Enzymatic and Chemical Modifications of Oligoenes and Polyenes

Dissertation

zur Erlangung des Doktorgrades der Naturwissenschaften
(Dr. rer. nat.)

der

Naturwissenschaftlichen Fakultät II
Chemie, Physik und Mathematik

der Martin-Luther-Universität
Halle-Wittenberg

vorgelegt von

Herrn Vico Keve Bernhard Adjedje

1st Reviewer: Prof. Dr. Wolfgang H. Binder
2nd Reviewer: Prof. Dr. Stefan Mecking

Date of public defense: 05.11.2024

Danksagung

Zuallererst möchte ich mich bei Prof. Dr. Wolfgang H. Binder für die Bereitstellung dieses interessanten Themas bedanken. Die intensiven Diskussionen meiner Ergebnisse und seinen steten Glauben an mich möchte ich hierbei herausstellen.

Mein Dank gilt all denen, die mich in meiner Zeit als Doktorand begleitet haben. Insbesondere danke ich meinem Kooperationspartner Prof. Dr. Martin J. Weissenborn von dem ich viel lernen durfte. Den Partnern des Leibnitz-Instituts für Pflanzenbiochemie (IPB) Halle Eugen Schell, Dr. Annegret Laub und der gesamten Gruppe Weissenborn bin ich sehr dankbar für die gemeinsame Zeit und die Unterstützung bei dem Erarbeiten dieser Arbeit. Yannick L. Wolf möchte ich hier gesondert meinen Dank für die gemeinsame Zeit und die zahlreichen Diskussionen aussprechen. Ich danke der Abteilung NWC des IPB für das Ermöglichen der massenspektrometrischen Messungen. Herrn Dr. D. Ströhl und seinem Team danke ich für die Messung zahlreicher NMR-Proben. Herrn Dr. G. Hause bin ich dankbar für die Messungen mit Transmissionselektronenmikroskopie. Frau Dr. L. de Souza bin ich dankbar für die Unterstützung zu Anfang des Projekts. Herrn Prof. Dr. D. Jendrossek danke ich für das Bereitstellen des originalen Lcp_{K30} Plasmids, das dieses Projekt mitermöglichte.

Bei der AG Binder bedanke ich mich insbesondere bei Anke Hassi, die mich bei allem Organisatorischen immer unterstützt hat und die gute Seele der AG für mich ist. Bei Julia Großert und Susanne Tanner bedanke ich mich für die kontinuierliche Hilfe bei Laborwünschen und zahlreichen Messungen. Auch allen anderen Kollegen, mit denen ich in dieser Zeit zusammenarbeiten, sowie mir ein Büro und Labor teilen durfte, möchte ich meinen Dank aussprechen. Hier denke ich im Besonderen an Matthias Rohmer, Justus F. Thümmler, Philipp S. Hilgeroth, Yue Cai, André Paschold und Zviadi Katcharava. Die zahlreichen schönen, gemeinsamen Erlebnisse im Labor, Büro und auf Konferenzen haben diese Zeit enorm bereichert. Meinem Masteranden Mohamed Hassan bin ich für die gemeinsame Zeit, die für uns beide so lehrreich war, dankbar. Ein herzlicher Dank gilt Frau Dr. Anja Marinow, die immer ein offenes Ohr für mich hatte und mich wissenschaftlich wie menschlich unterstützt hat.

Außerdem möchte ich mich bei meiner Familie, insbesondere meinen Eltern, und meinen Freunden für ihren Glauben und ihre Zuversicht während dieser Zeit, in der sie mich stets unterstützt haben, bedanken. Meinen Kommilitonen aus dem Studium, Franz, Frederik und Konstantin, die mir aus der Ferne immer wieder wertvolle Ratschläge gegeben haben, möchte ich hier insbesondere meinen Dank aussprechen. Meinen Freunden Dietrich, Mirthe und Christoph will ich auch einen gesonderten Dank aussprechen, weil dies Menschen für mich sind, die meinem Leben Struktur gaben. Ohne sie wäre ich heute nicht, der, der ich bin. Abschließend möchte ich meiner Partnerin Carolin danken für ihre Liebe, ihren Glauben an mich, ihre Unterstützung und ihre Geduld in dieser aufregenden Zeit.

Abstract

The poor solubility of polyisoprene (PI) in water is a substantial limit to accomplish enzymatic degradation. Increasing the interface of polyenes is therefore a major factor to enhance the attack of enzymes, such as rubber degrading enzymes (rubber oxygenases). In this thesis the chemical modification of natural and synthetic rubber has been investigated, using both, synthetic and enzymatic catalysts. Two different emulsification methods have been established to generate surfactant-free emulsions of PI in aqueous media, utilizing either a co-solvent or acoustical emulsification. The hydrodynamic diameters of the so formed emulsions of polyisoprene with different number average molar masses of 3000 g/mol and 14000 g/mol were determined by dynamic light scattering. Stability of the emulsions was investigated by transmittance studies and by zeta potential measurements for the co-solvent emulsified system (**C 1**). For the investigation of the effect of surfactant-free emulsification onto the enzymatic degradation behaviors, the degradation of latex milk was first replicated with the rubber oxygenase Lcp_{K30}. This was used as a reference system and positive control for the expansion of the degradation scope onto synthetic PIs and natural rubber derived PI with HPLC and UHPLC. Optimizations of the enzymatic degradation with Lcp_{K30} for the degradation of synthetic PIs with a significant 1,4-*trans* ratio were conducted. UHPLC-UV comparative analysis of the enzymatic degradation experiments clearly showed that the bioinspired emulsification approach with either acoustical emulsification or co-solvent emulsified system led to an increase in the integrated area of degradation fragments. **C 1** exhibited the most significant increase, showing a 4-fold higher integrated degradation fragments area compared to the non-emulsified PI 3000 (**N 1**) chromatogram. UHPLC-ESI-HRMS/MS measurements confirmed that the fragmentation patterns of **C 1** were identical to the bioinspiration latex milk. The tolerance of Lcp_{K30} towards other isomeric motifs than the 1,4-*cis*-isomer of PI showed its potential as a sustainable degradation catalyst for polymers, which require new sustainable methodologies of recycling. Protein-engineered variants of the rubber oxygenase Lcp_{K30} by PROSS showed increased thermostability according to NanoDSF. The most promising variant Lcp_{K30}-P7 was investigated for its catalytic behavior and showed the capability of withstanding thermal stress at 60 °C regarding catalytic activity towards latex milk, 1,4-*cis*-PI, according to UHPLC-UV-ESI-HRMS. To facilitate future catalytic degradations of polyenes, a new rubber oxygenase degradation assay was developed with GPC-UV. Different synthetic polyenes were chemically degraded by epoxidation and subsequent oxidative degradation with periodic acid, resulting in mixtures of telechelic polyenes and undegraded polyenes. Quantitative conversion of the derivatization agent was determined according to NMR methodologies and UHPLC-UV-ESI-HRMS. Application of the rubber oxygenase degradation assay allowed for the tracking of degradation with a background of undegraded polymer for the chemically degraded and the enzymatically degraded samples of PI by Lcp_{K30}. The activity of the first round of protein-engineered enzymes was screened alongside the native enzyme and the FuncLib protein engineered enzymes using the established methodology, allowing for a comparative analysis. Revealing promising results for the degradability of polybutadiene, which were investigated further with UHPC-ESI-HRMS. UHPLC-ESI-HRMS showed that the catalytic activity was too low to conclusively prove the degradation.

The post-modification of polyenes with new catalytic entities could allow for the remediation of waste polyene materials. Incorporation of cyclopropanating functionalities to provide novel catalytic entities as single chain nanoparticles was investigated with three different approaches. The transesterification of post-modified poly(pentafluorophenyl acrylate) and poly(pentafluorophenyl methacrylate) with hydroxyl bearing bis-*N*-heterocyclic carbene copper lead to the formation of single chain nano particles with the addition of auxiliary cross-linker 1,6-hexanediol. This is supported by evidence of a reduction in hydrodynamic diameter observed through DLS, GPC, and DOSY NMR analyses.

Kurzzusammenfassung

Die geringe Löslichkeit von Polyisopren (PI) in Wasser stellt einen wesentlichen limitierenden Faktor in chemischen und enzymatischen Abbauprozessen dar, da – zusammen mit der oftmals eingeschränkten Stabilität der Enzyme - die verfügbare Oberfläche für den enzymatischen Abbau von Polyisopren dadurch erheblich begrenzt ist. In dieser Promotionsarbeit wurden chemische und enzymatische Modifikationsmethoden von synthetischen und natürlichen Polyenen untersucht. Zwei verschiedene Emulsionsmethoden wurden etabliert, um tensidfreie Emulsionen von PI in wässrigen Medien zu erzeugen, wobei entweder ein Co-Lösungsmittel oder akustische Emulsifikation verwendet wurden. Der hydrodynamische Durchmesser der so gebildeten Emulsionen von Polyisopren mit den verschiedenen mittleren molaren Massen von 3000 g/mol und 14000 g/mol wurde mittels dynamischer Lichtstreuung bestimmt. Die Stabilität der Emulsionen wurde durch Transmissionsstudien und durch Zetapotenzialmessungen für das mit Co-Lösungsmittel emulgierte System (**C 1**) untersucht. Zur Untersuchung der Auswirkung der tensidfreien Emulsifikation auf das enzymatische Abbauverhalten wurde der Abbau von Latexmilch zunächst mit der Rubberoxygenae Lcp_{K30} repliziert. Dies diente als Referenzsystem und positive Kontrolle für die Erweiterung des Abbaubereichs auf synthetische PIs mit HPLC und UHPLC. Optimierungen des enzymatischen Abbaus mit Lcp_{K30} für den Abbau von synthetischen PIs mit einem signifikanten 1,4-*trans*-Verhältnis wurden durchgeführt. Die UHPLC-UV-Vergleichsanalyse der standardisierten enzymatischen Abbauexperimente zeigte deutlich, dass der bioinspirierte Emulsionsansatz mit akustischer Emulsifikation oder mit dem Co-Lösungsmittel emulgierten System zu einer Zunahme der integrierten Fläche der Abbaubruchstücke führte. **C 1** zeigte den größten Anstieg mit einer 4-fachen Zunahme der integrierten Fläche der Abbaubruchstücke im Vergleich zum nicht emulgierten **PI 3000** Chromatogramm. UHPLC-ESI-HRMS/MS-Messungen bestätigten, dass die Fragmentierungsmuster von **C 1** identisch mit Latexmilch waren. Die Toleranz von Lcp_{K30} gegenüber anderen isomeren Motiven als dem 1,4-*cis*-Isomer von PI zeigte ihr Potenzial als nachhaltiger Abbaukatalysator für Polymere, die neue nachhaltige Recyclingmethoden erfordern. Protein-engineerte Varianten der Rubberoxygenase Lcp_{K30} durch PROSS zeigten eine Erhöhung der Thermostabilität. Die vielversprechendste Variante, Lcp_{K30}-P7, wurde auf ihr katalytisches Verhalten untersucht und zeigte die Fähigkeit, thermischem Stress bei 60 °C in Bezug auf die katalytische Aktivität gegenüber Latexmilch, 1,4-*cis*-PI, standzuhalten, gemäß UHPLC-UV-ESI-HRMS. Um zukünftige katalytische Untersuchungen von Polyenen zu erleichtern, wurde ein neuer Abbauassay für Rubberoxygenasen mit GPC-UV entwickelt. Verschiedene synthetische Polyene wurden epoxidiert und anschließenden oxidativ abgebaut mit Periodsäure. Dies führte zu Mischungen von telechelen Polyenen und unabgebauten Polyenen. Die quantitative Umsetzung des Derivatisierungsreagenz wurde mittels NMR-Methoden und durch UHPLC-UV-ESI-HRMS bestimmt. Die Anwendung des Rubberoxygenase-Abbausassays ermöglichte die Verfolgung des Abbaus mit einem Hintergrund aus unabgebautem Polymer für die chemisch abgebauten und die enzymatisch abgebauten Proben von PI durch Lcp_{K30}. Die Aktivität der ersten Runde von protein-engineerten hergestellten Enzymen wurde neben dem nativen Enzym und den FuncLib-protein-engineerten hergestellten Enzymen unter Verwendung der etablierten Methodik gescreent, was eine vergleichende Analyse ermöglichte. Die vielversprechenden Ergebnisse für die Abbaufähigkeit von Polybutadien wurden mit UHPC-ESI-HRMS weiter untersucht. UHPLC-ESI-HRMS zeigte allerdings, dass die katalytische Aktivität zu gering war, um den Abbau vollständig nachzuweisen. Die Post-Modifikation von Polyenen mit neuen katalytischen Einheiten könnte die Wiederverwendung von Gummiabfällen bereichern. Hierfür wurden der Einbau von cyclopropananierenden Funktionalitäten als neuartiger katalytischer Spezies mit drei verschiedenen Ansätzen untersucht. Die Transesterifizierung von post-modifizierten Poly(pentafluorophenylacrylat) und Poly(pentafluorophenylmethacrylat) mit Kupferhaltigen Carben-Komplexen führte zur Bildung von Single Chain Nanopartikeln mit Zugabe des Hilfsquervernetzers 1,6-Hexandiol. Dies wurde aus der Abnahme des hydrodynamischen Durchmessers geschlossen, die durch DLS-, GPC- und DOSY-NMR-Analysen beobachtet wurden.

List of Abbreviations

°C	degree Celsius
ACN	acetonitrile
AIBN	azobisisobutyronitrile
Asc.	ascorbate
ATRP	atom transfer radical procedure
BC	before Christ
BR	butadiene rubber
bis-NHC-Cu	bis(*N*-heterocyclic carbene) copper complex
cat	catalyst
CDAB	1,4-*cis*-diacetoxy-2-butene
CSRD	Corporate Sustainability Reporting Directive
CTA	chain transfer agent
CuAAC	copper catalzye azide alkyne cycloaddtion
d	day
DLS	dynamic light scattering
DMAP	4-dimethylaminopyridine
DMF	*N*,*N*-dimethylformamide
DNA	deoxyribonucleic acid
DNPH	2,4-dinitrophenylhydrazine
EDA	ethyl diazoacetate
EPR	electron paramagnetic resonance spectroscopy
equiv.	equivalent
ESI-TOF-MS	electron spray ionization time of flight mass spectrometry
EU	European Union
FT-IR	Fourier transformative infrared spectroscopy
GPC	Gel permeation chromatography
Grubbs I	Grubbs first generation
Grubbs II	Grubbs second generation
GTC	Grubbs-type catalyst
h	hours
HG II	Hoveyda Grubbs second generation
HPLC	high performance liquid chromatography
HRMS	high resolution mass spectrometry
KPi	potassium phosphate buffer
LCC	leaf-branch compost cutinase
Lcp	latex clearing protein
min	minute
M_n	number average molar mass
M_w	mass average molar mass
NaH	sodium hydride
NanoDSF	nano differential scanning fluorimetry
NC	negative control
n. d.	not determined
n. e.	not emulsified
NHC	*N*-heterocyclic carbene
NMP	nitroxide mediated polymerization
NMR	nuclear magnetic resonance
br	broad
s	singlet
d	doublet
dd	doublet of doublets
t	triplet
m	multiplet
q	quartet
NR	natural rubber
n. r.	not reported
ODTD	12-oxo-4,8-dimethyl-trideca-4,8-dien-1-al
P1-9	PROSS variant 1-9
PB	polybutadiene
PDI	polydispersity index
PEG	poly(ethylene glycol)
PEGMA	poly(ethylene glycol methacrylate)
PI	polyisoprene
PROSS	Protein Repair One Stop Shop
r. t.	room temperature
RAFT	reversible addition fragmentation
RDBE	ring double bond equivalent
Ref.	reference
Rox	rubber oxygenase
Rx.	reaction
SBR	styrene butadiene rubber
SBS	styrene-butadiene-styrene
SCNP	single chain nanoparticle
SD	standard deviation
SDS	sodium dodecyl sulfate
SEM	scanning electron microscope
SIS	styrene-isoprene-styrene
SPI	synthetic polyisoprene
TEA	triethylamine
TEM	transmission electron microscopy
THF	tetrahydrofuran
T_m	meting temperature
UHPLC	ultra-high-performance liquid chromatography
UV	ultraviolet
w/v%	weigh per volume percentage

Table of Content

1. INTRODUCTION 1

1.1 Polyene-based rubbers 1
1.2 Polyisoprene and polybutadiene polymerization 3
1.3 Degradation strategies for rubber 4
1.3.1 Mechanical degradation of polyene rubbers 5
1.3.2 Photooxidation and pyrolysis of polyisoprene and polybutadiene 5
1.3.3 Chemical degradation of polyisoprene and polybutadiene 6
1.3.4 Organometallic degradation of polyisoprene and polybutadiene 9
1.4 Rubber degradation by microorganisms and enzymes 11
1.4.1 Rubber degrading enzymes 12
1.4.2 Polyisoprene degradation determination of enzymes and microorganisms 14
1.5 Surfactant-free emulsification 16
1.6 Protein engineering by directed evolution 18
1.7 Single chain nano particles as artificial enzymes 19

2. AIM AND CONCEPT 22

2.1 Aim 22
2.2 Concept 23

3. RESULT AND DISCUSSION 26

3.1 SURFACTANT-FREE EMULSIFICATION OF POLYISOPRENE AND POLYBUTADIENE 26

3.1.1 General Procedure 27
3.1.2 Acoustically emulsified system 28
3.1.2.1 Preliminary experiments of acoustical emulsification 28
3.1.2.2 Surfactant-free acoustical emulsification 30
3.1.3 Co-solvent emulsified system establishment 33
3.1.4 Characterization of the surfactant-free co-solvent emulsified systems of polyisoprene 35
3.1.5 Co-solvent emulsified polybutadiene systems 39

3.2 ENZYMATIC DEGRADATION OF POLYISOPRENE AND POLYBUTADIENE 41

3.2.1 Preliminary investigations of enzymatic degradation behavior of LcpK30 towards latex milk, synthetic polyisoprenes, and natural rubber derived polyisoprenes 42
3.2.1.1 Analytical methodology for enzymatic degradation of latex milk 42
3.2.1.2 Enzymatic degradation of non-emulsified polyisoprenes 43
3.2.2 Optimization of enzymatic degradation parameters 44
3.2.3 Comparative and optimized surfactant-free degradation studies of polyisoprene with Lcp_{K30} 48
3.2.3.1 Enzymatic degradation of surfactant-free emulsions of polyisoprene by Lcp_{K30} according to UHPLC and ESI-TOF-MS 49
3.2.3.2 UHPLC-ESI-MS of the surfactant-free synthetic polyisoprene emulsions 49
3.2.3.3 Influence of emulsification onto the enzymatic degradation 51
3.2.3.4 Enzyme stability investigations in the presence of synthetic polyisoprene, *N*-hexadecane, and surfactant-free emulsion 54
3.2.4 Degradation studies of polyisoprene with Lcp_{K30}-P7 55
3.2.4.1 Characterization of PROSS variants of Lcp_{K30} 55
3.2.4.2 Degradation studies after thermal stress on the variants 57
3.2.5 Rubber Oxygenase Degradation Assay by UV-labelling and Gel Permeation Chromatography 59
3.2.5.2 Establishment of derivatization methodology 59
3.2.5.3 Derivatization assay for synthetic polyisoprene 63
3.2.5.4 Application of derivatization assay onto Lcp_{K30} enzymatically degraded samples 64
3.2.5.6 Investigations into enzymatic degradation of polybutadiene by FuncLib 66

3.3 CYCLOPROPANATION OF OLIGOENES: NOVEL CATALYTIC ENTITIES 68

3.3.1 Preliminary investigations into squalene cyclopropanation 69
3.3.2 Approaches for the formation of single chain nanoparticles to incorporate cyclopropanating functionalities 71
3.2.2.3 Copper-NHC complexation as internal folding for SCNPs 71

3.3.2.1 Precursor polymer synthesis 73
3.3.2.2 Folding of SCNP by external cross-linker with copper catalyzed alkyne azide click reaction 76
3.2.2.4 Transesterification strategy with bis-(*N*-heterocyclic carbene) copper complexes 79

4. CONCLUSION 83

5. EXPERIMENTAL SECTION 87

5.1 Materials and methods 87
5.2 Procedures 91
5.3 Synthesis 97

6. REFERENCES 113

Curriculum Vitae 131
Eigenständigkeitserklärung 132

7. APPENDIX 133

Publication List

Parts of the Aim and Concept, Results and Discussion, Experimental Section as well as the Conclusion were already published in

1. Adjedje, V. K. B.; Schell, E; Wolf, Y. L.; Laub. A; Weissenborn, M. J.; Binder, W. H. Enzymatic degradation of synthetic polyisoprenes *via* surfactant-free polymer emulsification, *Green Chem*. **2021**, *23*, 9433-9438 DOI: https://doi.org/10.1039/D1GC03515K

2. Adjedje, V. K. B.; Wolf, Y. L.; Weissenborn, M. J.; Binder, W. H. Rubber Oxygenase Degradation Assay by UV-Labeling and Gel Permeation Chromatography, *Macromol*. *Rapid Commun*. **2024**, 2400032. DOI: https://doi.org/10.1002/marc.202400032

1. Introduction

The European Green Deal[1] and the Corporate Sustainability Reporting Directive (CSRD)[2] of the European Union (EU) are intended to empower a transformation of the EU into a clean and circular economy. This includes a zero-pollution ambition for a toxic free environment, which ensures no net emissions of greenhouse gases by 2050 and an economic growth decoupled from the usage of resources. Sustainability in this regard can either be seen as chance or problem.[3] The production of both natural and synthetic rubbers, derived from polyene-polymers, holds immense economic and environmental significance in this regard, with an estimated annual production in the millions of tons.[4, 5] Sustainable and green degradation methodologies for polyene-polymers and synthetic rubbers could become indispensable in aligning with the objectives of the Green Deal and CSRD. The 12 principles of green chemistry by P. T. Anastas and J. C. Warner, who suggested "the design, development and implementation of chemical products and processes that reduce the use and generation of hazardous substances" are aligned with the goals of legislation by the EU in this aspect and should be seen as a guiding principle for sustainable chemistry.[6] Those principles have been extended further by 12 principles with mainly process technological and thermochemical considerations.[7] Polyene derived rubbers like polyisoprene (PI) and polybutadiene (PB), could pose significant environmental challenges due to their resistance to sustainable, controlled and green degradation methodologies until now.[8] Research towards more sustainable methodologies for the controlled degradation, recycling, or repurposing of these materials could become imperative to reduce waste and pollution, conserve resources, and transition into a circular polymer chemistry in the future. In 2017, natural rubber (NR) has already been designated a critical raw material by the European Commission,[9] which makes the development and optimization of chemical or biotechnological recycling methodologies for end-of-life tires, NR and synthetic polyisoprene (SPI) even more pressing. Even though the recycling input rate improved from 1% in 2017 to 5% in the latest report from 2023,[10] there still remains a clear need for action to significantly improve this recycling rate and to establish more sustainable degradation methodologies. Degrading polymers without hydrolysable functional groups in the polymer backbone represents a challenge in polymer recycling especially with the goal of a circular economy.[11] In the following sections the different methodologies for the degradation of the polyenes, PI and PB, will be introduced as well as different concepts that could possible improve the remediation of polyene wastes, protein-engineering or single chain nano particles as artificial enzymes.

1.1 Polyene-based rubbers

Humanity has used rubber, harvested as a latex acquired from the *Castilla elastica* tree and processed with juice from *Ipomoea alba*, a species of morning glory vine, for a variety of rubber products, as solid rubber balls, medicines, art and rubber bands, since 1600 BC in Mesoamerican cultures.[12] But rubber did not find commercial use until 1838, when Charles Goodyear was able to overcome the thermic constraints of liquid rubber becoming sticky in the heat and rigid in the cold by discovering a commercially applicable way of vulcanization.[13] Vulcanization is the cross-linkage of sections of polymer chains leading to a curing of an elastomer, which can have a beneficiary effect onto the elastic properties over a range of temperatures (Figure 1). The rubber from *Hevea brasiliensis* has been established as practically the only naturally occurring rubber source, although over 2000 species of higher plants and fungi, have been reported to contain PI hydrocarbon.[14] NR is harvested as latex milk, which is a white colloidal suspension obtained from the *hevea* tree by tapping (Figure 1).[15] The dry material of latex milk is a mixture of NR, predominantly consisting of 1,4-*cis*-PI, and non-rubber components such as proteins, carbohydrates and lipids.[16] A distinction is made between NR and synthetic rubber. Synthetic rubber refers to various polymers, mostly petroleum-based, such as styrene-butadiene rubber (SBR), butadiene rubber (BR) or nitrile rubber.[17]

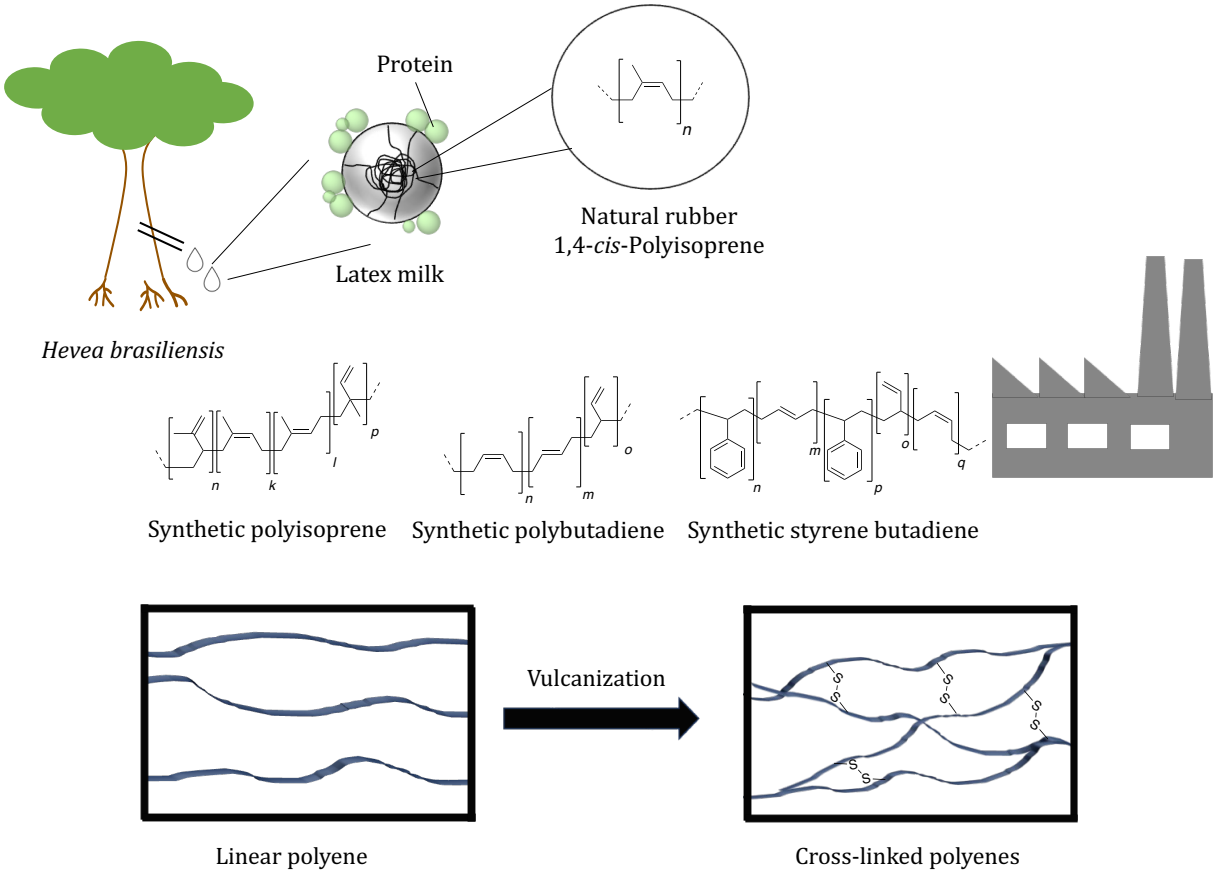

Figure 1. Sources of natural rubber (NR), 1,4-*cis*-polyisoprene, synthetic polyisoprene, synthetic polybutadiene and synthetic copolymer of styrene and butadiene with the corresponding possible isomeric motifs (I). Vulcanization of the linear polyene to the corresponding rubber materials (II).

Synthetic rubber has been gaining importance since the middle of the 20th century as either a replacement or additive to NR.[18] Most synthetic rubbers are of higher thermostability and better resistance to oil and other solvents than NR.[19] Nonetheless, nowadays, PI is still ubiquitously applied in industry as motor mounts, pipe gaskets, sporting equipment and many other molded and mechanical goods due to its exceptional mechanical properties.[20] Unlike NR, SPI, depending on the polymerization method used can exhibit different microstructures, the 1,4-*cis*, 1,4-*trans*, 1,2-, and 3,4-isomer (Figure 1). Depending on the respective fractions of these different repeating units, thermal and mechanical properties such as glass-transition temperature, temperature resistance, and mechanical stress resistance can significantly vary. PB has no natural analog and is solely synthetically produced, as a mixture of the 1,4-*cis*, 1,4-*trans* and 1,2-isomer, dependent on the polymerization procedure. Rubber-like solids can be referred to the group of elastomers because of their viscoelastic properties. Elastomers are polymers with cross-linkages that feature elastic behavior that allows the entangled polymer chains to partially entangle when force is applied with the ability to reshape the polymer chains to their coil structure after the mechanical force is removed. Here, 1,4-*cis*-PI as NR or SPI and styrene-butadiene or PB can be seen as some of the most relevant elastomeric rubber materials. These polymers are crucial for car tires and other molded mechanical goods, which are accumulating in the environment and require more sustainable degradation methodologies.[21]

1.2 Polyisoprene and polybutadiene polymerization

The microstructure of the polyenes PI and PB is highly dependent on their polymerization (Scheme 1). A general overview over the polymerization possibilities as well as the influence onto the isomeric motifs of PI and PB is provided in the following section.

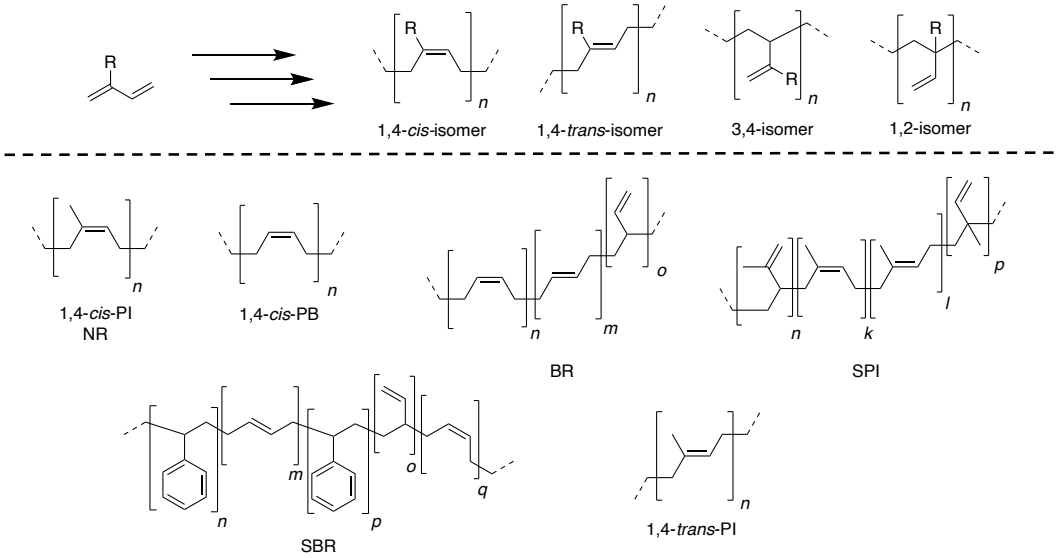

Scheme 1. Polymerization of isoprene (R = CH_3) and butadiene (R = H) resulting in the isomeric motifs of 1,4-*cis*-, 1,4-*trans*, 3,4- and 1,2-isomers for PI and 1,4-*cis*-, 1,4-*trans*- and 1,2-isomers for PB. Most relevant polymers: natural rubber (NR), 1,4-*cis*-PI, 1,4-*cis*-PB, butadiene rubber (BR), synthetic PI (SPI), styrene-butadiene rubber (SBR), and 1,4-*trans*-PI with their corresponding possible isomeric motifs.

PI can be synthesized by free radical polymerization *via* miniemulsion polymerization. In miniemulsion polymerization the monomer is dispersed in an aqueous solution of surfactant with a concentration exceeding the critical micelle concentration and the polymerization is started by means of an initiator system.[22] Miniemulsion polymerization allows for the preparation of PI latexes with different initiator systems, such as redox initiation systems tert-butyl hydroperoxide and tetraethylene-pentamine or potassium persulfate and sodium bisulfite[23] or solely by potassium persulfate.[24] In case of radical polymerization of PI soluble, low-dispersity product formation is competing with remaining unsaturated linkages in the first-formed polymer.[25] Butadiene is not easily polymerized to high molecular weights by conventional free-radical initiators in solution or in bulk, because the products are mixtures of a low molecular weight soluble fraction and a cross-linked gel with the fractions dependent on the reaction conditions and temperatures.[26] Emulsion polymerization of PB leads to high molar mass and broad polydispersity. Free radical polymerization for PB generally leads to 15 to 20% 1,2-isomer and a 1,4- *cis*: *trans* ratio dependent on the polymerization temperature.[27, 28]

Preparation of PI and PB has also been investigated with controlled radical polymerization methodologies such as nitroxide mediated polymerization (NMP). Herein, the reversible end-capping of the growing radical chains to give dormant species reduces the concentration of active species and inhibits side reactions leading to a control of the radical mechanism. This led to good control of the polydispersity and number average molar masses (M_n) for PI and for PB but no control over the microstructure.[29] The solvent had a significant effect onto the polymerization in the case of PI showing the best results in pyridine.[30, 31] The microstructure for PI was typically about 80% of 1,4-repeating units, in both *cis*- and *trans*-configurations, and about 20% of 1,2- and 3,4-isomers. Atom transfer radical procedure (ATRP) was not successful in the controlled radical polymerization of isoprene due to the chelation of the copper by isoprene,[32] whereas for PB the ATRP led to control over the M_n up to high molecular weights and with polydispersity ranging from 1.3 to 1.5.[33] In reversible addition

fragmentation polymerization (RAFT) the control is dependent on the chain transfer agent. The chain transfer agent is degenerative and the reversible transfer of the functional chain end-group between the dormant chains and the propagating radicals are in an equilibrium that provides polymerization control.[34] RAFT-polymerization of PI required temperatures above 110 °C for conversions of 30% but lead to polydispersity below 1.4 without control of the microstructure.[35]
Ring opening metathesis can also be applied for the polymerization of PB from cyclooctadiene[36] and PI from 1,5-dimethyl-1,5-cyclooctadiene[37] with respective chain transfer agents. It led to the formation of polyenes but without control of the microstructure.
The biosynthesis of NR is debated to be a carbocationic polymerization.[38] Consequently, PI can also be polymerized in a cationic manner. One of the main features observed for the cationic polymerization with catalytic systems such as, BF_3,[39] $AlEtCl_2$,[40] and $TiCl_4$,[41] was a first stage of rapid and linear isoprene consumption followed by a second stage of moderate to very low activity.[42] Double bond content diminished in PI as well as PB during cationic polymerizations. For isoprene and butadiene cyclization, termination and chain transfer have been observed as side reactions in cationic polymerizations.[43] But the microstructure is highly 1,4-*trans* for PI[44, 45] as well as PB.[46]
Polyisoprene and polybutadiene are polymerized with anionic catalytic systems in industry. Anionic polymerization of PB does not lead to highly stereoregular PB but allows for tuning of the microstructure.[47] Polar solvent with alkali metal as counterion have shown to have led to high 1,2-isomer content for PB,[48] whereas high 1,4-*trans*-PBs were reported for multi-metallic system with for example alkyllithium, alkylaluminum or barium alkoxide.[49]
Most control over the stereoregularity for polyenes is allowed by coordination polymerization. The catalysts utilized industrially are heterogeneous Ziegler-Natta-type multicomponent systems that consist typically of rare-earth metals such as neodymium[50, 51] yttrium,[52] or lanthanum[53, 54] Coordination polymerization allows for the preparation of high 1,4-*cis*-PIs and 1,4-*cis*-PBs.[55] Furthermore it is possible to synthesize high 1,4-*trans*-PBs[56] and high 1,4-*trans*-PIs with those kind of catalytic systems.[57] The methodologies for the polymerization and cross-linkage of PI and PB are manifold. But their degradation remains challenging and can be conducted with different approaches.

1.3 Degradation strategies for rubber

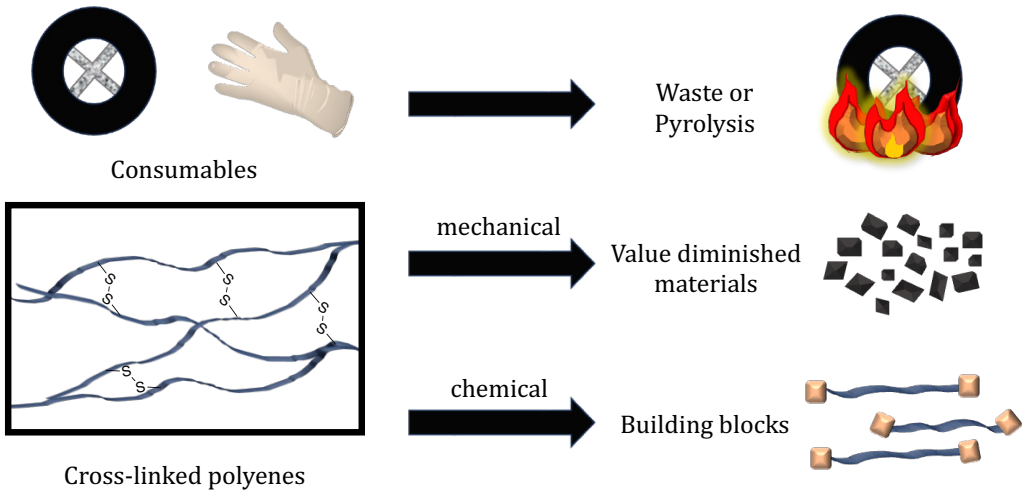

Figure 2. Approaches for the waste management of rubber materials by landfill disposal or pyrolysis, mechanical degradation, and chemical degradation.

Rubber can be degraded with different approaches (Figure 2). The least controlled methodology is the disposal of rubber materials in landfills. Since the EU waste landfill directive, the landfilling of tires for example has been banned, which encourages other reutilization strategies.[21] Nonetheless globally rubber, especially in the form of end-of-life tires is still often not recycled. Pyrolysis of rubber can

repurpose the inherent polymeric structure of the rubber into energy recovery, gases, distillates and char, albeit in widely variable relative amounts dependent on the operating conditions.[58] Mechanical degradation has found broad application in the recycling of rubber materials but can lead to value diminished materials. The degradation of rubber into new building blocks, for instance through chemical degradation, could allow for a circular economic approach for polyenes. In the following the different degradation approaches are introduced.

1.3.1 Mechanical degradation of polyene rubbers

In the case of polyenes, cross-linking or vulcanization is often essential to create the necessary mechanical properties for most applications. Current methodologies for PI and PB derived rubber recycling predominantly relies on mechanical grinding, either at ambient temperature or through cryofracturing.[59, 60] Ambient processing typically leads to irregularly shaped particles with relatively large and rough surface areas. Physical binding of the rubber particles with other matrix material is observed when using this grinding methodology that can promote additional interaction as seen for example in paving bitumen.[60, 61] The generation of heat during the grinding process can be higher for aged rubber, which in turn leads to increased degradation of the polymer chains and more irregular particle properties.[62] In the cryogenic grinding process, small pieces of frozen vulcanized rubber are ground in a ball mill, in the presence of liquid nitrogen generating rubber particles of different sizes.[63] Those can be used as fillers in virgin rubbers or thermoplastics, but typically with somewhat diminished properties.[64]

1.3.2 Photooxidation and pyrolysis of polyisoprene and polybutadiene

Diene derived elastomeric materials are susceptible to oxidative degradation also by photo-oxidation. PI and PB photo degradation is often observed on films to have led to degradation products, such as ethers, esters, hydroperoxides, ketones and aldehydes.[65,66] The first study on photo-oxidation of dienic elastomers was carried out already in 1911, it established that the oxygen consumption during NR degradation depended upon the ultraviolet (UV) radiation exposure time and its wavelength.[67] The bond dissociation energy of C-C bond (375 kJ/mol) and C-H bond (420 kJ/mol) can be overcome by photolysis but it can also lead to radical side reactions.[68] Consequently, the photooxidation of rubber waste has not found broad application due to its energetic cost and uncontrolled radical mechanism. Microwave assisted degradation of rubber has also been reported to have led to low efficiency and it is presumed that the degradation only occurs at the carbon–sulfur and sulfur–sulfur bond, which has limited the application of these methodologies.[63, 69] But it could be a viable technology for pretreatment of rubber waste by devulcanization.[70]

Pyrolytic conversion is one of the most used reutilization approaches for rubber materials. Pyrolysis is the thermal decomposition of organic materials in the absence of oxygen, which relies on the addition of heat to break chemical bonds.[71] The high calorific value of rubber waste, for end-of-life tires 30–40 MJ/kg, which is higher than that of coal for example, has led to its usage as an alternative fuel in the cement industry.[72] The pyrolysis can yield fuel gas, low-grade carbon black, and other in comparison to the feed stock, value-diminished materials as products dependent on the operating conditions. However, it can also lead to air pollution from emissions[73] and has the disadvantage that the rubber is not brought back into the life cycle of other rubber materials to utilize the chemical structure of the polyenes.

1.3.3 Chemical degradation of polyisoprene and polybutadiene

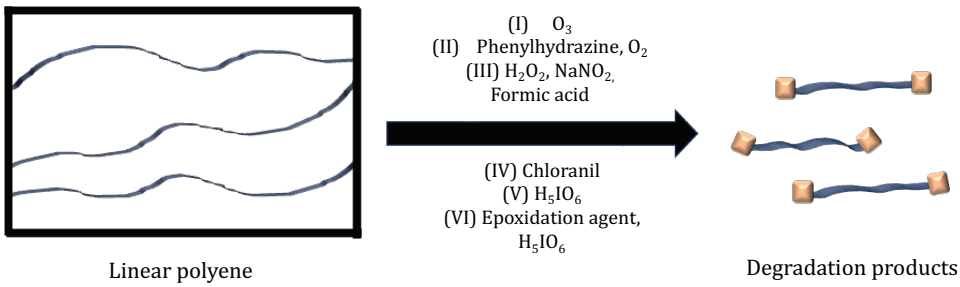

Figure 3. Chemical degradation approaches of polyenes by ozonolysis with ozone (O_3 (I)), radical generating agents (phenylhydrazine, O_2 (II)), peroxynitrous acid as oxidizing agent (H_2O_2, $NaNO_2$, formic acid (III)), chloranil, tetrachlor-*p*-benzochinon, as oxidizing agent (IV), periodic acid (H_5IO_6) as oxidizing agent (V) and epoxidation with subsequent oxidation by periodic acid (VI).

The chemical degradations of PI and PB have commonly been conducted to utilize the specific highly ordered *cis*-isomeric motifs as telechelic polyenes with defined end groups (Figure 3). Especially in regard to NR different methodologies have been employed to enable the preservation of the 1,4-*cis* isomeric motifs for applications as "liquid" NR, because of the molecular weight viscosity and the viscosity processability relationships.[74]

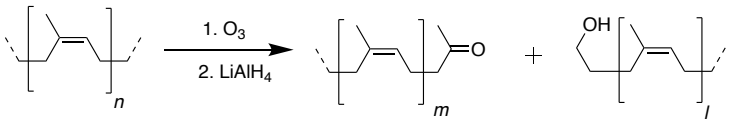

Scheme 2. Ozonolysis of 1,4-*cis*-PI with ozone (O_3) with subsequent reduction by lithium aluminum hydride ($LiAlH_4$).

Ozonolysis of rubber materials has been investigated since the 1950s.[75, 76] According to the Criegee mechanism,[77] ozone forms an unstable primary ozonide intermediate, which is an unstable species because it contains two very weak O-O bonds, that can rapidly decompose into a stable carbonyl compound, aldehyde, or ketone, and an unstable zwitterionic carbonyl oxide. The carbonyl oxide can rearrange into stable compounds dependent of the nature of the environment. Those reactions can lead to a decrease in the NR molecular weight accompanied by an introduction of functional end-groups such as aldehydes, ketones, carboxylic acids, or peroxides (Table 1).[78] The production of low molecular weight hydroxyl-telechelic polyenes from 1,4-*cis*-PB and 1,4-*cis*-PI by ozonolysis and subsequent reduction by lithium aluminum hydride was also already reported in the 1970s (Scheme 2).[79]

Table 1. Chemical degradation of polyenes by ozonolysis and redox couples to the corresponding lowest M_n after the degradation or the method of degradation detection.

Chemical structure	Descriptor	Reagent	M_n (before)	M_n (after) / Degradation determination	Ref.
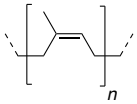	NR	O_3	271 000	840	[78]
	1,4-cis-PI	O_3	n. r.	800	[79]
	NR latex	Propanal, $K_2S_2O_8$	n. r.	3200	[80]
	Latex milk	H_2O_2, $NaNO_2$, Formic acid	650 000	10 500	[81]
	Deproteinized NR	H_2O_2, $NaNO_2$, Formic acid	1100000	56 300	[82]

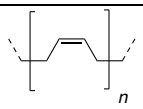	1,4-cis-PB	O_3	n. r.	1000	[79]
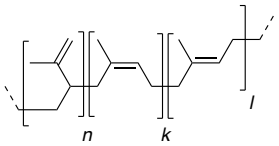	SPI	Phenylhydrazine, atmospheric O_2	9700	3650	[83]
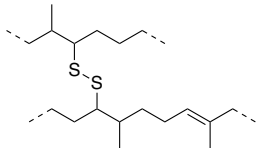	Vulcanized rubber	Phenylhydrazine, $Fe(III)Cl_3$	n. r.	Soluble fraction determination	[84]

The redox degradation of rubbers, which utilizes a free radical mechanism and a pairing of oxidizing agent and reducing agent, has been used more frequently due to the cheaper reaction conditions. Organic peroxides, hydrogen peroxide, and atmospheric oxygen as oxidizing agents coupled with phenylhydrazine or sodium nitrite as reducing agents are some examples of redox reagents. Depending on the redox couple used, the cleavage of polyene chains allows not only for obtaining low molecular weights but also for introducing reactive end-chain functionalities such as phenylhydrazones, carbonyl, or hydroxyl groups.[85] The combination of phenylhydrazine and atmospheric oxygen generates free phenyl radicals that can perform the PI chain degradation. This was applied to SPI and led to significant decreases in the M_n but not to the low molecular weights obtained for the degradation with ozonolysis. One of the drawbacks of the usage of phenylhydrazine and atmospheric oxygen is the formation of epoxides and hydroxyl functions as side products of the reaction.[83] For vulcanized rubber materials the degradation with phenylhydrazine and iron(III)chloride led to degradation according to soluble fraction determination, which was deemed to be independent of the cross-linkage disintegration.[84] Alternatively, propanal and potassium persulfate, a radical initiator, with sodium phosphate for pH control were applied for the degradation of NR latex by a radical mechanism.[80]

Hydrogen peroxide has been used in combination with sodium nitrite and formic acid for the oxidative degradation of PIs as NR in the latex milk form. It was proposed that in an acidic medium the hydrogen peroxide and sodium nitrite react to form peroxynitrite, which then protonated in acidic medium to peroxynitrous acid that can decompose to hydroxyl radical and nitrogen dioxide by homolytic scission.[81] Deprotonated liquid NR was degraded with hydrogen peroxide and sodium nitrite, but epoxidations were reported to occur as side reactions.[82]

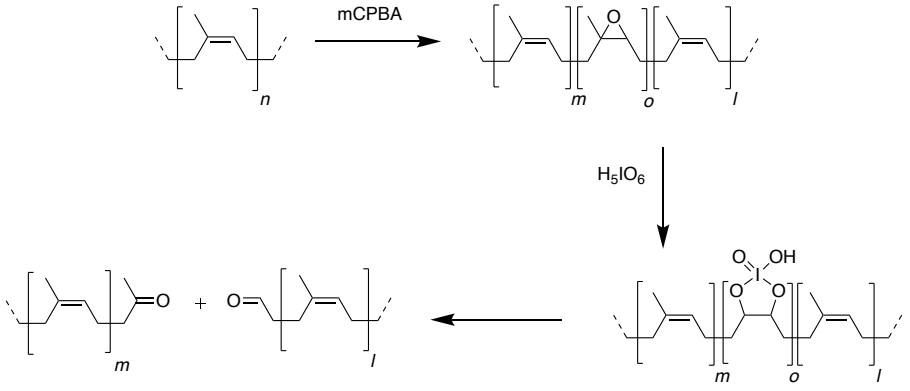

Scheme 3. Epoxidation of 1,4-*cis*-PI with *m*-chloroperoxybenzoic acid (mCPBA) subsequent oxidative degradation by periodic acid (H_5IO_6).

Strong oxidants, such as chloranil, tetrachlor-*p*-benzochinon, were reported to have led to PI oxidative degradation by ^{1}H NMR integration and viscosity decrease.[86] A similar effect was observed, when styrene butadiene rubber (SBR) was degraded better by sonication in the presence of periodic acid to 40000 g/mol rather than to M_n of 80000 g/mol without periodic acid.[87] Further investigations in to the effect of periodic acid showed that pre-epoxidized NR was oxidatively depolymerized in the presence of periodic acid (Table 2).[88] It was established that the degradation of PI by periodic acid is a two-step process involving two molecules of periodic acid per double bond. A first slow step involves the oxidation of the double bond in the polymer chain by periodic acid, which can lead to epoxide units or vicinal diols. The second, faster step is the oxidative cleavage of the modified double bond to aldehyde and ketone end-groups by a second periodic acid molecule.[89] The first epoxidation step can also be conducted with *m*-chloroperoxybenzoic acid (mCPBA)[89] for better control of the first step and subsequent oxidative degradation with periodic acid according to the epoxidation ratio (Scheme 3).[90] Investigations into the applicability to waste rubber tire granulates showed a degradation correlation between periodic acid concentration, reaction time and temperature according to NMR-studies.[91] This also showed that the degradation was possible with synthetic rubbers. The PB degradation was conducted according to a similar strategy with first epoxidation by formic acid and hydrogen peroxide or mCPBA and subsequent chain cleavage by periodic acid. This reaction was also conducted in one pot with butadiene rubber (BR) leading to satisfactory results.[92] The excess of periodic acid seems to have led to residual epoxides.[92] But vicinal diols were not reported for a similar procedure of the oxidative degradation of PB.[93] Phase transfer catalysts were utilized as an alternative sustainable and reusable epoxidation method with subsequent oxidative degradation by periodic acid.[94] A comparative degradation study of PI and PB by the oxidative degradation with either solely periodic acid or the combination of mCPBA and periodic acid revealed that the oxidative degradation was better controlled for PI than for PB. Furthermore it showed that the two step process of epoxidation and subsequent oxidation was distinctively better controlled for the oxidative degradation PB than the direct oxidation with solely periodic acid.[95]

Table 2. Organocatalytic degradations of polyenes by different oxidative reagents with the corresponding lowest M_n after the degradation or the degradation detection method.

Chemical structure	Descriptor	Reagents	M_n (before)	M_n (after) / Degradation determination	Ref.
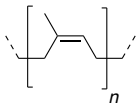	1,4-*cis*-PI	Chloranil	1040000	Viscosity decreases	[86]
	1,4-*cis*-PI	mCPBA, H_5IO_6	800000	4135	[89]
	1,4-*cis*-PI	mCPBA, H_5IO_6	184 000	1510	[90]
	1,4-*cis*-PI	mCPBA, H_5IO_6	635 000	4800	[95]
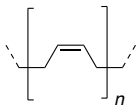	1,4-*cis*-PB	Chloranil	314000	Viscosity decreases	[86]
	1,4-*cis*-PB	mCPBA, H_5IO_6	150 000	5400	[95]

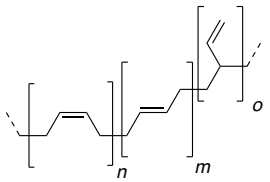	BR	HCOOH, H_2O_2 or mCPBA, H_5IO_6	n. r.	5500	[92]
	BR	HCOOH, H_2O_2 or mCPBA, H_5IO_6	n. r.	2800	[93]
	BR	CPC-PW_4O_{16}, H_2O_2, H_5IO_6	180000	6000	[94]
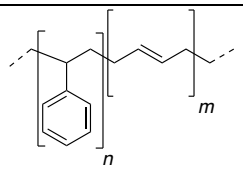	SBR	H_5IO_6, sonication	325000	40000	[87]
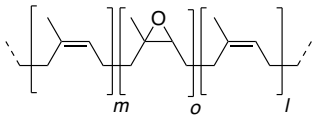	Epoxidized rubber	HCOOH, H_2O_2, H_5IO_6	145800	5100	[88]
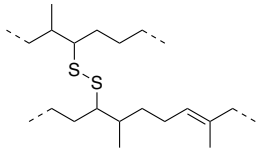	Waste rubber tires	mCPBA, H_5IO_6	-	^{1}H NMR	[91]

1.3.4 Organometallic degradation of polyisoprene and polybutadiene

The presence of the C=C double bonds in polyenes also allows for organometallic degradation. PI and PB depolymerization have been investigated with various catalytic systems with a historic focus on PI and the corresponding NR depolymerization. One of the first organochemical degradation of NR and SPI was reported with tungsten hexachloride and tetramethyl tin in chlorobenzene (Table 3).[96] Molecular weight decreased notably with reaction progress and temperature increase. However, a metathesis ring-chain equilibrium of 1,5,9-trimethyl-(1E,5E,9E)-cyclododecatrien and 1,4-*cis*-PI was reported as a side reaction to the depolymerization with tungsten hexachloride and tetramethyl tin in cross metathesis with ethylene.[97]

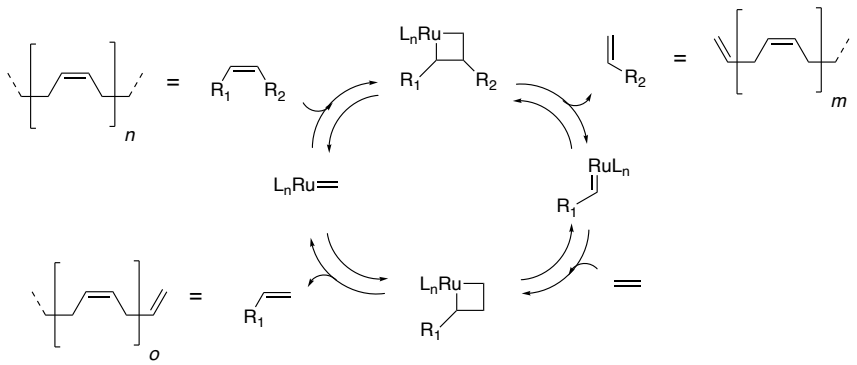

Scheme 4. Catalytic cycle of degenerative polyene cross metathesis with ethylene of 1,4-*cis*-PB segments with R_1 and R_2 as polybutadiene extensions.

A productive metathetic depolymerization takes place when an internal olefin and external olefin in the presence of an olefin metathesis catalyst lead to the cleavage of an internal double bond to give two terminal olefins. This leads to the scission of long chain unsaturated polymers into shorter degradation products with terminal olefins (Scheme 4).[98] The catalytic system for the depolymerization of polyene was enhanced by the introduction of Schrock tungsten complexes (STC), which led to more control over the depolymerization with a more stable catalyst, albeit under

conditions of low polymer concentrations and a surplus of olefins.[99] This limitation arises from the significant decrease in catalyst reactivity due to trisubstituted unsaturation in comparison to PB, as well as PI's susceptibility to side reactions like the aforementioned cationic cyclization.[100] Hence, sterically more hindered PI requires highly stable and selective metathesis catalysts for depolymerization. The development of highly active Ru-alkylidene catalysts opened vast new possibilities in olefin metathesis and their application to controlled depolymerization of polyenes.[101] As a comparative study the rate of reverse acyclic diene metathesis depolymerization with ethylene of styrene-butadiene-styrene (SBS) and styrene-isoprene-styrene (SIS) ABA triblock copolymers was investigated with alkoxy-imido molybdenum and tungsten complexes in comparison to the Ru-alkylidene catalysts, Grubbs first generation (Grubbs I) and Grubbs second generation (Grubbs II) catalysts. The metathetic degradation was most effective for PB and PI with the Grubbs II catalyst with slower degradation kinetics reported for the trisubstituted double bond.[102] The metathetic degradation of NR and SPI was reported with *cis*-1,4-diacetoxy-2-butene (CDAB) as the chain transfer agent and the Grubbs II catalyst.[103] The corresponding GPC data revealed a constant decrease of M_n in a controlled manner to 900 g/mol, with polydispersity values of 1.8. For NR solely the deproteinized rubber latex with acetonitrile as a co-solvent was successfully degraded. The degradation of NR was further improved by the usage of β-pinene as chain transfer agent leading to degradation products with 1200 g/mol according to GPC.[104] The developments in ruthenium catalysts[105] have allowed for the effective depolymerization of NR even with the natural occurring squalene with a Grubbs-type catalyst to oligoisoprenoids.[106] By now, even degradation of end-of-life tires with ethenolysis of Grubbs-type catalyst (GTC)[107] and cross-metathetic depolymerization with CDAB in ionic liquids were reported.[108] The metathetic degradation of 1,4-*trans*-PIs revealed that the degradation also functions effectively with other isomeric motifs but leads to better control with Hoveyda Grubbs second generation (HG II) than Grubbs I or Grubbs II in contrast to the 1,4-*cis*-PI. At number average molar masses lower than 10 000 isomerization of the *trans*- to the *cis*-PI was also observed.[109] One of the drawbacks of metathetic degradation of polyenes in regards of green chemistry is that it requires rare earth metals as well as non-benign solvents.

Table 3. Organometallic degradation of polyenes by different degradation agents and catalysts with the corresponding lowest M_n after the degradation or the observed degradation products.

Catalyst	Polyene	Degradation Agent	M_n (before)	M_n (after) / Degradation products	Ref.
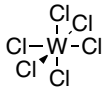	NR	$Sn(CH_3)_4$	1200000	5800	[96]
	NR	$Sn(CH_3)_4$, Ethylene	n. r.	Cyclized products	[97]
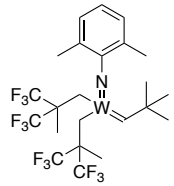 STC	1,4-*cis*-PI	3-Hexene	n. r.	Cyclized products	[99]
	1,4-*cis*-PB	3-Hexene	n. r.	Cyclized products	[99]
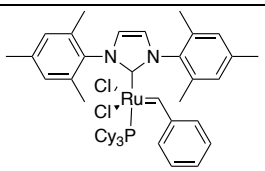 G II	SBS	Ethylene	40000*	540	[102]
	SIS	Ethylene	90000*	400	[102]
	NR	CDAB	222000	900	[103]
	SBR	CDAB	201000	1400	[103]
	NR	β-Pinene	1700000	1400	[104]

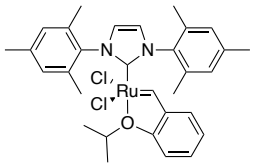 HG II	1,4-*cis*-PI	CDBA	114000	17000	[108]
	End-of-life tires	CDBA	n. r.	Soluble oligoisoprenes	[108]
	1,4-*trans*-PI	1-Octene	400 000	1100	[109]
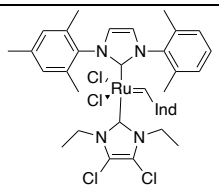 GTC	NR	Squalene	n. r.	Soluble oligoisoprenes	[106]
	End-of-life tires	Ethylene	n. r.	Soluble oligoisoprenes	[107]

*= M_w; Ind = 3-phenylindenylid-1-ene;

1.4 Rubber degradation by microorganisms and enzymes

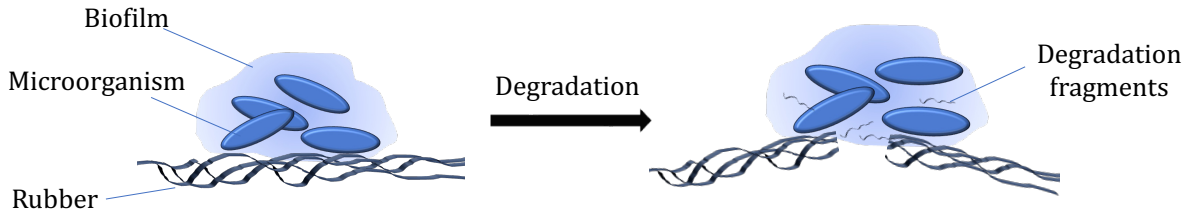

Figure 4. Microorganism degradation of rubber by the cleavage of double bonds by secreted enzymes in the biofilm.

Rubber degrading microorganism have been investigated since the early 20th century.[110,111] A historical focus has been placed onto the exploration and characterization of NR degrading organisms due to their long standing presence in the environment and the similarities in the molecular structures of isoprene units to many biomolecules such as terpenoids and carotenoids.[112] In contrast, synthetic rubbers and their molecular structure are relatively new in environmental contexts, resulting in rare examples of identified microorganisms capable of their degradation. Bacteria involved in the NR degradation can be categorized into two groups: those forming clearing zones and those not forming clearing zones around a colony of latex overlay agar plates.[112] The formation of clear zones around the developing colonies of rubber-degraders could be a consequence of the secretion of rubber-degrading enzymes. These enzymes diffuse into the agar and extracellularly cleave the polymer to lower molecular weight products that can be taken up by the bacteria (Figure 4). The non-clearing zone forming rubber degrading microorganisms require direct contact with the rubber substrate and grow adhesively.[5] *Gordinia westfalica*,[113] *Nocardia farcinica*,[114] and *Mycobacterium fortuitum*[115] are for example members of this group. These bacteria give rise to the formation of a biofilm, which leads to the disintegration of the rubber.[116]

Table 4. PI and vulcanized latex degradation by microorganisms according to weight loss.

Strain	Material	Weight loss [%]	Duration [week]	Reference
Gordonia polyisprenivorans VH2	SPI	50	4	[115]
Steroidobacter cummioxidans 35Y	NR latex	60	1	[117]
Streptomyces coelicolor 1A	Vulcanized latex gloves	18	6	[118]
Streptomyces lividans TK23	Vulcanized latex gloves	5.1	12	[119]
Streptomyces sp. K30	Vulcanized latex gloves	13.4	12	[119]

Various other rubber degrading microorganisms have been reported derived from bacteria as well as fungi.[120 121] The only strain that was capable of degrading PB with a M_n of 2400 as a carbon source was a *Moraxella* strain.[122] The biodegradation of NRs can be investigated by the weight loss in microorganism experiments (Table 4).[123] Alternatively mineralization experiments can determine the carbon dioxide formation of the decomposition of the rubber by microbial action during the cultivation duration.[114] It is crucial for the understanding of sustainable rubber remediation to investigate in detail the enzymes governing the degradation behavior as well as the factors influencing the degradation process and the specific degradation products. In the following the most intensively investigated enzymes derived from different bacterial stems are introduced; the rubber oxygenase A (RoxA), rubber oxygenase B (RoxB) and latex clearing proteins (Lcp).

1.4.1 Rubber degrading enzymes

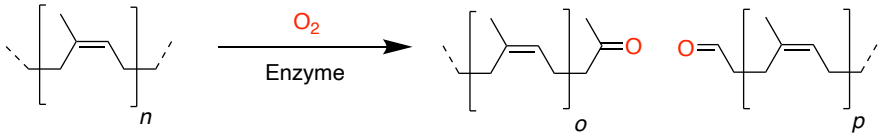

Scheme 5. Oxidative cleavage of the double bond of 1,4-*cis*-PI with atmospheric oxygen by enzymatic degradation.

Rubber oxygenases utilize atmospheric oxygen for the oxidative cleavage of the double bond (Scheme 5). The rubber oxygenase A (RoxA) and rubber oxygenase B (RoxB) derive from gram-negative organisms whereas latex clearing proteins (Lcp) have been found only in gram positive organisms. Gram positive or negative differentiates bacteria by the chemical and physical properties of their cell walls by staining. Degradation studies by Tsuchii und Takeda were the first to report a protein in *Steroidobacter cummioxidans 35Y* that had the ability to degrade 1,4-*cis*-PI.[117] The isolation and sequence analysis revealed that the protein had a size of 70-74 kDa.[124] Characterization of the enzyme revealed it to be a c-type heme, which refers to the attachment of the heme group to the protein *via* thioether bridges of cysteine residues.[125] $RoxA_{35Y}$ is a dioxygenase that produces one main degradation product, 12-oxo-4,8-dimethyl-trideca-4,8-dien-1-al, (ODTD) but the reaction mechanism has not been completely understood.[126, 127] $RoxA_{35Y}$ is an exotype rubber oxygenase, because it cleaves the PI in an exo-fashion, at the end of the polymeric structure in a distinctive manner leading to aldehyde and keto-functionalities at the end group.

Rubber oxygenase B_{35Y} has also been isolated from *Steroidobacter cummioxidans 35Y* after investigation of the draft genome sequence revealed only 38% amino acid sequence identity to a RoxA-types.[128, 129] $RoxB_{35Y}$ is of similar size as RoxA and also reported to be a c-type heme. The distinctive difference is that $RoxB_{35Y}$ degrades NR with an endo type cleavage. It cleaves the PI backbone randomly. This allowed for the investigation of synergistic degradation of $RoxA_{NS21}$ and $RoxB_{NS21}$

derived from *Rhizobacter gummiphilus NS21*, which lead to a higher amount of ODTD according to HPLC analysis. The endo cleavage of the $RoxB_{NS21}$ allowed the $RoxA_{NS21}$ to find the respective chain ends with higher probability.[130]

Latex clearing proteins that have been characterized in depth can be derived from *Streptomyces sp. K30*,[119] *Gordonia polyisprenivorans VH2,*[131] *Rhodococcus rhodochrous RPK1*[132] and *Nocardia nova SH22a*.[133] Lcps have molecular masses ranging from 40 to 46 kDa. Lcps are not related in amino acid sequence to RoxAs or RoxBs.[112] In contrast to RoxAs and RoxBs that are c-type diheme proteins, Lcps harbor only one, non-covalently bound b-type heme cofactor as the active site.[134] B-type hemes have a bis-histidine coordination site, where the iron atom is coordinated by two histidine residues. Lcps cleave the polyene backbone in an endo-type fashion. Lcp_{SH22a} was shown to have been responsible for the degradation of 1,4-*trans*-PI by *Nocardia nova SH22a*.[135, 136, 133] It was also reported to have been active towards the 1,4-*trans* and the 1,4-*cis*-isomeric motifs and its degradation process of *trans*-PI was deemed very similar to that of *cis*-PI.[133] However, it appeared that the degradation mechanism is dependent on more enzymes in the overall metabolic pathway in *Nocardia nova SH22a*.[135] For Lcp_{1VH2} distinctive degradation products were isolated but the degradation process was nonetheless determined to be a endo-type PI chain scission.[137] The effect of rubber additives onto the enzymatic degradation of Lcp_{1VH2} was investigated. It revealed that antioxidants interfered the most with either microbial or enzymatic rubber degradation. But it showed that degradation by Lcp_{1VH2} was much more resistant and less sensitive towards the investigated rubber additives, such as plasticisers and retarders, in comparison to an *in vivo* approach. Consequently, an enzymatic process was deemed to be a more promising method to enhance rubber degradation.[8]

The best characterized Lcp is the Lcp_{K30}. The X-ray crystal structure of the enzyme was determined and revealed for Lcp_{K30} that the heme is coordinated by a proximal histidine and a lysine as a distal axial ligand with the majority, 63%, of the Lcp_{K30} protein exhibiting an α-helical structure while the other 37% consist of connecting loops. EPR measurements showed two distinguishable heme species for the enzyme, which corresponds to the effect that Lcp_{K30} was present in two conformations in solution. One conformation as the closed state of Lcp_{K30} in which the heme cofactor has two axial ligands and produces a low spin signal and another open state were the heme iron is free at the axial position, which leads to a high spin signal.[138] Domains for activity have also been investigated by mutations, which provided preliminary insight into possible protein engineering.[139] The degradation of NR had also already revealed an endo type degradation process in line with the other Lcps.[112] The mechanism of the cleavage of the double bond by Lcp_{K30} is still under investigation. Two different mechanistic pathways for the oxidative degradation have been described.[138] The oxygen binds to distal axial position of the heme iron and subsequently binds to the double bond of a polyisoprene-moiety (Scheme 6, (I), (II)). Two pathways are feasible: a heme bound oxygen could lead to an epoxidation and an oxo-ferryl intermediate, which is subsequently cleaved by the nucleophilic attack of the oxo-ferryl intermediate (Scheme 6, (III)). The pathway with the oxygen bound in an open state of Lcp_{K30} forming an instable cyclic dioxetane intermediate that spontaneously rearranges into the cleavage products was deemed more favorable in molecular dynamic simulations and leads to the formation of an aldehyde and ketone (Scheme 6, (IV), (V)).[140] Recent investigations into the docking of a 1,4-*cis*-PI with 12 repetitive units indicated two dominant substrate tunnels that provided feasible routes for substrate binding, and the presence of two hydrophobic pockets was predicted near the heme cofactor, which could have an effect onto the degradation capabilities.[141] It was even shown that Lcp_{K30} could cleave double bonds in UV-pretreated polyolefins.[142]

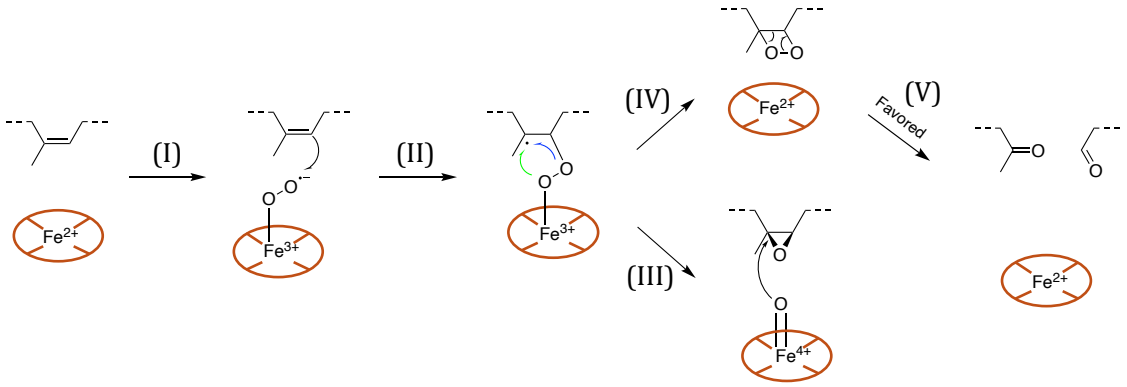

Scheme 6. Hypothetical mechanism of the Lcp_{K30}-catalyzed cleavage of 1,4-*cis*-PI. Redrawn from [140]

An alternative to the usage of rubber oxygenases for the rubber degradation are enzyme-mediator systems. Those systems promote the scission of the polyene chain by a radical β-scission mechanism. First, the enzymes promote the radical formation on the mediator molecules, which then successively generate radicals at the PI chains that lead to a subsequent cleavage.[123] The oxidative degradation of 1,4-*cis*- and 1,4-*trans*-PIs was reported by two types of enzyme-mediator systems, lipoxygenase with linoleic acid and horseradish peroxidase with 1-hydroxybenzotriazole in aqueous media.[143] Manganese peroxidase with manganese(III) was also reported to have led to a degradation of 1,4-cis-PIs.[144] Similarly, the reaction of 1,4-*trans*-PI by laccase with 1-hydroxybenzotriazole and linoleic acid was reported to have led to degradation. For PBs the degradation with horseradish peroxidase with 1-hydroxybenzotriazole was only effective for high 1,4-*cis*-PBs and mixtures of the 1,4-*trans* and 1,4-*cis* isomeric motifs but not for the pure 1,4-*trans*-PB.

1.4.2 Polyisoprene degradation determination of enzymes and microorganisms

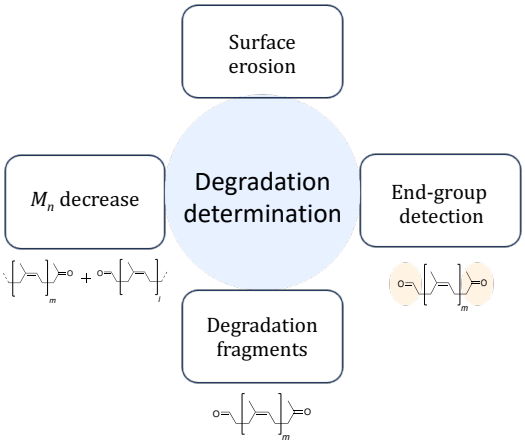

Figure 5. Degradation determination by different approaches: Surface erosion (e. g. SEM, IR), End-group detection (e. g. Schiff reagent, DNPH), M_n decrease (e. g. GPC), Degradation fragment detection (e. g. HPLC, UHPLC, ESI-TOF-MS, NMR).

As the initial activity determination, the detection of weight loss has been used commonly for microorganisms. It shows that the microorganism can use the respective polyene as a carbon source and as feeding medium for the respective cells. Weight loss is determined gravimetrically before and after the rubber transformation experiment.[145] But the specific detection of rubber degradation of microorganisms and enzymes has been conducted with different methodologies in particular surface erosion, end-group detection, M_n decrease and degradation fragment determination (Figure 5).

The decomposition of rubber surfaces by microorganisms or enzymes can be detected by changes in the surface morphology. Scanning electron microscopy (SEM) produces images by scanning the surface of samples with a focused beam of electrons. The electrons interact with atoms in the sample, producing signals that contain information about the surface topography and composition of the respective sample.[146] This allows in the case of rubber degradation for the detection of structural changes of samples subjected to microorganisms or enzymes and their corresponding negative controls.[147] SEM analysis can also provide insights into the respective colonization behavior and biofilm formation with microorganisms.[148] Alternatively, Fourier transform infrared spectroscopy (FT-IR) has found broad applicability in the investigation of degradative activity. The oxidative degradation of rubber leads to the formation of characteristic C=O stretching bands in the region of 1600 to 1750 cm^{-1} corresponding to the carbonyl function.[115] Characteristic bands of the PI backbone for CH_3 rock, CH_3 deformation, C=C stretch, CH_2 asymmetric stretch and the CH_3 asymmetric stretch[149] can be normalized and related to the occurrence of oxidative degradation.[150,113]

Investigations beyond the surface require extraction methodologies for the reactions in aqueous media of enzymes and microorganisms. Herein, liquid-liquid extractions are frequently used to transfer organic compounds between two immiscible solvents, generally an aqueous phase and an organic phase. Diethyl ether,[137] pentane,[114] chloroform[151] and the most commonly used ethyl acetate[152, 132, 118] are the solvents of choice for the isolation of degradation products of enzymatic and microorganismal PI degradation.

For the detection of carbonyl functionalities in PI degradation extracts and agar plates two staining agents have been implemented, Schiff's reagent and dinitrophenyl hydrazine (DNPH). Schiff reagent has been used since its invention by Schiff for the detection of aldehyde functionalities.[153] The Schiff reagent is the reaction product of a dye formulation such as fuchsin and sodium bisulfite or sulfurous acid.[154] It leads to a color shift of the chromophore from colorless to colorful by the formation of a conjugated π-system. This has been applied to enzyme and microorganism degraded samples to detect the aldehyde functionality.[155] DNPH has been used for its acid catalyzed reaction with carbonyl compounds forming hydrazones as an analytical tool for a long time.[156, 157] For rubber degraded samples DNPH has been used mainly as a derivatization agent for the detection of carbonyl functionalities *via* the UV shift of the respective hydrazone.[117]

GPC allows for the separation of the polyene and its respective degradation products according to their elution behavior and entropic interaction with the GPC-column.[158, 159] External standard calibration enables the determination of the number average molar mass und polydispersity. Polymeric degradation products that have been isolated from the degradation of enzymes and microorganisms are commonly investigated by GPC.[119, 148] It was reported that the results in GPC could vary depending of the extraction procedure because of the solubility of the degradation fragments.[160]

High performance liquid chromatography (HPLC) was used extensively in the determination of the degradation products of the enzymatic degradation of NRs.[161] It revealed the differences between the exo-type degradation of RoxAs and the endo-type degradation of RoxBs and Lcps.[129] The efficiency of the separation of complex mixtures allowed for the determination of the oligoisoprenoidic degradation products of these enzymes with the combination of mass spectrometry (MS).[112] HPLC-MS allowed for the assignment of the respective HPLC peaks to the mass to charge ratio of the respective degradation products. Mass spectrometry was also utilized independently from HPLC for the determination of degradation products from extracts.[162] Derivatization with Girard Reagent T was reported to have led to better peak detection, because the hydrazone derivate has a quaternary ammonium moiety, which facilitates the detection of the resulting derivate by positive-ion ESI-MS.[163]

1.5 Surfactant-free emulsification

Enzymatic degradation of rubber oxygenases is commonly conducted in water or potassium phosphate buffers.[112] This is primarily because most of the previous research has focused on the enzymatic degradation of 1,4-*cis*-PI, particularly in the form of natural latex milk. This latex milk is a white colloidal suspension, mainly composed of rubber and non-rubber particles, which is solubilized in water.[15] To mimic such a system with synthetic polyenes, different emulsification strategies could be feasible. Emulsions are defined as two immiscible liquids, where one liquid is dispersed in the other.[164] The large interfacial energy can make emulsions thermodynamically unstable but the usage of surfactants can counteract the droplet coalescence, the process of two or more droplets merging.[165] Surfactants are generally amphiphilic molecules that can stabilize the interface of the immiscible liquids. However, surfactants could denature enzymes, because they could disrupt the enzyme's tertiary structure and interfere with its active site through interactions with hydrophobic regions.

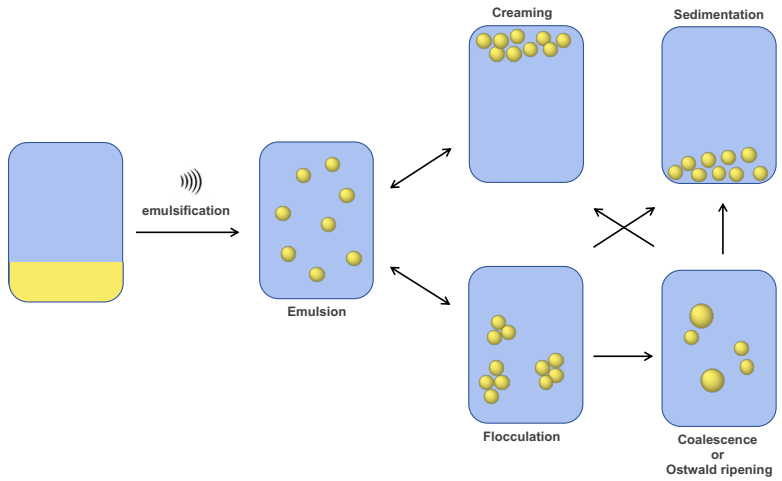

Figure 6. Illustration of the emulsion destabilization mechanisms prior to phase separation.

Emulsions of oil in water as meta stable systems can break down over time because of a variety of physicochemical processes. Gravitational force can cause droplets to migrate either to the top of the mixture, creaming, or to the bottom of the mixture, sedimentation (Figure 6).[166] The rate of creaming can also be related to the viscous properties of the emulsion.[167] Flocculation is a process where droplets aggregate because of the formation of hydrogen bonds or Van der Waals forces between the droplets. Flocculation leads to stronger creaming or sedimentation of the dispersed phase and promotes coalescence, as the droplets are brought closer together.[168] Ostwald ripening describes the process whereby larger droplets grow at the expense of smaller ones.[169]

Surfactant-free emulsions are commonly oil in water emulsions in the absence of any stabilizing agents.[170] Energy input is usually required to create oil in water droplets. This can for example be achieved by ultrasonication, sonication and high-speed homogenizing.[166] Ultrasonication refers to the irradiation of liquid sample with ultrasonic waves, 20-100 kHz, resulting in agitation of the sample.[171] The sound waves can propagate into the liquid media resulting in alternating high-pressure, compression, and low-pressure, rarefaction, cycles. During rarefaction, high-intensity sonic waves can create small vacuum bubbles or voids in the liquid. The cavitation of those bubbles can disrupt the oil water interface forming emulsions in the process,[172] with forces strong enough to lead to sonolysis and radical formation.

Emulsions of oils in water prepared by sonication can be stable for prolonged times.[173] Hydroxide ions seem to stabilize the oil and water interface,[174] dependent on the pH the stability can therefore be influenced.[175] The colloidal stability of surfactant-free oil droplets in water correlated to the chain length of alkanes, in comparison of *n*-hexane, *n*-octane, *n*-decane, *n*-dodecane, *n*-tetradecane and *n*-

hexadecane. The higher solubility of oil in water enhances the Ostwald ripening. Consequently oil droplets composed of shorter hydrocarbon grew easier through Ostwald ripening due to higher solubility.[176] Addition of *n*-hexadecane to *n*-hexane and water emulsion even with surfactant seemed to have led to an increase in stability because of the decrease in vapor pressure or solubility.[177] This also held true for surfactant-free emulsions, here *n*-hexadecane stabilized tetralin and water emulsions prepared with sonication baths for prolonged times even in molar fractions of 1 to 1000.[178]

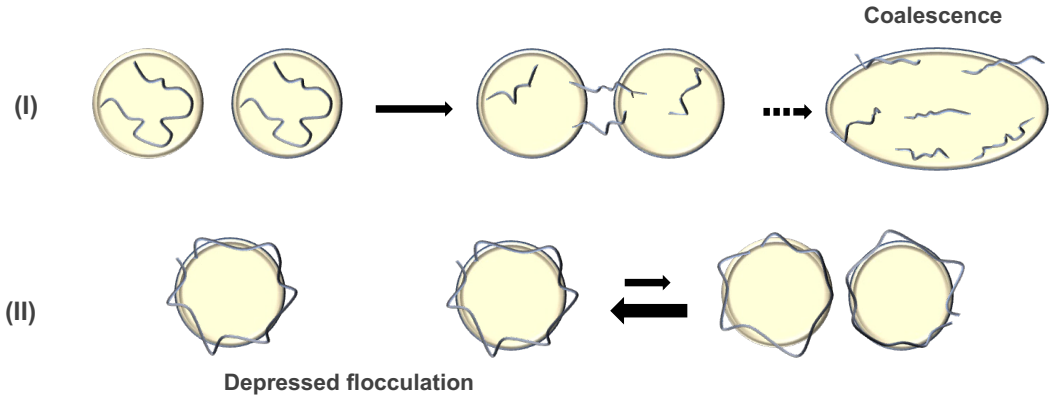

Figure 7. Coalescing effect of addition of polymer onto emulsions (I); proposed emulsion stabilization effect and depressed flocculation by addition of polymer in surfactant-free emulsions due to the formation of repellent emulsion polymer droplets (II).

This seemed to have inspired the idea of adding polymers to oil in water mixtures to investigate their stability. For polymers the entropic loss should also be lower upon mixing than smaller molecules. Polystyrene and benzene solutions in polymer and oil weight ratios of 1 to 10 remained stable up to one year in water in comparison to benzene and water emulsions, which remained stable for one day.[179] Figure 7 demonstrates the two counteracting mechanisms. The solvated polymer can either lead to accelerated flocculation and subsequent coalescence or to a flocculation suppression by surface modification of the respective oil droplets. This was hypothesized because of the increase in zeta potential for the mixtures of hydrophobic polystyrene and benzene in water.[179] Zeta potential is defined as the potential at the slipping and shear plane of a colloid particle or droplet moving under an electric field.[180] It can be correlated to the stability of emulsions in water[181] and is reported to be in the range of 30-50 mV for surfactant-free emulsions.[170] The other used analysis methodology dynamic light scattering measurements (DLS) can reveal the hydrodynamic radius of individual emulsion droplets or particles according to the fluctuation of scattering dependent of the Brownian motion of the emulsion droplets or particles.[182] Alternatively to hydrophobic polymer addition, tandem sonication can lead to prolonged stabilization of surfactant-free emulsions. Sequential radiation with ultrasonic, 40 kHz, ultrasound, 200 kHz, and megasound, 1 MHz, led to the stabilization of surfactant-free oleic acid in water emulsions.[183] The effect of megasound is more pronounced on submicrometer particles, which leads to a reduction of submicrometer droplets and less polydisperse and more stable emulsions.[184] The stability of surfactant-free oil in water emulsions relies on temperature dependent interaction between the intrinsic surface tension of oil and water.[185]

1.6 Protein engineering by directed evolution

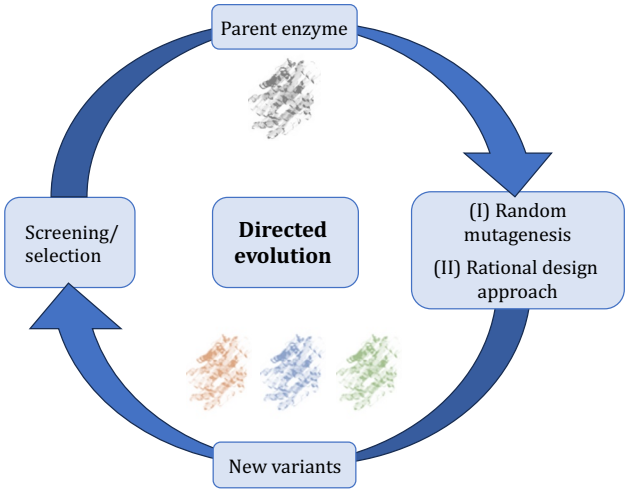

Figure 8. Conceptional approach for directed evolution. Random mutagenesis approach (I) or rational design approach (II), e.g. Protein Repair One Stop Shop (PROSS), leading to creation of new variants and the screening of new activity for the selection of a new round of engineering.

The biotransformation of PI in multiphase enzymatic reactors, aimed at the continuous extraction of oligo-isoprenoid molecules,[186] could benefit greatly from more robust Lcp-variants. This methodology together with a more effective, distinctively solvent-stable and kinetically longer enzymatically active variant could have a positive effect onto sustainable polyene degradation, especially in regards to circular polymer chemistry.[11] Surfactant-free emulsifications could allow for the presentation of the polyene without the need of protein destabilizing surfactants. Capabilities and natural properties of enzymes can be enhanced by protein engineering.[187] Directed evolution approaches intend to solve the optimization of proteins and enzymes through evolutionary pressure, with mutations gradually improving a protein towards the intended function by iterative testing (Figure 8).[188] To this end, random mutant libraries of proteins can be prepared by exploiting error prone DNA-polymerase to mutate genomic sequences for amino acid substitution.[189] Alternatively, DNA-shuffling methods can utilize DNA segments of different variants to create functional chimeric proteins to improve catalytic abilities.[190, 188] However, the stochastic nature of these random approaches can limit this method if the variants cannot be screened very efficiently by high-throughput.

In semi-rational design previous knowledge and understanding of the mechanism of the respective catalysed reaction by the enzyme is used to investigate novel protein features.[191] Site specific saturation mutagenesis can be utilized to determine the respective additive effects.[192] An example for the effect of semi rational protein engineering design are the polyethylene terephthalate degrading enzymes derived from leaf-branch compost cutinase (LCC).[193] Based on the X-ray crystal structure and molecular docking, site specific saturations were utilized to create a library of engineered variants and the most effective and thermostable variant, the LCC^{ICCG} was determined.[194]

Rational design approaches are targeted mutations based on computing algorithms enabling improvement of protein characteristics.[195] Protein Repair One Stop Shop (PROSS) is an algorithm aiming at improved expression and stability of proteins.[196] Increased solvent tolerance and thermostability can be beneficiary for reaction velocity at elevated reaction temperatures. Calculations with the PROSS algorithm are based firstly on a phylogenetic step that is targeted at identifying homologs of the protein under investigation and identifying positions of amino acids that are seldom in the homologues. This is based on the hypothesis that a rarer occurrence correlates to an evolutionary disadvantage, for example in the form of destabilising effects on the protein.[197] In silico the mutations which are more pronounced in homologs are tested for detrimental effects in regards

to the X-ray crystal structure. The most promising variants are individually calculated and energy calculations are performed for these combinations using the Rosetta model.[198]
Alternatively, the FuncLib Algorithm aims to increase the efficiency of choosing combinations of active site mutations in enzymes to create a small set of stable, efficient, and functionally diverse multipoint active-site mutants suitable for low-throughput experimental testing.[199] FuncLib calculation use rationally selected positions in the active site for mutation and check for non-additive effects by clustering and ranking the stability according to the Rosetta model.[199]
The drawback to these rational enzyme engineering approaches is that they require a diverse set of homologs as input for the phylogenetic analysis.[200] But due to the presence and investigations into rubber degrading bacteria a diverse set of homologs can be found for Lcps.

1.7 Single chain nano particles as artificial enzymes

Enzymes are highly evolved natural nano entities that are able to leverage self-confinement for catalysis. They consist of specific polypeptide chains forming precise tertiary 3D structures by intramolecular interactions such as hydrophobic interactions, hydrogen bonding, disulfide bridges, with catalytically active sites. A similar self-confinement effect arising from the folding of individual synthetic polymer chains can be employed for the construction of a type of enzyme-mimetic called single-chain nanoparticles (SCNPs).[201]
SCNPs are polymeric nanostructures with internal cross-linkages that are formed from an intramolecularly collapsed single polymer chain.[202] Remarkably, the imperfect folding of a unimolecular synthetic chain into a functional soft nano-object resembles, to some extent, the folding of a protein into its native and, more importantly, functional state.[203]
Synthetic strategies to prepare the SCNPs with the capability to form catalytic pockets are derived from different polymeric architectures. Here in, the polymer backbone can govern the structure of the embedded functionalities. Functionality can be incorporated into the structure of the polymer backbone by the selection of monomers in different copolymer compositions or by external cross-linkage.[201] Amphiphilic copolymers can self-fold dependent on their solvophilicity. Various polymers have found broad application such as (meth)acrylates,[204, 205] styrene derivatives[206] and norborene-derivatives.[207] The preparation of high molecular weight polymers with low polydispersity allows for the preparation of SCNPs of uniform size and properties.

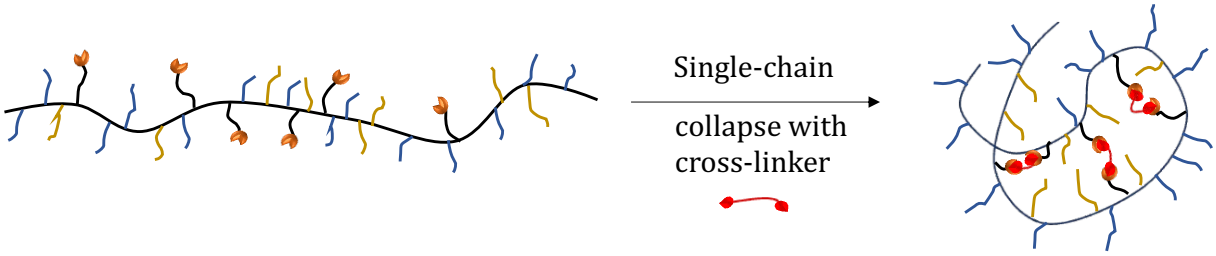

Figure 9. Random copolymer with hydrophilic (blue) and hydrophobic (brown) moieties collapsing into a single chain nano particle by cross-linkage with an external cross-linker (red).

SCNPs are synthesized by single-chain collapse at very high dilutions to exclusively achieve intramolecular cross-linkages of the respective individual chains and to prevent intermolecular interactions.[208] The folding of the SCNPs can be performed with different approaches dependent on the polymer backbone. Homofunctional chain collapse implies the formation of the nano particle by a copolymer with reactive self-complementary groups, such as thiols for disulfide bridges.[209] Heterofunctional chain collapse is the formation of the SCNP by two supplementary folding motifs, such as an diene and a dieneophile for a Diels Alder reaction.[210] External crosslinkers mediated collapse, which is the addition of a cooperative cross-linker for functional groups of the polymer backbone, for example the formation of amides by a diamine cross-linker (Figure 9).[211]

The folding strategies of SCNPs can be categorized in dynamic and covalent folding strategies. Dynamic folding strategies require strong supramolecular or non-covalent interactions for the formation of stable SCNPs. Hydrogen bonding motifs like 2-ureidopyrimidinone,[212] which can dimerize, or benzene-1,3,5-tricarboxamide with the ability to form helical assemblies *via* hydrogen bonding have been utilized for the preparation of SCNPs.[213] SCNPS can fold during the single-chain collapse into core-shell like structures with compartmentalized pockets.

Table 5. Examples of catalytically active entities incorporated into SCNPs with their corresponding folding strategy as well as catalyzed reaction.

Catalytic entities	Folding strategy	Catalytic reaction	Ref
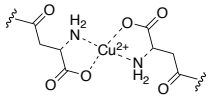	Complexation	Copper catalyzed azide alkyne cycloaddition	[205]
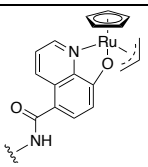	Helical self-assembly	Allyl carbamate cleavage	[214]
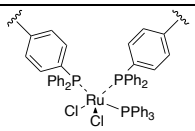	Complexation	Oxidation of alcohols	[215]
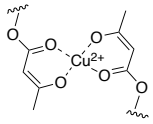	Complexation	Oxidative coupling of terminal acetylene	[216]
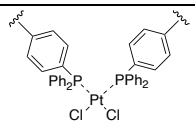	Complexation	Amination of allyl alcohol	[217]
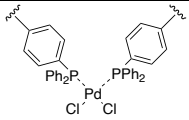	Complexation	Sonogashira coupling	[218]
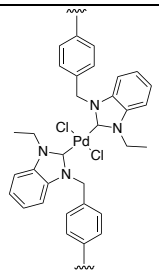	Complexation	Suzuki coupling	[219]
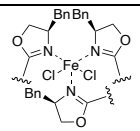	Complexation	Sulfa Michael addition	[220]
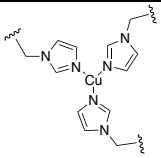	Complexation	Hydroxylation of phenol	[221]
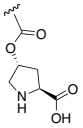	Helical self-assembly	Aldol reaction	[222]

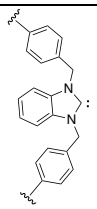	Self-quaternization	Benzoin condensation	[223]

This folding of a linear chain *via* intramolecular crosslinking into an SCNP can give rise to the formation of local domains within the nanoparticle, which when decorated with catalytic moieties can afford catalytic pockets.[224] The retardation of water in those catalytic hydrophobic pockets of SCNPS could be crucial for catalytic activity.[225] In the case of the organocatalytic L-proline bearing SCNPs, the aldol reaction of cyclo-hexanone and *p*-nitrobenzaldehyd was only functional in the folded conformation of the SNCP (Table 5).[222] Copper complexation into SCNPs has enabled the catalysis of the CuAAC-click reaction,[205] and the hydroxylation of phenol (Table 5).[221] Catalytic SCNPs can combine the benefits of both homogeneous and heterogeneous catalysts such as homogeneous reaction conditions, improved recyclability, high activity, and potentially high substrate specificity.[224] The amination of allyl alcohol was conducted with Pt(II)-SCNPs under homogenous conditions, but change of the solvent allowed for the isolation of the SCNP and the reutilization for further catalytic cycles (Table 5).[217] The aspect of lower required catalytic loading has been shown in the case of an oxidative coupling of terminal acetylene, but the shift towards unprecedented substrate specificity by the incorporation of catalytic moieties into a SCNP was remarkable (Table 5).[216]

2. Aim and concept

2.1 Aim

The aim of the thesis is to investigate the modification and degradation of polyenes by chemical and enzymatic methodologies. In the first part of the thesis, enzymatic degradation of polyenes and their degradation fragments with surfactant-free emulsification is investigated. The interdisciplinary project should establish enzymatic degradation approaches for the wildtype Lcp_{K30} with synthetic polyisoprenes and polybutadienes and implement polymeric degradation tracking possibilities for the Lcp_{K30} wildtype and protein-engineered variants.

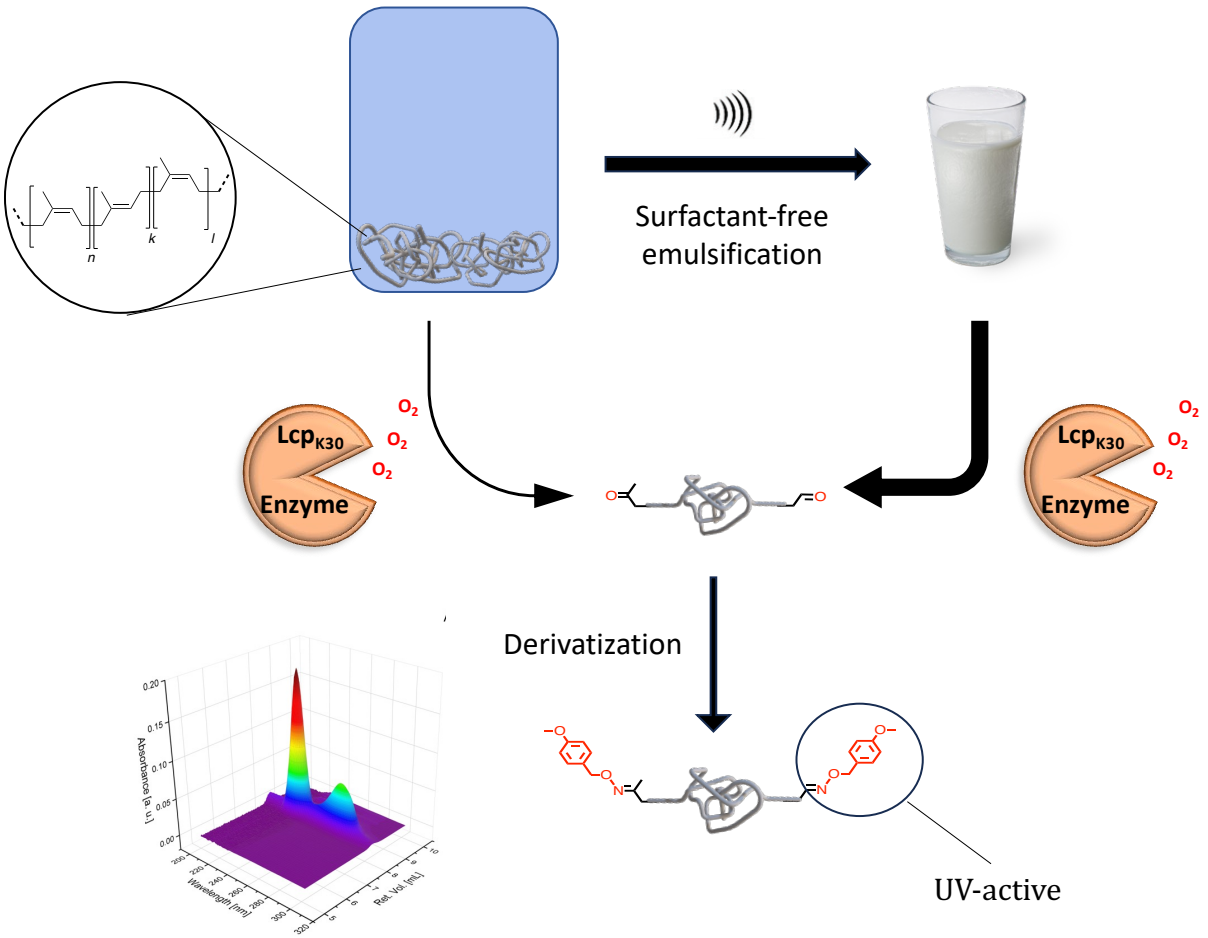

Figure 10. Surfactant-free emulsification by sonication for increased enzymatic degradation. Degradation fragmentation derivatization for an improved tracking of degradation activity by UV with GPC.

Controlled and sustainable recycling of PI and PB remains challenging due to the absence of hydrolysable functional groups in their polymer backbones. Nature has evolved an enzyme family dedicated to the degradation of PI, rubber oxygenases. Nevertheless, there remains a significant knowledge gap regarding the degradation of SPIs. Specifically, the enzymatic degradation of SPI with a 1,4-*cis*: *trans*-ratio below 97% has not yet been addressed. It is hypothesized that the major challenge to achieving efficient enzymatic degradation of SPI lies in its presentation in aqueous media. The poor solubility of the polymer in water substantially limits the available interface for enzymatic degradation (Figure 10). Furthermore, the enzymatic degradation of PBs has not been reported yet. Consequently, the investigation into methodologies for the enzymatic degradation of synthetic polyenes with rubber oxygenases is of great interest. Rational protein engineering methodologies could allow for the

modification of PI degrading enzymes to PB degrading enzymes. For the detection of low activity over a broad spectrum of molecular weights, new degradation tracking methodologies are required. More thermostable variants of the Lcp_{K30} could allow for better solvent stability and adaptability of degradation methodologies. Macromolecular degradation analysis with HPLC, UHPLC, ESI-TOF-MS, UHPLC-ESI-TOF-MS, NMR methodologies, and GPC could provide new insight into the acceptance of isomeric motifs of the wild type Lcp_{K30} as well as the activity of protein engineered variants after thermal stress or their promiscuous degradation capabilities towards PB.
In the second part of the thesis, the incorporation of cyclopropanating functionalities in novel artificial enzymatic single chain nano particles is investigated. Those catalytically active entities could allow for the remediation of polyene wastes by post-modification approaches and chemical modifications of oligoenes. The formation of the SCNPs is investigated by the reduction in hydrodynamic diameter or M_n by GPC, DLS and NMR spectroscopic methodologies.

2.2 Concept

(Partially published in 1. Adjedje, V. K. B.; Schell, E; Wolf, Y. L.; Laub. A; Weissenborn, M. J.; Binder, W. H. Enzymatic degradation of synthetic polyisoprenes *via* surfactant-free polymer emulsification, *Green Chem*. 2021, *23*, 9433-9438. DOI: https://doi.org/10.1039/D1GC03515K, 2. Adjedje, V. K. B.; Wolf, Y. L.; Weissenborn, M. J.; Binder, W. H. Rubber Oxygenase Degradation Assay by UV-Labeling and Gel Permeation Chromatography, *Macromol. Rapid Commun*. 2024, 2400032. DOI: https://doi.org/10.1002/marc.202400032)

(I) Surfactant-free emulsification of polyisoprene and polybutadiene

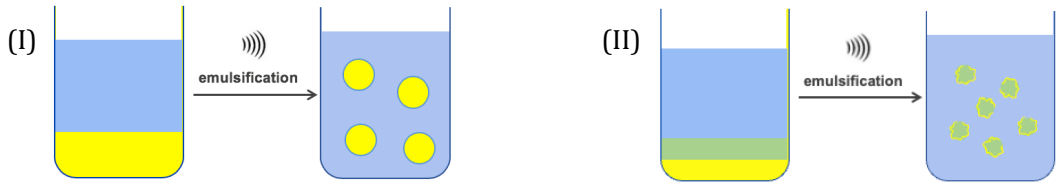

Figure 11. Acoustically induced emulsification of PI (yellow) by ultrasonic sonifier for the formation of metastable emulsion droplets (I). Co-solvent emulsification of polyenes by sonication and stabilization with a co-solvent (green) (II)

In previous research, the investigation of enzymatic degradation of rubber oxygenases was commonly conducted in KPi with latexmilk, as 1,4-*cis*-PI. For the investigation of polyenes without the natural suspension of latex milk, mainly composed of rubber and non-rubber particles, alternative surfactant-free approaches must be examined. Acoustical emulsification of oil in water emulsions can be achieved by the mechanical effects of power ultrasound due to cavitation. Moreover, the stability of oil in water emulsions can be influenced by the presence of hydrophobic polymers.[179] In this thesis surfactant-free emulsification approaches with acoustical emulsification with a sonifier and a co-solvent emulsification approach are investigated further for their capabilities of emulsifying synthetic polyenes (Figure 11). The emulsification parameters, in particular weight-per-volume-percentages and sonication details, are examined to obtain metastable emulsions stable enough for the enzymatic degradation duration of 24 hours. Stability of the so formed emulsions is tracked by DLS, transmittance studies and zeta potential. The emulsions are investigated for their stability in ultrapure water and the KPi optimum of the respective rubber oxygenase. The transferability of the co-solvent emulsification to polybutadiene as well as the stability at different temperatures are examined for the investigation of PB-degrading enzymatic activity.

(II) Enzymatic degradation studies of polyisoprene with wildtype Lcp_{K30} and protein engineered variants

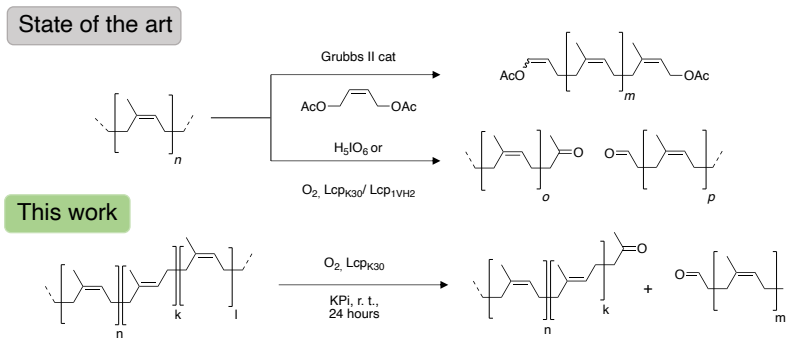

Scheme 7. Previous efforts of degrading 1,4-*cis*-PIs. Expansion of the enzymatic degradation scope to SPIs with significant 1,4-*trans*-ratios by surfactant-free emulsification.

After establishing the optimized emulsification parameters, the emulsification influence on the formation of degradation fragments by the increased available surface for enzymatic degradation in comparison to non-emulsified polyisoprene is investigated (Scheme 7). The influence of co-solvents onto the enzymatic degradation capabilities of the rubber oxygenase Lcp_{K30} is determined to ensure that the enzyme remained active in the presence of the respective solvents. Determination of the degradation is conducted according to the oligoisoprenoidic degradation fragments with HPLC or UHPLC methodologies and mass spectrometry. Optimization of the degradation parameters for the emulsified samples lead to insights into the acceptance of non-1,4-*cis* isomeric motifs by the rubber oxygenase Lcp_{K30}. Correlation of the degradation fragments to the mass-to-charge ratio allow for the determination of the degraded species. The comparative MS/MS fragmentation experiments of the degradation fragments of synthetic polyisoprene and latex milk provide further insights.

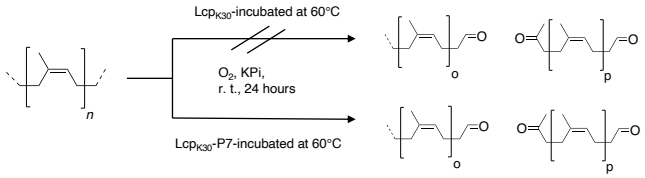

Scheme 8. Incubation of protein engineered variants at characterized thermostability temperatures and subsequent degradation of latex milk.

The protein engineering of the rubber oxygenase is expected to lead to an increase in the thermostability. Characterization of the Lcp_{K30}-variants enables the investigation of the reactivity of the enzyme towards latex milk after incubation at elevated temperatures without the loss of enzymatic degradation activity (Scheme 8).

(III) Rubber oxygenase degradation tracking *via* GPC-UV

For the detection of enzymatic degradation with a background of unreacted polymer above the detection limits of MS new degradation tracking is required. Chemical degradation of polyenes with mCPBA and periodic acid is conducted to establish the derivatization with *O*-(4-methoxybenzyl)-hydroxylamine hydrochloride (Scheme 9). The derivatization allows for the tracking of the degradation by UV detection with GPC at the wavelength of the absorption of the derivatized chemically and enzymatically degraded polyenes. This methodology is applied for detection of PB degradation with protein engineered rubber oxygenase variants in addition to UHPLC-ESI-MS measurements. Providing further insights into the degradation product formation beyond the detection of solely oligoisoprenoidic degradation fragments.

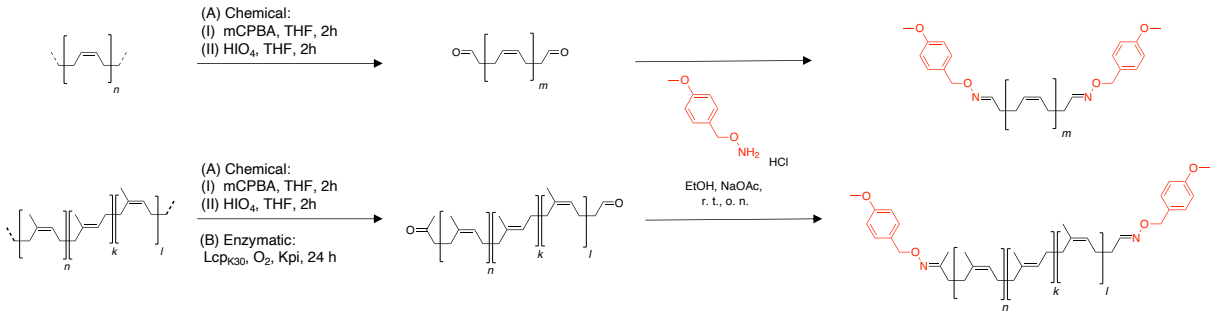

Scheme 9. Chemical and enzymatic degradation of PI and PB and subsequent establishment of derivatization strategy for rubber oxygenase degradation assay *via* GPC-UV.

(IV) Artificial enzymatic catalyst design with cyclopropanating functionalities

Post-modification of polyenes can allow for the remediation of waste materials. Herein, recyclable catalyst with the capability of conducting reactions in aqueous media could be beneficial. Cyclopropanation of squalene and the investigation into the regioselectivity could allow for insight into the selective modification of polyenes. Incorporation of cyclopropanating catalysts into a macromolecular structure as artificial enzymes could be achieved as single chain nano particles. For the formation of SCNPs different collapse and synthetic strategies are implemented.

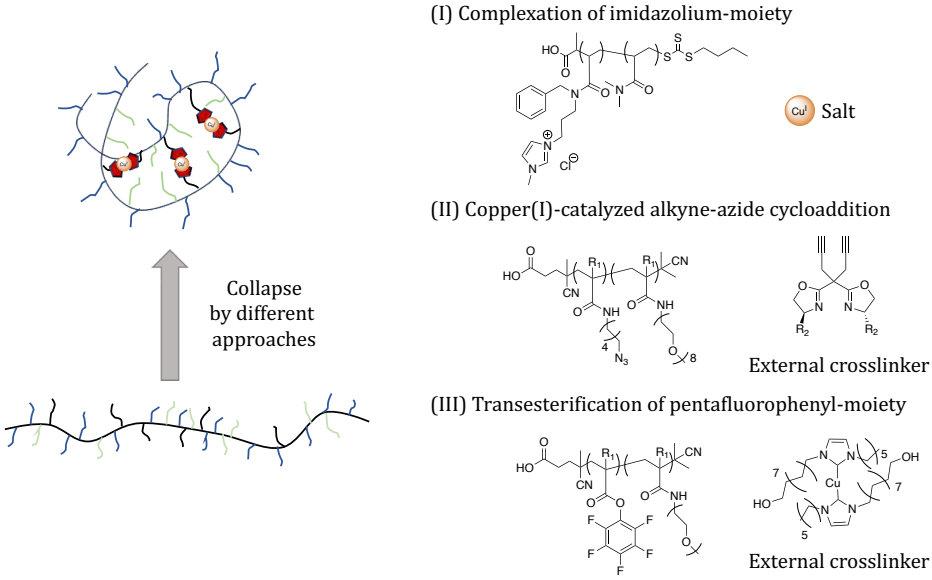

Figure 12. Preparation approaches of SCNP with cyclopropanating functionalities by complexation of a copper salt (I), copper catalysed alkyne-azide cycloaddition reaction with a cross-linker (II) and transesterification of pentafluorophenyl-moieties (III). R_1= CH_3 or H, R_2= *t*-Butyl or Phenyl.

Syntheses of monomers with functional imidazolium moieties for copolymerization with a hydrophilic monomer are conducted. Folding could be achieved by the complexation with a copper salt resulting in bis-(*N*-heterocyclic carbene) copper complexes (bis-NHC-Cu) containing SCNPs. Alternatively, the folding of SCNP with external crosslinkers is investigated. An amphiphilic polymer with azide functionalities is examined for collapse by a cross-linker with bisoxazoline moieties to incorporate the cyclopropanating functionality externally. Transesterification of pentafluorophenyl with bis-NHC-Cu complexes is also investigated as an approach to incorporate an external crosslinker for the formation of SCNPs (Figure 12).

3. Result and Discussion

Parts of the Results and Discussion as well as the Experimental Section were already published in

1. Adjedje, V. K. B.; Schell, E; Wolf, Y. L.; Laub. A; Weissenborn, M. J.; Binder, W. H. Enzymatic degradation of synthetic polyisoprenes *via* surfactant-free polymer emulsification, *Green Chem*. **2021**, *23*, 9433-9438. DOI: https://doi.org/10.1039/D1GC03515K

2. Adjedje, V. K. B.; Wolf, Y. L.; Weissenborn, M. J.; Binder, W. H. Rubber Oxygenase Degradation Assay by UV-Labeling and Gel Permeation Chromatography, *Macromol*. *Rapid Commun*. **2024**, 2400032. DOI: https://doi.org/10.1002/marc.202400032

and were in parts adapted with permission from the Royal Society of Chemistry ©2021 and John Wiley and Sons. Inc. ©2024

3.1 Surfactant-free emulsification of polyisoprene and polybutadiene

Water or potassium phosphate buffers are commonly used as the solvent for the enzymatic degradation of rubber oxygenases.[112] This is primarily because most of the previous research has focused on the enzymatic degradation of 1,4-*cis*-PI, particularly in the form of natural latex milk. This is a white colloidal suspension, mainly composed of rubber and non-rubber particles solubilized in water.[15] It was hypothesized that the major challenge in achieving efficient enzymatic degradation of synthetic polyenes lies in their presentation in aqueous media. The poor solubility of these polymers in water substantially reduces the available interface for biodegradation. One strategy to remedy this problem could be the application of surfactants, which reduce the surface tension between immiscible phases and act as emulsifiers. However, surfactant could denature enzymes, because they could disrupt the enzyme's tertiary structure and interfere with its active site through interactions with hydrophobic regions.[152] An alternative strategy is the surfactant-free emulsification. Different emulsification approaches were tested to achieve a surfactant-free emulsion of polymer and water either aided by a co-solvent or solely by acoustic emulsification. The influence of co-solvents onto the enzymatic degradation capabilities of the rubber oxygenase Lcp_{K30} had not been investigated and therefore the concentration of the co-solvents was kept as low as possible (chapter 3.2). A comparison of a non-emulsified, an acoustically emulsified and a co-solvent emulsified system was deemed crucial to understand the effect of the different approaches. Comparing these three approaches provides insight into the effect of the co-solvent onto the degradation in comparison to an approach without a co-solvent. The emulsions had to be investigated both for their stability in ultra-pure water and in the potassium phosphate buffer (KPi) optimum of the respective rubber oxygenases and their stability at temperatures deemed optimal for the enzymatic degradation of the respective enzyme. A metastable emulsion, which stayed stable for the enzymatic degradation time of 24 hours was the main objective. The preparation of a co-solvent emulsified system had to be established and the transferability of the system to PB investigated. The focus of the co-solvent emulsified system methodology transfer to PB was the stability in the KPi optimum for the wild type rubber oxygenase Lcp_{K30} as well as stability at different temperatures. Surfactant-free emulsification utilizes physicochemical processes, such as acoustical energy or co-solvents or a combination of both, to disperse immiscible substances such as polyenes into fine droplets suspended in a continuous phase such as water.[170]

3.1.1 General Procedure

Three SPIs (**PI 3000**, **PI 4500** and **PI 14000**), a PI derived from NR, 1,4-*cis*-PI (**PI *cis* 7000**) and two synthetic polybutadienes (**PB 3500** and **PB 12 000**) were examined in the scope of this study (Table 6). The microstructure of the SPIs were predominantly 1,4-regiosisomers at comparable *cis*: *trans* ratios. The remaining microstructure of the PIs consisted of 1,2- and 3,4-regisomers. These PIs (**PI 3000, PI 4500** and **PI 14000**) were selected for investigation due to their significant *trans* ratio, similar microstructures with different degrees of polymerization and their M_n, which correlates with the entanglement and intermolecular interactions in polymers. **PI *cis* 7000** was also included in the scope as an all-*cis*-PI isomer without the natural emulsion of latex milk as well as a polymer with broad polydispersity index. The synthetic polybutadienes were included to the scope to show the transferability of the established methodologies onto similar polymer structures at comparable M_n. For the establishment of the surfactant-free emulsification strategies the **PI 3000**, **PI 14000**, and **PI *cis* 7000** were investigated to determine the effect of M_n, microstructure and polydispersity onto the emulsification capabilities (Table 6).

Table 6. Polyisoprenes (PI) and polybutadienes (PB) investigated for their capability to form surfactant-free emulsions.

Samples	M_n [g/mol][a]	Đ[a]	Microstructure [%][b]			
			3,4-units	1,4-units *cis*	1,4-units *trans*	1,2 units
PI 3000	3100	1.1	16	56	27	1
PI 4500	4500	1.1	16	56	27	1
PI 14000	14000	1.1	16	55	28	1
PI *cis* 7000	7000	6.6	-	98	2	-
PB 3500	3500	2.0	-	75	24	1
PB 12000	11500	1.2	-	33	55	12

[a]= determined *via* GPC; [b]=determined by ^{1}H NMR

The range of investigated polymers was assessed for their stability as emulsions in water by different analytical methodologies. Visual inspection involved observing the emulsions over time to detect changes in appearance, such as phase separation, creaming, sedimentation, flocculation, and coalescence. This provides qualitative insights into emulsion stability and serves as an expedient initial screening tool. It was employed to establish the coarse parameters of emulsification for both the acoustical and the co-solvent based emulsification approaches during the preliminary analysis.
Samples and approaches that cleared the initial broad screening by visual inspection, were subjected to particle size analysis, a crucial step in evaluating emulsion stability. DLS was employed to determine the droplet size distribution within the emulsion. An increase in droplet size over time was indicative of droplet coalescence or destabilization, suggesting a loss of stability. Conversely, a decrease in transmittance and droplet size could indicate the occurrence of creaming.

3.1.2 Acoustically emulsified system

3.1.2.1 Preliminary experiments of acoustical emulsification

The first approach to obtain meta stable surfactant-free acoustically emulsified PI droplets in a continuous water medium was inspired by microemulsion polymerizations techniques. In microemulsion polymerization, monomer droplets are created and stabilized in a continuous phase, such as water, with the assistance of ultrasound sonication. But this process involves the usage of surfactants as stabilizers and osmotic pressure agents to counteract the Ostwald ripening.[226, 227]
Landfester and co-workers[24] synthesized PI nanoparticles using sodium dodecyl sulfate (SDS) as surfactant. The emulsions remained stable up to 2 years but the main drawbacks of surfactants are that they can denature enzymes and that they can have a negative environmental impact.[170] Nevertheless the conditions for acoustical emulsification of isoprene monomer droplets during microemulsion polymerizations were adopted as the initial framework for the establishment of a surfactant-free emulsification strategy without those drawbacks. This framework was used for a comprehensive exploration of parameters for the new emulsification strategy of PIs and for the investigation of the feasibility of dispersing polymers *via* ultrasonication without the presence of surfactants.
Dispersion and emulsification generally stem from the mechanical effects of power ultrasound due to cavitation. These effects encompass surface erosion, interface disruption, enhancement of mass transfer occurring near the interface, and are typically favored at lower frequencies.[166] Previous studies have reported the range of 20-50 kHz as the most efficient for these processes.[228] Ultrasound treatments for the acoustically emulsified system were executed using a VCX 500 ultrasonic processor equipped with a 3 mm micro tip. Cycles of pulsed ultrasound at varying frequency of 20 kHz were applied with different percentages of the maximum amplitude, following a sequence of 10 s pulse and 5 s pause.

Table 7. Preliminary acoustical emulsification of PI-polymers under various conditions.

Entry	Polymer	Polymer [w/v%]	Squalene [w/v%]	Hexadecane [w/v%]	SDS [w/v%]	Amplitude: Duration: Cycles	Stability
1	**PI *cis* 7000**	20				30: 5 min: 3	unstable
2	**PI *cis* 7000**	20		2		35: 5 min: 4	unstable
3	**PI *cis* 7000**	20			0.5	35: 5 min: 4	unstable
4	**PI *cis* 7000**	12				30: 1 min: 3	unstable
5	**PI *cis* 7000**	12		2.5	0.8	30: 1 min: 3	unstable
6	**PI *cis* 7000**	2	2			20: 30 min: 1	unstable
7	**PI *cis* 7000**	0.2				20: 30 min: 1	unstable
8	**PI *cis* 7000**	0.2				30: 1 h: 1	unstable
9	**PI 14000**	12				30: 1 min: 4	unstable
10	**PI 14000**	8				30: 1 min: 4	unstable
11	**PI 14000**	0.2	0.2			30: 1 h: 1	unstable
12	**PI 3000**	10	2			30: 1 h: 1	unstable
13	**PI 3000**	10		2		30: 1 h: 1	unstable
14	**PI 3000**	2	2			30: 1 h: 1	1 h
15	**PI 3000**	0.2				30: 1 h: 1	1 d

A collection of the experimental parameters for the preliminary acoustic emulsification is given in Table 7. The stability was defined as the time until phase separation became visible. To facilitate extensive sample screening with enzymes, a polymer stock solution was intended, therefore a weight per volume ratio (w/v%) of 20 was selected as a starting point for the acoustic emulsification establishment. Starting with two separated phases, ultrasound could be applied directly. However, as

the disruption of a planar interface demands a substantial amount of energy, a primary coarse emulsion was prepared and stirred before the application of acoustic power.[228]

PI *cis* 7000 was examined (entry 1 of Table 7) without the utilization of an osmotic pressure agent and surfactant; however, a visibly stable emulsion was not achieved. Neither the addition of an osmotic pressure agent, *n*-hexadecane in a weight ratio of 10-to-1, polymer to osmotic pressure agent (entry 2 of Table 7) nor the increase of amplitude led to a stable emulsion. The possibility of emulsifying the PI through the addition of a surfactant was explored but this did not yield significant improvement (entry 3 of Table 7). In entry 4, an attempt was made to reduce the weight per volume percentage along with a decrease in amplitude, and this was compared to entry 5, which employed a setup involving both an osmotic pressure agent as well as a surfactant. Both did not lead to a stable emulsion due to the high w/v%. Accordingly, the latter was decreased while simultaneously increasing the ratio of an osmotic pressure agent increased in order to counteract the Ostwald ripening more pronouncedly (entry 6 of Table 7). A further reduction of the w/v% was attempted, coupled with an increase in amplitude and the duration of sonication. However, in none of these cases a visual emulsion could be observed (entry 7 of Table 7).

The polydispersity of **PI *cis* 7000** was identified as a potential limiting factor in the acoustic emulsification attempts. These attempts appeared to partially emulsify the PI but never achieved to complete emulsification. This partial emulsification could have been possibly due to shorter polymer chains being emulsified, while longer polymer chains could have entangled due to more pronounced intermolecular interactions. To investigate this hypothesis, **PI 14000**, with a M_n of 14000 g/mol and low polydispersity according to GPC, was examined for acoustic emulsification. The parameters employed in entry 4 of Table 7 served as the initial basis for entry 9 of Table7, with the addition of an extra cycle of emulsification. However, the stability of the resulting emulsion was found to be negligible. A reduction of the w/v% to 8 at the same sonication parameters was attempted, but this did not yield substantial improvement for the emulsion formation (entry 10 of Table 7). Lower w/v% could lead to smaller droplet sizes in emulsions, which could translate to increased stability and enhanced homogenization. Smaller droplets should have a higher surface area-to-volume ratio, which in turn should make them less prone to coalescence or creaming.

Consequently, a significant reduction of w/v% to 0.2 was made in another attempt (entry 11 of Table 7), which corresponds to the PI loading in the standard procedure for the enzymatic degradation of latex milk by Lcp_{K30}.[139] In addition to this reduction, squalene was applied as an osmotic pressure agent, and the sonication time was increased. Nevertheless, this combination of adjustments did not result in a visually stable emulsion.

Considering the negative results for the various w/v% and sonication parameters examined up to that point, it became apparent that another system parameter might be a limiting factor in the acoustical emulsification approach. Accordingly, experiments with **PI 3000** with a decreased M_n were performed. The w/v% of 10 was examined with squalene (entry 12 of Table 7), and *n*-hexadecane (entry 13 of Table 7), using the sonication parameters employed in entry 11 for PI 14000. In both cases, stable emulsions were not achieved. A reduction in the w/v% to 2, accompanied by the addition of squalene as an osmotic pressure agent, resulted in the formation of a visual emulsion (entry 14 of Table 7). Further reduction of the w/v% to 0.2 resulted in an emulsion that remained turbid for up to one day (entry 15 of Table 7). This marked the first instance in which a PI had been emulsified acoustically *via* sonication for a duration of one day without the usage of a surfactant. Consequently, a more comprehensive investigation of the parameters dictating the emulsification process became of importance.

3.1.2.2 Surfactant-free acoustical emulsification

It became evident from the preliminary investigations that both the polydispersity, as observed for **PI *cis* 7000**, and polymer chain length, as exemplified by **PI 14000**, played pivotal roles in the acoustical emulsification. The acoustical emulsification of **PI 3000** led to the most promising results and was consequently investigated in more detail by dynamic light scattering to determine the stability of the so formed emulsions. To optimize the emulsification parameters, the KPi optimum concentration of 5 mM, as determined in chapter 3.2, was employed.
Sodium chloride has the capacity to bind water molecules tightly and to suppress cavity fluctuations, which can reinforce the hydrophobic effect and can promote the salting out of hydrophobic solvents, among other effects.[229] However, it should be noted that the impact of this phenomenon has not been determined for the KPi concentration under investigation. Nevertheless, it is reasonable to expect that such ionic salts could lead to similar effects, necessitating their consideration.

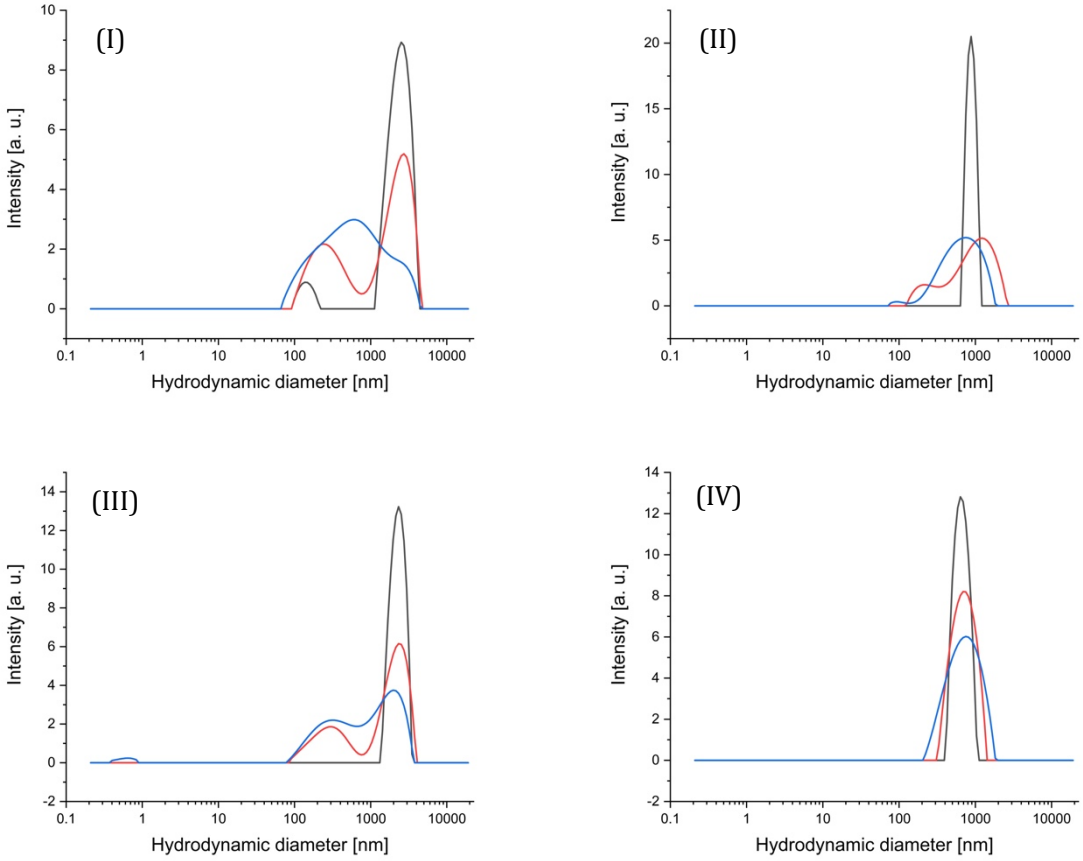

Figure 13. DLS measurements at different amplitudes and durations for **PI 3000** after preparation (black), after 30 minutes (red) and after 60 minutes (blue) for (I) 30 min, 20% amplitude, (II) 30 min, 30% amplitude, (III) 60 min, 20% amplitude, and (IV) 60 min, 30% amplitude.

The hydrodynamic diameter of acoustically emulsified PI 3000 was determined in a 5 mM KPi solution. This assessment was conducted by variating sonication durations and amplitudes while maintaining a w/v% of 0.2, which showed the most favorable results in the preliminary investigations. The pulse duration was set at 10 seconds with 5 seconds of pause, serving the purpose of ensuring that the energy input remained within acceptable limits for extended durations while allowing for repeated pulsing of the mixture. Extended pulse durations can potentially lead to elevated temperatures and homolytic cleavage of the aqueous medium.[230] The latter had to be mitigated to prevent the cross-

linkage of double bonds in the PI. The measurements were conducted immediately after preparation of the acoustically emulsified samples.

In Figure 13, the initial DLS results revealed monomodal distributions of the emulsions after 30 minutes at 30% amplitude (II), 60 minutes at 20% amplitude (III), and 60 minutes at 30% amplitude (IV) within the micrometer size range. Except for 30 minutes at 20% amplitude (I), where a bimodal distribution was observed. After 30-minute period bimodal distributions were detected under the sonication conditions for (I), (II), and (III), accompanied by a broadening of the hydrodynamic diameter distributions. After a 60-minute period the bimodal distributions for (I) and (II) vanished, giving rise to a broad distribution that was smaller than the initial one. This reduction in hydrodynamic diameter is a phenomenon commonly associated with emulsion creaming. For (III), a bimodal distribution is also evident after 60 minutes, with the emergence of a new species in the sub-nanometer size range. The hydrodynamic diameter distribution of (IV) remains monomodal and undergoes only a slight broadening during the duration of the dynamic light scattering experiment under investigation. The hydrodynamic diameters of the emulsions exhibited significant variation, (I) 3140 ± 1010 nm, (II) 1430 ± 450 nm, (III) 4000 ± 490 nm, to (IV) 800 ± 205 nm due to differences in the dispersion conditions. Given the objective of achieving a monomodal emulsion consisting of polymer droplets with the highest surface possible and consequently a small hydrodynamic diameter, the sonication conditions employed for (IV) were selected for further experiments and investigations. However, meta-stable emulsions were also achieved under the other sonication conditions, warranting further investigation in the future.

The results regarding the sonication time align with findings reported by Leong *et al.*,[231] who similarly noted that prolonged sonication led to a reduction in polydispersity in nanodroplets of oil in water nanoemulsions of sunflower oil, albeit in the presence of a surfactant. On the contrary, Consoli *et al.* [232] observed that excessively long sonication could potentially result in over-processing and droplet coalescence. Consequently, there is an optimal sonication time, which varies depending on the specific process conditions and components used.[233]

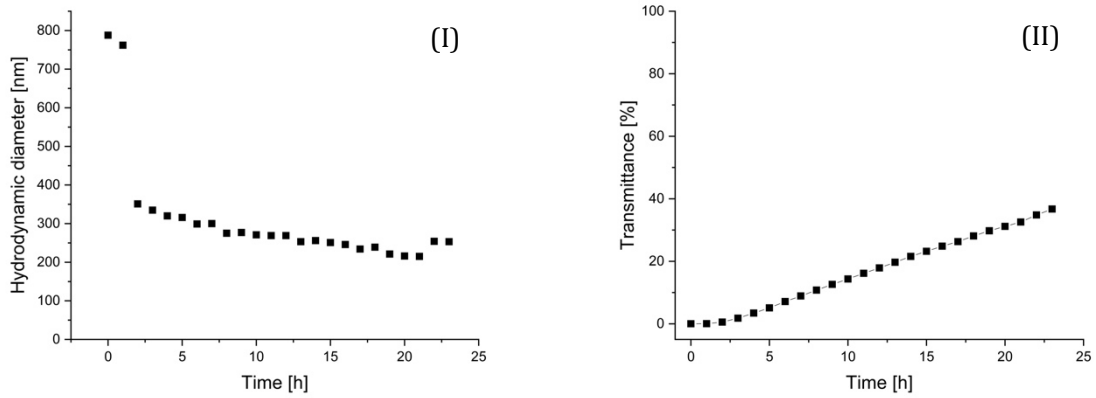

Figure 14. Hydrodynamic diameter measurements of acoustically emulsified **PI 3000** (I) and transmittance study in KPi 5mM (II).

The hydrodynamic diameter of the emulsion droplets was 800 nm, with a polydispersity index of 26%, according to DLS measurements immediately after preparation (Figure 14). Under the sonication conditions optimized for the acoustically emulsified **PI 3000**, the emulsion droplets remained stable for one hour with a broadening of the polydispersity. A decrease of the hydrodynamic diameter and the transmittance, as evidenced by measurements taken at one-hour intervals over a span of 24 hours using DLS, can be explained by the creaming of the hydrophobic polymer in the aqueous KPi at the investigated concentration of 5mM.

The hydrodynamic diameter remained stable after the first two measurements at approximately 300 nm with a broad polydispersity throughout the 24-hour measurement time frame. This decrease

in the hydrodynamic diameter after the first two measurements was also observed for the other sonication conditions but exhibited a faster decline with a faster decay in their respective hydrodynamic diameters. An increase in the hydrodynamic diameter, attributed to Ostwald-ripening or polymer coalescence could not be observed. The reason could be that the measurements was conducted at a fixed position, which was the middle of a 1 mL cuvette. The polymer underwent creaming at the water-air interface, which was not tracked. The resultant reduction in the hydrodynamic diameter can be correlated to such a behavior in emulsions. Conducting transmittance studies was therefore important to verify that the emulsion stays turbid for the duration of the envisioned enzymatic degradation and to gain further insight into the emulsion stability. The transmittance study revealed that the transmittance decreased to 36.7% over the course of 24 hours. Consequently, **PI 3000** remained acoustically emulsified for the targeted reaction duration and temperature range of the enzymatic degradation studies.

The next investigation was the evaluation of the stability of the PI against solvolysis under these sonication conditions. Sonotrodes can generate local acoustic power that can be a hundred times higher than that achieved in an ultrasonic bath. However, the maximum corresponding energy is only available in proximity to the vibrating tip.[228] To this end, GPC analysis was conducted before and after the sonication of **PI 3000** with the previously established parameters.

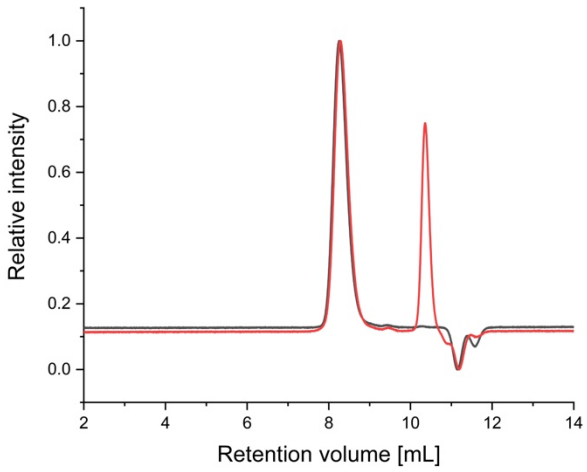

Figure 15. Gel permeation chromatography of **PI 3000** before (black) and after sonication (red).

Figure 15 illustrates that the retention volume of the **PI 3000** remains unchanged before and after acoustical emulsification. The second peak appearing after sonication is a solvent peak from residue water. This provides evidence that there is no polymer decomposition resulting from the acoustical emulsification process. Degradation of the PI backbone would lead to a reduction in the number average molar mass, which would result in a shift to higher retention volumes in GPC analyses. Cross-linkage of the double bonds due to the activation of the double bonds and the generation of reactive double bonds by the energy input of the acoustical emulsification procedure was also not observed under the optimized acoustical emulsification conditions. Cross-linkage could either lead to the generation of insoluble particles or an increase of the M_n in the GPC analyses, neither of which were observed in the conducted experiments.

A further parameter that affects the performance of the enzymatic degradation is the pH. Maintaining a constant pH level is essential for enzymatic degradation to ensure enzyme stability as well as the optimal conditions for enzymatic activity. As ultrasonication, at specific frequencies, is known to lead to the generation of OH radicals from water[183] potentially causing a decrease in the pH level this was probed. The pH levels were investigated before and after acoustical emulsification using a freshly calibrated pH meter. The pH remained unchanged before and after the acoustical emulsification procedure.

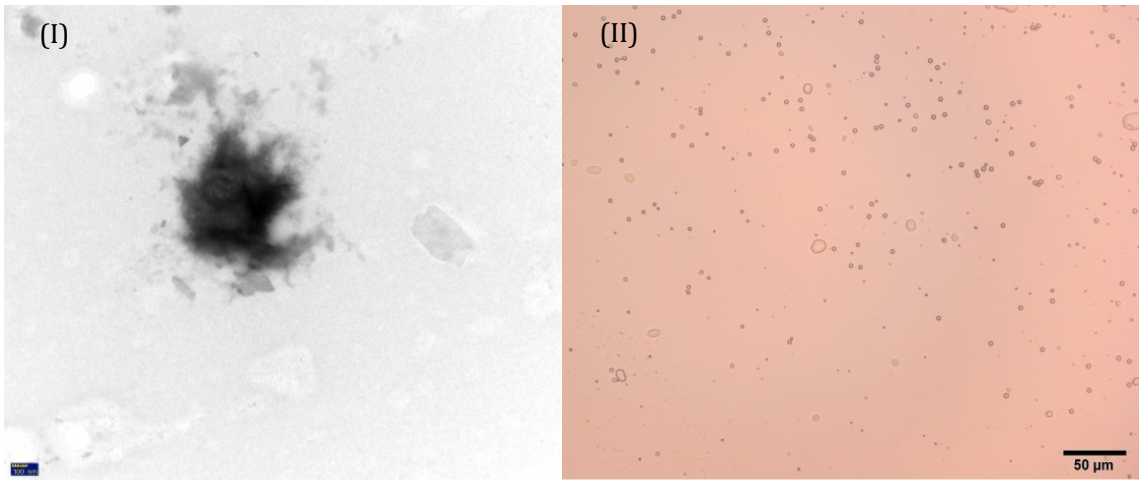

Figure 16. Transmission electron microscopy (I) and light microscopy image of the acoustically emulsified **PI 3000** (II).

To investigate the appearance of the acoustically emulsified system, transmission electron microscopy (TEM) images were taken, as shown in Figure 16 (I). The image shows polymer droplets in the micrometer range, which is in accordance with the findings from the dynamic light scattering investigations. Light microscopy images of the acoustically emulsified system, taken 6 hours after preparation, showed a dispersed system with polymer droplets in the micrometer range as well, see Figure 16 (II). Droplet sizes were determined using the image analysis software ImageJ, capable of measuring distances, areas and other graphical data of Figure 16.[234, 235] A coagulation of the polymer droplets is observed, as anticipated for a hydrophobic polymer in the hydrophilic aqueous phase. However, this observation appears to contradict the DLS results, which indicated a decrease in the hydrodynamic diameter over time. The discrepancy can be resolved by considering that during the DLS measurement, the hydrophobic polymer is aggregating at the air-water interface, leaving only well-dispersed emulsions of polymer droplets within a specific size range in the solution. Meanwhile, polymer droplets of a certain size were creaming out of the water phase. In light microscopy the coagulation or creaming of the emulsion at the glass-water interface was able to be tracked.

3.1.3 Co-solvent emulsified system establishment

The co-solvent emulsified systems were initially subjected to a broad screening process based on the visual appearance of the emulsified systems. The standard w/v% of latex milk of 0.2[161] in buffer served as the starting point for determining the required conditions to achieve metastable emulsions.

Table 8. Preliminary surfactant-free emulsification attempts with PI and cosolvents.

Entry	Polymer	[w/v%]	Co-Solvent	[w/v%]	Sonication time	Stability[a]
1	**PI *cis* 7000**	0.2	*n*-Hexadecane	20	1 h	1 h
2	**PI *cis* 7000**	0.2	*n*-Hexadecane	2	1 h	2 h
3	**PI *cis* 7000**	0.2	Squalene	2	1 h	2 h
4	**PI *cis* 7000**	0.2	Squalene	0.2	1 h	unstable
5	**PI *cis* 7000**	2	*n*-Hexane	2	1 h	unstable
6	**PI *cis* 7000**	0.2	*n*-Octane	0.2	1 h	unstable
7	**PI 14000**	0.2	Squalene	2	1 h	1 h
8	**PI 14000**	0.2	Squalene	0.2	1 h	24 h
9	**PI 14000**	0.2	*n*-Hexadecane	0.2	1 h	24 h
10	**PI 3000**	0.2	Squalene	0.2	1 h	24 h
11	**PI 3000**	0.2	*n*-Hexadecane	0.2	1 h	24 h

[a] = Stability was defined as the time until phase separation became visible

The aim for these emulsions was to maintain stability throughout the entire 24-hour enzymatic reaction period. The first co-solvent investigated in the emulsification of **PI *cis* 7000** was *n*-hexadecane. *n*-Hexadecane has been emulsified in water for extended durations by sonication using a sonication bath.[176] Additionally, it is utilized as an osmotic pressure agent in mini-emulsion polymerizations, which shows its capability of counteracting the Ostwald-ripening.[24] Polymer and co-solvent were stirred to ensure the dissolution of the polymer in the excess or equal ratios of the co-solvent. Subsequently, water was added and pre-emulsified by stirring to facilitate the emulsification process by sonication.[228] The solubility of the polymer in the solvent can be of crucial importance in the surfactant-free emulsification process and therefore solely hydrophobic solvents were investigated.[179]

A co-solvent to polymer ratio of 100 to 1, exhibited stability for up to 1 hour until phase separation became evident (Table 8). Better stability was achieved by reducing the co-solvent to polymer ratio to 10-to-1 (entry 2 of Table 8). However, transitioning to squalene as the co-solvent (entry 3 of Table 8) did not result in a significant improvement. Using a 1-to-1 ratio at 0.2 w/v% did not result in stable emulsions (entry 4 of Table 8). Dissolution of **PI *cis* 7000** in *n*-hexane required an increase of the w/v% to 2 (entry 5 of Table 8). Nevertheless, this adjustment did not result in stable emulsions with the addition of water and sonication. It was hypothesized that the length of the hydrophobic entity in water might have an influence onto the stabilization of emulsions.[176]

Increased solubility of oil in water enhances Ostwald ripening, causing oil droplets consisting of shorter hydrocarbons to grow more readily through this process due to their increased solubility.[176] Therefore, *n*-octane was investigated in comparison to *n*-hexane, using a 1-to-1 ratio (entry 6 of Table 8). However, stable emulsions could not be achieved under these conditions. The polydispersity as a factor in the formation of surfactant-free co-solvent emulsions was investigated by replacing **PI *cis* 7000** with **PI 14000** under the conditions that appeared the most promising. **PI 14000** exhibits a higher M_n while simultaneously showing a significantly reduced polydispersity index, which should be beneficial in the controlled emulsification. Applied conditions, a 10-to-1 co-solvent to polymer ratio (entry 7 of Table 8) were also previously reported to have resulted in highly stable surfactant-free emulsions in water for polystyrene-benzene solutions.[179] As demonstrated (entry 7 of Table 8) the stability was observed for one hour when squalene was used. Significantly improved stability of metastable emulsions was achieved by reducing the co-solvent ratio to 1-to-1, resulting in emulsions that remained turbid for 24 hours (entry 8 of Table 8).

The enhanced stability might arise from a minimized saturation of the aqueous phase and the formation of smaller droplet sizes within the emulsion, a common factor contributing to increased stability. Smaller droplets have a higher surface area-to-volume ratio, making them less prone to coalescence or creaming. Furthermore, lower concentrations could facilitate better mixing and dispersion of the hydrophobic phase into the aqueous phase. Additionally, an alternative co-solvent to squalene, *n*-hexadecane (entry 9 of Table 8), led under the same conditions to stable emulsion, which also remained turbid for 24 hours. The w/v% of 0.2, combined with a polymer-to-co-solvent ratio of 1-to-1, was also investigated for **PI 3000**. This resulted in turbid emulsions for 24 hours with both *n*-hexadecane and squalene (entries 10 and 11 of Table 8). The polydispersity as well as the ratio of co-solvent to polymer seemed to govern both the stability and the homogenization of the surfactant-free co-solvent emulsified systems of **PI 3000** and **PI 14000**. To further investigate these preliminary conditions, dynamic light scattering, and transmittance studies were conducted.

3.1.4 Characterization of the surfactant-free co-solvent emulsified systems of polyisoprene

The parameters for surfactant-free emulsification of *n*-hexadecane in water have been investigated.[176] However, the stability of *n*-hexadecane at the KPi optimum concentration of 5 mM, determined in chapter 3.2, has not been examined. Furthermore, it was intended to compare the results established in the preliminary results with the literature inspirations.[179]

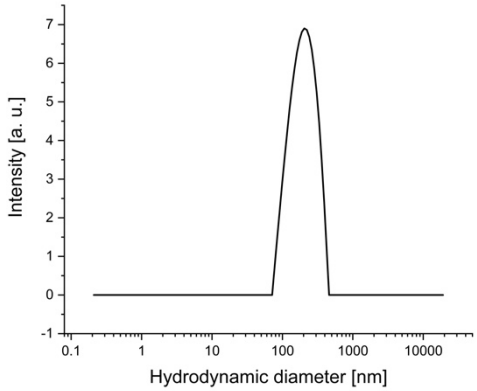

Figure 17. DLS of *n*-hexadecane in KPi 5 mM, as the negative control and point of reference of the surfactant-free co-solvent emulsified system without the addition of PI, with a hydrodynamic diameter of 190 nm.

The hydrodynamic diameter of the *n*-hexadecane in 5 mM KPi was 190 nm (Figure 17), which is more than double the diameter of the 50 nm reported in the literature for *n*-hexadecane in water emulsions.[176] It was hypothesized that the salting out effect of the *n*-hexadecane may contribute to this phenomenon, either by increasing Ostwald ripening or by hindering the dispersion of the hydrophobic solvent into the aqueous phase due to the salt content, resulting in larger hydrodynamic diameters. Furthermore, the stability of the surfactant-free emulsion of *n*-hexadecane was found to be lower compared to the emulsification procedure reported in the literature.

Transmission measurements indicated a rapid increase in transmittance of *n*-hexadecane in 5 mM KPi after 1 hour, stabilizing at around 70% for the 24 hour-duration of the reaction. The magnitude of molecular diffusion is dependent on the solubility of the hydrophobic moiety in the water phase, and changes in droplet size can occur due to the inherently greater solubility of the disperse phase as small droplets. Consequently, larger droplets can grow at the expense of smaller ones.[176] Additionally, the concentration of *n*-hexadecane used in this study was higher than the 1 mM concentration used in the literature,[176] which could also be a reason for the increased coalescence and Ostwald ripening observed in the sample reported here. Weiss *et al*. reported that the kinetics of the solubilization process were strongly dependent on the initial droplet size and concentration in *n*-hexadecane in water emulsions.[236] This could also explain the significant increase in transmittance observed in *n*-hexadecane in 5 mM KPi, especially without the stabilizing influence of a hydrophobic polymer.

The preliminary results for the co-solvent emulsified systems of **PI 3000** and **PI 14000** indicated emulsions that remained stable for the entire reaction duration of 24 hours (entry 9 and 11 in Table 8). To further investigate their stability dynamic light scattering measurements as well as transmittance studies were conducted. *n*-Hexadecane was chosen as the co-solvent from that point on due to results parallelly obtained in chapter 3.2, which showed less inhibition of enzymatic activity by *n*-hexadecane in comparison to squalene.

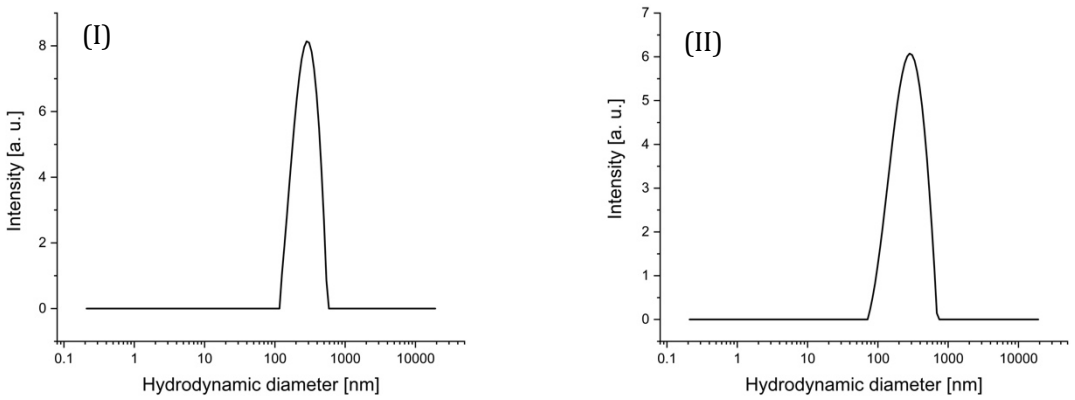

Figure 18. DLS of co-solvent, *n*-hexadecane, emulsified systems of **PI 3000** (I) and **PI 14000** (II).

The co-solvent stabilized emulsions of PI showed size distributions in DLS measurements, of 280 nm for **PI 3000** and 270 nm for **PI 14000** with a 1-to-1 ratio of *n*-hexadecane to the respective polymer in 5 mM KPi. The hydrodynamic diameter distribution of the co-solvent emulsified systems of **PI 3000**, with a polydispersity of 21%, was slightly narrower than that of the co-solvent emulsified systems of **PI 14000**, which had a polydispersity of 22% (Figure 18).

In contrast to the polystyrene and benzene emulsions reported to have initial droplet sizes of 50-100 nm at weight ratios of 1: 500, 1: 300, 1: 100 and 1: 10,[179] the initial droplet sizes for the PI and *n*-hexadecane system were larger. However, this difference could be explained by the high affinity of polystyrene to benzene, as well as the negative effect of KPi content on to the dispersion of the emulsion droplets.

Surfactant-free emulsions of polystyrene and cyclohexane with weight ratios of 1-to-10 and 1-to-100 were reported to have led to bimodal distributions in the range of 70-100 nm and 200-300 nm.[179] These findings align more closely with the co-solvent-stabilized PI and *n*-hexadecane systems described in this investigation. However, it should be noted that the concentration of the polymer-co-solvent mixture varied because of the lower co-solvent content employed in the procedures established here, as compared to the literature, where concentrations of 100 and 10 mmol/L of co-solvent in water were utilized. When a polymer doesn't have a strong affinity for the co-solvent, there might be a slight tendency for the expulsion of the polymer toward the surface, potentially forming a polymer-coated hydrophobic solvent droplet. This surface shell could induce repulsion among polymer chains adsorbed onto different emulsion droplets, thereby contributing to the creation of meta-stable emulsions.[179]

It was evident that, at the investigated polymer to co-solvent ratio of 1-to-1, the addition of polymers **PI 3000** and **PI 14000** should have led to an increase in the viscosity of the oil phase. Consequently, viscosity measurements of the oil phase were not conducted in this study.

To track the stability of the co-solvent emulsified systems, the hydrodynamic diameter was measured with DLS over a 23-hour period at one-hour intervals. Transmittance studies and hydrodynamic diameter tracking were carried out at fixed positions, as previously described for the acoustically emulsified system, and at a temperature of 25 °C.

The hydrodynamic diameter of the co-solvent emulsified system **PI 3000**, immediately after preparation, was 280 nm. After one hour, it exhibited a slight increase in hydrodynamic diameter but over the entire tracking period it remained in the range of 260-350 nm (Figure 19 (I)). This range fell within the standard deviation reported by the Anton-Paar algorithm for hydrodynamic diameter by intensity measurements. A similar pattern was observed for the co-solvent emulsified system of **PI 14000**, which had an initial hydrodynamic diameter of 270 nm. It remained within the range of 250-320 nm throughout the tracking period (Figure 19 (II)). In the first three hours of the measurement, a slight increase in the maximum hydrodynamic diameter of the co-solvent emulsified

system of **PI 14000** was observed, which could be interpreted as a small indicator of coalescence but is also within the range of the standard deviation.

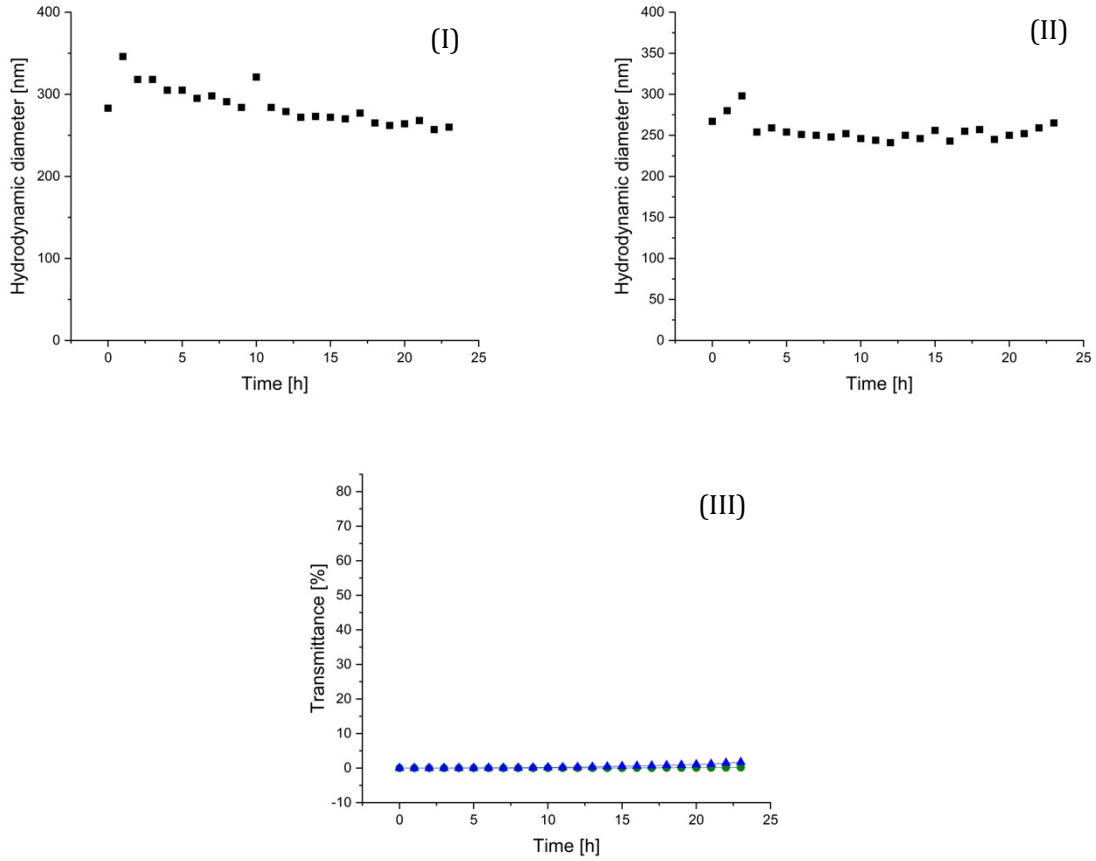

Figure 19. Emulsion droplet hydrodynamic diameters (DLS) for co-solvent emulsified system of **PI 3000** (I) and co-solvent emulsified system of **PI 14000** (II) for 24 hours and transmittance study for the reaction time duration of co-solvent emulsified system **PI 3000** (III; green circles) and **PI 14000** (III; blue triangles).

For further insight into the emulsion's stability, transmittance studies were conducted. In this study, the co-solvent emulsified system of **PI 14000** remained turbid, with transmittance reaching 1.7% after 24 hours, (Figure 19 (III)). The co-solvent emulsified system of **PI 3000** also remained turbid for the entire reaction duration, with a transmittance of 0.2% after 24 hours. To verify the superior stability of the co-solvent emulsified system of **PI 3000** compared to that of **PI 14000**, the transmittance study was extended until the transmittance reached 20%. For the co-solvent emulsified system of **PI 14000**, the transmittance reached 23.6% after 144 hours, whereas for the co-solvent emulsified system of **PI 3000**, the transmittance reached 20.4% after 230 hours. The hydrodynamic diameter of 290 nm after 230 hours for the co-solvent emulsified system of **PI 3000** and 350 nm after 144 hours for the co-solvent emulsified system of **PI 14000**, respectively was observed. Consequently, it appeared that the co-solvent emulsification approach had delayed the creaming of the sample.

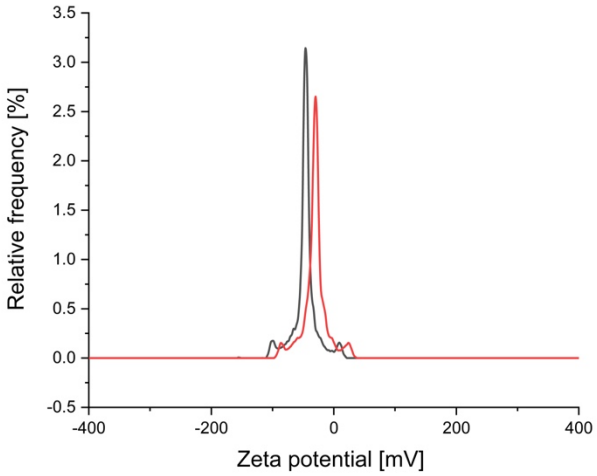

Figure 20. Zeta potential measurements of co-solvent emulsified system of **PI 3000** (black) and *n*-hexadecane (red)

The surface electric properties of the co-solvent-stabilized **PI 3000** emulsion were analyzed (Figure 20). A comparison was made between *n*-hexadecane and the **PI 3000**/*n*-hexadecane system to determine if the combination of hydrophobic polymer and hydrophobic solvent influenced the potential stability of the system. A possibility to assess this property is measuring zeta potential, which is a measure of the electric charge at the surface of emulsions or colloidal dispersions, indicating their stability and propensity to attract or repel one another. When emulsion droplets have a high positive or negative zeta potential, they tend to repel each other, preventing coalescence. However, when the zeta potential is low, there is no force to prevent them from coagulation or flocculation.

The zeta potential value for *n*-hexadecane under the dispersion conditions was relatively high, at −35 mV, compared to the transmittance study, which showed a fast decay. The reason could be that the zeta potential measurement was not conducted with 5 mM KPi, which should have led to less stability of the emulsion. The buffer KPi was not used for the measurements because of its high ionic strength and specific ion composition, which can interfere with accurate zeta potential measurements by altering the surface charge and the electrical double layer of particles in suspensions and emulsions. Nonetheless, there was a significant decrease in the zeta potential for co-solvent-stabilized **PI 3000**, reaching −47 mV. This change serves as another clear indication of the stability achieved through the surfactant-free emulsification approach with *n*-hexadecane. Kamogawa *et al.* also reported a change in the electric surface properties of cyclohexane emulsions in water from −37 mV to −59 mV for their polystyrene/cyclohexane system immediately after preparation.[179]

TEM imaging of the co-solvent-stabilized **PI 3000** system showed PI droplets of approximately 300 nm in size. The increased size, compared to dynamic light scattering, may have resulted from water evaporation before measurement, leading to droplet agglomeration. Additionally, the emulsion droplet size appeared rather coarse, potentially due to the sample staining procedure. ImageJ software was utilized to determine distances, areas, and other graphical data. The suggested structure for **PI 3000**-coated *n*-hexadecane droplets, as depicted in the schematic representation chapter 1.5, or the literature for the styrene-benzene emulsions[179] could not be confirmed by TEM imaging.

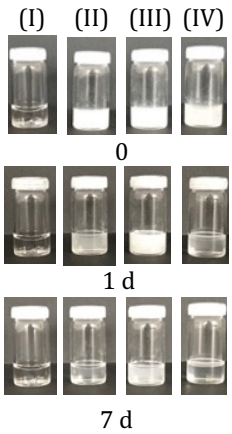

Figure 21. Pictures of **PI 3000** systems: non emulsified (I), *n*-hexadecane without **PI 3000** (II), co-solvent emulsified **PI 3000** (III), acoustically emulsified **PI 3000** (IV); after preparation (0), after one day (1 d) and after seven days (7 d).

Pictures of the differently emulsified **PI 3000** systems were captured immediately after preparation, at the one-day mark, and after seven days to illustrate the stability of these systems. The pictures in Figure 21 depicted the stability of the emulsions, including the co-solvent emulsified system, the acoustically emulsified system, and the non-emulsified system. It reveals that the acoustically emulsified system of **PI 3000** exhibited significantly faster emulsion decay than the co-solvent emulsified system of **PI 3000**, primarily due to the absence of a stabilizing co-solvent.

3.1.5 Co-solvent emulsified polybutadiene systems

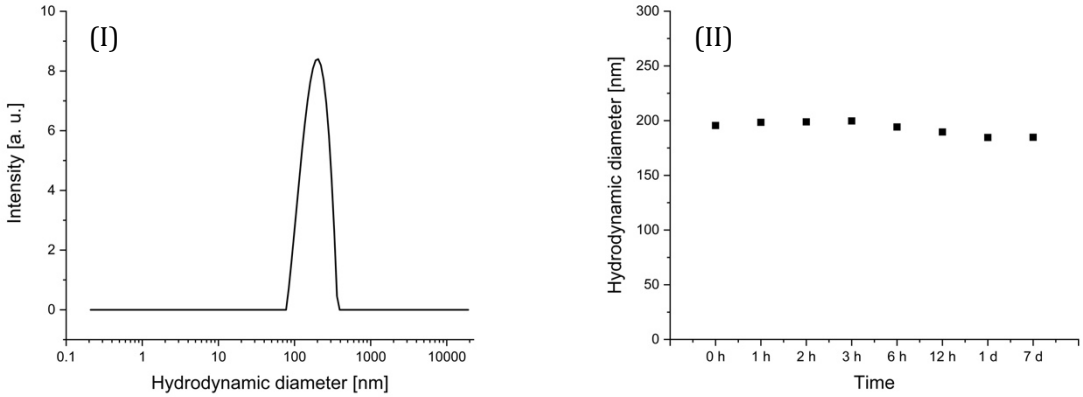

Figure 22. DLS of the co-solvent emulsified system of **PB 3500** (I) and the tracking of the hydrodynamic diameter over 7 days of the same system (II).

The transferability of the system to PB was investigated by applying the same 1-to-1 ratio of co-solvent *n*-hexadecane to PB as optimized for PI. **PB 3500** was chosen due to its comparable M_n to **PI 3000** similar hydrophobicity, similar chemical structure, and a higher PDI of 2.0 (Table 6). DLS measurements revealed a hydrodynamic diameter of 200 nm with a hydrodynamic diameter distribution smaller than the co-solvent emulsified systems of PI (Figure 22). Hydrodynamic diameter tracking over 7 days demonstrated that the emulsion remained stable, with the hydrodynamic diameter consistently within the range of 200 nm.

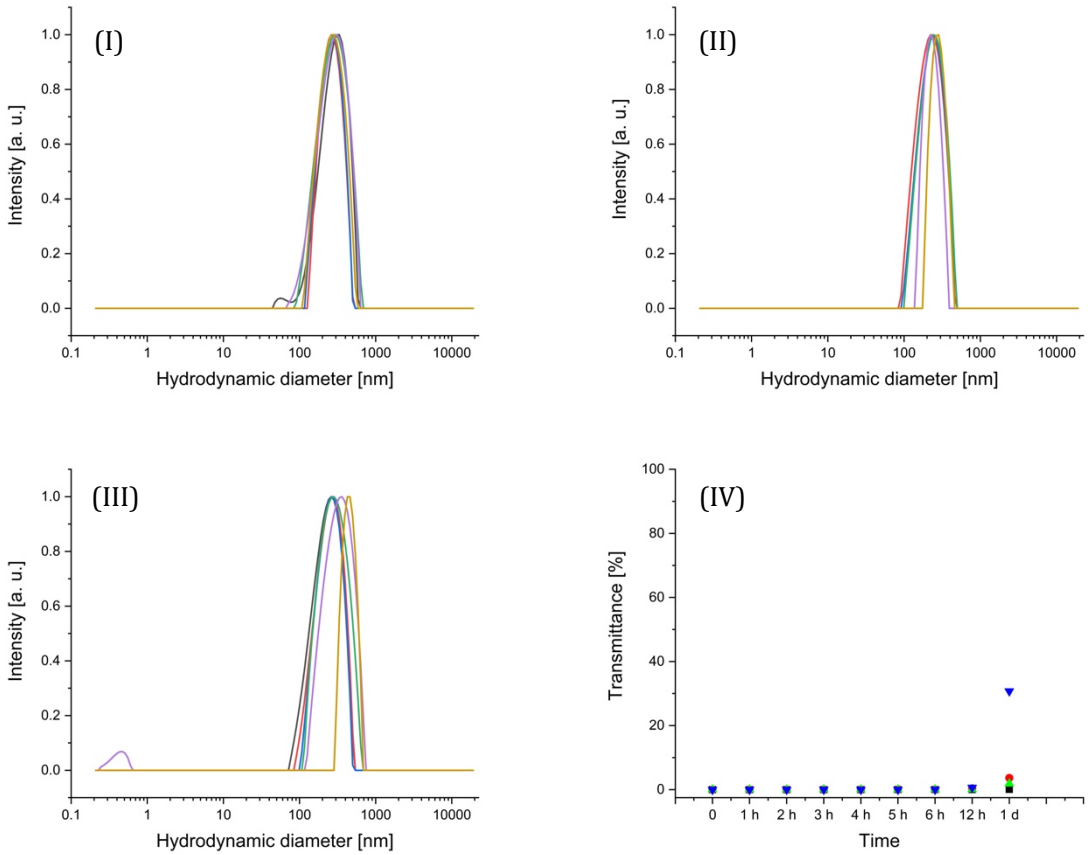

Figure 23. Hydrodynamic diameter of co-solvent emulsified **PB 3500** at 37 °C (I), at 45 °C (II) and at 55 °C (III) after 0 h (black), 1h (red), 3 h (blue), 6 h (green), 12 h (purple) and one day (light brown); Transmittance study of the co-solvent emulsified system of **PB 3500** (IV) at 25 °C (black; Square), 37 °C (red; circle), 45 °C (green; upward triangle) and 55 °C (blue; downward triangle).

Investigations of the thermostability of the co-solvent emulsified PB were conducted at 37 °C, 45 °C, and 55 °C to demonstrate that, if enzymatic activity would be optimized for higher temperatures, the system maintains its applicability (Figure 23). The hydrodynamic diameter at 37 °C (Figure 20 (I)) remained constant for 24 hours, while the hydrodynamic diameters at 45 °C (Figure 23 (II)) and 55 °C (Figure 23 (III)) increased slightly over 24 hours. The increase in hydrodynamic diameter with rising temperature suggests that coalescence of the emulsion droplets appears to be predominant in comparison to the creaming effect observed in the co-solvent emulsified system at 37 °C. The transmittance study of the co-solvent emulsified system of **PB 3500** revealed that the stability of the emulsions was significantly lower at 55 °C compared to the other investigated temperatures (25 °C, 37 °C, and 45 °C). This observation suggests that co-solvent emulsified of **PB 3500**, unlike surfactant-free emulsions of triolein in water, which were reported to have increased colloidal stability at temperatures above 40 °C,[185] has decreased stability above 45 °C. However, the decrease in the interfacial tension between triolein and water with increasing temperature can be linked to the transformation of short-range ordered domains of triolein molecules in the liquid state, leading to enhanced colloidal stability. According to Eotvos's equation, it is well-established that the surface tension of most liquids decreases as temperature rises. The increased kinetic energy imparted to the surface molecules at higher temperatures tends to overcome the net attractive force of the bulk liquid. Furthermore, as the temperature of the liquid approaches its critical value, the cohesive force between the molecules significantly weakens. It is thus expected that the surface tension will decrease considerably at a certain critical temperature.

The decrease in surface tension is primarily attributed to the increased thermal energy of the surface molecules, which leads to a weakening of the net attractive forces within the bulk liquid. However, the hydrophobic nature of the polymer seems to result in a separation of the co-solvent emulsified system at elevated temperatures. This behavior aligns with known hydrophobic interactions, which tend to cause aggregation or phase separation in aqueous systems. Variations in temperature could indeed impact the interfacial properties of the co-solvent emulsified system, including interfacial tension and emulsion stability. At higher temperatures, the interfacial tension between the hydrophobic polymer droplets and the aqueous phase may decrease. This reduction in interfacial tension can weaken the stability of the emulsion. Additionally, this effect might be enhanced by the salting out effect, which can be temperature dependent at least in the case of proteins.[237] Furthermore, as the temperature rises, the viscosity of the continuous aqueous phase may decrease. Lower viscosity implies reduced resistance to droplet movement within the emulsion. This increased mobility of the emulsion droplets can further contribute to changes in stability. In the case of a hydrophobic polymer, this increased mobility could lead to the creaming out of polymer droplets toward the upper part of the system, inducing phase separation. At elevated temperatures, the significance of hydrophobic interactions between polymer chains may also increase. This heightened interaction can result in the aggregation or coalescence of polymer molecules, leading to the formation of larger droplets or even polymer-rich domains. These aggregated droplets or domains can subsequently ascend within the emulsion, giving rise to creaming. Further investigations into hydrophobic polymers stabilized by co-solvents, without the use of surfactants, could provide additional insights into the results that have been reported here.

3.2 Enzymatic degradation of polyisoprene and polybutadiene

Nature has evolved an enzyme family dedicated to the degradation of PI, rubber oxygenases. Nevertheless, there remains a significant knowledge gap regarding the degradation of SPIs. Specifically, the enzymatic degradation of SPI with a 1,4-*cis*: *trans*-ratio below 97% 1,4-*cis* has not yet been addressed. It was hypothesized that the major challenge to achieving efficient enzymatic degradation of SPI lies in its presentation in aqueous media. The poor solubility of the polymer in water substantially limits the available interface for enzymatic degradation. Consequently, surfactant-free emulsification strategies were established in Chapter 3.1. Subsequently the impact of these emulsification strategies on enzymatic degradation had to be systematically investigated. Moreover, the analytical methodologies for monitoring the enzymatic degradation, both for preliminary sampling and the optimization of degradation parameters, particularly for SPI with a substantial *cis*: *trans* ratio had to be implemented. The enzymatic degradation had to be first replicated with latex milk and then the expansion of scope onto SPIs and NR derived PI had to be investigated. Investigations were conducted to determine the applicability of detection for degradation fragments using HPLC, ESI-TOF-MS and UHPLC with a comparison of their respective effectiveness. Additionally, protein-engineered variants of the rubber oxygenase Lcp_{K30} were cultured, expressed by the group of Weissenborn, and assessed for their catalytic behavior under optimized conditions in collaboration. Following the establishment of a methodology for surfactant-free enzymatic degradation of PIs with significant *cis*: *trans* ratios, the focus shifted to the investigation of the enzymatic degradation of synthetic PB with the established surfactant-free emulsification methodology from Chapter 3.1. To facilitate this investigation, a new rubber oxygenase degradation assay was developed to measure the degradation of protein-engineered variants even at low enzymatic activity levels. The activity of the protein-engineered enzymes was screened alongside the native enzyme using the established methodology, allowing for a comparative analysis.

3.2.1 Preliminary investigations of enzymatic degradation behavior of LcpK30 towards latex milk, synthetic polyisoprenes, and natural rubber derived polyisoprenes

3.2.1.1 Analytical methodology for enzymatic degradation of latex milk

High-pressure liquid chromatography (HPLC) has emerged as a powerful analytical tool for the separation and characterization of complex mixtures in various scientific disciplines. HPLC was employed for the preliminary analysis of telechelic degradation fragments of PIs. HPLC methods for the separation of oligoioprenoids were evaluated in terms of their chromatographic resolution, peak symmetry, retention time, and sensitivity based on the procedure implemented by Röther *et al.*[161] The results revealed distinct differences in the separation efficiency and overall performance among the tested methods with the HPLC under investigation and consequently an adaption was conducted.

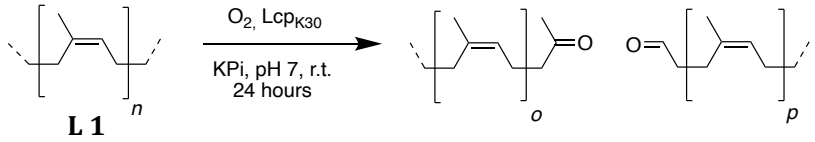

L 1

Scheme 10. Enzymatic degradation of latex milk, 1,4-*cis*-PI, (**L 1**) by Lcp_{K30}.

The enzymatic degradation of latex milk to the respective isoprenoidic degradation fragments is the most extensively studied system for evaluating the activity of Lcp_{K30} (Scheme 10). Rubber oxygenases, as heme-containing enzymes, enable the oxidative cleavage of PI into low molecular weight oligoisoprenoidic degradation fragments with terminal aldehyde and keto groups between a variable number of intact isoprene units, depending on the type of rubber oxygenase.[112] To implement the HPLC methodology, the standard procedure to produce oligoisoprenoidic degradation fragments was applied.[152] Latex milk was provided by Weber and Schaer GmbH and washed according to a procedure by Röther et *al.*[238] prior to the usage. Prof. Dr D. Jendrossek provided the original Lcp_{K30} plasmid that was expressed by Eugen Schell and provided for the enzymatic degradation studies. The enzymatic degradation of latex milk (**L 1**) was conducted for 24 hours, at KPi concentration of 100 mM, at room temperature and an enzyme concentration of 5 µg/L, which correlated to 115.6 nM/mL. The products were then isolated with liquid-to-liquid extraction with ethyl acetate. The ethyl acetate extracts were dried *in vacuo* and then redispersed in methanol for analysis with HPLC.

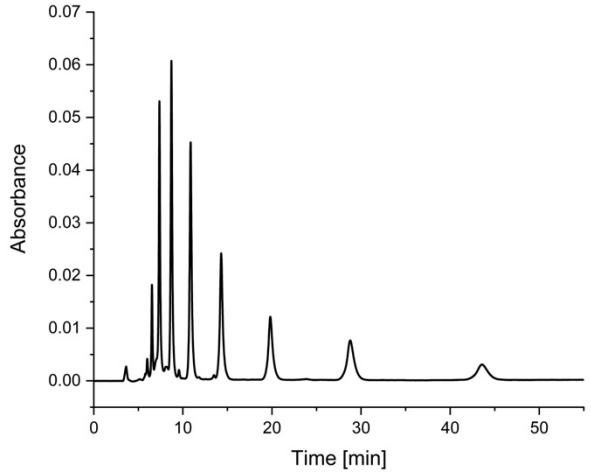

Figure 24. HPLC of enzymatic **L 1** degradation by Lcp_{K30}.

The HPLC-chromatogram (Figure 24) showed the characteristic degradation pattern of the oligoisoprenoidic degradation fragments with keto- und aldehyde-end-groups (Scheme 10).[161] Evaluation of the product formation was conducted *via* area integration with OriginLab. In literature, the quantification of the enzymatic activity of Lcp_{K30} involved the addition of the distinct oligoisoprenoidic degradation fragment produced by the rubber oxygenase RoxA, which cleaves the PI in exo-fashion and therefore leads to one distinct oligoisoprenoidc degradation fragment known as 12-oxo-4,8-dimethyltrideca-4,8-diene-1-al (ODTD).[239] ODTD was not used as an internal standard in this study, because it was shown by Birke et *al.*[134] that Lcp_{K30} can also produce ODTD in amounts that were detected by HPLC. The usage of standards in HPLC analysis of complex samples can present challenges due to matrix effects, which are to be circumvented for the screening of new enzymatic activities towards SPIs. These effects may interfere with the analysis and make it difficult to accurately quantify the target analyte using a standard. Furthermore, the objective of the analysis was to compare relative differences between the samples under investigation. Additional analysis was then conducted with ESI-TOF-MS to assess whether the degradation products were correlating to the formed oligosisoprenoidic degradation fragments found in literature. The ESI-TOF-MS revealed the expected degradation fragments as a $[M+Na+MeOH]^+$ series, consistent with previous findings in literature.[161]
L 1 was used to determine the effect of squalene and *n*-hexadecane onto the enzymatic degradation of Lcp_{K30}. Squalene and *n*-hexadecane had shown to be co-solvents that could have a beneficiary effect onto the emulsification of PIs in chapter 3.1. Squalene, being a hydrophobic triterpene, shares structural similarities to PI. This was hypothesized to be beneficiary for the inhibition effect onto the rubber oxygenase. To investigate this hypothesis enzymatic degradation experiments of **L 1** were conducted with squalene and *n*-hexadecane *via* HPLC analysis. The experiments were conducted in one batch of the same enzyme at room temperature, with identical stirring speeds, freshly prepared KPi, extracted with liquid-to-liquid extraction with ethyl acetate and corresponding negative controls without the enzyme Lcp_{K30}. The inhibition effect of the co-solvent *n*-hexadecane and squalene was apparent according to the decrease in the intensity of the respective oligoisoprenoidic degradation fragments in comparison to the sample without the co-solvent (HPLC-chromatograms in Appendix). Therefore *n*-hexadecane was deemed the better co-solvent for the enzymatic degradation of SPIs. Additional studies were undertaken to further validate the impact of *n*-hexadecane onto the enzymatic degradation. These investigations are presented in the following chapter.

3.2.1.2 Enzymatic degradation of non-emulsified polyisoprenes

SPIs with a significant 1,4-*cis*: *trans* ratio below 97% had not previously been investigated in terms of their enzymatic degradation capabilities for Lcp_{K30}, especially as a sustainable alternative to conventional degradation methods. The polymers under investigation were labeled as non-emulsified (N), acoustically emulsified (A), and co-solvent emulsified (C) (Table 9).

Table 9. Polymers used in the emulsification and degradation studies of polyisoprenes.

PIs	M_n[a]	M_w[a]	PDI[a]	1,4-*cis*: t*rans*-ratio[b]	ID
PI 3000	3100	3500	1.1	56:27	**N 1**, **A 1**, **C 1**
PI 14000	14000	16000	1.1	55:28	**N 2**, **C 2**
PI *cis* 7000	7000	48300	6.6	98:2	**N 3**, **C 3**

[a]Determined by GPC; [b]Determined by ^{1}H NMR.

The standard degradation parameters were used for **N 1** and **N 2**, resulting in neither the distinct degradation pattern nor the detection of oligoisoprenoidic degradation fragments according to HPLC

and ESI-TOF-MS analysis, which implies an unsuccessful degradation attempt. To enhance the enzymatic activity, the enzyme concentration was increased to 5 μmol/L. However, this adjustment did not lead to distinguishable degradation patterns when compared to the negative controls according to HPLC. The negative controls were degradation experiments conducted under identical conditions as the enzymatic reaction but without the addition of the enzyme Lcp_{K30}. Nonetheless, ESI-TOF-MS analysis did reveal oligoisoprenoidic degradation signals at low intensity.
An improved isolation and enhanced degradation efficacy were reported by Andler *et al*.[160] through the sequential addition of the rubber oxygenase Lcp_{1VH2} in a bioreactor under continuous extraction with organic solvent. Attempts to adapt this methodology to our lab-scale set up employing the standard procedure neither lead to a significant improvement of degradation fragment isolation nor to degradation product formation according to HPLC and ESI analysis. Even upscaling the reaction threefold, to increase the amount of formed degradation products, and combining of the triplicate, did not lead to the expected signals according to ESI-TOF-MS analysis. This could be attributed to the potential denaturation of the enzyme in this approach, preventing a cumulative effect. As an alternative strategy, the synthesis of PI nanoparticles was investigated to enhance the available degradation surface in an emulsified system. PI nanoparticles were synthesized according to Lorenz et *al*.[24] with microemulsion polymerization and according to Cheong *et al*.[23] with an *ab initio* redox emulsion polymerization. The properties of the resulting nanoparticles were analyzed with DLS and after freeze-drying with GPC. The enzymatic degradation attempts proved to be unsuccessful according to HPLC, and ESI-TOF-MS analysis. The reason being the utilization of SDS as a surfactant to stabilize the monomer emulsion droplets in the respective emulsion polymerization. Birke *et al*.[152] demonstrated that the presence of 1 mM of SDS or even nonionic surfactants such as Tween 20 or Triton X-100 led to a drastic reduction in the relative activity of the Lcp_{K30} to 0.1%.
Acoustical and co-solvent emulsified systems were established in Chapter 3.1. To investigate the effect of the surfactant-free emulsification, the initial step involved determining whether the NR derived predominantly 1,4-*cis*-PI would be degraded by the enzyme in the here established procedure. For a more comprehensive and efficient screening methodology to assess the various factors that could influence the enzymatic degradation of polyenes, a partial transition and adaption of the HPLC procedure to UHPLC was conducted. UHPLC can provide superior screening capabilities by increased separation, enhanced resolution, and heightened sensitivity in comparison to HPLC. This reduction in screening time can lead to quicker analysis times, sharper peak detection, and superior trace detection, which could be crucial in the assessment of new enzymatic activities. Additionally, UHPLC contributes to sustainability by the reduction of solvent consumption, an aspect worthy of consideration for broad and extensive screening efforts. Consequently, the HPLC methodology employed for the EC-C8 InfinityLab poroshell was transposed and adapted to UHPLC implementation for subsequent screening. With this methodology at hand, the subsequent chapter focused on a thorough and in-depth optimization of the enzymatic degradation parameters.

3.2.2 Optimization of enzymatic degradation parameters

The first objective was the assessment of the suitability of parameters for the surfactant-free systems in regard to the enzymatic degradation of PI. A key aspect was the evaluation of different solvents in respect to the compatibility towards the enzyme Lcp_{K30}. Experiments were conducted with different solvents, including chloroform, dichloromethane, ethyl acetate, *n*-hexane, toluene, and *n*-hexadecane, in a biphasic manner, inspired by bioreactors, which showed better product isolation.[240] The selection of solvents was guided by their hydrophobic nature, which allowed for biphasic experimental set ups as well as their potential capability of acting as co-solvents in the surfactant-free emulsification systems. To determine the retention times and intensity of the characteristic degradation pattern of oligoisoprenoidic degradation fragments, as seen for HPLC, positive controls of **L 1** were prepared in UHPLC.

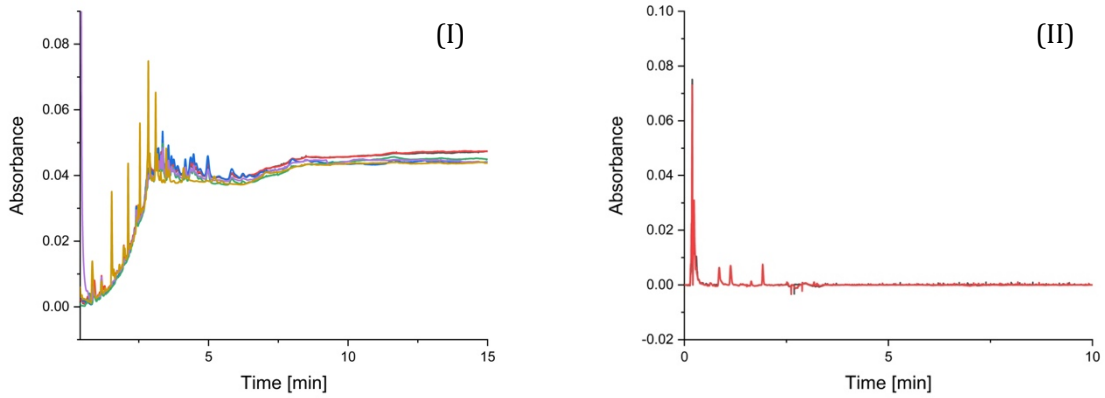

Figure 25. Degradation inhibition by different solvents of the enzymatic degradation of **PI *cis* 7000**. Stacked UHPLC chromatograms, with gradient, of enzymatic degradations of **PI *cis* 7000** in the presence of chloroform (black), dichloromethane (red), ethyl acetate (blue), *n*-hexane (green), toluene (purple) and *n*-hexadecane (light brown) (I). Stacked, baseline corrected, UHPLC-curves of ethyl acetate extracts of a blind run with solely Lcp_{K30} enzyme (black) and the corresponding negative control (red) (II).

The characteristic peaks, as seen for the positive controls of **L 1**, in the UHPLC chromatogram were visible at the respective retention times for the enzymatic degradation of **PI *cis* 7000** as **N 3**. For a comparative assessment of the impact of solvent onto the degradation capabilities of the enzyme Lcp_{K30} the intensity of those peaks was investigated. The stacked UHPLC-chromatograms revealed that the distinctive degradation pattern due to the enzymatic degradation of **PI *cis* 7000** by Lcp_{K30} was least suppressed in the presence of *n*-hexadecane (Figure 25). Degradation was least inhibited in the presence of the solvent *n*-hexadecane but a significant suppression for all the other investigated solvents was observed. This could be attributed to the denaturation of the enzyme in the presence of less hydrophobic entities than *n*-hexadecane. The enzyme's acceptance of *n*-hexadecane could also be attributed to the rubber oxygenase's capacity to interact with the hydrophobic PI as a carbon source, which is most resembled by the *n*-hexadecane.

For verification that the peaks were not artifacts from denatured enzyme, an experiment was conducted using solely enzyme Lcp_{K30} without the presence of PIs. Negative controls were included under identical conditions without the addition of enzyme. Figure 25 (II) depicts the respective UHPLC-chromatogram, showing that the product peaks do not originate from the enzyme Lcp_{K30} itself.

The subsequent step was the investigation of the KPi concentration optimum for the stability of surfactant-free PI emulsions. Metastable hydrocarbon-polymer in water systems, as envisioned, proved to be less stable in the presence of buffers as seen in chapter 3.1. However, these buffers are necessary for the stabilization of the enzyme. To this end, experiments were conducted in triplicates, with Yannick L. Wolf, to determine the KPi optimum of the enzymatic degradation of **L 1**. This approach aimed to ensure that the balance of interacting effects could be minimized and to determine the most effective conditions for the enzymatic degradation process.

The distinct oligoisoprenoidic degradation fragments typical for the enzymatic degradation of **L 1** by the enzyme Lcp_{K30}[161] were tracked *via* UHPLC and the area of peaks of the respective degradation fragments was integrated (Figure 26). A comparative analysis of those oligoisoprenoidic degradation fragment peak areas was conducted at different KPi concentrations. The correlation between these degradation fragments and their retention times was established with Yannick L. Wolf. Interestingly, the optimal KPi were found to be 1 mM and 2 mM, which is a significant discrepancy to the previously reported 100 mM.[5, 112] Due to this discrepancy subsequent experiments were conducted at a concentration of 5 mM to account for the possible deviation of degradation optimum for longer oligoisoprenoidic degradation fragments, which might have a different degradation optimum outside of the scope of the investigated UHPLC peak areas.

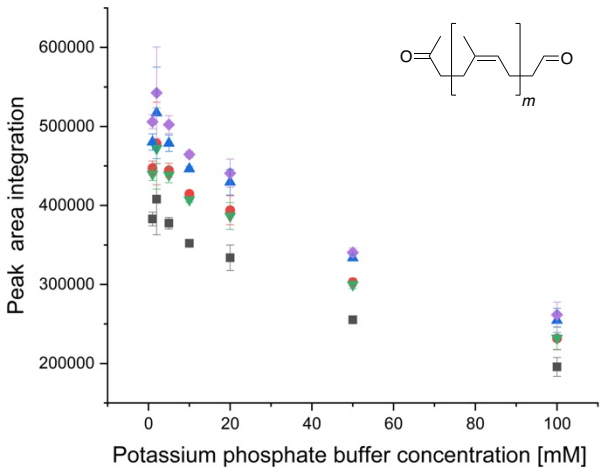

Figure 26. Peak area integration of oligoisoprenoidic degradation fragments dependency of KPi concentration investigated using UV-UHPLC measurements of enzymatic degradation of **L 1**. (*m* = 4 = black square; *m* =5 = red dot; *m* = 6 = blue triangle; *m* = 7 = green triangle; *m* = 8 = purple square).

The pH was tested prior to all of the experiments and standardized to 7, aligning with the pH optimum previously determined by Birke *et al.* for the degradation of latex milk.[152] At these conditions the enzymatic degradation of **N 1** was repeated, which led to distinctive degradation patterns detected by UHPLC. These peaks were not detected in the corresponding negative controls. ESI-TOF-MS analysis of the respective samples showed signals of degradation fragments that correlated to the enzymatic degradation of the reference probe **L 1** and absent in the respective negative controls. The sum area of product peaks from the enzymatic degradation of **N 1** was investigated with UHPLC. This quantification was determined by integration of UV-UHPLC chromatograms and subtraction of the background observed in negative controls conducted under identical conditions without the addition of enzyme Lcp_{K30}. These experiments aimed at determining if the enzyme concentration had already plateaued beneath 5 μMol/L. While the sum of product peak area increased with the increased loading of the enzyme Lcp_{K30}, a non-linear retardation was detected. Nevertheless, 5 μMol/L had led to the highest sum of product peak areas and was consequently continued to be used in subsequent experiments.

The enzymatic degradation of latex milk was commonly conducted at 37 °C.[5, 112, 123] It was not determined if a decrease temperature would retard the enzymatic degradation with SPIs. Consequently, experiments at three different temperatures 25 °C, 30 °C and 40 °C aimed to explore the temperature dependency of the enzymatic degradation of **PI 3000** and to determine whether the commonly used temperature of 37 °C was indeed the optimal for SPIs. This assessment provided insights into the feasibility of conducting the enzymatic degradation at standard laboratory conditions and indeed increasing the temperature did not lead to more degradation products according to UHPLC analysis. Consequently, the reactions could be conducted at standard laboratory conditions in subsequent reactions.

The stirring speed could play a pivotal role in enzymatic degradation processes by affecting mass transfer and substrate accessibility to the respective enzyme's active sites. On one hand, insufficient stirring could lead to incomplete mixing, leading to localized substrate deficiency, and subsequently impacting enzymatic activity. On the other hand, excessive stirring could subject mechanical stress onto the enzyme, potentially denaturing it and decreasing its catalytic efficiency. It was observed that the stirring speed had a significant effect onto the enzymatic degradation of SPIs, resulting in accelerated enzyme degradation and accumulation at the air-buffer interface. To determine the adequate stirring speed, experiments were conducted in collaboration with Eugen Schell.

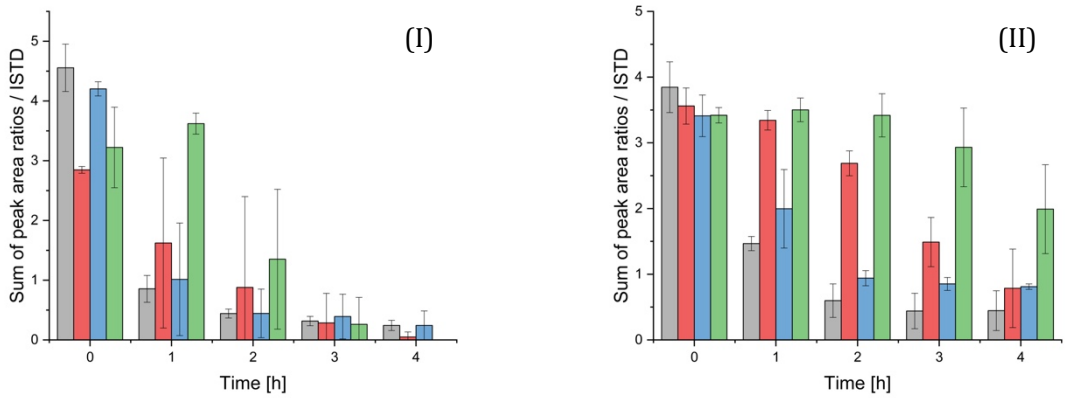

Figure 27. Enzyme stability with emulsion, PI, *n*-hexadecane and KPi buffer at 700 rpm (I) and 450 rpm (II). Co-solvent stabilized system of **PI 3000** (**C 1**) (grey), **PI 3000** (red), *n*-hexadecane (blue) and KPi (green).

The activity of the enzyme Lcp_{K30} was assessed after stirring for different durations at the respective stirring speed, in the presence of either *n*-hexadecane, KPi, **PI 3000** or **C 1** at room temperature. The enzyme was then transferred into a reaction set up for the enzymatic degradations with **L 1** and subsequent degradation studies in triplicates at room temperature were conducted. Figure 27 shows the cumulative product peak areas of these degradation fragments, which correspond the enzyme's stability in the presence of either *n*-hexadecane, **PI 3000** or both. It becomes evident, that the enzyme stability is significantly diminished with large standard deviation at 700 rpm (Figure 27 (I)), whereas higher enzyme stability was observed for 450 rpm (Figure 27 (I)). Consequently, 450 rpm was used for further investigations into the enzymatic degradation of SPI. Additionally, these investigations revealed the effect of the combining of *n*-hexadecane and **PI 3000**. The combination of both led to a cumulative decrease in the enzyme's stability. But it is noteworthy that the stability of the enzyme also diminished significantly in the presence of KPi. Accordingly, one of the objectives of the subsequent studies was the protein-engineering of a more thermostable Lcp-Variant in collaboration with the Weissenborn group in further studies in chapter 3.4.

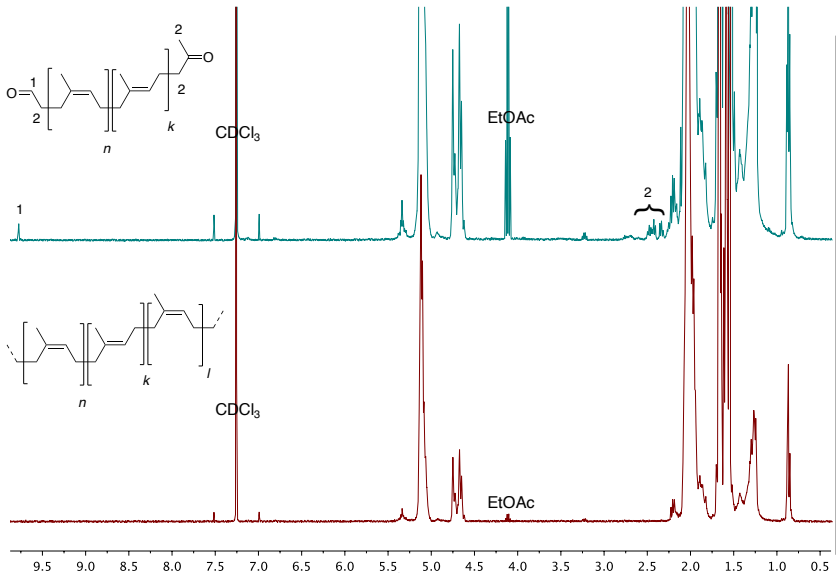

Figure 28. Stacked ^{1}H NMR spectra of degraded and extracted non-emulsified PI 3000 (**N 1**, blue) and the respective negative control without the addition enzyme.

Under the optimized conditions, the enzymatic degradation of **PI 3000** was conducted in triplicates, with the products pooled to enhance the degradation fragment concentrations while maintaining the

reaction scale. To allow for comparability with the established experiments of enzymatic degradation of latex milk, a w/v% for degradation studies was selected. This choice aligns with the most common practice in literature for Lcp_{K30},[112] facilitating consistency across all experiments.
Characterization of these degradation products by ^{1}H NMR revealed a peak at 9.76 ppm, corresponding to the aldehyde proton attached to a methylene group (Figure 28). According to the literature, signals generated between 2.2 and 2.4 ppm are indicative of the microstructure of protons adjacent to the methylene next to the aldehyde and ketonic end groups.[241] This microstructure is also reported in literature for the chemical and microbial degradations of NR, 1,4-cis-PI.[91, 137] This marks the first time that the enzymatic degradation of a SPI with a substantial *cis*: *trans* ratio of 56: 27 has been reported by ^{1}H NMR spectroscopy.

3.2.3 Comparative and optimized surfactant-free degradation studies of polyisoprene with Lcp_{K30}

Table 10. Surfactant-free PI systems with positive control latex milk with hydrodynamic diameters and emulsion stability.

Emulsions	ID	Diameter [nm][c]	Stability[d]
(A)			
PI 3000	**A 1**	800	14 h
(C)			
PI 3000	**C 1**	280	8 d
PI 14000	**C 2**	270	5 d
PI cis 7000	**C 3**	n. e.	n. e.
(L)			
Latex milk	**L 1**	750	n. d.

[c]Determined by DLS. [d]Determined by transmittance study at a threshold of 20% transmittance; n. e. = no emulsion formed; n. d. = not determined

Natural latex milk comprises from a white colloidal suspension primarily composed of both rubber and non-rubber particles.[15] To mimic such a well-dispersed PI system, two surfactant-free preparation methods were investigated in Chapter 3.1: an acoustic methodology (A) and a co-solvent stabilized (C) emulsification. For a comprehensive evaluation of different PI emulsions, four different degradation set ups were examined and compared: the non-emulsified PIs (**N 1-3**), PI and potassium phosphate buffer (KPi), the acoustically and surfactant-free emulsified **PI 3000** (**A 1**), PI and KPi, the surfactant-free and co-solvent emulsified PIs (**C 1-3**), PI, KPi and the hydrocarbon *n*-hexadecane as co-solvent, and the natural latex milk and KPi (**L 1**) (Table 10). The acoustically emulsified **A 1** showed broad size distributions of 800 $\pm$ 300 nm according to DLS and a stability of 14 h according to transmittance studies. The surfactant-free co-solvent stabilized emulsions of PI showed size distributions in dynamic light scattering measurements of 280 nm for **C 1** and 270 nm for **C 2**. Both exhibit stabilities far exceeding the reaction time intended for the enzymatic degradation. **C 3** was partially emulsified but did not lead to distinct size distributions in DLS. **L 1** was included in the comparative study as the model substrate.

3.2.3.1 Enzymatic degradation of surfactant-free emulsions of polyisoprene by Lcp_{K30} according to UHPLC and ESI-TOF-MS

The different dosage forms were subjected to the identical enzymatic degradation procedure to ensure comparability. UHPLC measurements were performed of the extracted degradation products, revealing distinctive degradation patterns that correlated to the retention times of **L 1** for all samples. For verification that the UHPLC peaks correspond to the oligoisoprenoidic degradation fragments of **L 1**, ESI-TOF-MS was conducted, and the results were summarized in Table 11. The mass of the respective degradation fragment should remain consistent regardless of the isomeric motif. In ESI-TOF-MS, the detected mass remains identical irrespective of the microstructures of PI, including any variations in constitutional or stereoisomerism.

Table 11. Degradation fragments detected by enzymatic cleavage by Lcp_{K30} according to ESI-TOF-MS

Number of intact isoprene units	m/z $[M+Na+CH_3OH]^+$ (calculated)	**N 1** (measured) $[m/z]$	**N 2** (measured) $[m/z]$	**N 3** (measured) $[m/z]$	**A 1** (measured) $[m/z]$	**C 1** (measured) $[m/z]$	**C 2** (measured) $[m/z]$	**C 3** (measured) $[m/z]$
4	427.32	427.32	427.31	427.31	427.32	427.32	427.31	427.32
5	495.38	495.40	495.37	495.37	495.40	495.40	495.38	495.38
6	563.44	563.47	563.44	562.42	563.46	563.46	563.44	563.44
7	631.50	631.53	631.51	631.50	631.52	631.52	631.51	631.50
8	699.57	699.62	699.57	699.55	699.57	699.58	699.57	699.56
9	767.63	767.65	767.63	767.61	767.65	767.65	767.62	767.62
10	835.69	835.72	835.69	835.68	835.72	835.71	835.69	835.68

The mass-to-charge ratio (m/z) of the respective extracted degradation fragments in ESI-TOF-MS revealed that the measured m/z ratios for all the samples were in good accordance with the calculated values.

3.2.3.2 UHPLC-ESI-MS of the surfactant-free synthetic polyisoprene emulsions

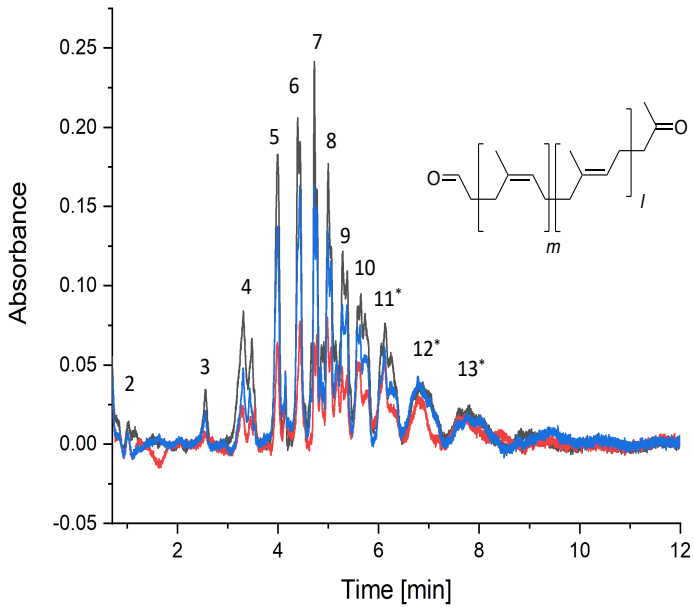

Figure 29. Stacked UHPLC-UV-chromatograms of enzymatically degraded **PI 3000** with the assigned degradation fragments (number of intact isoprene units (m + l)). Co-solvent stabilized (**C 1**, black); acoustically stabilized (**A 1**, blue); non-emulsified (**N 1**, red). Numbers with * were detected with an Orbitrap Elite mass spectrometer, others with QTOF-System.

To verify the correspondence of UHPLC peaks with the respective mass-to-charge ratios, ultra-high-performance ultraviolet-electron spray ionization high-resolution quadrupole time-of-flight mass spectrometry (UHPLC-UV-ESI-QTOF-HRMS) measurements were performed with Annegret Laub, at 210 nm wavelength (λ) for **N 1**, **C 1**, and **A 1**. UHPLC-ESI-QTOF-MS combined the benefits of UHPLC and ESI-MS, providing high-resolution chromatography and highly accurate mass measurement within a single platform, facilitating the comprehensive degradation fragment analysis, characterization, and correlation between UHPLC peaks and m/z ratios. Figure 29 shows the typical pattern of oligo-isoprenoids for Lcp_{K30},[112] varying in the number of intact isoprene units (m + l = 2–10) for **PI 3000**-derived degradation fragments from **N 1**, **C 1**, and **A 1**. The correlation between the UHPLC peaks and ESI-HRMS mass-to-charge ratios was successfully detected. Emulsified samples **C 1** and **A 1** exhibited distinctively more degradation products according to the UHPLC-UV chromatograms than the non-emulsified **N 1**, with **C 1** displaying the highest abundance of degradation products. The broadening of signals in the UHPLC-UV chromatograms could stem from the varying regioisomers in the degradation fragments of SPI, particularly when compared to the all-*cis* **L 1**. The presence of different microstructures in **C 1** can result in different composition of regioisomers within the degradation fragments. This resulted in broadening of the product peaks, caused by the isomeric motifs interacting differently with the reversed phase C8 column.

Comparative analysis between **L 1** and **C 1** in the UHPLC-ESI-QTOF-MS data indicated that the m/z ratios were detected at similar retention times and were in good accordance with the calculated m/z ratios. However, HRMS analysis of the SPI samples revealed that the m/z ratios of the longer-chain degradation fragments could not be ionized under the given ESI spray conditions and were therefore not detected by the TOF analyzer. Consequently, UHPLC-ESI-HRMS measurements using an Orbitrap system to detect the longer chain PI degradation products with 11-13 intact isoprene units were conducted with Annegret Laub (Table 12). An Orbitrap mass spectrometry system can offer a superior mass accuracy and resolution compared to a Q-TOF system, because of the ability to trap ions in an electrostatic field and measures their oscillation frequencies to determine their m/z ratios. This makes an Orbitrap mass spectrometry system more suitable for the precise and high-resolution analysis of complex molecules. This was deemed necessary for the detection of the difficult to ionize long oligoisoprenoidic degradation fragments, which could be difficult to ionize, due to their hydrophobic nature, potentially uneven charge distribution and limited solubility in the solvent. These factors could hinder their efficient entry into the ionization process and contribute to the poor ionization efficiency observed in UHPLC-ESI-QTOF-MS.

Table 12. Degradation fragments generated by enzymatic cleavage of **C 1** by Lcp_{K30} according to UHPLC-ESI-HRMS in positive ion mode

Number of intact isoprene units	$[M+H]^+$ measured	$[M+H]^+$ calculated	Elemental Composition	RDBE[a]
1	169.1224	169.1223	$C_{10}H_{17}O_2^+$	2.5
2	237.1850	237.1849	$C_{15}H_{25}O_2^+$	3.5
3	305.2475	305.2475	$C_{20}H_{33}O_2^+$	4.5
4	373.3096	373.3101	$C_{25}H_{41}O_2^+$	5.5
5	441.3725	441.3727	$C_{30}H_{49}O_2^+$	6.5
6	509.4346	509.4353	$C_{35}H_{57}O_2^+$	7.5
7	577.4969	577.4979	$C_{40}H_{65}O_2^+$	8.5
8	645.5595	645.5605	$C_{45}H_{73}O_2^+$	9.5
9	713.6230	713.6231	$C_{50}H_{81}O_2^+$	10.5
10	781.6857	781.6857	$C_{55}H_{89}O_2^+$	11.5
11	849.7474	849.7483	$C_{60}H_{97}O_2^+$	12.5
12	917.8104	917.8109	$C_{65}H_{105}O_2^+$	13.5
13	985.8733	985.8735	$C_{70}H_{113}O_2^+$	14.5

[a]RDBE = ring double bond equivalent;

The $[M+H]^+$ and $[M+H-H_2O]^+$ ions of the different degradation products detected in both UHPLC-(UV)-ESI-HRMS measurements of **N 1**, **C 1** and **A 1**, as well as of the natural latex milk **L 1**, were not observed in the corresponding negative controls.

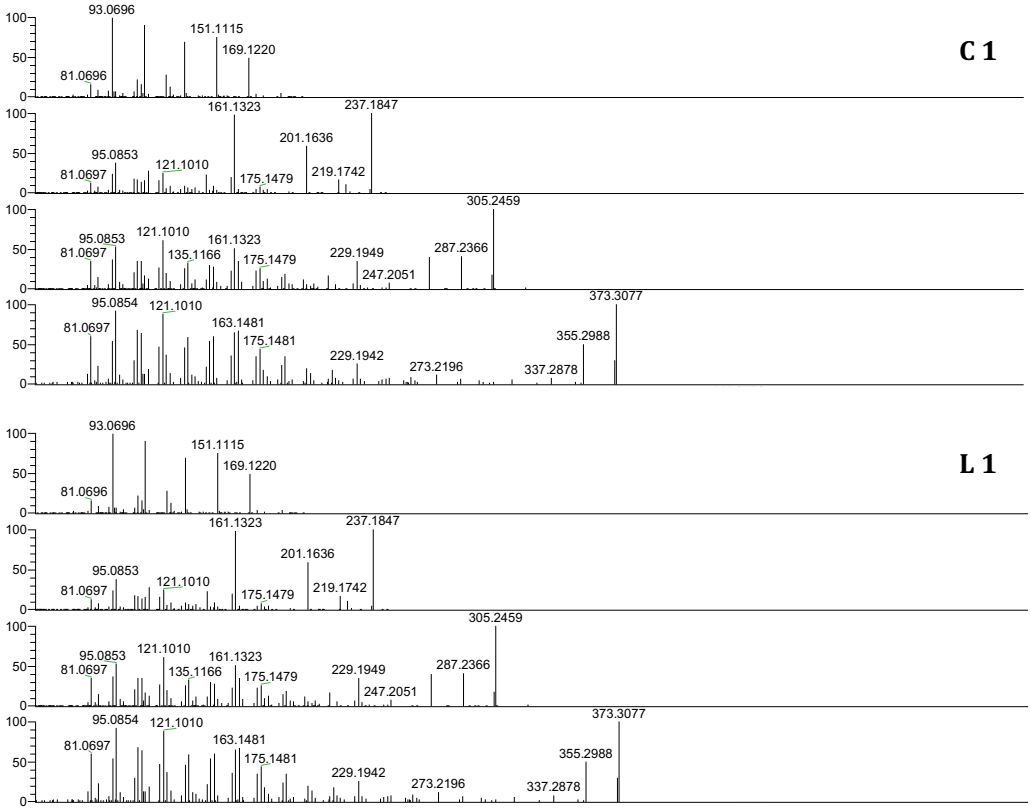

Figure 30. Comparison of the positive ion UHPLC-ESI-HRMS/MS spectra of the detected degradation products of **C 1** (top) to **L 1** (bottom).

For verification that the detected degradation products are indeed the same chemical species UHPLC-ESI-HRMS/MS spectra were measured. **C1** degradation fragments showed a distinct fingerprint (Figure 30, **C 1**), matching the UHPLC-ESI-HRMS/MS measurements of the degradation fragments of **L 1** (Figure 30, **L 1**). This proves that the degradation fragments of the SPIs are indeed the identical oligoisoprenoidic degradation fragments as observed for the products of the enzymatic degradation of **L 1**.

3.2.3.3 Influence of emulsification onto the enzymatic degradation

Table 13. Qualitative data of the enzymatic degradation with Lcp_{K30} of the investigated polymers

Emulsification Strategy	ID	Area integration	Emulsification effect
non emulsified:			
PI 3000	**N 1**	560 (±308)	n. e.
PI 14000	**N 2**	340 (±155)	n. e.
PI *cis* 7000	**N 3**	1290 (±460)	n. e.
A:			
PI 3000	**A 1**	1860 (±301)	200%
C:			
PI 3000	**C 1**	2860 (±359)	400%
PI 14000	**C 2**	420 (±120)	20%
PI *cis* 7000	**C 3**	2640 (±280)	100%
L:			
Latex milk	**L 1**	13000 (±250)	n. d.

The effect of emulsification onto the degradation process was evaluated with a comparative analysis of standardized experiments using UHPLC-UV chromatograms. The analysis compared non-emulsified degradation experiments and emulsified degradation experiments, with the exclusion of the background signals through the usage of negative controls (Table 13). Experiments were executed in a standardized manner, following protocols that had been established and optimized in the preceding chapters. To ensure the production of valid and representative qualitative data, the experiments were conducted in triplicates, in a parallelized manner with corresponding negative controls. Additionally, the same batch of enzyme was consistently employed to minimize and mitigate the effect of potential enzyme stability fluctuations, thereby improving the statistical validity of the enzymatic degradation comparison. Negative controls were prepared by using the same PIs but excluding the addition of the enzyme Lcp_{K30} and instead replacing it with phosphate buffer, thereby ensuring consistent weight/volume percentages of the respective PI to the solvent. The determination of the area of integration was performed using the software Origin. It should be noted that the error associated with the area of integration remained relatively constant across all samples, with a slight exception for **PI 15000** (Table 13). However, this error may appear relatively high when compared to the area of integration for the non-emulsified samples (Table 13, **N 1**-**2**). This could arise from the low level of degradation without emulsification, which allows UV-active contaminants of the SPIs as well as the latex milk and the baseline noise to influence the integrated chromatogram area. Nonetheless, our investigated area was not confined solely to the absorbances of the latex milk due to the presence of various isomeric motifs in the SPIs (Table 9).

Consequently, the integration area can be regarded as indicative of the different degradation products. In the case of **A 1**, it was found to be 200% higher than for **N 1**, signifying an improved polymer accessibility to the enzyme in the acoustically emulsified system (Table 13). This result underscored the substantial impact of acoustical emulsification onto the enzymatic degradation rate of Lcp_{K30} towards **PI 3000**. The accessibility of PIs to enzymatic degradation, as well as the exposed surface area towards enzymatic degradation was significantly improved by the acoustical emulsification process.

To ensure enzyme activity a control experiments with **L 1** were conducted, which resulted in significant higher area of integration than the SPI, due to the 1,4-*cis*-isomeric motif as well as the emulsification of the latex in the aqueous medium (Table 13).

The partial emulsification of **PI *cis* 7000** as **C 3** with a co-solvent demonstrated that even highly metastable and polydisperse emulsions could result in an increase of the integration area for naturally derived 1,4-*cis*-PI by 100%. In the absence of the inherent emulsifying properties of natural latex milk,[15] the degradation of **PI *cis* 7000**, a 1,4-*cis*-PI, with the enzyme Lcp_{K30} lead to an improved surface area and, consequently, increased availability for the enzymatic degradation. This had an effect onto the production of oligoisoprenoidic degradation fragments of varying lengths but with consistent terminal functions.[138] This further indicates the correlation between emulsification and degradation rate mediated by the rubber oxygenase Lcp_{K30}.

However, the co-solvent emulsification of **C 2** did not significantly affect the enzymatic degradation. The area of integration according to UHPLC revealed that the degradation was more pronounced for **PI 3000** and **PI *cis* 7000** than for **PI 14000** systems. The lower emulsification effect for **C 2** could be explained by the weaker stabilizing effect of the comparatively high molecular weight polymer with the limited amount of *n*-hexadecane. [179]

A higher molecular weight could require a higher volume for the co-solvent to dissolve the hydrophobic **PI 14000** more effectively. The solubility of hydrophobic polymers like PI in a co-solvent emulsification system is dependent on the interaction between the polymer and the solvent. Higher molecular weight PIs have a greater number of repeating units, resulting in larger, bulkier molecules that may have lower solubility in the respective co-solvent or require an increased volume of the co-solvent, which could have detrimental effects onto the enzymes stability. Furthermore, **PI 14000** in **C 2** is interacting more pronounced with itself due to the increased intermolecular interactions in the longer polymer chain than the **PI 3000** in **C 1**, resulting in less exposure and consequently availability

for enzymatic degradations on the *n*-hexadecane droplet surface. This could be due to the van-der-Waals interactions that arise more pronouncedly in a longer PI chain. A longer polymer chain can lead to a more extensive and entangled structure, which could additionally create a greater degree of steric hindrance. This hindrance could potentially limit the enzyme's ability to approach and bind to the PI substrate effectively, especially if the PI is not well dissolved in the beneficial co-solvent, which should counteract this limitation.

In contrast, **PI 3000** in emulsion **C 1**, with a well-dispersed 1:1 *n*-hexadecane ratio, appears to be significantly better exposed and available for enzymatic degradation on the surface of the *n*-hexadecane droplets. Unsurprisingly, this emulsion **C 1** demonstrated also the best stability as an emulsion in the conducted transmittance studies. Zeta potential measurements were conducted (chapter 3.1), revealing a relatively high value that suggest a greater repulsion of individual co-solvent PI droplets for **PI 3000**. This result indicates, that for the investigated **C 1**, the conformation of the PI chains of **PI 3000** at the investigated ratios of co-solvent to polymer lead to a more extended polymeric structure compared to the probably more coiled conformational structure of **PI 14 000**. This conformational structural discrepancy could have led to an enhanced accessibility for enzymatic degradations and could have had a significant beneficiary influence onto the degradation rate. The improved emulsification effect of the metastable co-solvent stabilized system **C 1** resulted in a remarkable increase in the area of integration of 400% when compared to **N 1** in triplicate experiments (Table 13).

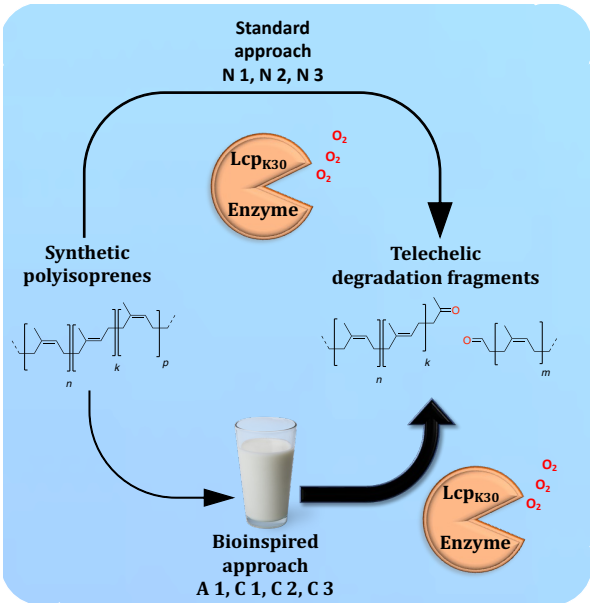

Figure 31. Visualization of the effect of the bioinspired surfactant-free emulsifications (**A 1**, **C 1**, **C 2**, **C 3**) beneficiary effect onto the enzymatic degradation of SPIs with a significant ratio of other isomeric motifs than 1,4-*cis*-PI in comparison to the non-emulsified approach (**N 1**, **N 2**, **N 3**).

The UHPLC-UV comparative analysis of the standardized enzymatic degradation experiments clearly showed that the bioinspired emulsification approach with either acoustical emulsification or co-solvent emulsified system led to a significant improvement of area of integration and therefore to more oligosioprenoidic degradation fragments (Figure 31). For **C 1** the improvement was 4-fold in comparison to the non-emulsified samples, which barely was degraded according to the UHPLC-UV chromatogram.

3.2.3.4 Enzyme stability investigations in the presence of synthetic polyisoprene, *n*-hexadecane, and surfactant-free emulsion

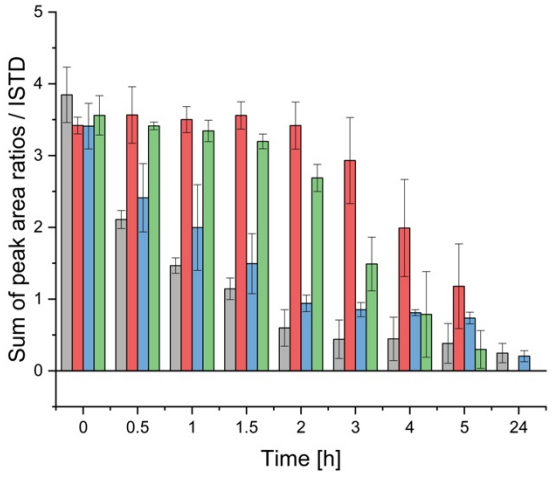

Figure 32. Enzyme degradation capability tracking over 24 hours. **C 1** (grey), **PI 3000** (red), *n*-hexadecane (blue) and KPi (green).

For a more comprehensive assessment of the impact of the emulsified systems onto the enzyme Lcp_{K30} itself, an enzyme stability experiment was designed with Eugen Schell. The enzyme was subjected to a storage condition in the presence of either **C 1**, **PI 3000**, *n*-hexadecane or KPi. Subsequently, the storage stability was evaluated according to a standardized experiment with **L 1**, and then investigating the resulting characteristic oligoisopreoidic degradation fragments[152] with UHPLC-UV chromatogram analysis in triplicates. To gain insights into the enzyme stability over time, multiple time points were evaluated (Figure 32). The kinetics of enzymatic degradation of Lcp_{K30} were also investigated in later investigations (Appendix), revealing that the enzymatic degradation is quick in the initial hours but then plateaus. Lcp_{K30} exhibited the longest residual activity for the co-solvent stabilized system (**C 1**) and the negative control of *n*-hexadecane in KPi 5 mM buffer. However, the initial enzyme stability seemed to notably decrease in the presence of **C 1**, which was correlated with enzyme decomposition during the degradation of **C 1**, resulting in less active enzyme available for the subsequent degradation of **L 1** in the activity and stability determination step. The mere presence of *n*-hexadecane resulted in a reduction in enzymes stability, observed already after 30 minutes. This unexpected detrimental effect onto the enzyme's stability came as a surprise. Especially in comparison to the enzyme's stability in the presence of the hydrophobic **PI 3000**, which did not clearly reduce the enzyme's stability but appeared to have stabilized the enzyme over the course of the investigation (Figure 32). The negative control with KPi, without the presence of any additional entities, demonstrated that the enzyme is decomposing over time, potentially due to the mechanical forces of stirring (Figure 27). Interestingly, only the samples containing **C 1** and *n*-hexadecane exhibited residual enzymatic activity after 24 hours, which could be attributed to the stabilization of the enzyme at the hydrophilic and hydrophobic interfaces within the systems, offering a larger surface area than the **N 1**.

It is noteworthy that, even though the enzyme's deactivation was observed to be higher in **C 1**, it still resulted in a significant increase in the area of integration (Table 13) for **C 1** when compared to **N 1** (PI 3000). This accentuates the immense effect that the emulsification seemed to have had onto the enzymatic degradation even further.

The acoustic and co-solvent stabilized emulsification of SPI in water without surfactant to form metastable bioinspired colloids for improved enzymatic degradation with Lcp_{K30} can be reported. The tolerance of Lcp_{K30} towards other isomeric motifs than the *cis*-isomer of PI shows its potential as a

sustainable degradation catalyst for polymers, which require new sustainable methodologies of recycling.
Analysis of the gel permeation chromatograms of the SPI scope (Table 9) did not lead to reproducible significant shifts in the retention volume. This showed that the degradation of the non-all *cis*-isomers with the rubber oxygenases required either an improvement of the enzyme by directed evolution or the implementation of new rubber oxygenase degradation assays.

3.2.4 Degradation studies of polyisoprene with Lcp_{K30}-P7

The degradation efficiency of the rubber oxygenase Lcp_{K30} was significantly influenced by the dosage form when degrading low molecular weight SPIs. However, another hurdle arises in case of solid rubber polymers due to their structural integrity, which hinders accessibility for rubber degrading enzymes. Surfactant-free emulsification has demonstrated the ability to circumvent this by the utilization of co-solvents or acoustical emulsification of the SPIs. While this approach increases the substrate's accessibility by enlarging the interface, the use of co-solvent can lead to a heightened risks of denaturation of the enzyme. Additionally, the biotransformation of 1,4-*cis*-PI in multiphase enzymatic reactors, aimed at the continuous extraction of oligo-isoprenoid molecules,[186] could benefit greatly from more robust Lcp-Variants. This methodology together with a more effective, distinctively solvent-stable and kinetically longer enzymatically active, PROSS-variant in tandem with sustainable organocatalytic depolymersation could have a positive effect onto sustainable polyene degradation in regards to circular polymer chemistry.[11] Especially with a corresponding, specifically automated, degradation assay for the various degradation fragments. At first, enhancements in temperature stability can potentially be associated with improved enzyme stability against various solvents, as well as other critical factors that could contribute to an increased degradation rate or prolonged enzymatic activity.[242-244] Notably, this correlation is not straightforward, because the catalytic activity can be complex and is influenced by various factors, including the specific mutations introduced and the prevailing environmental conditions.[245] But bolstering protein stability became imperative to have a better platform for future investigations in the sustainable degradation of polyenes.[246] To address these challenges, a rational engineering process employing a PROSS algorithm[196] was conducted in cooperation with Eugen Schell and Yannick L. Wolf and then investigated in collaboration for a novel approach. Initially, efforts may focus on enhancing the thermostability of the outer sphere of a rubber oxygenase, followed by active, rational engineering of the active center but with a need for future engineering to further refine these processes.[247, 248]
The PROSS algorithm is a computational tool specifically designed to improve the thermostability, solubility as well as the expression rates of enzymes through protein engineering. Through the identification and recommendation of amino acid substitutions, PROSS offers a systematic and rational approach to enhance enzyme resilience at elevated temperatures, thereby expanding their potential applications in various biotechnological processes.[196, 249] It is noteworthy that all suggested mutations are located outside the active center of the enzyme and, as such, should not directly impact the enzyme's activity. But should be used preferably surfactant-free and with minimized stress on the respective optimized enzyme without the usage of excessive amounts of water and preferably with biobased solvents, which could potentially also improve catalytic efficiency synergistically in future optimization rounds to a better catalyst.[200, 244]

3.2.4.1 Characterization of PROSS variants of Lcp_{K30}

The cooperation partner applied the PROSS algorithm after discussions of the most beneficial mutations and cultivated the respective potentially applicable Lcp-PROSS variants. Expression of the enzyme variants, except for Lcp_{K30}-P1 and Lcp_{K30}-P2, lacked behind the protein expression of the wild type Lcp_{K30} but was nonetheless acceptable for further investigation of the variants.[250] Improved

protein expression is commonly expected from mutagenesis but due to, the aforementioned, complex interactions it does not directly correlate to all aspects of applicability. Especially in a heme-containing enzyme like Lcp rubber oxygenases, where the incorporation of the iron can be challenging.[244, 249, 251, 252] This was also reported for the Lcp from *Gordonia polyisoprenivorans VH2*, which showed that in that case an interaction with histidine was of crucial importance for the non-covalent association of heme-b as a cofactor[253] as well as for Rox rubber oxygenases by Birke *et.al*.[112]

To assess the stability of the respective Lcp-PROSS-variants, their thermostability was determined by Eugen Schell using Nano Differential Scanning Fluorimetry (NanoDSF), which is a commonly used biophysical technique to analyze protein thermal stability, unfolding and refolding behavior. It can monitor changes in the intrinsic fluorescence as a function of temperature, which can provide valuable insights into protein stability, folding, and interactions.[214, 249, 254] The melting temperature of the different PROSS engineered Lcp-variants and the corresponding Lcp_{K30} (wild type) were determined in triplicates (Table 14).

Table 14. Lcp_{TM} values of Lcp_{K30} and PROSS variants according to Nano-DSF-measurements.

Lcp-Variant	Mutations	Mutations [%]	Average [°C]	SD [°C]
Lcp_{K30}(Strep)opt	-	-	45.9 °C	0.2 °C
Lcp_{K30}(Strep)opt-GFP11	-	-	46.0 °C	0.2 °C
Lcp_{K30}-P1	16	4.31	45.8 °C	0.3 °C
Lcp_{K30}-P2	26	7.1	69.7 °C	0.2 °C
Lcp_{K30}-P3	30	8.09	69.9 °C	0.2 °C
Lcp_{K30}-P4	33	8.89	65.4 °C	0.7 °C
Lcp_{K30}-P5	42	11.32	75.4 °C	0.3 °C
Lcp_{K30}-P6	47	12.67	73.2 °C	1.7 °C
Lcp_{K30}-P7	54	14.56	74.6 °C	0.2 °C
Lcp_{K30}-P8	65	17.52	80.8 °C	0.4 °C
Lcp_{K30}-P9 1. Elution	84	22.64	78.5 °C	0.3 °C
Lcp_{K30}-P9 2. Elution	84	22.64	80.2 °C	0.2 °C

The results of the thermostability measurements with NanoDSF revealed a clear positive correlation between the extent of mutations and the corresponding improvements in thermostability with acceptable standard deviations (SD). The variant with the fewest mutations, Lcp-PROSS-P1, did not exhibit any significant enhancement in thermostability (Table 14). In contrast, the other variants P2 through P6 demonstrated an increase in their melting temperature (T_m) by approximately 24 °C without the detection of a refolding of the enzyme. The most substantial improvements of thermostability were observed, with an increase in T_m of roughly 34 °C, for the Lcp-PROSS variants P7 to P9 (Table 14). Such an enhancement in thermostability shows the effect of protein engineering with the PROSS algorithm.

The most promising candidate for further investigations, balancing a high thermostability, favorable expression behavior and enzymatic activity against **L 1**, was identified as Lcp_{K30}-P7. Because PROSS variants were expected to exhibit enhanced stability due to their PROSS-induced mutations, kinetic studies were conducted over a 24-hour reaction time, comparing the wild type enzyme with the most promising variant, Lcp_{K30}-P7. These investigations revealed an overall lower reaction rate for the more thermostable protein variant. However, the enzyme's activity duration was considerably extended. In accordance with the expectation of enhanced enzyme stability with increased thermostability. The degradation studies were conducted with **L 1** and sampling at specific time intervals for analysis with UHPLC. This extended enzymatic activity was accompanied by an increased production of degradation fragments with lower degrees of isoprenoidic repeating units, further evidenced by separate UHPLC-ESI-HRMS stack measurements. To establish a correlation and validate the data obtained from the kinetic studies with UHPLC, UHPLC-ESI-HRMS measurements were conducted to align the retention times with the oligoisoprenoidic degradation fragments.

Investigations with SPIs, whether in non-emulsified, acoustically emulsified or co-solvent emulsified dosage forms, under various reaction conditions, such as reaction time, enzyme concentration, or KPi concentrations, did not lead to significantly more degradation fragments than the Lcp_{K30} wild type, according to HPLC, ESI-TOF-MS, GPC, UHPLC and UHPLC-ESI-HRMS analysis. This suggests that the mutations did not have a beneficial effect onto the acceptance of other isomeric motifs. One possible reason is that the active center and substrate channel where not substantially altered through the rational protein engineering algorithm. This might be requiring mutagenesis at the active center, which could enhance the enzymatic activity towards non-1,4-*cis* isomeric motifs.

3.2.4.2 Degradation studies after thermal stress on the variants

Enzymatic degradation studies of **L 1** were conducted to investigate whether the enzymatic activity of PROSS-variants would persist after incubation at elevated temperatures. Specifically, incubation at 60 °C of the respective PROSS-variants P2 to P7 was investigated to assess their residual activity after incubation to determine, which PROSS-variant would retain its catalytic activity. The separate incubation was necessary to investigate the thermal stress resistance and remaining enzymatic activity because of the susceptibility to denature at elevated temperature. Interestingly, the PROSS-Variant P7 seemed to have retained almost 100% of its original enzymatic activity towards **L 1** after incubation and reaction times of one hour in preliminary experiments with Eugen Schell. Consequently, it was concluded that for PROSS-Variant P7, incubation did not lead to a significant reduction in the production of degradation fragments of **L 1** as indicated by UHPLC-analysis.

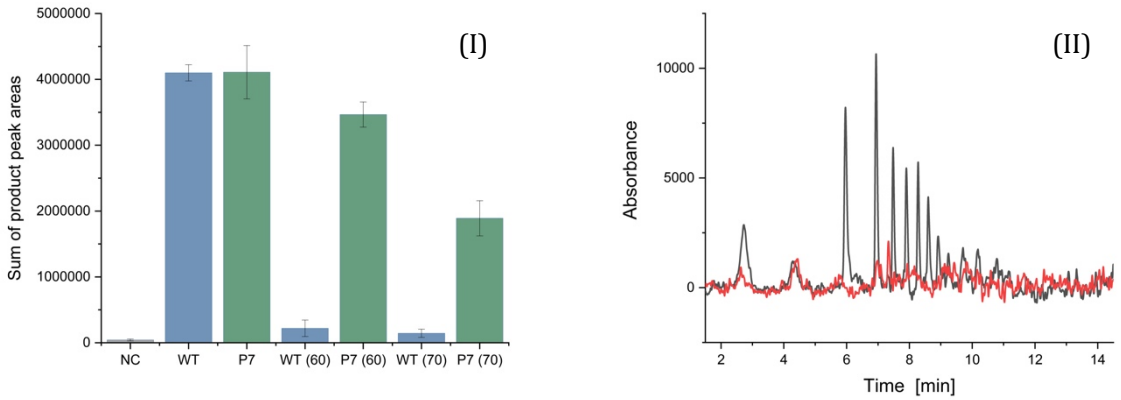

Figure 33. Cumulative area of the degradation fragments of the enzymatic degradation of **L 1** according to UHPLC-UV-ESI (I) and corresponding UV-chromatogram of Lcp_{K30}-P7 (II) incubated at 60 °C (black) and Lcp_{K30}-WT incubated at 60 °C (red).

For this most promising variant standardized degradation studies with **L 1** with incubation at 60 °C or 70 °C were conducted, with corresponding negative controls either without incubation at elevated temperatures or without the presence of enzyme in triplicates. The phosphate buffer concentration was adapted according to KPi optimum determination studies by Yannick L. Wolf. Furthermore, the reaction time was extended to 24 hours to leverage the kinetics of the Lcp_{K30}-P7. The samples were investigated using UHPLC-ESI-HRMS to directly correlate the mass of the degradation fragments to the UV-absorption. The resulting data was analyzed automatically with XCalibur and revealed that the cumulative area of the degradation fragments for Lcp_{K30}-WT at 60 °C and 70 °C was in stark contrast, almost approaching baseline levels to the Lcp-P7 variants under these conditions (Figure 33). The residual activity of Lcp_{K30}-P7 did not approach the same level as in preliminary investigations but was nonetheless significantly higher than the apparently denaturated Lcp_{K30}-WT. Additionally, Lcp_{K30}-P7 remained catalytically active even after incubation at 70 °C. The positive controls without incubation

proved that the Lcp_{K30}-WT was, catalytically active, whereas the negative controls showed that there were no absorptions without the presence of enzymes.

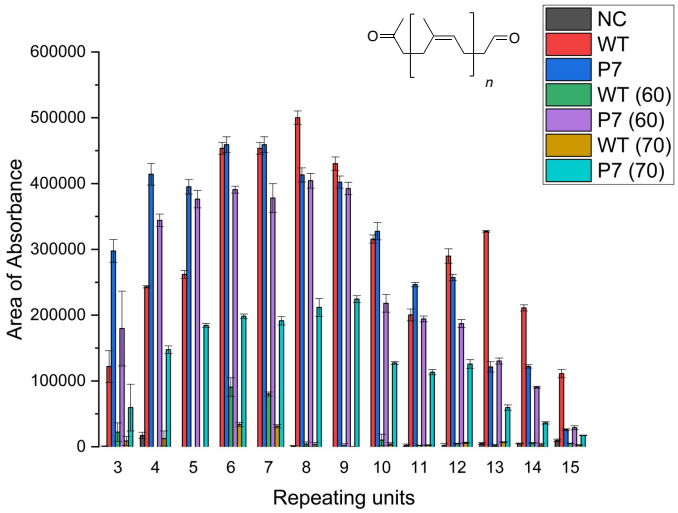

Figure 34. Comparison of residual UV-area of the degradation fragments peaks according to UHPLC-ESI-HRMS integration (*n* = repeating units)of the enzymatic degradation of **L 1**. Negative control = black; Lcp_{K30} WT = red; Lcp_{K30}-P7 = blue; Lcp_{K30} WT 60 °C incubated = green; Lcp_{K30}-P7 60 °C incubated = purple; Lcp_{K30} WT 70 °C incubated = brown; Lcp_{K30}-P7 70 °C incubated = light blue.

The UHPLC-UV-ESI-HRMS analytics measured and analyzed with A. Laub showed that through the quantitative analysis with Xcalibur the residual UV-area of the distinct degradation patterns were comparative to the Lcp_{K30} wildtype levels for small degradation fragments (Figure 34).

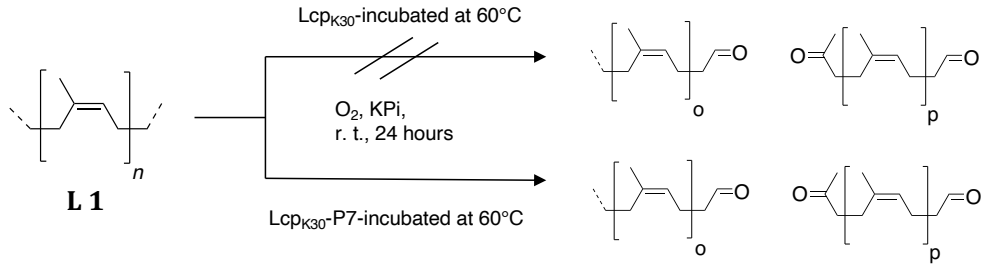

Scheme 11. Enzymatic degradation after incubation of **L 1** by Lcp_{K30} (WT) and Lcp_{K30}-P7.

The Lcp_{K30}-P7 remained catalytically active even after incubation at 60 °C after only one round of mutagenesis (Scheme 11), which on one hand proves the increased thermostability of the enzyme as well as the significant effect of the rational engineering PROSS algorithm.[196] For a deeper understanding of the enzymatic degradation, it was necessary to implement, test and optimize a new methodology tailored for the degradation of rubber oxygenases. This methodology applies GPC to understand the scope not under a lens but also from a broader macromolecular perspective and context.

3.2.5 Rubber Oxygenase Degradation Assay by UV-labelling and Gel Permeation Chromatography

The enzymatic degradation of low molecular weight SPIs showed that the dosage form played a crucial role in the degradation efficacy of the rubber oxygenase Lcp_{K30}. However, to further enhance the understanding and improve the sustainable enzymatic degradation of synthetic polyenes and to screen for the enzymatic activity of rubber oxygenases towards not only SPIs but also polybutadiene, even at low enzymatic activity, new analytical methodologies were required.
The analysis of enzymatic and bacterial rubber-degrading activity had been mostly limited to synthetic high molecular weight PI of usually 96% 1,4-*cis*-content, high molecular weight PB and NR so far.[5, 255] The occurrence of the aldehyde and keto-functionality end-groups of the oxidative degradation products can be proven by chemical methods for example by staining with Schiff reagent[255] or 2,4-dinitrophenylhydrazine[239] or spectroscopically by FTIR[148] and NMR spectroscopy.[255] U/HPLC-UV-MS had been used for the analysis of the molecular mass of mainly oligoisoprenoidic degradation products.[161] The derivatization with Girard reagent T was reported to enable better detection by positive-ion ESI-TOF-MS, which could be used as a further determent of new degradation behavior.[163] GPC has predominantly been utilized for determining the number-average molar mass of the initial polymer and for assessing the bioconversion of the polymer into its corresponding degradation products with refractive index detection.[255] This gives an additional macroscopic information about the degradation fragment nature.
But quantitative derivatization for the Schiff reagent, dinitrophenylhydrazine and Girard reagent T have not been shown specifically, and arguably generally, for PI and PB with aldehyde or keto end-groups.
There is currently no methodology to investigate the enzymatic degradation of either SPI or synthetic PB by gel permeation chromatography at low degradation activity or by standard UV detection methods with complete derivatization for high molecular weight polymers without side reactions at mild conditions. The lack thereof in the range between oligo and macroscopic degradation species needs to be better understood for effective, targeted future engineering endeavors. Inspired by recent advances in the derivatization strategies for oximes,[256, 257] a methodology for the detection of low enzymatic activity of the enzymatic degradation of SPIs and the potential detection of enzymatic degradation of synthetic PB by gel permeation degradation tracking of rubber oxygenase with a new UV-active derivatization methodology was implemented.

3.2.5.2 Establishment of derivatization methodology

Herein, a new methodology to track the enzymatic degradation of SPIs using a new derivatization strategy was investigated, which leads to a shift in the UV absorbance of the polymer that can be tracked with the UV-detector of a GPC. The derivatization strategy was firstly established with organochemically degraded polyenes. Subsequently, the applicability onto the enzymatic degradation was investigated. Synthetic PB was utilized because of the UV sensitivity and to implement the conversion to the oxime with the derivatization reagent *O*-(4-methoxybenzyl)-hydroxylamine hydrochloride with the two easily trackable aldehyde end-groups. In general, oxime conjugates obtained from ketones have higher stability than the respective aldehyde derivatives, which made the establishment of stable aldehyde derivatives at first crucial.[256] Other derivatization agents were screened, such as 2,4-dinitrophenylhydrazine (DNPH), but the best results in the preliminary investigations were obtained for *O*-(4-methoxybenzyl)-hydroxylamine hydrochloride (Scheme 12).

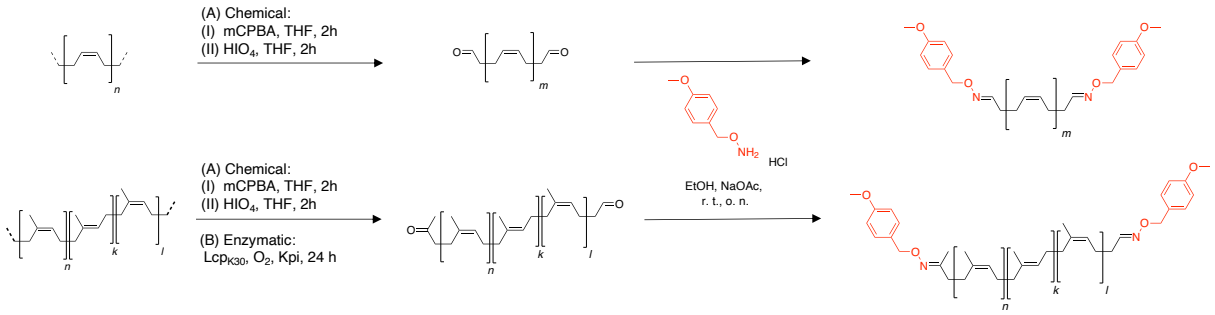

Scheme 12. Assay of chemical and enzymatic degradations of PI and PB with the derivatization strategy of the respective end-groups.

Table 15. Polymers chemically and enzymatically degraded and subsequent derivatized samples.

Polyenes	Microstructure [%][a]				M_n [g/mol]	PDI	ID	M_n [g/mol]	PDI
	3,4-units	1,4-units *cis*	1,4-units *trans*	1,2-units					
							PI 3000-Ox	1700	1.6
PI 3000	16	56	27	1	3100	1.1	**PI 3000-D**	1800	1.5
							PI 3000 WT-D	2600	1.1
							PI 4500-Ox	2300	1.5
PI 4500	16	56	27	1	4500	1.1	**PI 4500-D**	2400	1.5
							PI 4500 WT-D	3300	1.1
PB 3500	-	75	24	1	3500	2.0	**PB 3500-Ox**	2400	2.3
							PB 3500-D	2200	2.5
PB 12000	33	55	12	33	11500	1.2	**PB 12000-Ox**	5400	2.0
							PB 12000-D	5100	1.7
PB 200k	98	-	2	98	190000	1.3	**PB 200k-Ox**	6100	2.9
							PB 200k-D	5900	2.4

[a] Determined by ^{1}H NMR

The scope of the investigated synthetic polymers included the low molecular weight PI (**PI 3000**), which has previously been shown to lead to the most degradation products with the co-solvent based surfactant-free emulsification strategy, a PI of similar isomeric motifs but higher number average molar mass (**PI 4500**), a PB of low molecular weight but high *cis*-content (**PB 3500**), a PB of comparatively high *trans*-ratio (**PB 12000**) and a high molecular weight 1,4-*cis*-PB (**PB 200k**) (Table 15). **PB 3500** and **PB 12000** were investigated because of their relatively high *cis*-content and their molecular weight, which allowed for the formation of surfactant-free emulsions with a co-solvent (Chapter 3.1). This makes them good candidates for the potential enzymatic degradation investigations of synthetic PB with the co-solvent emulsified system approach. For telechelic polybutadienes with very defined end groups, it is best to start with precursors of the highest molar mass possible.[95] Consequently, a high molecular mass 1,4-*cis*-PB was included in the scope. The oxidatively degraded samples, e. g. **PI 3000-Ox**, and the derivatized samples, e. g. **PI 3000-D**, of the respective polymers, are listed in Table 15. The microstructure of the samples did not change significantly, as can be observed in the corresponding ^{1}H NMR spectra.

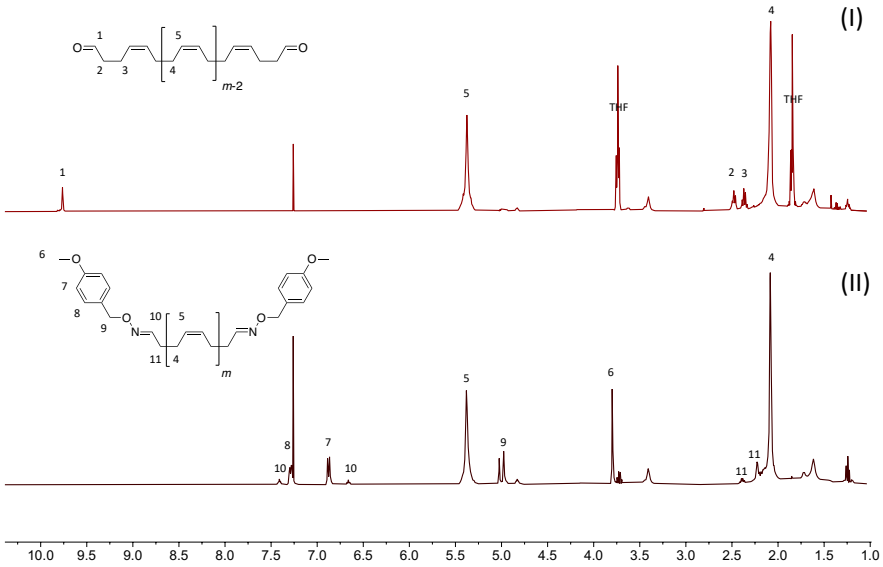

Figure 35. ^{1}H NMR spectra of the chemically degraded **PB 200k-Ox** (I) and the derivatized telechelic **PB-200k-D** (II).

PB 200k was degraded by epoxidation with mCPBA and subsequent oxidative chain cleavage of the epoxide C-C bond by periodic acid as reported in literature.[95] The resulting telechelic PB (**PB 200k-Ox**) was analyzed by ^{1}H NMR, GPC and UHPLC-ESI-HRMS (Appendix). **PB 200k-Ox** was then subjected to derivatization with *O*-(4-methoxybenzyl)-hydroxylamine hydrochloride and sodium acetate in ethanol overnight for derivatization.[258] ^{1}H NMR showed that the aldehyde proton (Figure 35, Index 1) at 9.77 ppm disappeared in the derivatized sample, and the adjacent methylene protons α to the aldehyde (Figure 35, Index 2/3) at 2.38 and 2.47 ppm changed as well. In the derivatized telechelic PB (**PB 200k-D**) the methyl group of the derivatization reagent was detectable at 3.80 ppm (Figure 35, Index 6), together with the aromatic protons at 7.30 and 6.88 pm (Figure 35, Index 7/8) and the methylene group at 5.0 ppm. The protons at 7.41 and 6.66 ppm could be assigned to the oxime proton of the respective *E*/*Z* isomer (Figure 35, Index 10).^{1}H-^{1}H correlation spectroscopy (COSY) NMR revealed that the proton of the *E*/*Z* isomers of the oxime at 7.41 and 6.66 ppm correlated to the protons at either 2.40 or 2.22 ppm. The assignment of the carbons with heteronuclear single quantum spectroscopy (HSQC) and heteronuclear multiple bond spectroscopy (HMBC) measurements also showed this correlation. This is a clear indication that the aldehyde functionality of the telechelic PB is fully converted with this derivatization strategy.

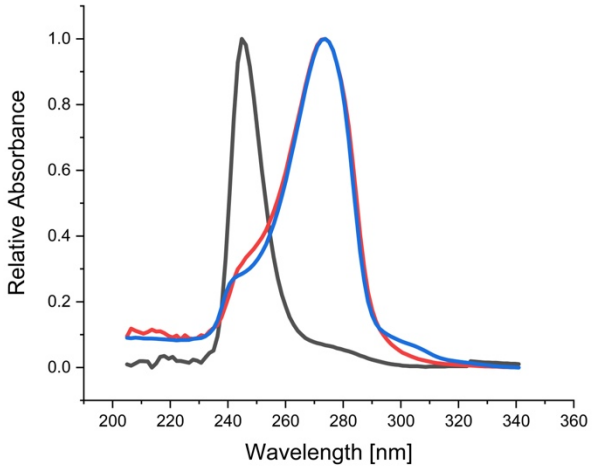

Figure 36. UV absorption spectra of the underivatized **PB 3500** (black), derivatized polymer **PB 200k-D** (red) and the derivatization agent (blue).

The derivatized sample, **PB 200k-D** was measured by GPC with a UV detector indicating absorption maximum shifts from 244 nm for an unreacted PB (Figure 36, black) to the absorption maximum of the free derivatization agent (Figure 36, blue) at 274 nm but with a shoulder of the PB backbone at 244 nm for **PB 200k-D** (Figure 36, red). The shift in the absorption maximum allows for the distinction between an unreacted polymer and the respective derivatized sample in the same GPC run by a change in the tracking wavelength from 244 nm to 274 nm for the investigated polybutadienes. Consequently, derivatization enables the detection of degradation activity at the derivatized UV absorption maximum of 274 nm for the respective polybutadienes, independently of the indirect molecular weight determination with standards.

To explore the boundaries of this method, mixtures of telechelic polymers and undegraded polymers were synthesized *via* chemical degradation. This approach enabled the examination of the derivatization strategy amidst a backdrop of unreacted polymer, simulating conditions anticipated for the enzymatic degradation of SPI with a significant *trans* ratio or synthetic polybutadienes with low enzymatic activity. The chemical degradations were conducted according to a modified procedure outlined by Pillard and co-workers,[95] who established and refined the chemical degradation of high molecular mass 1,4-*cis*-PI and 1,4-*cis*-polybutadiene. Initially, the polyenes were first epoxidized, followed by oxidative cleavage with periodic acid, with the mCPBA concentrations selected to achieve an epoxidation rate of approximately 2%. Theoretical and experimental epoxidation values, ranging from 0.7% to 1.5%, differ due to deviations in the microstructure of the internal double bonds in the investigated polyenes (Table 15) from the all *cis*-polybutadienes or all *cis*-PIs reported in the literature.[95] Periodic acid concentration was set to 1.2 equiv. of the respective mCPBA concentration to avoid a significant excess of the periodic acid, which could lead to an uncontrolled degradation of the double bonds in PI.[89] The molecular weights of **PI 3000-Ox**, **PI 4500-Ox**, **PB 3500-Ox**, and **PB 12000-Ox** decreased significantly, according to GPC (Table 15). ^{1}H NMR showed that the aldehyde proton at 9.77 ppm as well as the microstructure around the aldehyde appeared in all the chemically degraded samples. Determination of the $M_{n\,(\mathrm{NMR})}$ *via* end group correlation to the repetitive units in the polymer backbone led to higher values than the $M_{n\,(\mathrm{GPC})}$ due to the intended residue of undegraded polymer. Unreacted polyene does not result in telechelic end groups associated with the $M_{n\,(\mathrm{NMR})}$ resulting in a higher value than the respective $M_{n\,(\mathrm{GPC})}$, which is determined based on the relative retention time of the entirety of the polyene.

3.2.5.3 Derivatization assay for synthetic polyisoprene

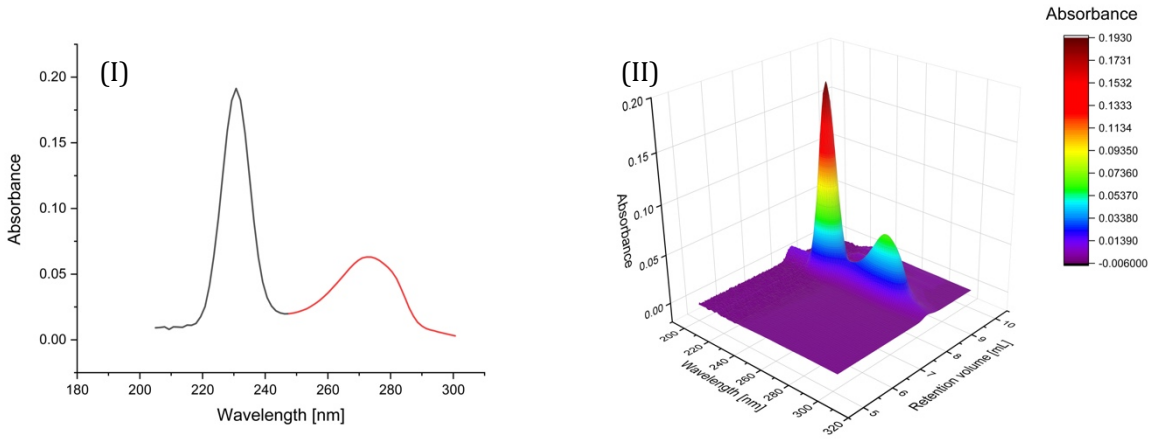

Figure 37. (I) UV absorption spectra of the underivatized (black) and derivatized (red) **PI 3000-D** in one GPC run, (II) corresponding 3D visualization of the **PI 3000-D** intensity with an additional axis displaying the retention volume.

The derivatized **PI 3000-Ox** (**PI 3000-D**) exhibited two absorption maxima in the UV absorption spectrum (Figure 37). The maximum at 227 nm can be attributed to unreacted PI when compared to a GPC run with solely unreacted PI 3000. The other maximum at 272 nm was therefore assigned to the derivatization of **PI 3000-D**. The ^{1}H NMR spectrum of **PI 3000-D** showed the shift of the aldehyde proton (^{1}H NMR: 9.83 ppm) to the corresponding oxime derivate as a mixture of E- and Z-isomers (^{1}H NMR: 7.39 and 6.65 ppm). The microstructure around the derivatized oxime functionality was also detected by ^{1}H-^{1}H correlation spectroscopy (COSY) NMR for **PI 3000-D** revealing that the proton of the *E*/*Z* isomers of the oxime correlated to protons of the adjacent methylene. The methyl group of the derivatized keto-functionality seemed to be overlapped by the methyl-groups of the PI backbone. The derivatization of **PB 3500-Ox** and **PB12000-Ox** also showed full conversion of the aldehyde functionality and a shift to the corresponding oxime in ^{1}H NMR with the standard procedure for derivatization of polybutadienes. The molecular weights and the PDIs were not significantly affected by the derivatization procedure for all of the derivatization attempts (Table 15).

Table 16. Derivatized degradation fragments generated by chemical degradation of PI (**PI 3000-D**) according to UHPLC-ESI-HRMS (Orbitrap) in positive ion mode.

Number of intact repeating units	RT (min)	$[M+H]^+$ measured	$[M+H]^+$ calculated	Error (ppm)	Elemental Composition	RDBE
1	4.00	439.2579	439.2591	2.8	$C_{26}H_{35}N_2O_4^+$	10.5
2	6.37	507.3207	507.3217	2.1	$C_{31}H_{43}N_2O_4^+$	11.5
3	7.14	575.3830	575.3843	2.3	$C_{36}H_{51}N_2O_4^+$	12.5
4	7.65	643.4451	643.4469	2.8	$C_{41}H_{59}N_2O_4^+$	13.5
5	8.08	711.5081	711.5095	2.0	$C_{46}H_{67}N_2O_4^+$	14.5
6	8.48	779.5704	779.5721	2.3	$C_{51}H_{75}N_2O_4^+$	15.5
7	8.79	847.6326	847.6347	2.5	$C_{56}H_{83}N_2O_4^+$	16.5
8	9.19	915.6955	915.6973	2.0	$C_{61}H_{91}N_2O_4^+$	17.5
9	9.66	983.7578	983.7599	2.1	$C_{66}H_{99}N_2O_4^+$	18.5
10	10.25	1051.8204	1051.8225	2.0	$C_{71}H_{107}N_2O_4^+$	19.5
11	11.06	1119.8832	1119.8851	1.7	$C_{76}H_{115}N_2O_4^+$	20.5
12	11.86-12.36	1187.9443	1187.9477	2.9	$C_{81}H_{123}N_2O_4^+$	21.5
13	13.55-14.35	1256.0103	1256.0103	2.4	$C_{86}H_{131}N_2O_4^+$	22.5

For additional confirmation of the conversion of the keto-functionality and validation of the applicability also for low molecular weight degradation species UHPLC-ESI-HRMS measurements

were conducted. UHPLC-ESI-HRMS measurements of **PI 3000-D** revealed the expected derivatized low-molecular weight degradation products at specific retention times (Table 16). The respective negative controls did not show the products. For the data evaluation with XCalibur, the target *m/z* values were extracted from the total ion chromatogram using a 25 ppm mass window with a mass accuracy of four decimals to obtain the corresponding extracted ion chromatogram for each analyte according to the expected degradation fragments. The analysis of the sample triplicates neither showed partially derivatized nor underivatized degradation fragments in the analysis of the extracted ion chromatograms or in the total ion chromatograms. Congruent results were obtained for the triplicate and the corresponding negative controls of **PI 4500-D**. (+)-ESI-HRMS spectra of the degradation fragments with elemental composition obtained from **PI 3000-D** were also analyzed individually.
For validation the samples of PB were also investigated. **PB 3500-D** showed the expected derivatized low-molecular weight degradation products in triplicates and did not reveal them in the respective negative controls (Table 17). The analysis of the sample triplicates neither showed partially derivatized nor underivatized degradation fragments in the analysis of the extracted ion chromatograms or in the total ion chromatograms. (+)-ESI-HRMS spectra of the degradation fragments from PB 3500-D were also analyzed individually. Samples of **PB 200k-D** and **PB 12000-D** also showed the respective degradation fragments. This is a clear indication for the full conversion of both telechelic end-groups by the here established derivatization strategy for either polyene.

Table 17. Derivatized degradation fragments generated by chemical degradation of PB (**PB 3500-D**) according to UHPLC-ESI-HRMS (Orbitrap) in positive ion mode.

Number of intact repeating units	RT (min)	$[M+H]^+$ measured	$[M+H]^+$ calculated	Error (ppm)	Elemental Composition	RDBE
3	6.65	519.3219	519.3217	0.4	$C_{32}H_{42}N_2O_4^+$	12.5
4	7.19	573.6393	573.6387	1.2	$C_{36}H_{48}N_2O_4^+$	13.5
5	7.60	627.4164	627.4156	1.2	$C_{40}H_{54}N_2O_4^+$	14.5
6	8.01	681.4632	681.4626	0.9	$C_{44}H_{61}N_2O_4^+$	15.5
7	8.23	735.5097	735.5095	0.2	$C_{48}H_{67}N_2O_4^+$	16.5
8	8.51	789.5567	789.5565	0.3	$C_{52}H_{73}N_2O_4^+$	17.5
9	8.82	843.6038	843.6034	0.4	$C_{56}H_{79}N_2O_4^+$	18.5
10	9.13	897.6504	897.6504	0.0	$C_{60}H_{85}N_2O_4^+$	19.5
11	9.50	951.6969	951.6973	0.5	$C_{64}H_{91}N_2O_4^+$	20.5
12	9.90	1005.7442	1005.7443	0.1	$C_{68}H_{97}N_2O_4^+$	21.5
13	10.44	1059.7909	1059.7912	0.3	$C_{72}H_{103}N_2O_4^+$	22.5
14	11.10	1113.8366	1113.8382	1.4	$C_{76}H_{109}N_2O_4^+$	23.5
15	11.59-12.11	1167.8838	1167.8851	1.1	$C_{80}H_{115}N_2O_4^+$	24.5
16	13.00-13.76	1221.9228	1221.9321	7.6	$C_{84}H_{121}N_2O_4^+$	25.5

3.2.5.4 Application of derivatization assay onto Lcp_{K30} enzymatically degraded samples

The benefits of the new derivatization method by applying it to the enzymatic degradation of SPIs was demonstrated. Bioinspired, metastable, surfactant-free co-solvent stabilized emulsions have been shown to lead to increased enzymatic degradation of SPI with *cis*: *trans* ratios of 56:27 with the rubber oxygenase Lcp_{K30} compared to non-emulsified SPI. For the formation of these metastable emulsions, the ratio of hydrophobic solvent, polymer, and water was identified to be of crucial importance to form stable emulsions. As a consequence of its high dispersion stability, *n*-hexadecane was chosen as the hydrophobic solvent.[176] The stabilizing effect of the co-solvent stabilized PI stems either from the coalescence depression through a rise of viscosity of the droplet or the steric repulsion among the polymer chains adsorbed on the droplet surface.[179]

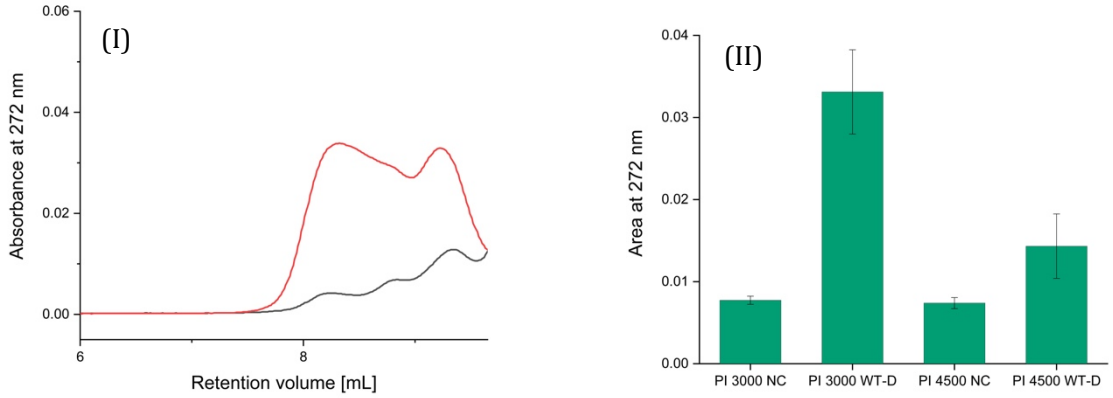

Figure 38. GPC measurements at a wavelength of 272.4 nm for **PI 3000 WT-D** (red) and **PI 3000** negative control (black) (I) and the resulting qualitative area integration of the enzymatic degradation of the triplicates of **PI 3000 WT-D**, **PI 4500 WT-D** and their respective negative controls (NC) (II).

As the absorption of the derivatized oximes is strongest at a wavelength of 272 nm, this one was chosen as the tracking wavelength to determine the absorption of the enzymatically degraded and derivatized PIs (**PI 3000 WT-D**, **PI 4500 WT-D**). The area under the curve of the 272 nm absorption was integrated for the retention volumes from 6 mL to 9 mL, which was correlated to molecular masses above 1000 according to external standard calibration (Figure 38 (I)). This provides a new insight into the degradation capabilities of Lcp_{K30} even with a background of unreacted polymer above the detection limit of UHPLC-ESI-HRMS. By adding the new absorption maximum with the derivatization agent, the degradation of endo-type rubber oxygenases can be tracked and compared (Figure 38 (II)). This degradation is not readily observable in the maximum of gel permeation chromatography using sole refractive index detection. The integrated area of absorption at 272 nm of the co-solvent emulsified system **PI 3000 WT-D** was significantly higher than the integrated area of absorption at 272 nm of the co-solvent emulsified system **PI 4500 WT-D**. All experiments were conducted in triplicates with corresponding negative controls. Negative controls were prepared without the enzyme Lcp_{K30}. The arrangement of microstructures within the investigated SPIs appears to be a significant factor for their degradation susceptibility and the observed differences in absorption. This interplay may be influenced by factors such as chain mobility and crystallinity,[259, 260] as well as the substrate's access to the active site and the pathways for product exit during the endo-type degradation by Lcp_{K30}.[141] This could lead to more degradation products above 1000 g/mol for PI **3000 WT-D** than **PI 4500 WT-D**.

A new methodology, that allows for further insight into the enzymatic activity of rubber oxygenases with SPI, was demonstrated. This methodology will enable the tracking of enzymatic activity with new rubber oxygenases or protein-engineered enzymes and is also applicable for the screening of enzymatic activity for the degradation of synthetic PB even with no significant shift in the retention volume by refractive index. The simple and robust end-group derivatization could also be utilized for the screening in higher throughput screenings.[261, 262] Consequently, this methodology can be seen as a valuable tool in the endeavor of finding new sustainable ways of degrading rubbers in the future and the quest for a more circular polymer chemistry world. This could be further augmented to a multidimensional system with MALDI-TOF-MS. [257, 263]

3.2.5.6 Investigations into enzymatic degradation of polybutadiene by FuncLib

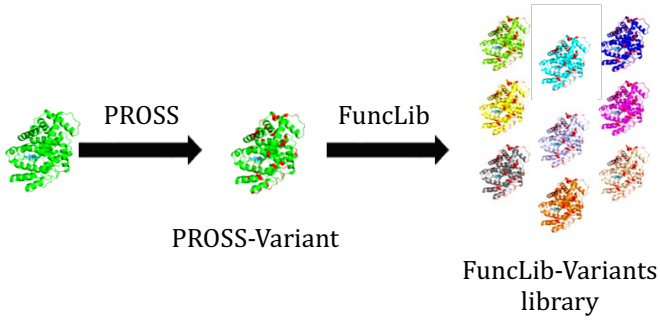

Figure 39. Lcp_{K30} thermostability improvement through PROSS and creation of library for new enzymatic catalytic activity screening by FuncLib. Reproduced from [264].

FuncLib is a substrate-independent method, based on which the resulting enzyme library can be tested on substrates. The main goal is to create an enzyme library consisting of mutants that are as different as possible but still stable. This is intended to minimize the screening effort and still offer a selection of proteins as diverse as possible.[199] Yannick Wolf of the Weissenborn group investigated the creation of a broad variety of rubber-degrading enzymes through protein engineering to enable the degradation of synthetic rubber polymers.[264] The improvement of rubber-degrading enzymes using the PROSS algorithm with Eugen Schell were implemented,[250] the enzyme diversified with the FuncLib algorithm and in collaboration the obtained library for its capacity to degrade synthetic polyenes was investigated (Figure 39).

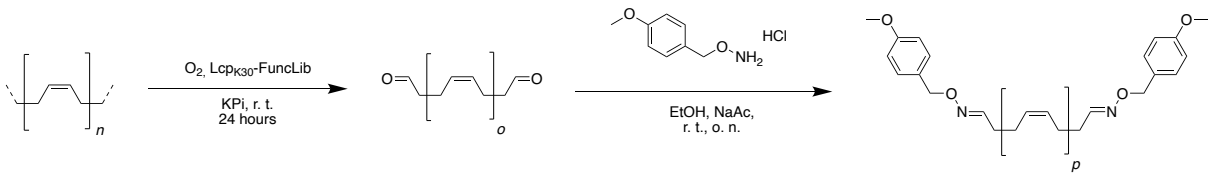

Scheme 13. Degradation capability investigation of PB with Lcp_{K30}-FuncLib Variants and derivatization for screening of activity.

After expression of the respective 50 different FuncLib-Variants of the most promising PROSS-Variant Lcp_{K30}-P7, the enzymatic degradations were screened and investigated with the established derivatization UV-detection assay *via* GPC (Scheme 13).
The M_n and polydispersity index were additionally investigated for all 50 samples and revealed that the M_n of the negative control was larger than that of all other samples. The wild type of Lcp_{K30}, the more thermostable variant Lcp_{K30}-P7 and interestingly, free heme had a slight effect onto the M_n. But the decrease in M_n was more pronounced for the FuncLib Variants.
UHPLC-ESI-HRMS measurements were performed for the samples of the most promising Lcp_{K30}-FuncLib variants, FL6, FL9, FL18, FL19, FL29, FL37, FL 41 and FL50, with chemically degraded PB as positive controls and negative controls without enzyme addition. The meta data analysis of the automated integration processing of the LC-MS extracted ion chromatograms by XCalibur revealed that the intensity of the expected degradation fragments was 10^5 for FuncLib variants. However, the intensity of the positive control was significantly higher with 10^7, as expected due to the low enzymatic degradation activity. Interestingly, intensities of 10^4 were detected in the negative controls, despite the absence of such intensities in the blanks, control measurements with solely solvent. But these promising results warranted further attempts for optimization of the measurement methodologies as well as the degradation procedure.

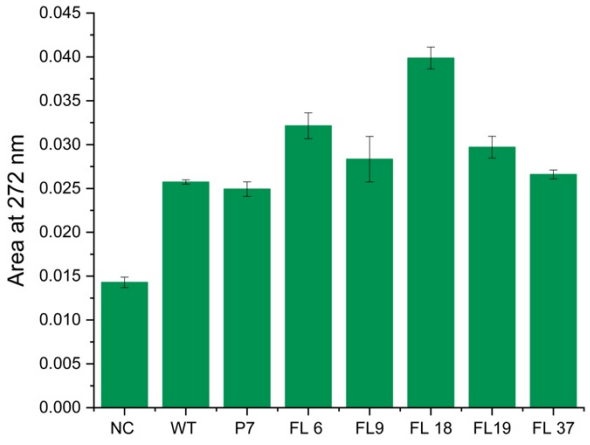

Figure 40. UV-absorption of the respective derivatized Lcp_{K30}-FuncLib variants at 272 nm according to GPC.

The intensity of the UV-absorption of the derivatized Lcp_{K30}-FuncLib variants 6 and 18 at 272 nm was significantly higher than the negative controls according to GPC (Figure 40). The GPC curve of Lcp_{K30}-FuncLib18 at 272 nm exhibited significantly higher absorption and a slight tilt towards lower number average molar masses, along with a broadened polydispersity index, which could also be interpreted as an indicator for enzymatic degradation. For Lcp_{K30}-FuncLib18 the highest absorption was detected and for Lcp_{K30}-FuncLib37 the most interesting results in the meta UHPLC-HRMS data analysis as well as the highest polydispersity in the preliminary investigations were observed. Consequently, those variants were investigated further. UHPLC-ESI-HRMS was performed of the entire sample spectrum of all Lcp_{K30}-FuncLib variants, and for Lcp_{K30}-FuncLib18 and Lcp_{K30}-FuncLib37, also enzyme concentration at 1 µM, 2 µM and 5 µM, in triplicates were investigated. The data did not conclusively demonstrate that the enzymatic degradation fragments were not also present in the respective negative controls. This could be attributed to the low activity of the respective enzyme towards the PB or suboptimal ionization of the hydrophobic degradation fragments. The presence of interfering compounds or matrix effects in the sample, arising from impurities or by-products of the synthetic polybutadiene, could have masked or suppressed the signals of the degradation fragments in the measurements as well. It is plausible that the small intensities observed in the negative controls are due to autoxidation of the polybutadiene. This phenomenon could also be detected due to the extremely high sensitivity with an ESI-HRMS Orbitrap.

Additionally, MALDI-TOF analysis was conducted to investigate the derivatized degradation fragments, which should be significantly more ionizable than the underivatized aldehyde functionalities. However, MALDI-TOF analysis did not reveal distinguishable degradation fragments with the differently applied sample preparation and measurement methodologies, suggesting that the sensitivity might not have been sufficient to detect these low concentrations of hydrophobic degradation fragments, especially if they were present in trace amounts with a high background of unreacted polybutadiene.

Nonetheless, the promising results of the rubbery oxygenase degradation assay and the necessity for more sustainable degradation methodologies for polyenes should warrant further investigations into the first enzymatic degradation of synthetic polybutadienes. Molecular dynamic calculations and docking of the respective variants, for example, could provide insights into the degradation behavior and could lead to improvement of the degradation efficacy.

3.3 Cyclopropanation of oligoenes: novel catalytic entities

In previous studies, the efficacy of cyclopropanation reactions of PI employing copper catalysis and *N*-heterocyclic carbenes (NHCs) had lagged behind that of styrene, due to higher reactivity of the latter.[265] Cyclopropanation reactions typically involve the addition of a carbene to a carbon-carbon double bond to form a three-membered ring. The reaction's efficiency and stereoselectivity are influenced by various factors, such as the steric and electronic nature of the alkene substrate.[266] For trisubstituted double bonds, the reaction tends to be less efficient due to steric hindrance, electron distribution and stereochemical considerations.[267] As a simplified and controllable model system, oligoenes were chosen to facilitate the optimization of the cyclopropanation process of trisubstituted double bonds. Squalene was selected as the representative oligoene because of its structural resemblance to the polyene PI (Scheme 14). This characteristic holds potential for more environmentally sustainable cyclopropanation reactions in aqueous environments.
The objective was to embed functionalities for cyclopropanation into single-chain nanoparticles (SNCPs) by three approaches (Scheme 15). The replacement of molecular ligands in organometallic catalysts with bulkier polymer chains can profoundly affect their functionality. However, strategic design can exploit this "shielding" effect to allow only specific substrates into the pocket, thereby enhancing chemical selectivity, site-selectivity as well as stereoselectivity and sometimes even catalytic turnover numbers.[268] Consequently, embedding these catalysts within a polymer framework and strategically positioning functional handles could increase local concentrations of catalytically active species thereby optimizing the overall reaction efficiency.[216] This approach could potentially even provide control over the regioselectivity in the cyclopropanation of squalene, which was deemed the “arithmetic demon” for regioselectivity reasons in a seminal publication on the dihydroxylation of squalene.[269]

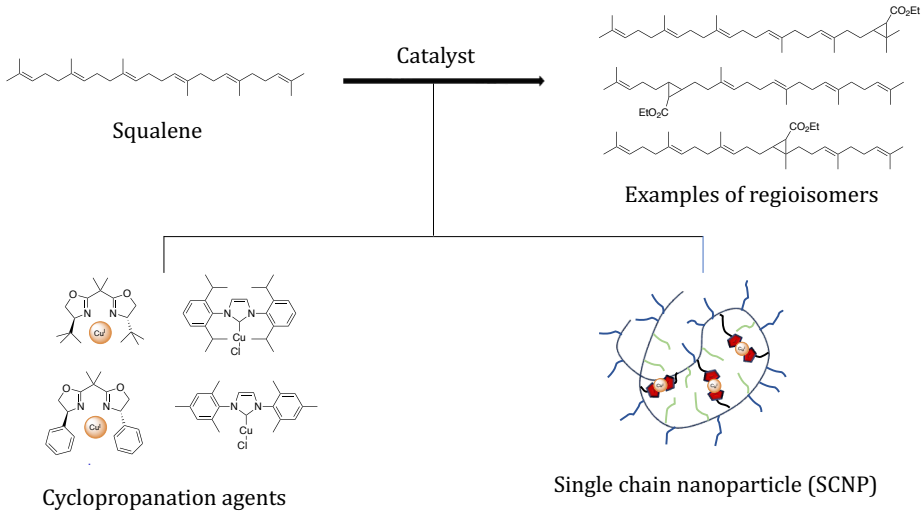

Scheme 14. Cyclopropanation of squalene with scope of cyclopropanation agents and possible regio isomers. SCNP with the cyclopropanating functionalities embedded as alternative novel catalytic entity.

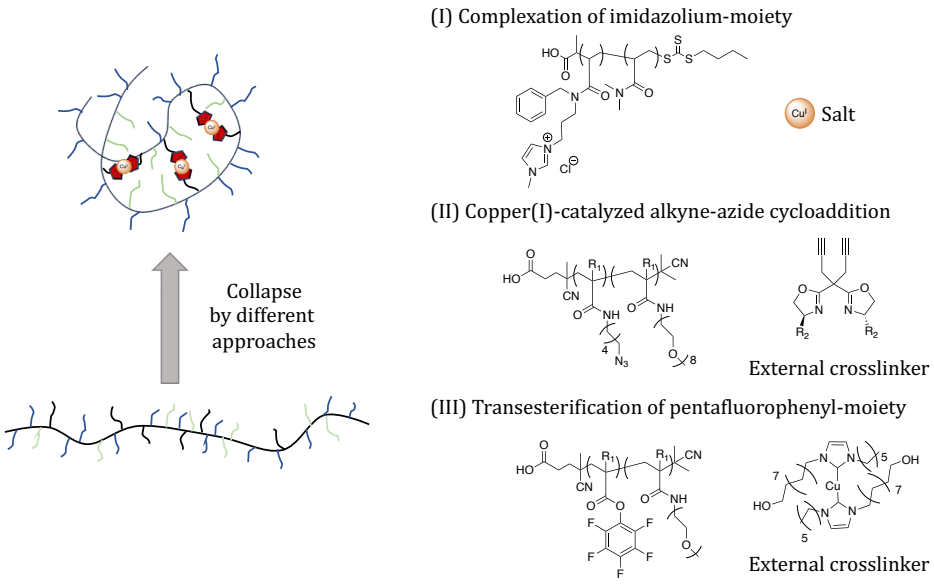

Scheme 15. Approaches to incorporate cyclopropanating moieties into a SCNP by complexation (I), CuAAC-click reaction (II) and transesterification (III). R_1= CH_3 or H, R_2= *t*-Butyl or Phenyl.

3.3.1 Preliminary investigations into squalene cyclopropanation

Initially, a screening of various copper catalysts in the cyclopropanation of squalene was conducted to assess the catalytic potential of molecular catalysts towards the selective modification of squalene. Initial reactions were conducted using an equimolar amount of ethyl diazoacetate to squalene and a 0.05 mol% loading of different copper catalysts (Scheme 16). Diazo compounds have been extensively employed as bench-stable, commercially available carbene sources in organic chemistry.[270] Despite the efficiency of different transition metals in the incorporation of such fragments into a variety of substrates, the undesirable homocoupling of the diazo compound remains one of the notable challenges in utilizing ethyl diazoacetate. The homocoupling is leading to the formation of diethyl maleate and diethyl fumarate as undesirable byproducts.[271] Fructos *et al.* reported that the cyclopropanation of styrene using IrPrCuCl did not result in these respective side products.[272] Consequently, IPrCuCl and SIMesCuCl were investigated as potential catalysts. Additionally, the suitability of two chiral enantiopure, C_2-symmetiric bidentate bis-oxazoline (box) ligands known for their cyclopropanation capabilites, in combination with various copper salts was tested.[266]

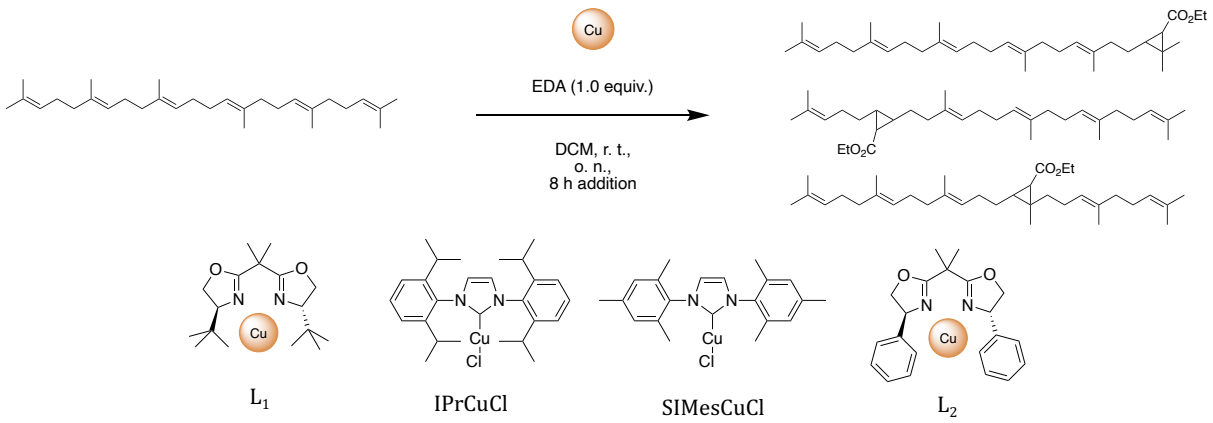

Scheme 16. Equimolar cyclopropanation of squalene with different copper catalysts leading to the formation of different regioisomers of monomodified squalene.

Table 18. Overview over catalyst scope for cyclopropanation of squalene

ID	Catalyst	Rate of diethyl maleate & fumarate [%][a]	Product formation[b]	Double bond ratio [mmol][a]
Cu-1	$L_1Cu(OTf)_2$	40	yes	0.275
Cu-2	$L_2Cu(OTf)_2$	35	yes	0.179
Cu-3	$L_1[Cu(NCMe)_4]PF_6$	28	yes	0.055
Cu-4	$L_2[Cu(NCMe)_4]PF_6$	28	yes	0.249
Cu-5	IPrCuCl	37	yes	0.309
Cu-6	SIMesCuCl	37	yes	0.361

[a]= according to ^{1}H NMR; [b]=according to ESI-MS

The catalytic efficacy for the formation of different regio isomers was tracked with ^{1}H NMR and ESI-MS. ^{1}H NMR provides insights into both the formation of the main product and the generation of side products, whereas ESI-MS allowed for the detection whether the mass to charge ratios of differently modified squalenes are formed during the process. The squalene contains six double bonds, and integrating the data related to these bonds enabled us to assess the formation of modified squalene in the equimolar experiments, as shown in Table 18. A full conversion of the double bond would have resulted in no more detection of excess integral of the respective double bonds and the corresponding double bond ratio (Table 18). This was not achieved in the experiment set but ESI-MS analyses confirmed the presence of monomodified squalene in all the reactions. However, the ESI-MS findings not only confirmed the existence of monomodified squalene but also indicated the presence of dimodified squalene in certain experiments. The incomplete conversion can be attributed to homocoupling, a phenomenon observed in all reactions. Interestingly, this effect was notably less pronounced for **Cu-3** and **Cu-4** compared to **Cu-5** and **Cu-6**. The side product formation with copper NHC complexes had already been reported by Shinde *et al.*[265] conversely to the results obtained by Fructos *et al.*[272] The copper salt $[Cu(NCMe)_4]PF_6$, because it was reported to have led to good results with sterically demanding substituents in the cyclopropanation with bis-oxazoline ligands,[273, 274] was compared to $Cu(OTf)_2$[275, 276] in the substrate scope. The ethyl diazo acetate (EDA) was added with a syringe pump decreasing the side product formation due to better control of the reaction rate and the minimization of the side reaction.

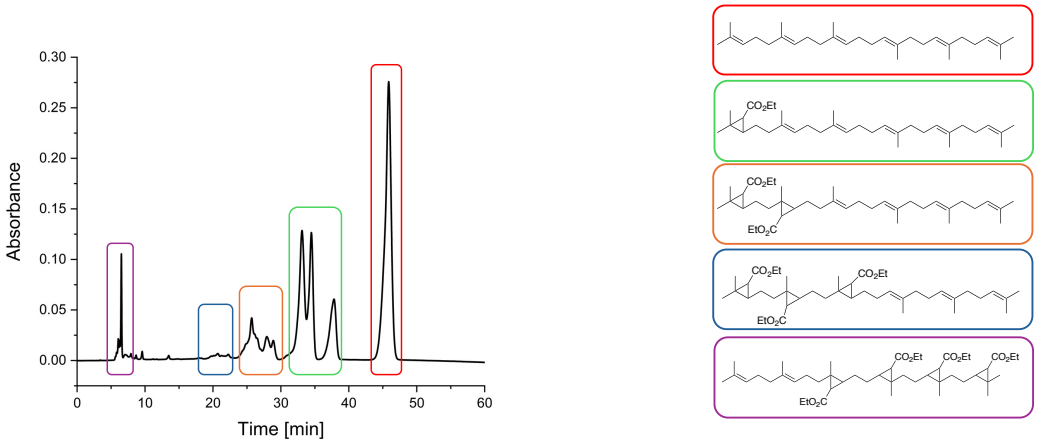

Figure 41. HPLC-ESI-MS coupling to determine the different products of cyclopropanation of squalene. Squalene (red), mono-modified (green), di-modified (orange), tri-modified (blue) and tetra-modified (purple).

To gain deeper insights into the site-selectivity of this process, HPLC analysis was conducted to determine whether the monomodified squalene would elute as a single peak, which would have meant that one regioisomer formed, or multiple peaks, which would have indicated a mixture of diastereomers. The HPLC results revealed a complex profile of peaks (Figure 41). Subsequently, HPLC-MS was employed to investigate the mass and to distinguish between peaks in respect to their molecular mass. The peaks could be attributed to several compounds, including three regioisomers of mono-modified squalene, di-, tri- and tetra-modified squalene derivatives as well as unreacted starting material. In the case of mono-modified squalene, the presence of a C_2 axis led to the formation of three distinct regio isomers, each exhibiting different elution behavior. In di-modified squalene, there was the potential for the formation of six different diastereomers, but their elution behavior was less distinct than for the monomodified squalene leading to overlapping signal pattern.
Overall, it became evident that the equimolar reaction resulted in various products, far exceeding the intended formation of only three distinct regioisomers. Based on these results from the initial catalyst screening (Table 18), it became evident that the bis-oxazoline ligand in combination with $[Cu(NCMe)_4]PF_6$, **Cu-3** and **Cu-4**, led to the most promising results.
Subsequent cyclopropanation experiments on squalene using the most promising catalysts identified during the initial screening were conducted. These subsequent experiments involved the addition of an excess of EDA to assess the feasibility of achieving complete modification of squalene. According to ^{1}H NMR analysis, full modification of squalene was observed when employing **Cu-3** and **Cu-4**. However, ESI-MS analysis still revealed traces of pentamodified squalene. This discrepancy indicated that complete conversion with EDA was not achieved.
Enzymes have garnered considerable attention in recent years due to their proficiency in cyclopropanating double bonds.[277, 278] However, to the best of our knowledge, no reports exist of regioselective cyclopropanation of three substituted double bonds using enzymes. Single chain nano particles (SCNPs) as artificial enzymes have demonstrated the potential to influence the catalytic selectivity of reaction products.[216] Based on the preliminary data, in a collaboration with Mohamed Hassan, the incorporation of cyclopropanating functionalities into SCNPs as a proof of concept for modification of oligoenes and polyenes with cyclopropanation reactions in the future was investigated.

3.3.2 Approaches for the formation of single chain nanoparticles to incorporate cyclopropanating functionalities

3.2.2.3 Copper-NHC complexation as internal folding for SCNPs

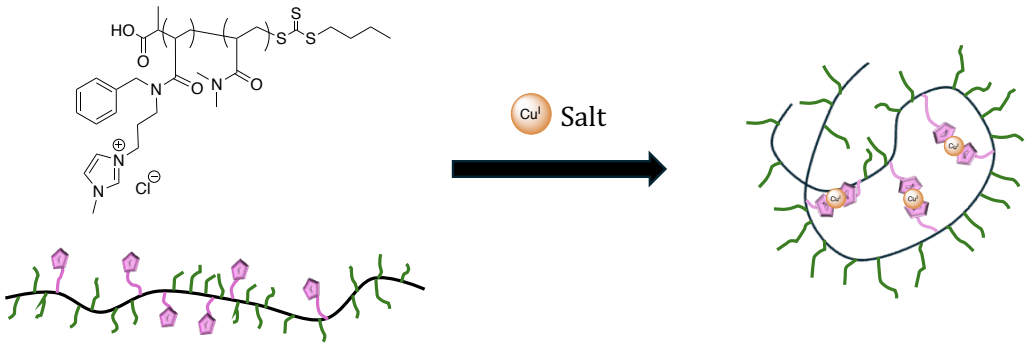

Scheme 17. Internal complexation of *N*-heterocyclic carbenes with copper salts as folding strategy for the incorporation of copper bis-*N*-heterocyclic carbenes into SCNPs.

Previous studies in our group have documented the formation of bis-*N*-heterocyclic carbene copper networks by precursor polymers with imidazolium functionalities and subsequent complexation with a copper source, such as $[Cu(MeCN)_4][PF_6]$[279] or Cu_2O.[280] Drawing inspiration from these works,

monomers that incorporate imidazolium moieties bearing acrylate and methacrylate functionalities were designed. These monomers were envisioned to be copolymerized with *N*,*N*-dimethylacrylamide, resulting in the formation of amphiphilic copolymers (Scheme 17). To increase the hydrophobicity of the core, tertiary amides bearing methyl or benzyl groups were investigated over the more hydrophilic secondary amides. The incorporation of aromatic structures was expected to have a beneficial impact on the core-shell structure through π-π stacking within the hydrophobic core. This phenomenon has been leveraged in the formation of other SCNPs.[207, 281] To this end, a library of monomers was synthesized (Scheme 18).

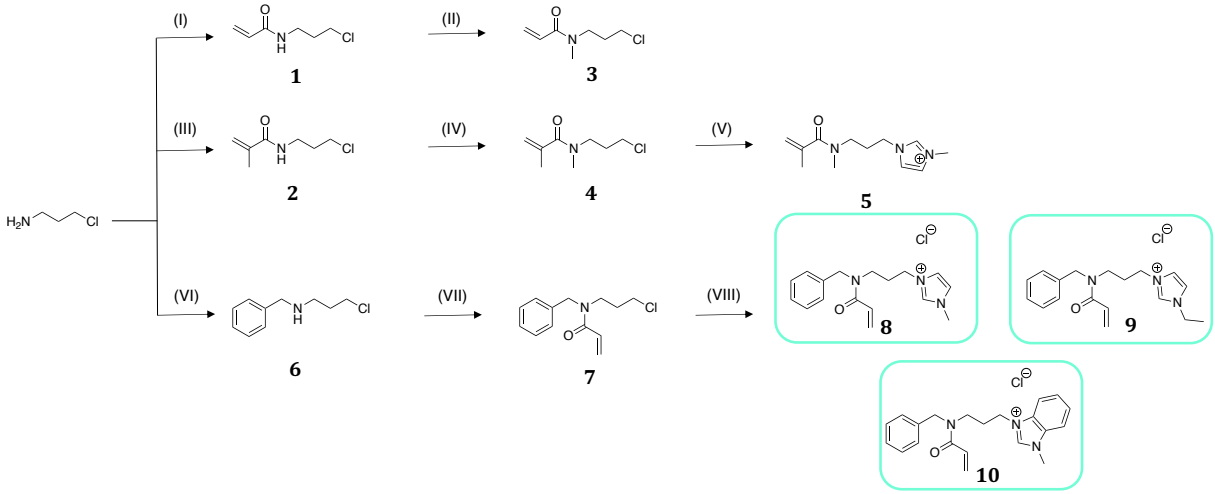

Scheme 18. Library and synthetic approaches for imidazolium bearing acrylamides for the incorporation of copper into SCNPs.

Starting from 3-chloropropylamine, three different substances were synthesized. The first reaction involved the use of triethylamine (TEA) to deprotonate and catalyze the acylation reaction, where the amine nucleophile attacks the acryloyl chloride, resulting in the formation of **1** (Scheme 18 (I)).[282, 283] In a similar reaction using methacryloyl chloride and TEA, **2** was obtained (Scheme 18 (II). It was observed that methylation of the amide bond was more successful when using sodium hydride (NaH) for amide deprotonation compared to TEA, due to the significant higher pKa value of circa 38 for NaH than roughly 11 for TEA. (Scheme 18 (II), (IV)).[284] The reaction led to a very low yield for **4** after purification *via* column chromatography, possibly due to undefined side reactions, which were monitored with ^{1}H NMR. Attempts to quaternate **3** led to a variety of side reactions, and despite extensive purification attempts using various solvents, pure products were not obtained. The quaternization of **4** in acetonitrile (ACN) using methylimidazole was successful. But due to the low yield of the second step being a limiting factor, an alternative route was devised.

As an alternative route, 3-chloropropylamine was subjected to a reductive amination with benzyl aldehyde and sodium boron hydride resulting in **6** (Scheme 18 (VI)).[285] **6** was subsequently reacted with acryloyl chloride, forming **7**. (Scheme 18 (VI). The reactions utilized TEA as base and catalyst in a nucleophilic substitution. Quaternization of **7** in ACN was successful, employing methyl imidazole, ethyl imidazole, and methylbenzylimidazole as quaternizing agents. The removal of side products was most effective using reverse-phase liquid chromatography and dynamically applying water and methanol as eluent.

SCNPs require amphiphilic polymer chains for the formation of a core-shell structure. *N*,*N*-dimethylacrylamide (DMAA) is a well-established acrylamide with high hydrophilicity and was therefore deemed a good comonomer. Prior to the copolymerization attempts of the imidazolium monomers with DMAA, the polymerization of DMAA was investigated as free radical polymerization and RAFT-polymerization in *N*,*N*-dimethylformamide (DMF)[286] and dioxane[287] employing 2-

(butylthiocarbonothioylthio)propanoic acid (BTPA) as the chain transfer agent. This resulted in a controlled RAFT-polymerization in DMF with BTPA.
The attempts to copolymerize **8**, **9**, and **10** with DMAA, using BTPA as the chain transfer agent at a ratio of 200:100:1:0.1 $[M]_0$(DMAA):$[M]_0$:[CTA]:[I], did not yield molecular weights exceeding 2000 g/mol, as determined by GPC, even though the chain transfer agent and azobisisobutyronitrile (AIBN) were reported as compatible for the RAFT-polymerization of acrylamides.[288] While GPC is a widely accepted method for characterizing the molecular weight of many neutral polymers, determining the molecular weight of polyionic liquids through GPC presents challenges. This is primarily due to their unique hydrodynamic radii and undesired interactions with GPC columns.[289, 290] For well-defined polyionic liquids with defined end-groups, such as a RAFT-agent, GPC standards can be specifically synthesized or the end-group can be correlated in ^{1}H NMR to the number average molar mass.[291] However, ^{1}H NMR spectroscopic measurements did not allow for the clear determination of the M_n in the case of these copolymerizations.
Free radical polymerizations of **8**, **9**, and **10** led to a notable increase in viscosity but also without distinct shifts above 2000 g/mol in GPC. Attempted MALDI-TOF measurements of the polymers did not produce interpretable spectra. As the polymerizations failed to yield well-defined polymers, an alternative strategy for the incorporation of cyclopropanating functionalities was devised.

3.3.2.1 Precursor polymer synthesis

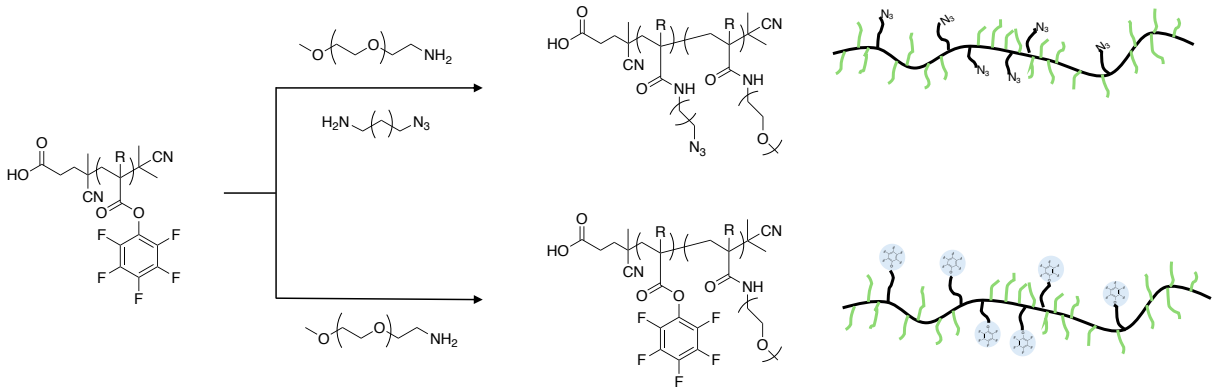

Scheme 19. Precursor synthetic strategy for the preparation of amphiphilic post-modified poly(pentafluorophenyl acrylate) or post-modified poly(pentafluorophenyl methacrylate) either bearing azide functionalities for CuAAC reaction or pentaflurophenyl for transesterification. R = H for acrylate; R = CH_3 for methacrylate

The synthesis of SCNPs with tailored functionalities often necessitates the incorporation of diverse, and, at times, complex monomers. However, using such functional monomers in polymerization processes can present challenges, potentially leading to poorly controlled copolymer compositions or a loss of control during radical polymerization.[222, 292] As a viable alternative, the incorporation of functional handles could be conducted after the polymerization process, thereby overcoming the limitations and challenges, mentioned earlier. A precursor polymer serves as an initial polymer that can undergo post-polymerization modifications and can overcome those limitations (Scheme 19). Polymers featuring reactive ester side groups, known to readily react with amines have proven to be valuable facilitating the synthesis of intricate single chain nanoparticles.[293, 294] As established by Theato *et al.*,[295, 296] poly(pentafluorophenyl acrylate) and poly(pentafluorophenyl methacrylate) can be synthesized using RAFT polymerization. These polymers exhibit notably high reactivity towards amines and have shown solubility in a wide range of solvents.

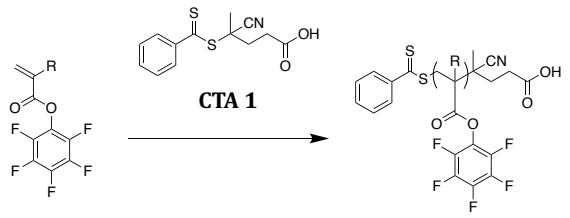

Scheme 20. RAFT-Polymerisation of pentafluorophenyl acrylate (**11**) to poly(pentafluorophenyl acrylate) (**PFPA-1**) and pentafluorophenyl methacrylate (**12**) to poly(pentafluorophenyl methacrylate) (**PFPM-1**). 11/PFPA-1 R = H; 12/PFPM-1 R = CH_3

Table 19. RAFT-polymerizations of **11** using **CTA 1**, **CTA 2** to **PFPA-1**.

Entry	Temperature [°C]	Rx. Time [h]	M_n [g/mol]	Đ	Yield [%]	CTA	$[M]_0$:[CTA]:[I]
1	70	3	7600	1.4	67	2	200:1:0.25*
2	70	3	14500	1.8	39	1	200:1:0.25*
3	80	3	10500	1.4	29	1	200:1:0.25*
4	70	3	16700	1.6	33	1	200:1:0.25
5	80	3	15700	1.6	25	2	200:1:0.25
6	70	4	10300	2.0	<10	2	200:1:0.25
7	80	4	10600	2.0	59	1	200:1:0.25
8	80	16	-	-	<10	1	200:1:0.25
9	80	3	12300	1.7	35	1	200:1:0.25
10	80	3	12100	1.7	58	1	200:1:0.25
11	70	3	12200	1.3	22	1	148:1:0.1
12	80	3	9100	1.3	63	1	85:1:0.125

*=ABCVA as initiator

RAFT-polymerizations of pentafluorophenyl acrylate were conducted according to modified procedures by Alex *et al*.[297] The chain transfer agent (CTA) employed in both the aforementioned study and the original procedure by Theato *et al*.[298] was 4-(phenylcarbonothioylthio)pentanoic acid (**CTA 1**) (Scheme 20). This particular CTA was selected as the featured chain transfer agent for the polymerization attempts. During kinetic investigations of the homopolymerization of pentafluorophenyl acrylate (PFPA),[297] notable solvent effects for the CTA under investigations were observed. The best control for the RAFT homopolymerisation was reported for 1,4 dioxane and acetonitrile, which were the solvents investigated in all of the polymerization attempts. The ratio of CTA to initator set at 1:0.25,[297] was investigated under various reaction durations and temperatures, drawing inspiration from other established procedures.[292, 299-301] However, unsatisfactory results were obtained in regards to the polydispersity and the control of the RAFT polymerization. Furthermore, changing the CTA to 2-(butylsulfanylthiocarbonylsulfanyl)-2-methyl propionic acid (**CTA 2**) as reported by Alex *et al*.[297] did not result in significantly better results. The subsequent change of CTA to initiator ratio ([CTA]:[I]) to 1:0.1, aligning with the procedure by Chalarca *et al*.[302] resulted in a controlled RAFT polymerization with polydispersity below 1.3 (Table 19 entry 11). To validate the significance of this ratio in controlling the RAFT-polymerization, a different ratio [CTA]:[I] of 1:0.125 was examined according to Jochum *et al*.[300] This variation also resulted in improved control of the polydispersity but with a reduced M_n (Table 19 entry 12).

For homopolymerization with PFPA slow growth in molar mass occurred beyond a monomer conversion of approximately 75%, indicating the presence of termination reactions. This observation aligned with a declined radical concentration observed in a semilogarithmic kinetic plot.[297] Consequently, the monomer feed was deliberately set significantly higher than the required degree of

polymerization to enhance reaction control by circumvent uncontrolled termination reactions.[19]F NMR spectroscopic tracking of the conversion showed that conversion did not exceed this critical threshold of 75% in the most promising polymerization attempts.

Table 20. RAFT-polymerization of **12** using **CTA 1** to **PFPM-1**.

Entry	Temperature [°C]	Rx. Time [h]	M_n [g/mol]	Đ	Yield [%]	CTA	$[M]_0$:[CTA]:[I]
1	80	3	11500	1.6	14	1	200:1:0.25
2	80	3	10100	1.7	33	1	200:1:0.25
3	80	3	13500	1.6	54	1	200:1:0.25
4	80	3	11400	1.4	17	1	200:1:0.1
5	80	3	12800	1.5	28	1	85:1:0.1
6	80	24	9400	1.4	24	1	85:1:0.1
7	80	3	16300	1.3	30	1	85:1:0.125
8	80	3	12600	1.3	57	1	85:1:0.125
9	80	3	12000	1.4	58	1	85:1:0.125

Polymerization of pentafluorophenyl methacrylate was also conducted according to a modified procedure by Alex *et al.*[297] (Table 20). However, the control of the polydispersity in the RAFT polymerization was lackluster (Table 20, entry 1-3), therefore, the ratio of [CTA]:[I] was adjusted from 1:0.25 to 1:0.1, according to the procedure by Battistella *et al.*[303] This adjustment resulted in improved control of the polymerization in regards to the polydispersity index, but at the cost of decreased yield (Table 20, entry 4). Interestingly, reduced monomer to CTA ratio improved the reaction yield. A lower monomer-to-CTA or monomer-to-initiator ratio reduces the concentration of active propagating radicals in the reaction mixture. This reduction could have enhanced the control over the polymerization process by potentially minimizing undesired termination reactions and side reactions. Finally, the most promising results were obtained by adjusting the [CTA]:[I] ratio to 1:0.125, according to a procedure by Barz *et al.*[304] leading to controlled RAFT-polymerizations with satisfactory yields of 58% and polydispersity of circa 1.3-1.4 (Table 20, entry 8 & 9).

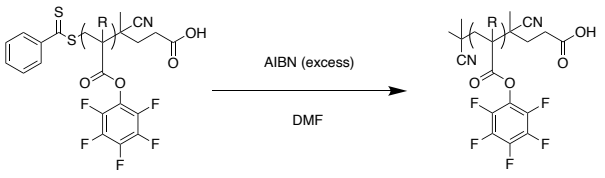

PFPA-1/PFPM-1 **PFPA-2/PFPM-2**

Scheme 21. End-cap modification of **PFPA-1** and **PFPM-1** by azobisisobutyronitrile (AIBN) in DMF. PFPA-1/PFPA-2 R = H; PFPM-1/PFPM-2 R = CH_3

The end-cap modifications of the precursor polymers were conducted to remove the phenylcarbonothioylthio-sulfur-containing end-group (Scheme 21). Removal of the RAFT-end group can be essential due to their intrinsic reactivity, which could cause unintended side reactions.[305, 306] This precaution ensures the polymer's integrity. During the post modification of the precursor polymer, the CTA can be susceptible to side reactions due to its potential instability at high temperatures. Additionally, it can potentially react with various nucleophiles, including water, which can lead to side reactions during the post-modification procedure.[305]

The modification was achieved using a radical method, whereby the polymer solution was treated with a large excess of a radical initiator, azobisisobutyronitrile (AIBN), to initiate the release of the polymeric radical. Subsequently, the released radical was end-capped with an unreactive initiator-derived group, similar to a Barton-McCombie deoxygenation. For PFPM-1, AIBN was used as the initiator in a 20-fold excess relative to the targeted end-groups.[34] The cyanoisopropyl radicals generated from the decomposition of AIBN became the new ω end-groups of the polymers. For poly(pentafluorophenyl acrylate)s, a secondary initiator addition, such as lauroyl peroxide,[307] can be

beneficiary. The C-S bond undergoes homolytic cleavage, and the stabilization of the resulting secondary acrylic polymeric radicals is less effective in comparison to the tertiary methacrylic radicals. Consequently, it may require initiator-derived radicals with superior ability to stabilize the radical.[292]

3.3.2.2 Folding of SCNP by external cross-linker with copper catalyzed alkyne azide click reaction

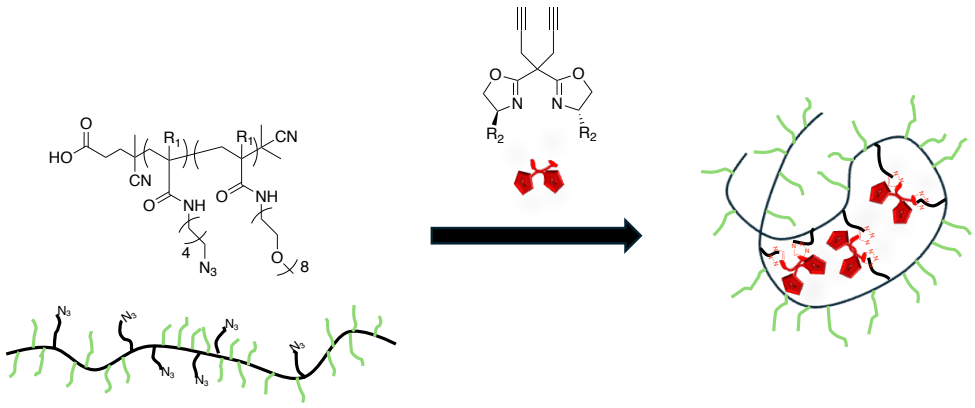

Scheme 22. CuAAC-click strategy to cross-link with bifunctional bisoxazoline ligands. R_1 = H for acrylate; R_1 = CH_3 for methacrylate; R_2 = *t*-Butyl; R_2= Phenyl

Our synthetic strategy, established with Mohamed Hassan, intended to utilize bivalent bisoxazoline functionalities and, if needed, an auxiliary crosslinker as external crosslinkers *via* copper catalzye azide alkyne click reaction to form SCNPs (Scheme 22). This approach was inspired by a methodology employed by Thümmler *et al.*[308] To this end the precursor polymers strategy with pentafluorophenyl esters has emerged as a highly efficient and versatile approach to construct well-defined multifunctional (co)polymers.[294] SCNPs require amphiphilic copolymers and therefore it was necessary to introduce hydrophilic moieties. Thus, the precursor polymers were post-modified with ω-amino-poly(ethylene glycol) to introduce hydrophilicity for amphiphilic SCNPs, along with azide bearing amine suitable for subsequent crosslinking *via* copper catalyzed azide alkyne cycloaddition reaction. Post-modification with unhindered amines has been reported to achieve nearly quantitative yields.[309] Also post-modification with poly(ethylene glycol) (PEG) amines of 500 g/mol has been reported by Chua *et al.*[310] to work satisfactorily. However, aminolysis may become less efficient when using sterically demanding amines, amines with high molecular weight, or secondary or tertiary amines.[311]

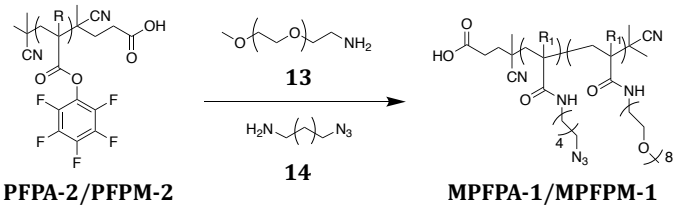

Scheme 23. Post-modification of **PFPA-2** and **PFPM-2** with ω-amino-poly(ethylene glycol) (**13**) and 6-azido-hexylamine (**18**). MPFPA-1/PFPA-2 R = H, MPFPM-1/PFPM-2 R = CH_3

At first, ω-amino-poly(ethylene glycol) was synthesized according to a modified procedure by Liu *et al.*[312] Methoxy poly(ethylene glycol) was activated with thionyl chloride and the obtained chloride was converted into an azide group *via* nucleophilic substitution employing sodium azide. Triphenlyphosphine was then used to reduce the azide group in a Staudinger reaction to the corresponding primary amine. The conversion of the reactions was tracked *via* IR spectroscopy and ^{1}H NMR. For the SCNP collapse with CuAAC-click chemistry, an azide had to be introduced to the

polymer backbone, consequently a 6-azido-hexylamine was synthesized. 1,6-Dibromohexane was converted to 1,6-diazido-hexane with a nucleophilic substitution with sodiumazide. Subsequently a Staudinger reaction employing triphenyl phosphine was utilized to reduce 1,6-diazido-hexane to the corresponding 6-azido-hexylamine.[313]

Table 21. Post-modification of **PFPM-2** and **PFPA-2** with ω-amino-poly(ethylene glycol) and 6-azido-hexylamine.

Entry	Polymer	Solvent	*T* [°C]	Catalyst	[equiv.]	Time [days]	M_n [g/mol]	PDI
1	**PFPM-2**	THF	55	-	-	6	27600	1.5
2	**PFPM-2**	THF	60	-	-	5	27300	1.5
3	**PFPM-2**	DMF	70	TEA	2	2	14000	1.6
4	**PFPM-2**	DMF	70	TEA	1	2	29700	1.6
5	**PFPM-2**	DMF	70	TEA	1	3	18400	1.6
6	**PFPM-2**	DMF	50	DMAP	0.2	2	22000	1.5
7	**PFPM-2**	DMF	70	TEA	1	2	11400	1.4
8	**PFPA-2**	THF	50	-	-	3	28300	1.7
9	**PFPA-2**	DMF	45	DMAP	0.2	3	22100	1.5

The post-modification reactions were conducted using different solvents and catalysts: THF[314] was used under catalyst-free conditions, while DMF[311] was used with either TEA[301, 315] or DMAP[316] as catalyst to achieve aminolysis (Scheme 23, Table 21). The progress of the reaction was tracked using *in situ* ^{19}F NMR spectroscopy. Aminolysis generates pentafluoro phenolate as the leaving group, resulting in a transition from broad polymer peaks to sharp signals corresponding to pentafluoro phenolate in the ^{19}F NMR spectrum of the reaction mixture. The completion of aminolysis was deemed when the polymeric peaks were no longer detectable.

The aminolysis reaction was observed to proceed significantly faster in polar aprotic solvents, such as DMF, which could be reasoned by increased nucleophilicity of the amine and stronger dipole moment of the C=O bond, thereby promoting the formation of the crucial tetrahedral intermediate.[317] This observation led to the change from THF toward DMF as the solvent and the most favorable results were obtained in DMF with DMAP as the catalyst at 45 °C and 50 °C (Table 21, Entry 6 & 9). However, increasing the temperature accelerated the reaction but also resulted in ester hydrolysis in the presence of catalysts.

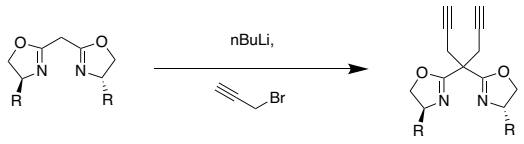

15/16

Scheme 24. Synthesis of "clickable" bis-alkyne bisoxazoline ligands (**15**, **16**). **15** R = *t*-Butyl; **16** R= Phenyl

Single-chain collapse and crosslinking could be accomplished by CuAAC click chemistry of the post-modified polymers with azide functionalities and external bis-alkynes as crosslinkers. Two bisoxazolines with alkyne functionalities were synthesized for the collapse and crosslinking experiments with CuAAC click chemistry **15** and **16**. The introduction of the alkyne functionality was accomplished by deprotonation of the bisoxazolines using *n*-butyllithium and subsequent nucleophilic substitution with propargyl bromide (Scheme 24). The formation of different nanosized compartments in amphiphilic single-chain nanoparticles could be controlled by collapsing in different reaction media.[308] Consequently, water, THF and DMF were probed for their applicability as collapse and crosslinking media, Table 22.

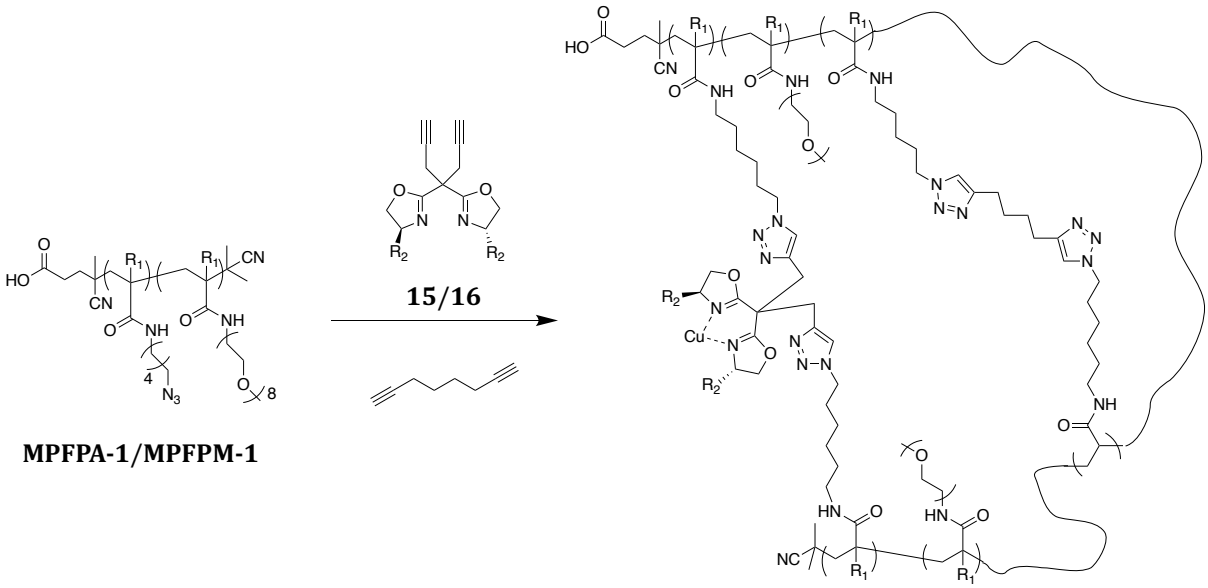

Scheme 25. Collapse of **MPFA-1**/**MPFM-1** with **15** or **16** and octadiyne to the respective SCNPs. MPFPA-1 R_1 = H, MPFPM-1 R_1 = CH_3, 15 R_2 = t-Butyl; 16 R_2= Phenyl

Table 22. Collapse and crosslinking attempts in different solvents at room temperature.

Entry	Polymer	Crosslinker	Catalyst	Solvent	DLS_{before}	DLS_{after}	$M_{n\ before}$	$M_{n\ after}$
1	**MPFPM-1**	Octadiyne	$CuSO_4$, NaAsc	water	10± 1	12± 2	27600	115400
2	**MPFPM-1**	Octadiyne	$CuSO_4$, NaAsc	water	7± 1.3	21± 2.9	27600	58600
3	**MPFPM-1**	Octadiyne	$CuSO_4$, NaAsc	water	7.9± 1.5	12.8± 1.4	27300	64600
4	**MPFPM-1**	Octadiyne	CuBr, bipyridine	THF	7.4± 1.3	7.0± 1.3	29700	27600
5	**MPFPM-1**	**16**	CuBr, bipyridine	THF	7.4± 1.3	8.6± 1.4	29700	33600
6	**MPFPM-1**	**15**	CuBr, bipyridine	THF	7.4± 1.3	7.2± 1.3	29700	33500
7	**MPFPM-1**	**16**	CuBr, bipyridine	THF	6.8± 1.2	5.0± 0.9	22000	33200
8	**MPFPM-1**	**16** + Octadiyne	CuBr, bipyridine	DMF	6.6± 1.1	6.5± 1.1	14000	16100
9	**MPFPA-1**	**16** + Octadiyne	CuBr, bipyridine	THF	7.0± 1.1	9.0± 1.1	11400	13800

Achieving the necessary conditions for single chain folding requires careful adjustment of concentrations, making the slow addition of the post-modified polymer solution to an aqueous $CuSO_4$/NaAsc solution *via* a syringe pump a crucial step. In this setup, it was anticipated that the amphiphilic post-modified polymer would adopt a preorganized intramolecular core–shell structure, where the hydrophilic PEG sidechains were expected to form the shell, while the reactive azide-groups comprised the core in water (Scheme 25).[318] Octadiyne was employed as an external crosslinker to initiate the procedure, but it resulted in an increase of the number average molar mass, suggesting the occurrence of intermolecular cross-linkage. DLS measurements revealed an increased hydrodynamic diameter when water was used as the folding medium. Changing the medium from water and $CuSO_4$ and sodium Asc. to using THF, along with CuBr and bipyridine, significantly improved the CuAAC click reaction. This enhancement was accompanied by a noticeable reduction in hydrodynamic diameter as observed through DLS, and a decrease in the number average molar mass, as well as the disappearance of the azide-band observed *via* IR spectroscopy. These changes serve as clear indicators of the successful formation of SCNPs,[202] which may be attributed to the increased solvation of the polymer

in the non-aqueous solvent. Solvation might have potentially hindered the preorganization of the core-shell structure, thereby limiting the flexibility required to bring the reactive sites into close proximity. This limitation could be attributed to the comparably sufficient but modest degrees of polymerization of the post-modified polymers. Switching from octadiyne to **15** or **16** once again resulted in intermolecular crosslinking events, as evidenced by the increase in M_n and hydrodynamic diameter. The steric demand and rigidity inherent within the bisoxazoline structures likely contributed to this behavior. The rigidity of alkyne functionalities, combined with their spatial proximity in both bisoxazoline derivatives, particularly due to the presence of only one methylene spacer to a quaternary carbon, may have restricted their reactivity. This limitation seemed to have prevented these structures from effectively acting as crosslinkers in intramolecular cross-linkage. Test reactions with **MPFPA-1** or **MFPM-1** and the auxiliary crosslinker octadiyne, which are expect to aid in preorganizing the single-chain nanoparticles could not overcome this limitation.[308] An alternative design of bisoxazoline crosslinkers with more flexible spacers could be beneficial for future endeavors.

3.2.2.4 Transesterification strategy with bis-(*N*-heterocyclic carbene) copper complexes

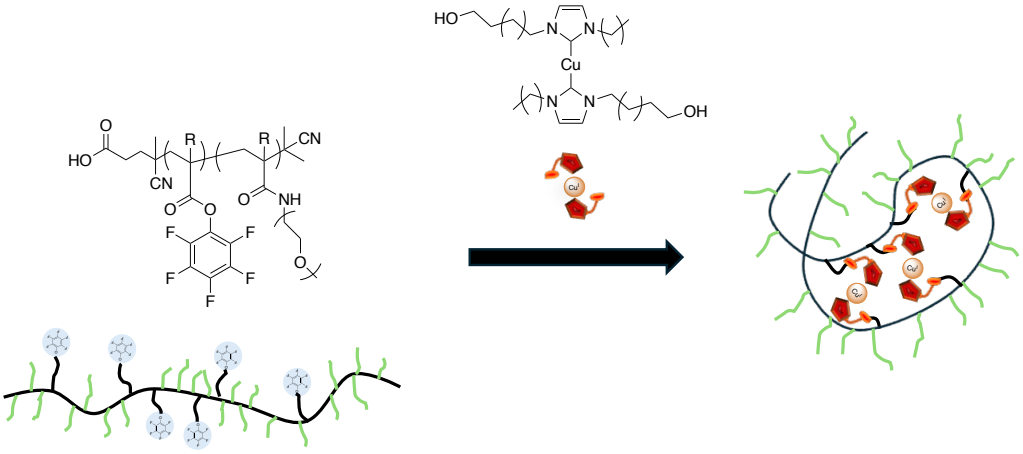

Scheme 26. Transesterification of the pentafluoro phenyl moiety as a collapse strategy to generate SCNPs. R = H for acrylate; R = CH_3 for methacrylate

Copper carbene complexes are known for their stability against air, moisture and bases.[319] Furthermore their catalytic activity for the envisioned cyclopropanation reaction had been reported.[272] The aforementioned precursor polymers allow for the post-modification of the pentafluorophenyl moieties to introduce the amphiphilic characteristics as well as the single chain folding capabilities into SCNPs.[281] An alternative post-modification strategy for the aminolysis has been established as by Das *et al.*,[299] the transesterification of pentafluorophenyl acrylates. Mechanistic investigations revealed the involvement of both DMAP and the nucleophilic solvent *N,N*-dimethylformamide (DMF) in catalyzing the transesterification reaction. This explained why nearly quantitative conversion was achieved solely in DMF and not in a non-nucleophilic solvent such as 1,4-dioxane. With this in mind, a bis(*N*-heterocyclic carbene) copper complex (bis-NHC-Cu), **17** was synthesized. The complex had two hydroxyl groups for the transesterification reaction with pentafluorophenyl moieties as a folding approach established with Mohamed Hassan of the post-modified polymers **MPFPM-2** or **MPFPA-2** (Scheme 26). To synthesize, a quaternization reaction was conducted using 11-bromo-1-undecanol and 1-hexylimidazole. The resulting 3-hexyl-1-(11-hydroxyundecyl)-1H-imidazol-3-ium bromide was then complexed with copper(I)oxide to form **17**.[320] To assess the compatibility of these complexes with DMAP, a stability test of the **17** under transesterification conditions was conducted. Aliquots were collected after 2, 24 and 73 hours and the

samples were analysed using ^{1}H NMR spectroscopy. No resonance for the highly acidic proton of the imidazolium moiety at 9.2 ppm was observed in the spectra. The absence of this signal suggested that the copper complex remained stable, even after 73 hours at 80 °C in DMF. This inspired the exploration of transesterification as a novel collapse methodology for single-chain nanoparticles. In this approach, complexes with hydroxyl groups are utilized as crosslinkers, and DMF serves as the folding medium (Scheme 26).

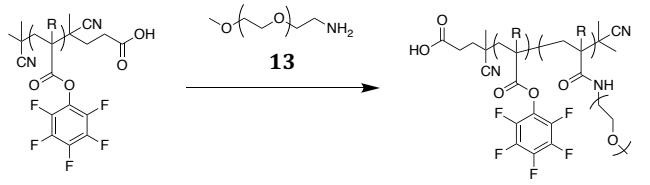

Scheme 27. Post-modification of **PFPA-2**/**PFPM-2** with **13** to **MPFPA-2**/**MPFPM-2**.

Table 23. Post-modification with ω-amino-poly(ethylene glycol).

Entry	Polymer	Solvent	*T* [°C]	Catalyst	[equiv.]	Time [days]	M_n [g/mol]	PDI
1	**PFPM-2**	THF	50	-	-	3	25000	1.4
2	**PFPM-2**	THF	55	-	-	4	27000	1.5
3	**PFPM-2**	DMF	80	TEA	1	1	25800	1.5
4	**PFPM-2**	DMF	80	TEA	1	1	22800	1.7
5	**PFPM-2**	THF	50	-	-	1	24300	1.5
6	**PFPA-2**	THF	50	DMAP	0.2	3	20900	1.4
7	**PFPA-2**	THF	60	DMAP	0.2	3	18000	1.5

PFPA-2 and **PFPM-2** were post-modified with ω-amino-poly(ethylene glycol) to synthesize polymers with a degree of functionalization of 0.8 and 0.2 of pentafluorophenyl moieties intended for the cross-linkage (Scheme 27). Similarly to the full post-modification approach discussed in chapter 3.2.2.3, post-modification was investigated in various conditions: without catalysts in THF[314] (Table 23, entry 1-2 & 5), in highly polar aprotic solvents like DMF[317] with TEA[301, 315] as catalyst (Table 23, entry 3-4), or in THF with DMAP[316] as catalyst (Table 23, entry 6-7). The conversion was tracked using *in situ* ^{19}F NMR spectroscopy, which revealed the most favorable results for **MPFPM-2** in DMF with TEA (Table 23, entry 3) and for **MPFPA-2** in THF without DMAP (Table 23, entry 5).

To establish and evaluate the transesterification as a novel methodology for synthesizing SCNPs, reactions were conducted using **PFPM-1** with DMAP as the catalyst and DMF as folding medium (Table 24). The first attempt did not result in a decrease in the number average molar but did show a slight decrease in DLS (Table 24, entry 1). Repeating the experiment at a higher dilution led to a decrease in the hydrodynamic radius according to DLS, as well as a decrease in the number average molar mass (Table 24, entry 2). These were both clear indications for the crosslinking of the polymer chain. For the single-chain nano particles collapse the experiments were conducted with the **MPFPA-2** and **MPFPM-2**. Although a reduction in hydrodynamic radius and number average molar mass was observed for the **MPFPM-2**, ^{19}F NMR spectroscopy indicated not a full conversion of the pentafluoro phenyl moieties. Upon repetition, the decrease in either DLS or number average molar mass became less pronounced when DMAP was used as a catalyst. It is possible that the presence of methyl groups in the backbone of the post-modified polymers imparts conformational rigidity and thereby reducing chain flexibility, making the polymer less adaptable to the necessary conformations for efficient substitution reactions with the sterically encumbered **17**. This hindrance could slow down or impede the full conversion of the reaction by limiting the accessibility of reacting species to the reaction site.

Table 24. Collapse and crosslinking attempts of **PFPM-1**, **MPFPM-2** and **MPFPA-2** *via* the transesterification methodology using **17** and 1,6-hexandiol at 80 °C.

Entry	Polymer	Crosslinker	Catalyst	Solvent	DLS_{before}	DLS_{after}	$M_{n\ before}$	$M_{n\ after}$
1	**PFPM-1**	**17**	DMAP	DMF	6.0 ± 0.6	5.3 ± 0.9	11400	13500
2	**PFPM-1**	**17**	DMAP	DMF	6.6 ± 0.3	5.5 ± 1	16600	16000
3	**MPFPM-2**	**17**	DMAP	DMF	8.4 ± 1.3	7.6 ± 1.3	24700	20700
4	**MPFPM-2**	**17**	DMAP	DMF	6.3 ± 1.2	6.3 ± 1.1	25800	25300
5	**MPFPM-2**	**17**	DMAP	DMF	7.6 ± 1.3	7.8 ± 1.3	25800	26100
6	**MPFPM-2**	**17**	TEA	DMF	8.3 ± 1.3	8.7 ± 1.4	22800	22800
7	**MPFPM-2**	**17** + 1,6-hexanediol	TEA	DMF	8.3 ± 1.3	6.7 ± 0.8	23000	18400
8	**MPFPA-2**	**17**	DMAP	DMF	6.4 ± 1.1	6.1 ± 1.1	18000	16300
9	**MPFPA-2**	**17** + 1,6-hexanediol	TEA	DMF	6.4 ± 1.1	6.8 ± 1.1	18000	14300

Consequently, crosslinking was explored using TEA as an alternative catalyst, and higher catalyst loading was investigated for the transesterification. While the DLS and GPC results did not exhibit a clear reduction in the size of the nanoparticles, ^{19}F NMR demonstrated almost complete conversion of the pentafluorophenyl moieties. To preorganize the polymer chain 1,6-hexanediol was employed as an auxiliary cross-linker, to facilitate the incorporation of the bulky **17** complex. This resulted in a significant decrease in the number average molar mass (Table 24, entry 7).

To confirm the formation of single-chain nanoparticles, diffusion ordered spectroscopy NMR (DOSY NMR) experiments were conducted of both, the post-modified polymers, and **NP 1**. DOSY NMR relies on the principle that the diffusion rate of a molecule or particle in a solution is inversely proportional to its size. Larger molecules or particles diffuse more slowly, whereas smaller ones diffuse more rapidly. SCNPs, being relatively smaller compared to the post-modified polymer, exhibit distinct diffusion behaviour in a DOSY NMR experiment. Consequently, the method provides data on diffusion coefficients, which can then be used to calculate hydrodynamic radii using the Stokes-Einstein equation (Eq. 1), where k_B is Boltzmann constant, T is temperature, η is the solvent viscosity and D is the diffusion coefficient.

$$r_h = \frac{k_B T}{6\pi \eta D} \qquad \text{Eq. 1}$$

This equation establishes a relationship between the diffusion coefficient of a particle and its corresponding hydrodynamic radius (Table 25).

Table 25. Comparison of **MPFPM-2** to **NP 1**.

			Hydrodynamic diameter [nm]	
	M_n [g/mol]	PDI	DLS	DOSY
MPFPM-2	23000	1.7	8.3 ± 1.3	13.4
NP 1	18400	1.7	6.7 ± 0.8	11.0

The results revealed a reduction in the hydrodynamic diameters, as evident in both DLS and DOSY NMR. Even though there is a difference in the determined hydrodynamic diameters between the DLS and DOSY NMR data. ^{19}F NMR demonstrated complete conversion of the pentafluorophenyl moieties. These findings support the successful formation of single-chain nanoparticles through the transesterification of pentafluorophenyl moieties and the incorporation of **17**. To conclusively confirm the successful incorporation of copper into the SCNP, inductively coupled plasma mass spectrometry (ICP-MS) could be employed in future endeavors.[321] Additionally, atomic force microscopy could be utilized to determine the morphological differences between the post-modified polymer and the folded single-chain nanoparticles.[212, 322]

The transesterification of **MPFPA-2** resulted in a reduction in hydrodynamic diameter, as observed in GPC analyses (Table 26). This reduction occurred with DMAP as catalyst in the presence or absence of 1,6-hexanediol as auxiliary crosslinker (Table 24). ^{19}F NMR spectroscopic studies revealed a complete disappearance of the polymeric signals originating from the pentafluoro phenyl moieties. This is an indication that transesterification appears to proceed more efficiently when not impeded by the methyl groups within the polymer backbone of poly(pentafluoro phenyl methacrylate). Similarly, to the **MPFPM-2**, the auxiliary cross-linker induced more reduction of the hydrodynamic diameter than the collapse without auxiliary cross-linker according to GPC analysis.

Table 26. Comparison of **MPFPA-2** to **NP 2** & **NP 3**.

			Hydrodynamic diameter [nm]	
	M_n [g/mol]	PDI	DLS	DOSY
MPFPA-2	18000	1.4	6.4 ± 1.1	8.0
NP 2	16300	1.4	6.1 ± 1.1	-
NP 3	14300	1.5	6.8 ± 1.1	7.5

DOSY NMR spectroscopic investigations comparing **MPFPA-2** to **NP 3** showed well-defined diffusions for the **NP 3** but also exhibited an undistinguishable diffusion pattern for **MPFPA-2**. It is possible that the sensitivity of DOSY NMR detected residual ω-amino-poly(ethylene glycol)methyl ether even after extensive dialysis in THF. AFM and ICP-MS measurements could serve as valuable supplements for the future characterization of the nanoparticles.

In summary, the formation of single-chain nanoparticles with two different polymer backbones, acrylate and methacrylate, both based on precursor polymers containing pentafluoro phenyl moieties, by transesterification can be reported. This is supported by evidence of a reduction in hydrodynamic diameter observed through GPC, DLS and DOSY NMR analyses.

The precursor polymers allow for the modification of hydrophilicity through post-modification methodologies. Strong indications of copper incorporation are evident through the observed reduction in hydrodynamic diameter. Further investigations can be conducted using techniques such as ICP-MS to confirm the presence of copper in the nanoparticles. Additionally, TEM may be employed for potential copper detection, utilizing staining or techniques such as Energy-Dispersive X-ray Spectroscopy[323] or Electron Energy Loss Spectroscopy.[324, 325]

The synthesized SCNPs could potentially be investigated regarding their capability to cyclopropanate squalene and be compared to the catalysts screened in chapter 3.1.1. One of the limitations inherent in the here established procedure for the synthesis of single-chain nanoparticles is related to the degree of polymerization of the precursor polymers. Despite extensive efforts to enhance the degree of polymerization for the homopolymers of **PFPM-1** and **PFPA-1** by RAFT-polymerization, it appears that there is a limit to the number average molar mass achievable.[297] Poly(pentafluorophenyl methacrylate) homopolymerization has shown a somewhat linear correlation between conversion and M_n up to 18 kDa but only with PDIs of roughly 1.3.[298, 303] Those values were almost reached with well-controlled RAFT-polymerizations up to 16 kDa. To circumvent these limitations the synthesis of the post-modified polymer for the transesterification methodology could also be attempted with a copolymerization of poly(ethylene glycol methacrylate) (PEGMA) and pentafluorophenyl methacrylate. The statistical copolymers of PEGMA and azidopropyl methacrylate of Thümmler *et al*.[308, 318] with their well-studied core shell structures, would also represent a suitable system for the incorporation of bis-NHC copper with azide functionalities or the herein-synthesized **15** or **16**. The complexes of **15** and **16** with tetrakis (acetonitrile) copper (I) hexafluoro phosphate could also be tested for the autocatalytic formation of SCPNs using the CuAAC click reaction in future endeavors. Other multifunctional bisoxazoline ligands may expand the scope of applicable reaction types beyond cyclopropanation to e. g. Diels-Alder reactions[326] and Michael Additions.[327, 328] Furthermore, transitioning from copper bisoxazoline complexes to other metals such as iron, could possibly lead to catalytic activity for oxyamination[329] and cyanofunctionalization by electrocatalytic activation.[330]

4. Conclusion

The European Green Deal and CSRD emphasize the need for a sustainable transformation across all sectors, including the polyene and rubber industry. By promoting the development of green chemistry and sustainable degradation methodologies, especially for challenging materials like PI and PB, the EU aims to reduce environmental impact, foster innovation, and create a circular economy. Moreover, in view of the European Commission's designation of NR as a critical raw material in 2017, the development and optimization of chemical or biotechnological recycling methodologies for end-of-life tires, NR, and SPI have become even more imperative. However, the absence of hydrolysable functional groups in the polymer backbones of PI and PB results in challenging recycling. Furthermore, the poor solubility of the polyenes in water is hypothesized to substantially limit the available interface for enzymatic degradation.

Accordingly, in this thesis two different emulsification methods have been established to generate surfactant-free emulsions of PI in aqueous media, utilizing either a co-solvent or acoustical emulsification, to tackle this obstacle. Acoustical emulsification was investigated for different sonication durations and amplitudes. The effect of M_n and the polydispersity was investigated and revealed that for **PI 3000** the most uniform emulsions were obtainable. The hydrodynamic diameter of the acoustically emulsified **PI 3000** was 800 nm according to DLS measurements after preparation (Figure 42 (I)). A decrease of the hydrodynamic diameter and the transmittance was observed and tracked within 24 hours DLS measurements, revealing creaming of the hydrophobic polymer in the aqueous KPi at the investigated concentration of 5 mM. Control experiments with GPC showed no indication for degradation by the acoustical sonication procedure.

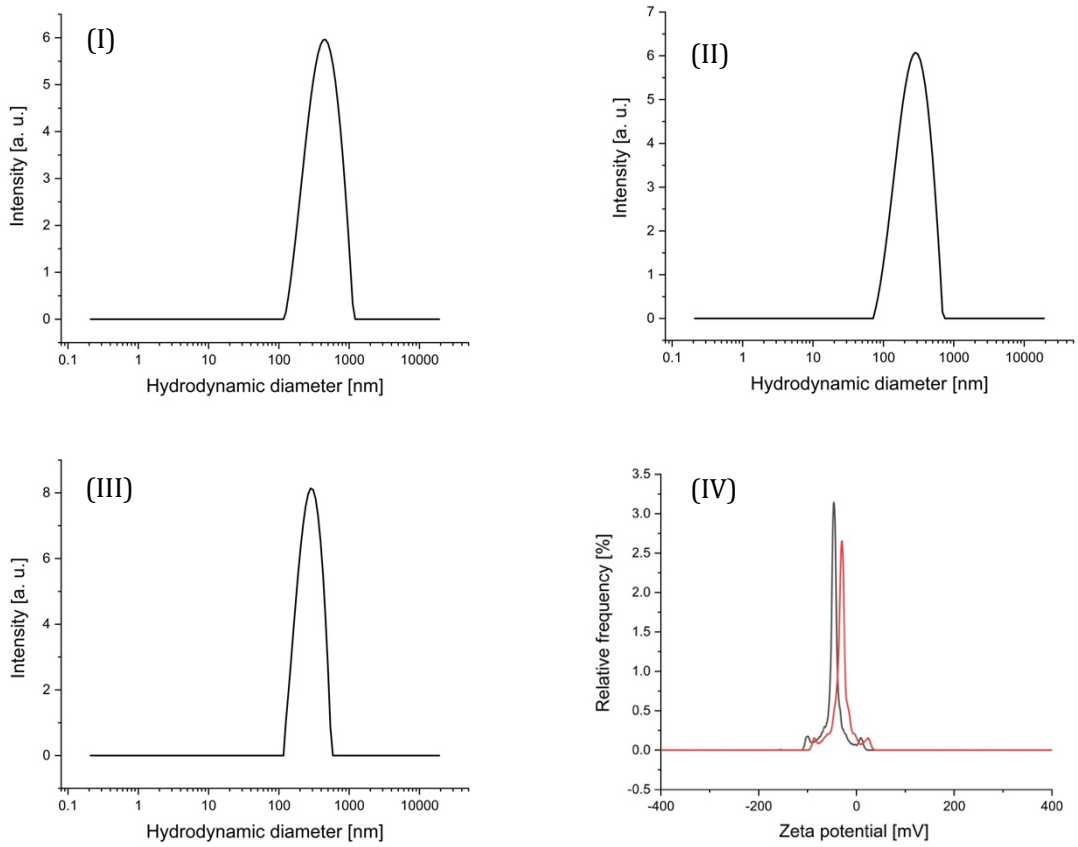

Figure 42. DLS of **A 1**, acoustically emulsified **PI 3000**, (I), DLS of **C 2**, co-solvent emulsified **PI 14 000** (II), DLS of **C 1**, co-solvent emulsified **PI 3000**, with the corresponding zeta potential measurement of **C 1** with *n*-hexadecane as negative control (IV).

The combination of a co-solvent with a hydrophobic polymer was investigated for increased emulsion stability for the first time for PI. Increased stabilization with the co-solvent *n*-hexadecane was observed for PIs, **PI 3000** and **PI 14000**, after emulsification. The co-solvent stabilized emulsions of PI showed size distributions in DLS measurements, of 280 nm for **PI 3000** (**C 1**) and 270 nm for **PI 14000** (**C 2**) with a 1-to-1 ratio of *n*-hexadecane to the respective polymer in 5 mM KPi (Figure 42 (II), (III)). The stabilization of the co-solvent emulsification approach was further evidenced by zeta potential measurements (Figure 42 (IV)). Transmittance studies revealed a stabilization of the emulsions for **C 1** up to 220 hours and for **C 2** up to 140 hours with the optimized surfactant-free emulsification approach. The transferability of the concept to PB for co-solvent emulsified systems was demonstrated. A surfactant-free cosolvent emulsification of **PB 3500** led to a hydrodynamic diameter of 200 nm. The influence of temperature was investigated to ensure surfactant-free emulsion stabilization at different hypothetical degradation temperatures. The stabilization of the surfactant-free emulsions decreased with increasing temperature according to DLS and transmittance studies.
For the investigation of the effect of surfactant-free emulsification on the enzymatic degradation behaviors the degradation of **L 1** was first replicated with the rubber oxygenase Lcp_{K30}. **L 1** was used as a reference system and positive control for the expansion of the degradation scope on SPIs and NR derived PI. The effect of the co-solvents with respect to the degradation fragment detection was investigated to confirm *n*-hexadecane as the best candidate for the enzymatic degradation with the least inhibition effect of the screened solvents. Optimizations of the enzymatic degradation parameters with Lcp_{K30} for the degradation of SPIs with a significant 1,4-*trans* ratio were conducted. Those parameters allowed for the first detection of enzymatic degradation of a SPI with a substantial *cis*: *trans* ratio of 56:27 by ^{1}H NMR spectroscopy.

Table 27. PIs and corresponding surfactant-free emulsions investigated in the comparative analysis of the enzymatic degradation with Lcp_{K30}.

PI	M_n [g/mol]	PDI	Microstructure [%]				Emulsification Strategies	Diameter [nm]	Effect of emulsification
			3,4-units	1,4-units *cis*	1,4-units *trans*	1,2 units			
PI 3000	3100	1.1	16	56	27	1	**N 1**	n. e.	n. e
							A 1	800	200%
							C 1	280	400%
PI 14000	14000	1.1	16	55	28	1	**N 2**	n. e.	n. e
							C 2	270	20%
PI *cis* 7000	7000	6.6	-	98	2	-	**N 3**	n. e.	n. e
							C 3	n. e	100%

UHPLC-UV comparative analysis of the standardized enzymatic degradation experiments clearly showed that the surfactant-free emulsification approach with either acoustical emulsification or co-solvent emulsified system led to an increase in the area of degradation fragments (Figure 43 (I)). **C 1** showed the most significant increase, with 4-fold higher integrated degradation fragments area than the non-emulsified **PI 3000** (**N 1**) according to UHPLC-UV analysis (Table 27). UHPLC-ESI-HRMS/MS measurements confirmed that the fragmentation patterns of **C 1** were almost identical to the bioinspiration **L 1**. The tolerance of Lcp_{K30} towards other isomeric motifs than the 1,4-*cis*-isomer of PI showed its potential as a sustainable degradation catalyst for polymers, which require new sustainable methodologies of recycling.

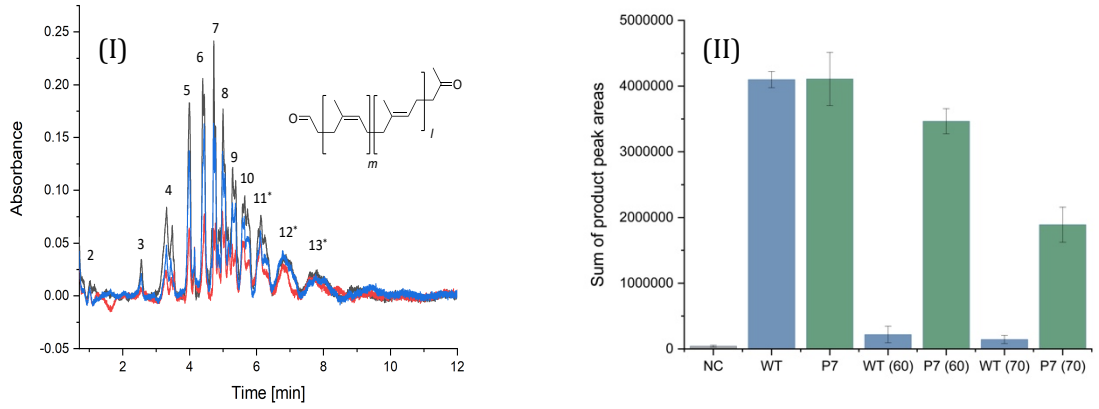

Figure 43. Stacked UHPLC-UV-chromatograms of enzymatically degraded **PI 3000** with the assigned degradation fragments (number of intact isoprene units (m + l)). **C 1**, black; **A 1**, blue; non-emulsified **N 1**, red. (I) Cumulative area of the product peak areas according to UHPLC-UV-ESI-MS of Lcp_{K30}-wild type (WT), Lcp_{K30}-PROSS variant 7 (P7) without incubation and with incubation at 60 °C and 70 °C prior to **L 1** degradation. (II)

Protein-engineered variants of the rubber oxygenase Lcp_{K30} by PROSS showed increased thermostability according to NanoDSF. The most promising variant Lcp_{K30}-P7 was investigated for its catalytic behavior and showed the capability of withstanding thermal stress at 60 °C and to a lesser degree at 70 °C regarding catalytic activity towards 1,4-*cis*-PI according to UHPLC-UV-ESI-MS (Figure 43 (II)).

To facilitate future catalytic investigations of polyenes, a new rubber oxygenase degradation assay was developed with UV-GPC. Synthetic PBs and PIs were chemically degraded by epoxidation and subsequent oxidative degradation with periodic acid. The resulting mixtures of telechelic polyenes and undegraded polyenes were derivatized for the detection of the new UV-absorption by GPC. Quantitative conversion of the derivatization agent was determined according to ^{1}H NMR, 2D-NMR methodologies and by investigation of the extracted ion chromatograms in UHPLC-UV-ESI-HRMS. Application of the rubber oxygenase degradation assay allowed for the tracking of degradation with a background of undegraded polymer for the chemically degraded samples and for the enzymatically degraded samples of **PI 4500** and **PI 3000** by Lcp_{K30} (Figure 44).

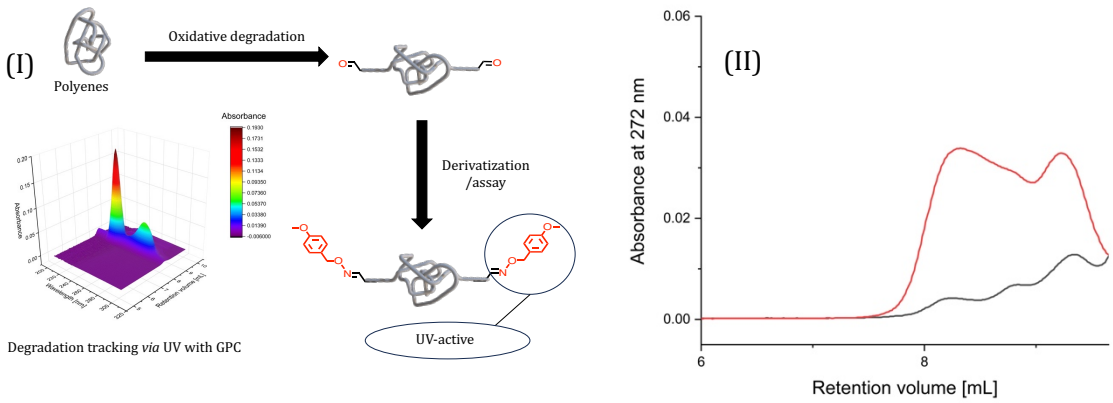

Figure 44. Concept of the rubber oxygenase degradation assay with oxidative degradation of polyenes, subsequent derivatization and tracking *via* GPC (I) GPC measurements at wavelength 272 nm for **PI 3000 WT-D** (red) and **PI 3000** negative control (black) (II)

The activity of the first round of protein-engineered enzymes were investigated alongside the native enzyme and the FuncLib protein engineered enzymes in a comparative analysis with the established

methodology. The promising results for the degradability of polybutadiene were investigated further with UHPC-ESI-HRMS. UHPLC-ESI-HRMS revealed that the catalytic activity was too low to conclusively proof the degradation. But nonetheless, the established methodologies and the investigations into their applicability onto the enzymatic degradation of polyenes can be seen as valuable tools in the endeavor of finding new sustainable ways of degrading rubbers in the future.

Regarding the second general problem of green chemistry tackled in this work the remediation and reduction of waste materials, investigations of novel catalytic entities, SCPNs, for cyclopropanation of oliogenes and polyenes were conducted. Cyclopropanations with different copper catalysts were investigated as a preliminary study for the reaction with the oligoene squalene. For the incorporation of cyclopropanating functionalities in SCNPs as an alternative catalytic system three different approaches were investigated. A library of imidazolium bearing acrylamides was synthesized but did not lead to the required polymeric architecture in copolymerization with *N*,*N*-dimethylacrylamide. Alternatively, a precursor polymer approach for poly(pentafluorophenyl acrylate) (**PFPA-1**) and poly(pentafluorophenyl methacrylate) (**PFPM-1**) was investigated. After polymerization the polymers were post-modified by two different approaches to result in amphiphilic polymers. Post-modifed polymers with azide-functionalities (**MPFPA-1**/**MPFPM-1**) were investigated in view of their folding behavior with alkyne-bearing cross-linkers (**15**/**16**) by copper catalyzed azide alkyne click reactions in two different media. These approaches did not lead to a clear reduction of the hydrodynamic diameter by DLS or GPC. Post-modified poly(pentafluorophenyl acrylate) (**MPFPA-2**) and poly(pentafluorophenyl methacrylate) (**MPFPM-2**) led the formation of SCNPs with hydroxyl bearing bis(*N*-heterocyclic carbene) copper complex **17** and with the addition of auxiliary cross-linker 1,6-hexanediol. This is supported by evidence of a reduction in hydrodynamic diameter observed through DLS, GPC, and DOSY NMR analyses. These new SCNPs could have the functionality for the cyclopropanation incorporated into their polymeric structure and could allow for the investigation of SCNPs as catalytic cyclopropanating entities in the future.

5. Experimental Section

5.1 Materials and methods

High Performance Liquid Chromatography (HPLC). HPLC studies were carried out on a Chromaster by Hitachi VWR equipped with a pump (L-5160), an autosampler (L-5260), a degasser, a diode array detector (DAD; L-5430), and a column oven (L-5310) with temperature control. The spectra were recorded on a reversed phase column (RP C-18) Waters Atlantis-T3, 5 µm, 100 Å, 4.6 × 250 mm or a reversed phase EC-C8 InfinityLab poroshell, 4 µm, 120 Å, 4.6 × 250 mm. DAD signals were recorded by using Chromaster software manager version 1.1 with an operating wavelength from 190 to 900 nm. The tracking wavelength was 210 nm.
The mobile phases for method A were water (A) and MeOH (B). Chromatographic separation of the samples (injection volume 10 µL) was realized using a gradient system starting from water 50% B (isocratic for 5 min) and increasing to 100% B within 2 min, followed by further 43 min at 100% B at a constant flow rate of 0.7 mL/min. The column re-equilibration time was set to 3 min at 50% B (flow 0.7 mL/min). The oven temperature was set at 30 °C and the analytes were detected at 210 nm.
The mobile phase for method B was MeOH (A). Chromatographic separation of the samples (injection volume 10 µL) was realized using an isocratic system starting from MeOH 100% A at a constant flow rate of 0.7 mL/min. The column re-equilibration was not necessary due to the isocratic measurement. The oven temperature was set at 30 °C and the analytes were detected at 210 nm.
The mobile phases for method C was MeOH (A). Chromatographic separation of the samples (injection volume 10 µL) was realized using an isocratic system starting from MeOH 100% A at a constant flow rate of 0.5 mL/min. The column re-equilibration was not necessary due to the isocratic measurement. The oven temperature was set at 30 °C and the analytes were detected at 210 nm.
The mobile phases for method D were water (A) and ACN (B). Chromatographic separation of the samples (injection volume 10 µL) was realized using a gradient system starting from water 50% B (isocratic for 5 min) and increasing to 100% B within 2 min, followed by further 43 min at 100% B at a constant flow rate of 0.7 mL/min. The column re-equilibration time was set to 3 min at 50% B (flow 0.7 mL/min). The oven temperature was set at 30 °C and the analytes were detected at 210 nm.

Ultra-high performance liquid chromatography (UHPLC). Chromatographic analysis was performed using a Waters Acquity UPLC system equipped with an UV-detector. The RP-C8 UHPLC column from Agilent (InfinityLab Poroshell 120 EC-C8, 2.1 x 50 mm, 1.9 µm) with a guard column (InfinityLab Poroshell 120 EC-C8, 2.1 mm, 1.9 µm) was used. The mobile phases were water (A) and MeOH (B). Chromatographic separation of the samples (injection volume 5 µL) was realized using a gradient system starting from 68% B (isocratic for 0.5 min) and increasing to 100% B within 2 min, followed by further 3.5 min at 100% B at a flow rate of 0.7 mL/min. Then the flow rate was increased within 1 min to 1 mL/min holding at 100% B for further 9 min. The column re-equilibration time was set to 3 min at 68% B (flow 0.7 mL/min). The oven temperature was set at 35 °C and the analytes were detected at 210 nm.

Electron spray ionization time of flight mass spectrometry (ESI-TOF-MS). ESI-TOF-MS measurements were performed on a Bruker Daltonics microTOF *via* direct injection at a flow rate of 180 µL/h in positive mode with an acceleration voltage of 4.6 kV. Samples were prepared by dissolving in LC-MS grade of the appropriate solvent, MeOH or THF or mixtures of both, ACN, ethyl acetate, ethanol, with additional salts, if required, such as sodium iodide salt in acetone or lithium chloride in LC-MS-grade water. The software Data Analysis (version 4.0) was used for data evaluation.

High Performance Liquid Chromatography-Mass spectrometry (HPLC-ESI-TOF-MS). Measurements were carried out on a Chromaster by Hitachi VWR equipped with a pump (L-5160), an autosampler (L-5260), a degasser, a diode array detector (DAD; L-5430), and a column oven (L-5310) with temperature control. A solution with a concentration of 1 mg/mL was prepared. The spectra were recorded on a reversed phase column (RP C-18) Waters Atlantis-T3, 5 µm, 100 Å, 4.6 × 250 mm or a reversed phase EC-C8 InfinityLab poroshell, 4 µm, 120 Å, 4.6 × 250 mm. DAD signals were recorded by using Chromaster software manager version 1.1 with an operating wavelength from 190 to 900 nm. The tracking wavelength was 210 nm. The mobile phase was MeOH (A). Chromatographic separation of the samples (injection volume 10 µL) was realized using an isocratic system starting from MeOH 100% A at a constant flow rate of 0.5 mL/min. The oven temperature was set at 30 °C and the analytes were detected at 210 nm. ESI-TOF-MS measurements were performed on a Bruker Daltonics microTOF in positive mode. The software Data Analysis (version 4.0) was used for data evaluation.

Ultra-high performance liquid chromatography electron spray ionization high resolution mass spectrometry (UHPLC-ESI-HRMS). The positive ion high-resolution ESI mass spectra (*m/z* range 150-1500) were obtained with an Orbitrap Elite mass spectrometer (Thermo Fisher Scientific, Germany) equipped with a heated electrospray ion source (spray voltage 3.8 kV, capillary temperature 325 °C, source heater temperature 300 °C, FTMS resolution 30.000). Nitrogen was used as a sheath and auxiliary gas. The MS system was coupled to an ultra-high-performance liquid chromatography (UHPLC) system (Dionex UltiMate 3000, Thermo Fisher Scientific), equipped with a RP-8 column (particle size 1.9 µm, 50 × 2.1 mm ID, InfinityLab Poroshell 120 EC-C8, Agilent; column temperature 40 °C) with a guard column (InfinityLab Poroshell 120 EC-C8, 1.9 µm, 2.1 mm ID). The mobile phases were H_2O (A; MilliQ-biocel apparatus from Millipore) and MeOH (B), each with 0.1% formic acid (additive for LC-MS). Chromatographic separation of the samples (injection volume 5 µL) was realized using a gradient system starting from 70% B (isocratic for 1 min) and increasing to 100% B within 3 min, followed by further 3 min at 100% B at a flow rate of 0.3 mL/min. Then the flow rate was increased within 0.5 min to 0.4 mL/min holding at 100% B for further 3.5 min. The column re-equilibration time was set to 3 min at 70% B (flow 0.3 mL/min). High energy collision dissociation (HCD) mass spectra were recorded at a relative collision energy of 40% using nitrogen as the collision gas. The instrument was calibrated externally using the Pierce ESI positive ion calibration solution (product no. 88323) from Thermo Fisher Scientific. The data were evaluated using the software Xcalibur 2.2 SP1.

UHPLC-UV-ESI-HRMS (QTOF). The UHPLC-UV-ESI-HRMS measurements were performed with a TripleToF 6600-1 mass spectrometer (Sciex), which was equipped with an ESI-DuoSpray-Ion-Source (operation in positive ion mode) and was controlled by Analyst 1.7.1 TF software (Sciex). The ESI source operation parameters were as follows: ion spray voltage: 5,500 V, nebulizing gas: 75 p.s.i., source temperature: 450 °C, drying gas: 60 p.s.i., curtain gas: 55 p.s.i. Data acquisition was performed in the MS1-TOF mode, scanned from 100 to 1500 Da with an accumulation time of 250 ms. The instrument was externally calibrated by the ESI positive ion calibration solution from Sciex. The MS system was coupled to an ultra-high-performance liquid chromatography (UHPLC) system (Waters I-class, Waters), equipped with a RP-8 column (particle size 1.9 µm, 50 × 2.1 mm ID, InfinityLab Poroshell 120 EC-C8, Agilent; column temperature 45 °C) with a guard column (InfinityLab Poroshell 120 EC-C8, 2.1 mm, 1.9 µm). The mobile phases were H_2O (A; MilliQ-biocel apparatus from Millipore) and MeOH (B; Chromasolv™, for LC-MS, Honeywell Riedel de Haën™), each with 0.1% formic acid (additive for LC-MS, LiChropur®, Merck). Chromatographic separation of the samples (injection volume 10 µL) was realized using a gradient system starting from 70% B (isocratic for 1 min) and increasing to 100% B within 3 min, followed by further 3 min at 100% B at a flow rate of 0.3 mL/min. Then the flow rate was increased within 0.5 min to 0.4 mL/min holding at 100% B for further 3.5 min. The column re-equilibration time was set to 3 min at 70% B (flow 0.3 mL/min). The wavelength range

of the PDA measurements was 200-600 nm used for detection. The data were evaluated using the software Peakview 1.2.0.3 (AB Sciex).

Matrix-assisted laser desorption/ionization time-of-flight mass spectrometry measurements (MALDI-TOF-MS). MALDI-TOF-MS measurements were performed on a Bruker Autoflex III system (Bruker Daltonics) using a nitrogen laser operating at a wavelength of λ = 337 nm in reflection mode. The used matrix: analyte: salt ratio was 100:10:1 and 1 µL of the solution was spotted on the MALDI target. The polymer samples were either dissolved or suspended in THF or DMF and DCTB or O-(4-Methoxybenzyl)-hydroxylamine-hydrochloride or Dithranol was used as matrix in THF or DMF, while NaTFA or AgTFA was used as salt in THF or DMF. Data evaluation was carried out *via* flexAnalysis software (3.4) and simulation of the isotopic pattern was performed by Data Analysis software (version 4.0).

Nuclear magnetic resonance (NMR). The NMR spectra were measured using an Agilent Technologies 400 MHz VNMRS and 500 MHz DD2 at 27 °C. Chemical shifts (δ) are reported in ppm and referred to the residual solvent signal (for example $CDCl_3$ 7.26 ppm for ^1H NMR).

Sonication. Co-solvent stabilized systems were sonicated in an ultrasonic cleaner (VWR) filled with MilliQ water at an ultrasound frequency of 45 kHz.

Ultrasonication. Ultrasound treatments for the acoustically emulsified system were performed with a VCX 500 ultrasonic processor (Sonics & Materials, CT, USA) equipped with a 3 mm micro tip. Cycles of pulsed ultrasound at a frequency of 20 kHz were applied using 30% of the maximum amplitude with a sequence of 10 s pulse and 5 s pause for 60 minutes.

Gel permeation chromatography (GPC). Tetrahydrofuran-based SEC measurements were performed at 30 °C on a Viscotek GPCmax VE 2001 from ViscotekTM using a CLM3008 precolumn and a CLM3008 main column. THF was used as the solvent at a flow rate of 1 mL/min. To determine the molecular weights, the refractive index of the sample under study was determined using a VE 3580 RI detector or a UV detector 2600 from ViscotekTM. External calibration was performed using either polystyrene (PS) standards (purchased from PSS) with a molecular weight range from 1050 to 115000 g/mol or polybutadiene (PB) standards (purchased from PSS) with a molecular weight range from 1070 to 1020000 g/mol. The UV data were acquired by scanning UV-Spectra mode of the deuterium lamp with a scan output speed of 1 nm/s and a range from 192 nm to 510 nm. OmniSEC software (version 4.6.2.359) was used to analyze the data.

Dynamic light scattering (DLS). The size distributions of the emulsions were determined on an Anton-Paar Litesizer 500. Samples were measured with a measurement angle of 175° and a focus position of -3.707 mm. A series of 6 runs with disposable measuring cells and 25 °C temperature was evaluated. A refractive index of 1.33 for the utilized dispersant was applied. Transmittance was determined under the same conditions using the Litesizer 500. The data were evaluated using the software Kalliope™.

Zeta potential measurement. The zeta potentials of the emulsions were determined on an Anton-Paar Litesizer 500 with omega cuvettes. Smoluchowski Approximation and Henry factor of 1.5 were applied. A relative permittivity of 78 was applied for the dispersant 0.1 mM KCl used. The data was evaluated using the software Kalliope™.

Determination of refractive index of 5 mM KPi. The samples for refractive index measurement were prepared freshly in a glass vial and the pH was checked prior to the measurement with a pH-meter. Subsequently, the sample was transferred into a quartz measurement cell to ensure accurate measurements. Refractive index measurements were carried out using an Anton-Paar Litesizer 500 instrument. Prior to the measurements, the instrument was calibrated using Milli Q water to ensure accurate results. The temperature of the sample was maintained constant at 25 °C throughout the measurements. The data was evaluated using the software Kalliope™.

Transmittance studies. The transmittance studies of the emulsions were determined on an Anton-Paar Litesizer 500. Samples were measured with a measurement angle of 175° and a focus position of -3.707 mm. The instrument was equipped with a semiconductor laser diode operating at 658 nm wavelength. A series of 6 runs with disposable measuring cuvettes were conducted and the temperature of the sample was maintained at a constant temperature of 25 °C throughout the measurements. The instrument settings were adjusted for optimal measurement conditions, including the measurement angle and duration, to obtain accurate and reliable results. A refractive index of 1.33 for the utilized dispersant was applied. The measurements were conducted with one hour delay measurements for at least 24 hours. Samples of transmittance studies investigated for over 24 hours were kept in the measurement apparatus at constant temperature to prevent solvent evaporation or disturbance of the emulsion. The data were evaluated using the software Kalliope™.

Lyophilization. The freeze-drying experiments were performed on a Telstar LyoQuest -85 laboratory freeze dryer. The samples were dissolved in water or KPi in low volumes of 1-10 mL in one-neck flasks. The samples were frozen while continuously rotated in liquid nitrogen to ensure a maximum cover of the flask surface with the frozen sample. The frozen samples were attached to a vacuum of 0.2 mbar and a condenser temperature of ~ -80 °C. After at least 24 hours the samples were removed from the freeze-dryer.

Light microscopy. Light microscopy images were obtained using Axiolab from Carl Zeiss. The sample was fixated on a microscope glass slide using suitable mounting media, ensuring proper adhesion and preservation of the sample integrity. The microscope was ensured to be properly calibrated, aligned, and maintained for optimal imaging conditions. The appropriate light source was set and the intensity, color balance, and filters were adjusted. The focus and stage position was adjusted to bring the sample into focus. Images were captured with a digital imaging system attached to the microscope, ensuring appropriate exposure time and image resolution. Measurables, such as length, area, or intensity, were implemented using calibrated scales within the software. Dimension, distances, or angles of features within the images were investigated using calibrated scales or measurement tools and the software ImageJ (Version 1.53a).

Transmission electron microscopy (TEM). TEM studies were carried out using an EM 900 transmission electron microscope from Carl Zeiss Microscopy GmbH. The sample was dehydrated using suitable dehydration methods. The microscope was calibrated and maintained for optimal imaging conditions. TEM components were aligned, including the condenser lens, objective lens, and projector lens, for proper imaging conditions. The focus, astigmatism, and contrast/brightness settings were applied to obtain clear and well-defined images. Dimension, distances, or angles of features within the images were investigated using calibrated scales or measurement tools and the software ImageJ (Version 1.53a).

Amino acid sequence of Lcp_{K30}. For protein expression the gene of the used latex-clearing protein Lcp_{K30} from *Streptomyces* sp. K30, was cloned into the pAGM22082-N[331] vector with an N-terminal Strep-tag and TEV protease cleavage site, and an C-terminal GFP11-tag linker with a GDS linker.[332]

MWSHPQFEKENLYFQGLQRPLWTWSPSASVAGTGVGVDPEYVWDEEADPVLAAVIDRGEVPAVNALLKQ
WTRNDQALPGGLPGDLREFMEHARRMPSWADKAALDRGAQFSKTKGIYVGALYGLGSGLMSTAIPRESRAV
YYSKGGADMKDRIAKTARLGYDIGDLDAYLPHGSMIVTAVKTRMVHAAVRHLLPQSPAWSQTSGGQKIPISQ
ADIMVTWHSLATFVMRKMKQWGVRVNTADAEAYLHVWQVSAHMLGVSDEYIPATWDAANAQSKQVLDPI
LAHTPEGEALTEVLLGIVAELDAGLTRPLIGAFSRYTLGGEVGDMIGLAKQPVLERLIATAWPLLVAFREGLIP
LPAVPAVLWTLEEALRKFVLLFLSEGRRIAIDIPDVNRPSDGGSGGGSTSRDHMVLHEYVNAAGIT

Nano differential scanning fluorimetry (Nano-DSF). Samples for protein stability assessment *via* Nano-DSF measurement were prepared with consistent enzyme concentrations within each measurement (6 or 10 µM). Samples were then stored on ice until measurement. Measurements were conducted using a Prometheus NT.48 instrument from Nanotemper. For each measurement, 10 µl of the samples were used. Absorbances at 330 nm and 350 nm, as well as light scattering, were measured with a temperature gradient ranging from 15 to 95 °C (0.8 °C/min). Light intensities were adjusted to maintain a similar level of absorption throughout the measurements.

5.2 Procedures

5.2.1 Preliminary experiments of acoustically emulsified system:

PI was placed in a pressure vial, and ultrapure water was added, followed by pre-emulsification through vigorous stirring at the polymer w/v% values specified in Table 7. Additional co-solvents, such as n-hexadecane or squalene, were introduced to the polymer before adding water. Sodium dodecyl sulfate, at the w/v% concentrations listed in Table 7, was dissolved in the aqueous medium before addition.
The emulsification process of the polymer was assessed through acoustic sonication, involving 10-second pulses followed by 5-second pauses, as detailed in Table 7. Visual monitoring of stability was commenced immediately after initial preparation. A transition to an opaque upper region, resulting from the floating or creaming of polymer or co-solvent, and a transparent lower region, accompanied by an increase in transmittance, were indicative of reduced colloidal stability. Emulsions that did not yield a uniformly dispersed opaque solution but instead resulted in separated phases were categorized as unstable.

5.2.2 Parameter optimization for surfactant-free acoustical emulsification:

PI (**PI 3000**, 6 mg, 0.2 w/v%) was placed in a pressure vial. A freshly prepared solution of potassium phosphate (5 mM) was added to the pressure vial and then pre-emulsified with stirring. Emulsification was achieved *via* sonication with 10 seconds of pulsing and 5 seconds of pausing. This process was conducted under continuous cooling in a sodium chloride-ice bath to prevent solvent evaporation. Subsequently, the emulsions were promptly transferred into a cuvette for dynamic light scattering measurements, using an Anton-Paar Litesizer 500 instrument. Measurements of transmittance and hydrodynamic diameter were taken every 10 minutes over a 90-minute duration, all while maintaining a constant temperature of 25 °C.

5.2.3 Determination of polymer stability in the surfactant-free acoustical emulsification:

To verify that the **PI 3000** was not degraded by the sonication procedure, particularly given the extended sonication time, at the comparatively long sonication times and the resultant energy input from the sonifier, a gel permeation chromatography (GPC) analysis of the PI before and after sonication was conducted. PI (**PI 3000**, 6 mg, 0.2 wt/vol%) was placed in a pressure vial. A freshly prepared potassium phosphate solution (5 mM) was added to the pressure vial and pre-emulsified with stirring. Emulsification was achieved through sonication at 30% amplitude for 60 minutes, using 10 seconds of pulsing and 5 seconds of pausing. This process was conducted under continuous cooling in a sodium chloride-ice bath to prevent solvent evaporation. After preparation, the sample was transferred to a 50 mL flask and frozen using liquid nitrogen. The solvent was removed *via* a Telstar LyoQuest bench freeze dryer. The resulting polymer was dissolved in THF at a concentration of 2 mg/mL. As a reference, a sample of PI 3000 at a concentration of 2 mg/mL was also prepared. Both samples were subjected to GPC measurements.

5.2.4 Determination of pH stability in surfactant-free acoustical emulsification:

A 5 mM KPi solution (6 mL) was subjected to the acoustical emulsification procedure using the optimized sonication conditions: 30% amplitude for 60 minutes with 10 seconds of pulsing and 5 seconds of pausing. This process was conducted under continuous cooling in a sodium chloride-ice bath to prevent solvent evaporation. Subsequently, the resulting solution was transferred to a vial, and its pH was measured using a freshly calibrated pH meter. The pH of 7 was found to be identical to that of the 5 mM KPi solution that was not subjected to the acoustical emulsification.

5.2.5 Standard procedure for surfactant-free acoustical emulsification:

PI (**PI 3000**, 0.2 w/v%) was placed in a pressure vial. A freshly prepared 5 mM potassium phosphate solution was added to the pressure vial and then pre-emulsified with stirring. Emulsification was achieved by subjecting the mixture to sonication at 30% amplitude for 60 minutes, with 10 seconds of pulsing followed by 5 seconds of pausing. This process was carried out under constant cooling in a sodium chloride-ice bath to prevent solvent evaporation.

5.2.6 Preliminary experiments for the establishment of surfactant-free co-solvent emulsified system:

PI was placed into a 5 mL vial, and then a co-solvent with the respective w/v% from table 8 was added, creating a hydrophobic phase. The mixture was stirred with a stirring bar to dissolve the polymer in the hydrophobic phase. MilliQ-water was added into the hydrophobic phase, and the mixture was stirred and sonicated for 1 hour. Ten minutes before completing the emulsification, the water was replaced with fresh cold MilliQ-water to prevent overheating.
The stability was visually assessed immediately after preparation and then at hourly intervals for 12 hours, and again after 24 hours. The transition to an opaque upper region, caused by floating or creaming polymer or co-solvent, along with a transparent lower region and an increase in transmittance, was indicative of lower colloidal stability. If a sample completely phase-separated and was no longer emulsified, the stability up to that point was noted. Attempts that resulted in separated phases rather than a dispersed opaque solution were considered unstable emulsions.

5.2.7 Stability of *n*-hexadecane in 5 mM KPi

n-Hexadecane was placed into a 5 mL vial, followed by the addition of freshly prepared potassium phosphate solution (5 mM) into the reaction vial. The mixture was stirred and sonicated for 1 hour. To prevent overheating, the water was replaced with fresh cold MilliQ-water 10 minutes before completing the emulsification process. Immediately after preparation, the emulsion was transferred to a cuvette for dynamic light scattering and transmittance studies. These measurements were performed using an Anton-Paar Litesizer 500.

5.2.8 Standard procedure for co-solvent stabilized system:

PI (0.2 w/v%) was placed into a 5 mL vial and then n-hexadecane (0.2 w/v%) was added, forming a hydrophobic phase. The mixture was stirred vigorously to dissolve the polymer in the hydrophobic phase. Potassium phosphate solution (5 mM) was freshly prepared and added to the reaction vial. The mixture was then vigorously stirred and sonicated for 1 h.

5.2.9 Latex milk preparation procedure

The stock latex milk, contained ammonia for stabilization, was subjected to washing before usage. A wash solution of 0.1 w/v% Nonidet P-40 in ultrapure water was prepared and equally combined with the 60 w/v% latex milk stock solution in a falcon tube. Careful mixing was achieved by inverting the tube 10 times to prevent polymer coagulation. Separation of the PI and washing solution was achieved by centrifugation (10000 g, 4 °C, 1 h), followed by the discarding of the wash solution. The falcon tube was refilled to the original volume with fresh wash solution, and the procedure was repeated three times. After the final centrifugation step, the remaining latex was weighed in and diluted to a concentration of 60 w/v% with 0.1 w/v% Nonidet P-40 solution.

5.2.10 Standard procedure latex degradation

Latex milk stock solution (60 w/v% PI) was diluted with freshly prepared potassium phosphate buffer pH 7 to result in a 0.2 w/v% and a KPi concentration of 100 mM at a volume of 1 mL. The Latex stock solution was charged into a 5 mL Vial. The Lcp_{K30} was added, and the reaction was stirred at room temperature under the exclusion of light. The degradation products were extracted via liquid to liquid extraction with ethyl acetate and occasionally additionally for GPC-analysis with n-hexane and chloroform. The solvent of the extracts was evaporated *in vacuo*. The residues were solubilized in the respective appropriate solvent for analysis by ESI or HPLC or GPC or UHPLC-ESI-HRMS.

5.2.11 Degradation inhibition of the enzymatic degradation of PI cis 7000 by different solvents

The **PI *cis* 7000** (1 w/v%) was placed into a 5 mL vial, followed by the addition of the respective organic solvent, $CHCl_3$ or DCM or toluene or hexane or *n*-hexadecane or ethyl acetate (1 mL), resulting in a hydrophobic phase that was vigorously stirred. 1 mL freshly prepared potassium phosphate solution (100 mM) was added to the reaction vessel along with Lcp_{K30} enzyme (1 μM). The vials were sealed with parafilm to prevent solvent evaporation. The reaction was stirred at room temperature, excluding light for 24 hours. The hydrophobic phase was isolated with a syringe, and 0.5 mL of the extract was used for further analysis. The solvent was evaporated, and the residue was dissolved in acetonitrile for UHPLC analysis.

5.2.12 Degradation inhibition of the enzymatic degradation of PI cis 7000 by *n*-hexadecane

The **PI *cis* 7000** (1 w/v%) was placed into a 5 mL vial, followed by the addition of *n*-hexadecane either in (1 w/v% or 10 w/v%), resulting in a hydrophobic phase that was vigorously stirred. A freshly prepared potassium phosphate solution (100 mM) was added to the reaction vessel along with Lcp_{K30} enzyme (1 μM). The vials were sealed with parafilm to prevent solvent evaporation. The reaction was carried out at room temperature, excluding light for 24 hours. The hydrophobic phase was isolated with a syringe, and 0.5 mL of the extract was used for further analysis. The solvent was evaporated, and the residue was dissolved in acetonitrile for UHPLC analysis.

5.2.13 Enzyme concentration dependency onto degradation of PI 3000

PI 3000 (0.2 w/v%) was placed in a 5 mL vial. Potassium phosphate solution was freshly prepared and added to the reaction vial. The mixture was stirred vigorously before the addition of the Lcp_{K30} enzyme at different concentrations 0,2 μM or 1 μM or 2 μM or 5 μM. After the addition of the enzyme, the vials were sealed with parafilm to prevent the evaporation of solvent. The reaction was stirred at room temperature with the exclusion of light for 24 hours. Ethyl acetate (1.5 mL) was added for liquid-liquid extraction. The hydrophobic phase was isolated with a syringe and 1 mL was used for further analysis. The solvent was evaporated then the residue was redissolved in acetonitrile for UHPLC analysis. Negative control samples were prepared as described above without addition of the enzyme Lcp_{K30}.

5.2.14 Temperature dependency onto degradation of PI 3000

PI 3000 (0.2 w/v%) was placed in a 5 mL vial. Potassium phosphate solution was freshly prepared and added to the reaction vial. The mixture was stirred vigorously before the addition of the Lcp_{K30} enzyme (5 μM). After the addition of the enzyme, the vials were sealed with parafilm to prevent the evaporation of solvent. The reaction was carried out at room temperature, in a thermostat at 30 °C and at 40 °C with the exclusion of light for 24 hours. After cooling down ethyl acetate (1.5 mL) was added for liquid-liquid extraction. The hydrophobic phase was isolated with a syringe and 1 mL was used for further analysis. The solvent was evaporated then the residue was redissolved in acetonitrile for UHPLC analysis. Negative control samples were prepared as described above without addition of the enzyme Lcp_{K30}.

5.2.15 Stability assay

Emulsions and corresponding controls (individual components, buffer only) were prepared as described above. The reaction was started by adding 5 μM Lcp_{K30} and stirred at 450 rpm. 50 μl samples were taken at different time points and added to 950 μL of 0.2 w/v% latex milk in 20 mM KPi buffer (pH 7). These secondary activity samples were shaken at 800 rpm and 37 °C for 1.5 hours. The activity assay was terminated by extraction with 1 mL ethyl acetate. In order to achieve a clear phase separation samples were centrifuged at 14500 rpm for 5 min. 700 μL of the organic phase was transferred into a new 1.5 mL reaction tube, evaporated in a vacuum centrifuge and redissolved in 700 μl acetonitrile. The samples were analyzed by UHPLC.

5.2.16 Optimized preparation of non-emulsified system

PI (0.2 w/v%) was placed in a 5 mL vial. Potassium phosphate solution (5 mM) was freshly prepared and added to the reaction vial. The mixture was stirred vigorously before the addition of the Lcp_{K30} enzyme (5 μM). After the addition of the enzyme, the vials were sealed with parafilm to prevent the

evaporation of solvent. The reaction was carried out at room temperature with the exclusion of light for 24 hours at a stirring speed of 450 rpm. Ethyl acetate (1.5 mL) was added, sonicated for 10 minutes and stirred for 30 minutes for liquid-liquid extraction. The hydrophobic phase was isolated with a syringe and 1 mL was used for further analysis. The solvent was evaporated with dried air and then the residue was redissolved in methanol and used for UHPLC, ESI-TOF-MS and UHPLC-(UV)-ESI-HRMS analysis. Negative control samples were prepared as described above without addition of the enzyme Lcp_{K30}.

5.2.17 Optimized preparation of acoustically emulsified system

PI (0.2 w/v%) was placed in a pressure vial. Potassium phosphate solution (5 mM) was freshly prepared and added to the reaction vial and then pre-emulsified with vigorous stirring. Emulsification was achieved by sonication at 20% amplitude for 30 minutes, 5 seconds of pulse and 10 seconds of pause under constant cooling in a sodium chloride-ice bath. The emulsion (0.2 w/v%) was transferred to 5 mL vials and then the enzyme Lcp_{K30} (5 µM) was added afterwards. Evaporation of the solvent was prevented by sealing the vial with parafilm. The reaction was carried out at room temperature excluding light for 24 hours with stirring of 450 rpm. For liquid-liquid extraction, ethyl acetate (1.5 mL) was added, sonicated and stirred for 30 minutes. The hydrophobic phase was isolated with a syringe and 1 mL was used for further analysis. The solvent was evaporated with dried air and then the residue was redissolved in methanol and used for UHPLC, ESI-TOF-MS and UHPLC-(UV)-ESI-HRMS analysis. Negative control samples were prepared as described above without addition of the enzyme Lcp_{K30}.

5.2.18 Optimized preparation of co-solvent stabilized system

PI (0.2 w/v%) was placed into a 5 mL vial and then *n*-hexadecane (0.2 w/v%) was added, forming a hydrophobic phase. The mixture was stirred vigorously to dissolve the polymer in the hydrophobic phase. Potassium phosphate solution (5 mM) was freshly prepared and added to the reaction vial. The mixture was then vigorously stirred and sonicated for 1 h. Lcp_{K30} (5 µM) was added and the vials were sealed with parafilm to prevent evaporation of solvent. The reaction was carried out at room temperature excluding light for 24 hours with stirring of 450 rpm. For liquid-liquid extraction, ethyl acetate (1.5 mL) was added, sonicated and stirred for 30 minutes. The hydrophobic phase was isolated with a syringe and 1 mL was used for further analysis. The solvent was evaporated with dried air and then the residue was redissolved in methanol and used for UHPLC, ESI-TOF-MS and UHPLC-(UV)-ESI-HRMS analysis. Negative control samples were prepared as seen above without addition of enzyme Lcp_{K30}.

5.2.19 Thermal stress incubation experiments with Lcp_{K30}-P7

Sample sets were prepared in 2.5-ml glass vials filled, each filled with 20 mM potassium phosphate buffer at pH 7 and 0.2 µM enzyme solution (Lcp_{K30} or Lcp_{K30}-P7 or negative control) up to a Volume of 100 µl. The different solutions were incubated at 60 °C or 70 °C or left unincubated for one hour in the glass vials. Then 900 µl latex milk solution with 20 µM KPi was added to achieve a PI loading of 0.2 w/v%. The glass vials were sealed with plastic caps to prevent evaporation and incubated for 24 hours at 450 rpm and 37 °C. After the reaction, the samples were extracted with ethyl acetate (1 mL) though sonication for 10 minutes. 800 µl of the organic phase was transferred into new glass vials, and the solvent was evaporated at 30 °C under continuous nitrogen flow. After complete solvent evaporation, the samples were redissolved in MeOH and sonicated for 10 minutes for analysis with UHPLC-ESI-HRMS.

5.2.20 Enzymatic degradation and derivatization

For the enzymatic degradation of SPI, an emulsion containing 0.2 (w/v%) SPI and 0.2 (w/v%) *n*-hexadecane in ultrapure water was prepared. 2.5-ml glass vials were filled with enzyme solution for 1 µM in 1 ml reaction volume and filled up to 600 µl with 20 mM potassium phosphate buffer at pH 7. The emulsion was stirred continuously with a stirring bar, to guarantee a consistent composition, while pipetting 400 µL of the PI emulsion into the reaction vials. The glass vials were sealed with plastic caps to prevent evaporation and incubated for 24 h at 450 rpm and 37 °C. After the reaction duration, the samples were extracted with 1 ml ethyl acetate by being vortexed for 10 seconds, sonicated for 10 min, and 10 min centrifuged at 8000 rpm. 700 µl of the organic phase was transferred into new glass vials and the solvent was evaporated at 30 °C under continuous nitrogen flow. To increase the extraction efficiency, the extraction procedure was repeated using 1 ml of ethyl acetate. The extracted organic phases were transferred into the same glass vial. After complete solvent evaporation under nitrogen flow at 30 °C, the mass of the dried product was determined. The derivatization reagent of 0.1 mg/ml O-(4-Methoxybenzyl)-hydroxylamine-hydrochloride and 0.071 mg/ml sodium acetate in pure ethanol was freshly prepared as stock solutions. 1 ml of the derivatization reagent was applied to each sample, vortexed for 10 seconds and sonicated 10 min. The derivatization reaction was conducted for 16 h at room temperature and 800 rpm after which the process was stopped by adding 20 µl of 50% formic acid in MilliQ-water and vortexing for 10 seconds. To prepare the samples for GPC measurements the solvent was evaporated under nitrogen flow at 30 °C. The dried derivatized product was dissolved at 3 mg/ml in tetrahydrofuran. 1 ml of each sample was filtered through a syringe filter, PTFE, 0.2 µM, and transferred into a new GPC vial which was closed with GPC caps.

5.2.21 Enzymatic degradation investigations with Lcp_{K30}-FuncLib

For the enzymatic degradation of synthetic polybutadiene, an emulsion containing 0.2 (w/v%) PB and 0.2 (w/v%) *n*-hexadecane in ultrapure water was prepared. 2.5-ml glass vials were filled with enzyme solution for either 1 µM or 2 µM or 5 µM in 1 ml reaction volume and filled up to 600 µl with 20 mM potassium phosphate buffer at pH 7. The emulsion was stirred continuously with a stirring bar, to guarantee a consistent composition, while pipetting 400 µL of the PI emulsion into the reaction vials. The glass vials were sealed with plastic caps to prevent evaporation and incubated for 24 h at 450 rpm and 37 °C. After the reaction duration, the samples were extracted with 1 ml ethyl acetate by being vortexed for 10 seconds, sonicated for 10 min, and 10 min centrifuged at 8000 rpm. 700 µl of the organic phase was transferred into new glass vials and the solvent was evaporated at 30 °C under continuous nitrogen flow. To increase the extraction efficiency, the extraction procedure was repeated using 1 ml of ethyl acetate. The extracted organic phases were transferred into the same glass vial. After complete solvent evaporation under nitrogen flow at 30 °C, the mass of the dried product was determined. The derivatization reagent of 0.1 mg/ml O-(4-Methoxybenzyl)-hydroxylamine-hydrochloride and 0.071 mg/ml sodium acetate in pure ethanol was freshly prepared as stock solutions. 1 ml of the derivatization reagent was applied to each sample, vortexed for 10 seconds and sonicated 10 min. The derivatization reaction was conducted for 16 h at room temperature and 800 rpm after which the process was stopped by adding 20 µl of 50% formic acid in MilliQ-water and vortexing for 10 seconds. To prepare the samples for GPC measurements the solvent was evaporated under nitrogen flow at 30 °C. The dried derivatized product was dissolved at 3 mg/ml in tetrahydrofuran. 1 ml of each sample was filtered through a syringe filter, PTFE, 0.2 µM, and transferred into a new GPC vial which was closed with GPC caps. The solvent was evaporated under continuous nitrogen flow and the residue was redissolved in THF and MeOH mixtures for the subsequent UHPLC-ESI-HRMS analysis.

5.3 Syntheses

5.3.1 General procedure for chemical degradation of PI to PI-Ox.

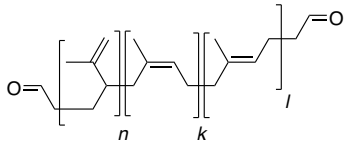

PI-Ox

PI of low molecular weight (1 g, 14.7 mmoL [isoprene unit]) solubilized in 10 mL of THF was first epoxidized by dropwise addition of a solution of mCPBA (52.8 mg, 0.3 mmol) in 1 mL THF at 0 °C. The reaction mixture was then stirred for 2 h at room temperature. A periodic acid solution (1.2 equiv. compared to mCPBA, 0.37 mmol), dissolved in 1 mL of THF, was added dropwise and stirred for 2 h at room temperature The solvent was then removed under reduced pressure and the crude product was dissolved in 10 mL of diethyl ether before filtration over celite to remove insoluble iodic acid. The filtrate was then concentrated before washing, 10 mL of each, twice with saturated $NaHCO_3$ solution and once with distilled water. The organic layer was dried over $MgSO_4$, filtered over celite, and the solvent was evaporated to dryness to obtain the product in yields of 69%.

^{1}H NMR (400 MHz, $CDCl_3$) δ [ppm] = 9.77 (m, 1H, CH_2-C*H*O), 5.14-5.07 (m, nH, -CH_2-C(CH_3)=C*H*-CH_2-), 4.76-4.63, (m, 2 nH, (CH-C(CH_3)=CH_2), 2.46 (m, 4H, -CH_2-CHO-CH_2-CH_2-C=O(CH_3)), 2.34 (m, 2H, - CH_2-CH_2-CHO), 2.12 (s, 3H, -CH_2-CH_2-C=O(CH_3)), 2.04 (s, 4 nH, -CH_2-C(CH_3)=CH-CH_2-), 1.68 (s, 3 nH, *cis* -CH_2-C(CH_3)=CH-CH_2-), 1.60 (s, 3 nH, *trans* -CH_2C(CH_3)=CH-CH_2-, CH-C(C*H*$_3$)=CH_2).
$M_{n\,(NMR)}$ = 6100 g/mol
$M_{n\,(GPC)}$ = 1700, Đ = 1.6

5.3.2 General procedure for chemical degradation of PB to PB-Ox.

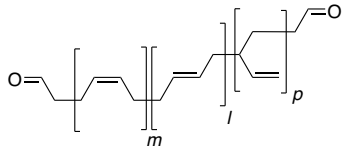

PB-Ox

PB of low molecular weight (1 g, 18.5 mmoL [butadiene unit]) solubilized in 10 mL of THF was first epoxidized by dropwise addition of a solution of mCPBA (65.2 mg, 0.4 mmol) in 1 mL THF at 0 °C. The reaction mixture was stirred for 2 h at room temperature. A periodic acid (1.2 equiv. in regard to mCPBA, 0.47 mmol) solution, dissolved in 1 mL of THF, was added dropwise and stirred for 2 h at room temperature The solvent was then removed under reduced pressure and the crude product was dissolved in 10 mL of diethyl ether before filtration over celite to remove insoluble iodic acid. The filtrate was then concentrated before washing, 10 mL of each, two times with saturated $NaHCO_3$ solution and once with distilled water. The organic layer was dried over $MgSO_4$, filtered over celite and the solvent was evaporated to dryness to obtain the product in yields of 74%.

^{1}H NMR (400 MHz, $CDCl_3$) δ [ppm] = 9.77 (m, 2H, CH_2-C*H*O), 5.58 (CH-C*H*=CH_2), 5.42-5.38(m, 2 nH, *cis*/*trans* -CH2-C*H*=C*H*-CH2-), 4.98 (m, CH-CH=CH_2), 2.47 (m, 4H, -CH_2-CH_2-CHO), 2.38 (m, 4H, -CH_2-CH_2-CHO), 2.09-2.04 (m, 4 nH, *cis*/*trans* -CH_2-CH=CH-CH_2-).
$M_{n\,(NMR)}$ = 5600 g/mol
$M_{n\,(GPC)}$ = 2400, Đ = 2.3

Table 28. Epoxidation rate of PI and PB

Polymers	$Epoxy_{theo}$	$Epoxy_{exp}$
PI 3000	2.0%	1.5%
PI 4500	2.0%	1.0%
PB 3500	2.0%	0.69%
PB 12000	2.0%	0.87%

5.3.3 General procedure for derivatization of PB-Ox to PB-D.

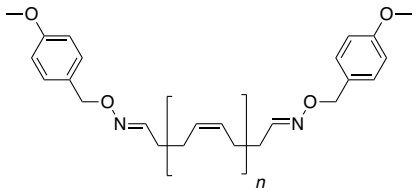

PB-D

Example of derivatization of polybutadienes. The chemically degraded PB (40 mg) was added to a vial. The derivatization reagent, consisting of *O*-(4-methoxybenzyl)-hydroxylamine-hydrochloride (20 mg, 0.16 mmol) and sodium acetate (14.6 mg, 0.28 mmol) in pure ethanol, was freshly prepared as stock solution and added to the vial at a volume of 10 mL. The vial was sonicated for 10 minutes, and the reaction was conducted for 16 h at room temperature under stirring. After completion, 20 µL of 50% formic acid in MilliQ-water was added and the vial was vortexed for 10 seconds. The solvent was evaporated *in vacuo* and precipitated from THF in methanol to obtain the product in a yield of 43%.

^{1}H NMR (400 MHz, $CDCl_3$) δ [ppm] = 7.43 – 7.39 (m, 1H, (*E*/*Z* N=C*H*-CH_2)), 7.28 (m, 4H, C($COCH_3$)-C*H*), 6.88 (m, 4H, C(C(CH_2)-C*H*-), 6.66 (m, 1H, (*E*/*Z* N=C*H*-CH_2)), 5.38 (s, 2nH, -CH_2-), 5.0 (m, 4H, C-CH_2-O), 3.80 (s, 6H, CH_3-O), 2.40 (m, 2H, (*E*/*Z*) N=CH-CH_2), 2.22 (m, 2H, (*E*/*Z* N=CH-CH_2), 2.09 (s, 4nH, -CH_2-CH=CH-CH_2-).
^{13}C NMR (126 MHz, $CDCl_3$) δ [ppm] = 159.30, 151.58, 150.72, 129.60, 128.04, 113.77, 75.29, 55.26, 27.4, 24.57.

5.3.4 General procedure for derivatization of PIs.

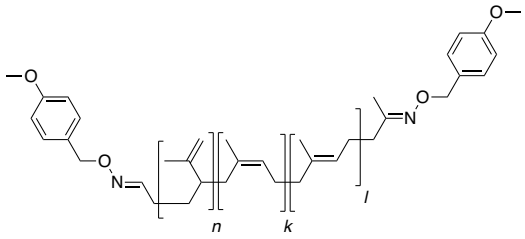

PI-D

Example of derivatization of PIs. The chemically degraded PI (40 mg) was added to a vial. The derivatization reagent, consisting of *O*-(4-methoxybenzyl)-hydroxylamine-hydrochloride (20 mg, 0.16 mmol) and sodium acetate (14.6 mg, 0.28 mmol) in pure ethanol, was freshly prepared as stock solution and added to the vial at a volume of 10 mL. The vial was sonicated for 10 minutes and the reaction was conducted for 16 h at room temperature under stirring. After completion, 20 µL of 50% formic acid in MilliQ-water was added and the vial was vortexed for 10 seconds. The solvent was evaporated *in vacuo* and the crude polymer was purified by column chromatography in chloroform to obtain the product in a yield of 24%.

^{1}H NMR (400 MHz, $CDCl_3$) δ [ppm] =7.41 – 7.38 (m, 1H, (*E*/*Z* N=C*H*-CH_2)), 7.31-7.27 (m, 4H, C($COCH_3$)-C*H*-), 6.88 (m, 4H, C(C(CH_2)-C*H*-), 6.66 (m, 1H, (*E*/*Z* N=C*H*-CH_2)), 5.14-5.07 (m, nH, -CH_2-C(CH_3)=C*H*-CH_2-), 5.0 (m, 4H, C-CH_2-O), 4.76-4.63, (m, 2 nH, CH-C(CH_3)=CH_2), 3.80 (s, 6H, CH_3-O), 2.40 (m, 2H, (*E*/*Z*) N=CH-CH_2), 2.27 (m, 2H, (*E*/*Z* N=CH-CH_2), 2.05 (m, 4 nH, CH_2-C(CH_3)=CH-CH_2), 1.68 (m, 3 nH, *cis* -CH_2-C(CH_3)=CH-CH_2-), 1.68 (m, 3 nH, *trans* -CH_2-C(CH_3)=CH-CH_2-, CH-C(CH_3)=CH_2).
^{13}C NMR (126 MHz, $CDCl_3$) δ [ppm] = 135.36, 129.78, 125.19, 124.38, 113.83, 111.48, 75.42, 55.39, 40.21, 32.36, 28.00, 26.53, 22.81, 18.80, 16.10.

5.3.5 Catalyst screening

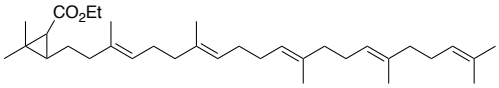

Equimolar reactions:
The respective catalyst (0.05 equiv.) was charged in a 25 mL Schlenk flask and dissolved in anhydrous DCM (1.2 mL) under nitrogen atmosphere. Subsequently, squalene (250 mg, 0.61 mmol, 1 equiv.) was added to the reaction vessel. A pre-dried solution of DCM (6.5 mL) and ethyl diazoacetate (69.45 mg, 0.61 mmol, 1 equiv.) was added *via* syringe pump over 8 hours. The resulting reaction mixture was stirred overnight. The DCM was removed in *vacuo* to result in the crude residue, which was analyzed with ^{1}H NMR and ESI-MS for product formation.

Full modification reactions:
The respective catalyst (0.05 equiv.) was charged in a 25 mL Schlenk flask and dissolved in anhydrous DCM (1.2 mL) under nitrogen atmosphere. Subsequently, squalene (250 mg, 0.61 mmol, 1 equiv.) was added to the reaction vessel. A pre-dried solution of DCM (6.5 mL) and ethyl diazoacetate (0.768 mL, 7.34 mmol, 12 equiv.) was added *via* syringe pump over 8 hours. The resulting reaction mixture was stirred overnight. The DCM was removed in *vacuo* to result in the crude residue, which was analyzed with ^{1}H NMR and ESI-MS for product formation.

Catalysts:
$L_1Cu(OTf)$, $L_2Cu(OTf)$, IPrCuCl, SIMesCuCl, L_1 $[Cu(NCMe)_4]PF_6$, $L_2[Cu(NCMe)_4]PF_6$

5.3.6 *N*-(3-chloropropyl)acrylamide (1)

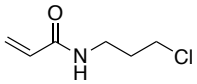

1

3-Chloropropylamine hydrochloride (1.0 g, 7.69 mmol), triethylamine (TEA) (2.3 mL, 16.9 mmol) and 4-(dimethylamino)pyridine (DMAP) (47.9 mg, 0.39 mmol) were mixed in dry dichloromethane (15 mL) under nitrogen atmosphere. The reaction mixture was cooled to 0 °C and then acryloyl chloride (0.75 mL, 9.2 mmol) was added dropwise. The reaction mixture was stirred overnight and allowed to gradually reach room temperature. The resulting precipitate was removed by filtration. The reaction mixture was subjected to washing with saturated $NaHCO_3$ aqueous solution (15 mL) and water (2 × 15 mL). The organic phase was dried with $MgSO_4$ and filtered. The filtrate was then treated with traces of butylated hydroxytolene (BHT) and concentrated *in vacuo* to result in an orange oil in the yield of 64%.

^{1}H NMR (500 MHz, $CDCl_3$) δ [ppm] = 6.28 (dd, *J* = 17.0, 1.4 Hz, 1H, CH=CH_2-CO), 6.09 (dd, *J* = 17.0, 10.4 Hz, 1H, CH=CH_2-CO), 5.85 (s, 1H,N*H*CO), 5.65 (dd, *J* = 10.3, 1.3 Hz, 1H, CH2=C*H*-CO), 3.60 (t, *J* = 6.4 Hz, 2 H, CH_2-CH_2- CH_2-Cl), 3.50 (q, *J* = 6.5 Hz, 2H, CH_2-CH_2-CH_2-Cl), 2.04 (p, *J* = 6.5 Hz, 2H, CH_2-CH_2-CH_2-Cl) ppm.
^{13}C NMR (126 MHz, $CDCl_3$) δ [ppm] = 165.9, 130.8, 126.8, 42.7, 37.3, 32.1 ppm.

5.3.7 *N*-(3-chloropropyl)methacrylamide (2)

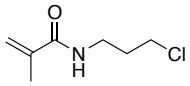

2

3-Chloropropylamine hydrochloride (2.0 g, 15.4 mmol, 1 equiv.) and TEA (4.7 mL, 33.8 mmol, 2.2 equiv.) were dissolved in dry dichloromethane (15 mL) under nitrogen atmosphere. The reaction mixture was cooled to 0 °C and then methacryloyl chloride (1.6 mL, 16.9 mmol, 1.1 equiv.) was added dropwise. Subsequently, the reaction mixture was stirred overnight and allowed to gradually reach room temperature. The resulting precipitate was removed by filtration. The reaction mixture was subjected to washing with saturated $NaHCO_3$ aqueous solution (20 mL), brine (2 x 20 mL) and water (20 mL). The organic phase was dried with $NaSO_4$ and filtered. Traces of butylated hydroxytolene (BHT) were then added to the filtrate, followed by concentration *in vacuo* to result in an orange oil with a yield of 58%.

^{1}H NMR (500 MHz, $CDCl_3$) δ [ppm] = 6.05 (s, 1H, N*H*CO), 5.68 (s, 1H, CH_3-C=CH_2-CO), 5.33 (s, 1H, CH_3-C=CH_2-CO), 3.60 (t, *J* = 6.4 Hz, 2H, CH_2-CH_2- CH_2-Cl), 3.47 (q, *J* = 6.5 Hz, 2H, CH_2-CH_2- CH_2-Cl), 2.04 (m, 2H, CH_2-CH_2-CH_2-Cl), , 1.96 (s, 3H, CH_3-C=CH_2-CO).
^{13}C NMR (126 MHz, $CDCl_3$) δ [ppm] = 168.50, 139.82, 119.42, 42.57, 37.20, 31.85, 18.53.
ESI-TOF-MS for $[M+Na]^+$ (m/z): found 184.050 calc. 184.050

5.3.8 *N*-(3-chloropropyl)-*N*-methylacrylamide (3)

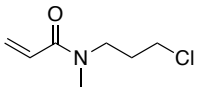

3

In a dry THF solution (60 mL) maintained at 0 °C, a suspension of sodium hydride (321 mg, 13.4 mmol, 2 equiv.) was prepared under nitrogen atmosphere. **1** (990 mg, 6.7 mmol, 1 equiv.) was then added dropwise to this cooled mixture. The reaction was allowed to proceed until gas evolution ceased. Subsequently, iodomethane (1.2 g, 13.4 mmol, 2 equiv.) was introduced dropwise. The reaction mixture was stirred overnight and allowed to gradually reach room temperature. Then water was added to quench the reaction. The ensuing mixture was extracted twice with chloroform (2 x 50 mL). The organic phases were collected, subjected to water washing, dried over sodium sulfate, filtrated and concentrated to result in the crude product. The crude product was purified by liquid chromatography using a hexane: ethyl acetate (2:1) eluent, to result in the product as a slight yellow oil with a yield of 38%.

^{1}H NMR (500 MHz, $CDCl_3$) δ [ppm] = 6.67 – 6.51 (m, 1H, CH=CH_2-CO), 6.36-6.29 (m, 1H, CH=CH_2-CO), 5.68 (d, *J* = 10.6 Hz, 1H, CH2=C*H*-CO), 3.56 (m, 4H, CH_2-CH_2-CH_2-Cl), 3.16 – 2.95 (m, 3H, NCH_3CO), 2.05 (m, 2H, CH_2-CH_2-CH_2-Cl).
^{13}C NMR (126 MHz, $CDCl_3$) δ [ppm] = 166.56, 166.43, 128.17, 127.98, 127.57, 127.22, 46.95, 46.03, 42.53, 41.59, 36.08, 34.00, 31.40, 30.36.
ESI-TOF-MS for $[M+Na]^+$ (m/z): found 184.0422 calc. 184.0500

5.3.9 *N*-(3-chloropropyl)-*N*-methylmethylacrylamide (4)

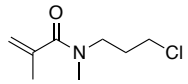

4

In dry THF (25 ml) maintained at 0 °C, a suspension of sodium hydride (415 mg, 17.3 mmol, 2 equiv.) was prepared under nitrogen atmosphere. **2** (1.4 g, 8.7 mmol, 1 equiv.) in dry THF (5 mL) was added dropwise. The reaction was allowed to proceed until gas evolution ceased. Subsequently, iodomethane (1.5 g, 17.3 mmol, 2 equiv.) was added dropwise. The reaction mixture was stirred overnight and allowed to gradually reach room temperature. To quench the reaction, the mixture was poured into water (25 mL). The ensuing mixture was extracted twice with ethyl acetate (2 x 20 mL). These organic phases were collected, subjected to water washing, dried over sodium sulfate, filtrated, and subsequently concentrated to recover the crude product. The crude product was purified *via* liquid chromatography (LC) using a hexane: ethyl acetate (2:1) eluent, to result in the product as a pale yellow oil with a yield of 5%.

^{1}H NMR (500 MHz, $CDCl_3$) δ [ppm] = 5.19 (s, 1H, CH_3-C=CH_2-CO), 5.02 (s, 1H, CH_3-C=CH_2-CO), 3.62-3.52 (m, 4H, CH_2-CH_2- CH_2-Cl), 3.03 – 2.95 (m, 3H, NCH_3CO), 2.04 (m, 2H, CH_2-CH_2-CH_2-Cl), 1.96 (s, 3H, CH_3-C=CH_2-CO).
ESI-TOF-MS for $[M+Na]^+$ (m/z): found 198.066 calc. 198.065

5.3.10 3-Methyl-1-(3-(*N*-methylmethacrylamido)propyl)-1*H*-imidazol-3-ium chloride (5)

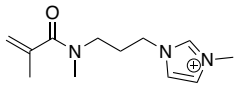

5

4 (291 mg, 1.7 mmol, 1 equiv.) was dissolved in dry ACN (2 mL) under nitrogen atmosphere. Methylimidazole (0.146 mL, 1.7 mmol, 1 equiv.) was subsequently added and the reaction was conducted for three days at 80 °C. The solvent was removed *in vacuo*, resulting in a residue that was then redissolved in water (2 mL). The resultant solution was subjected to a series of washing steps with chloroform (2 x 10 mL), dichloromethane (2 x 10 mL) and ethyl acetate (2 x 10 mL). The water was evaporated to result in the product as an orange oil with a yield of 57%.

^{1}H NMR (500 MHz, $CDCl_3$) δ [ppm] = 10.33 (s, 1H, N-C*H*=N), 7.81 (s, 1H, N-C*H*-CH), 7.32 (s, 1H, CH-C*H*-N), 5.22 (m, 1H, CH_3-C=CH_2-CO), 5.05 (m, 1H, CH_3-C=CH_2-CO), 4.38 (m, 2H, CH_2-CH_2-N=), 4.05 (s, 3H, N-CH_3), 3.48 (m, 2H, CO-NCH_3-C*H*), 3.07 (m, 3H CO-NCH_3), 2.27 (m, 2H, CH_2-CH_2-CH_2), 1.94 (s, 3H, CH_3-C=CH_2-CO).
^{13}C NMR (126 MHz, $CDCl_3$) δ [ppm] =173.48, 140.42, 123.30, 122.82, 116.21, 47.61, 43.56, 37.02, 36.84, 28.16, 20.33.
ESI-TOF-MS for $[M]^+$ (m/z): found 222.1393 calc. 222.1601

5.3.11 *N*-benzyl-3-chloropropan-1-amine (6)

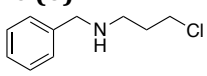

6

The synthesis of **6** was accomplished according to literature.[285] A solution of 3-chloropropylamine hydrochloride (3.0 g, 23.7 mmol, 1 equiv.) in DCM (25 ML) was prepared. To this solution, $MgSO_4$ (5.6 g, 46.1 mmol, 2 equiv.), TEA (3.5 g, 1.4 mL, 34.6 mmol, 1.5 equiv.) and benzaldehyde (2.4 g, 23.7 mmol, 1 equiv.) were sequentially added while stirring. The reaction mixture was stirred at room

temperature for 3 hours. The $MgSO_4$ was removed by filtration, washed with DCM, and the solvent of the filtrate was removed *in vacuo*. The resulting crude imine was dissolved in MeOH (30 mL) and cooled to 0 °C. $NaBH_4$ (2.6 g, 69.2 mmol, 3 equiv.) was added portion wise to this solution. The reaction mixture was stirred overnight at room temperature. The solvent was removed *in vacuo* and the residue was dissolved in water (30 mL) and extracted three times with DCM (20 mL). The combined organic phases were dried over Na_2SO_4, filtered and concentrated *in vacuo*, resulting in the product with a yield of 59%.

^{1}H NMR (400 MHz, $CDCl_3$) δ [ppm] = 7.37-7.31 (m, 4H, *o*/*m*-phenyl-C*H*), 7.26 (m, 1H, *p*-phenyl-C*H*), 3.80 (s, 2H, phenyl -CH_2-NH), 3.64 (t, *J* = 6.5 Hz, 2H, CH_2-Cl), 2.79 (t, *J* = 6.7 Hz, 2H, NH-CH_2-CH_2), 1.96 (m, 2H, CH_2-CH_2-CH_2).

5.3.12 *N*-benzyl-*N*-(3-chloropropyl)acrylamide (7)

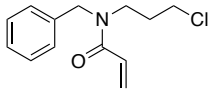

7

6 (7.5 g, 41.0 mmol, 1 equiv.) was dissolved in dry dichloromethane (75 mL) under nitrogen atmosphere. The solution was cooled to 0 °C, followed by the dropwise addition of TEA (3.68 mL, 45.1 mmol, 1.1 equiv.), and acryloyl chloride (3.68 mL, 45.1 mmol, 1.1 equiv.). The reaction mixture was stirred overnight and allowed to gradually reach room temperature. The reaction mixture was filtered, and the filtrate was washed twice with brine solution (2 x 75 mL), and once with water (75 mL). The organic phases were dried over $MgSO_4$, filtered, and traces of BHT were added before concentration *in vacuo*. The resulting crude product was purified by liquid chromatography using a gradient from chloroform to MeOH (100: 0 to 1: 1), resulting in the product as a slight yellow oil with a yield of 44%.

^{1}H NMR (500 MHz, $CDCl_3$) δ [ppm] = 7.41-7.26 (m, 4H, *o*/*m*-phenyl-C*H*), 7.19-7.17 (m, 1 H, *p*-phenyl-C*H*), 6.79-6.30 (m, 2H, CH_2=CH-CO), 5.88-5.62 (m, 1H, CH_2=C*H*-CO), 4.74-4.55 (m, 2H, phenyl-CH_2-NCO), 3.59-3.47 (m, 4H, NCO-CH_2-CH_2,CH_2-Cl), 2.05-1.95 (m, 2H, NCO-CH_2-CH_2).
^{13}C NMR (126 MHz, $CDCl_3$) δ [ppm] = 167.01, 166.49, 137.40, 136.76, 129.00, 128.73, 128.65, 128.16, 127.78, 127.58, 127.51, 127.22, 126.41, 116.12, 51.82, 49.21, 44.65, 44.36, 42.67, 41.81, 31.68, 30.66.
ESI-TOF-MS for $[M+Na]^+$ (m/z): found 260.0770 calc. 260.0818

5.3.13 3-(3-(*N*-benzylacrylamido)propyl)-1-methyl-1*H*-imidazol-3-ium chloride (8)

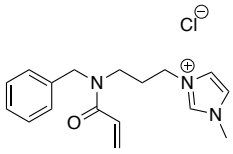

8

N-methylimidazole (0.22 mL, 2.5 mmol, 1.2 equiv.) and **7** (500 mg, 2.1 mmol, 1 equiv.) were dissolved in anhydrous ACN (1.5 mL) under nitrogen atmosphere. The reaction mixture was stirred at 80 °C for 3 days. The solvent was removed *in vacuo*, resulting in a residue that was then redissolved in water (5 mL). The resultant solution was subjected to a series of washing steps with *n*-hexane (3 x 10 mL) and chloroform (3 x 10 mL). The solvent was reduced *in vacuo* and the resulting solution was purified by reverse phase liquid chromatography from water: MeOH (95: 5) to pure MeOH (0: 100) resulting in the product as a colorless liquid with a yield of 17%.

^{1}H NMR (500 MHz, DMSO-D_6) δ [ppm] = 9.23 (s, 1H, N-C*H*=N), 7.90-7.67 (m, 2H, N-C*H*=C*H*-N), 7.43-7.06 (m, 5H, phenyl-C*H*), 6.86-6.60 (m, 1H, CH_2=CH-CO), 6.32-6.06 (m, 1H, CH_2=CH-CO), 5.79-5.60 (m, 1H, CH_2=C*H*-CO), 4.72-4.46 (m, 2H, phenyl-CH_2-NCO), 4.26-4.09 (m, 2H, NCO-CH_2-CH_2), 3.84 (s, 3H, N-CH_3), 3.33 (m, 2H, CH_2-N=C) 2.05-2.01 (m, 2H, CH_2-CH_2-CH_2).
^{13}C NMR (126 MHz, DMSO-D_6) δ [ppm] = 166.44, 138.21, 137.21, 129.17, 128.59, 128.06, 126.96, 124.00, 122.70, 50.53, 47.29, 43.19, 36.20, 29.59, 28.14, 20.03.
ESI-TOF-MS for $[M]^+$: found: 284.1776 cal. 284.1757.

5.3.14 3-(3-(*N*-benzylacrylamido)propyl)-1-ethyl-1*H*-imidazol-3-ium chloride (9)

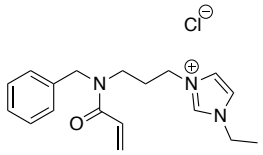

9

1-Ethylimidazole (0.24 mL, 2.5 mmol, 1.2 equiv.) and **7** (500 mg, 2.1 mmol, 1 equiv.) were dissolved in anhydrous ACN (5 mL) under nitrogen atmosphere. The reaction mixture was stirred at 80 °C for 3 days. The solvent was removed *in vacuo*, resulting in a residue that was then redissolved in water (5 mL). The resultant solution was subjected to a series of washing steps with diethyl ether (3 x 10 mL) and ethyl acetate (3 x 10 mL). The solvent was removed *via* lyophilization, and the resulting crude product was purified by reverse phase liquid chromatography from water: MeOH (95: 5) to pure MeOH (0: 100) resulting in the product as a colorless liquid with a yield of 32%.

^{1}H NMR (500 MHz, DMSO-D_6) δ [ppm] = 9.25 (s, 1H, N-C*H*=N), 7.88-7.71 (m, 2H, N-C*H*=C*H*-N), 7.48-7.14 (m, 5H, phenyl-C*H*), 6.82-6.67 (m, 1H, CH_2=CH-CO), 6.27-6.15 (m, 1H, CH_2=CH-CO), 5.85-5.66 (m, 1H, CH_2=C*H*-CO), 4.77-4.58 (m, 2H, phenyl-CH_2-NCO), 4.22-4.15 (m, 4H, NCO-CH_2-CH_2, N-CH_2-CH_3), 3.39-3.30 (m, 2H, CH_2-N=C), 2.10-2.01 (m, 2H, CH_2-CH_2-CH_2) 1.42 (*J* = 7.3 Hz, 3 H, N-CH_2-CH_3).
^{13}C NMR (126 MHz, DMSO-D_6) δ [ppm] = 165.32, 137.71, 135.87, 128.69, 128.10, 127.56, 126.47, 122.35, 50.00, 47.91, 46.85, 46.35, 44.19, 42.60, 28.94, 27.55.
ESI-TOF-MS for $[M]^+$: found: 298.1884 cal. 298.1914.

5.3.15 3-(3-(*N*-benzylacrylamido)propyl)-1-methyl-1*H*-benzo[*d*]imidazol-3-ium chloride (10)

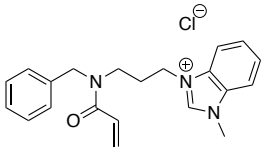

10

1-Methylbenzimidazole (333 mg, 2.5 mmol, 1.2 equiv.) and **7** (500 mg, 2.1 mmol, 1 equiv.) and were dissolved in anhydrous ACN (1.5 mL) under nitrogen atmosphere. The reaction mixture was stirred at 80 °C for 3 days. The solvent was removed *in vacuo*, resulting in a residue that was then redissolved in water (5 mL). The resultant solution was subjected to a series of washing steps with chloroform (3 x 10 mL) and ethyl acetate (3 x 10 mL). The solvent was reduced *in vacuo* and the resulting solution was purified by reverse phase liquid chromatography from water: MeOH (95:5) to pure MeOH (0: 100) resulting in the product as a colorless liquid with a yield of 36%.

^{1}H NMR (500 MHz, $CDCl_3$) δ [ppm] = 11.79 (s, 1H, N-C*H*=N), 7.84-7.61 (m, 4H, C*H*=C*H*-C*H*=C*H*), 7.40-7.15 (m, 5H, phenyl-C*H*), 6.58 (dd, *J* = 16.8, 10.4 Hz, 1H, CH_2=CH-CO), 6.34 (dd, *J* = 16.7, 2.0 Hz, 1H, CH_2=CH-CO), 5.69 (dd, *J* = 10.4, 2.0 Hz, 1H, CH_2=C*H*-CO), 4.78 (s, 2H, phenyl-CH_2-NCO), 4.63-4.60 (m, 2H, NCO-CH_2-CH_2), 4.24 (s, 3H, N-CH_3), 3.61 (t, *J* = 6.8 Hz, 2H, CH_2-N=C), 1.93 (m, 2H, CH_2-CH_2-CH_2).

^{13}C NMR (126 MHz, $CDCl_3$) δ [ppm] = 167.54, 144.01, 136.45, 131.90, 131.30, 128.92, 127.76, 127.52, 126.64, 113.15, 51.32, 45.51, 43.30, 33.54, 27.72.
ESI-TOF-MS for $[M]^+$: found: 334.1894 cal. 334.1924.

5.3.16 General procedure for RAFT homopolymerization of *N*,*N*-dimethylacrylamide

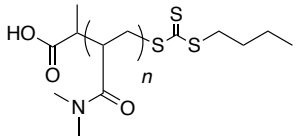

A Schlenk tube was charged with *N*,*N*-dimethylacrylamide (1 g, 10.1 mmol, 400 equiv.) 2-(butylthiocarbonothioylthio)propanoic acid (9 mg, 0.025 mmol, 1 equiv.), azobisisobutyronitrile (0.41 mg, 0.0025 mmol, 0.1 equiv.) and anhydrous 1,4-dioxane (3.36 mL). Four freeze-pump-thaw cycles were performed to degas the solution. The Schlenk tube was refilled with argon and placed into a preheated oil bath at 90 °C. After three hours the reaction was stopped by placing the Schlenk tube into a liquid-nitrogen bath. The crude polymer was precipitated in cooled diethyl ether three times from THF. The polymer was dried under vacuum and isolated in a yield of 90% as a slightly yellow powder.

M_n(GPC) = 24000; PDI (GPC) =1.3

5.3.17 Pentafluorophenyl acrylate (11)

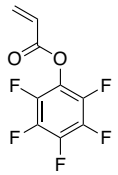

11

The synthesis of **11** was accomplished according to a modified literature procedure.[301] Pentafluorophenol (5 g, 27.2 mmol, 1 equiv.) was dissolved in anhydrous DCM (50 mL) under nitrogen atmosphere and cooled down to 0 °C. TEA (4.1 mL, 29.9 mmol, 1.1 equiv.) and acryloyl chloride (2.4 mL, 29.9 mmol, 1 equiv.) were added subsequentially dropwise to the reaction mixture. The reaction mixture was stirred overnight and allowed to gradually reach room temperature. Reaction monitoring was carried out by TLC using petroleum ether: ethyl acetate (10: 1). After full conversion and filtration, the reaction mixture was washed with brine solution (3 x 20 mL). The organic phase was dried over Na_2SO_4 and filtrated. Traces of hydroquinone were added, and the DCM was removed in *vacuo*. Vacuum distillation (0.055 mbar, 30 °C) yielded the product as a clear colourless liquid in yields of 64%.

^{1}H NMR (500 MHz, $CDCl_3$) δ [ppm] = 6.72 (dd, *J* = 17.3, 0.9 Hz, 1H, C*H*$_2$=CH-CO), 6.37 (dd, *J* = 17.3, 10.6 Hz, 1H, C*H*$_2$=CH-CO), 6.18 (dd, *J* = 10.6, 0.9 Hz, 1H, CH$_2$=C*H*-CO).
^{19}F NMR (470 MHz, $CDCl_3$) δ [ppm] = -152.50-152.74 (m, 2F), -158.04 (t, *J* = 21.7 Hz, 1F), -162.38-162.46 (m, 2F).

5.3.18 Pentafluorophenyl methacrylate (12)

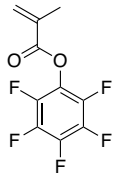

12

The synthesis of **11** was accomplished according to a modified literature procedure.[333] Pentafluorophenol (5 g, 27.2 mmol, 1 equiv.) was dissolved in anhydrous DCM (50 mL) under nitrogen atmosphere and cooled down to 0 °C. TEA (4.1 mL, 29.9 mmol, 1.1 equiv.) and methacryloyl chloride (2.6 mL, 27.2 mmol, 1 equiv.) were added subsequentially dropwise to the mixture. The reaction mixture was stirred overnight and allowed to gradually reach room temperature. Reaction monitoring was carried out by TLC using petroleum ether: ethyl acetate (10: 1). After full conversion and filtration, the reaction mixture was washed with brine solution (3 x 20 mL). The organic phase was dried over Na_2SO_4 and filtrated. Traces of hydroquinone were added, and the DCM was removed in *vacuo*. Vacuum distillation (0.035 mbar, 30 °C) yielded the product as a clear colourless liquid in yields of 66%.

^{1}H NMR (500 MHz, $CDCl_3$) δ [ppm] = 6.45 (t, *J* = 1.0 Hz, 1H, CH_3-C=CH_2), 5.95 – 5.86 (m, 1H, CH_3-C=CH_2), 2.09 (dd, *J* = 1.6, 1.0 Hz, 3H, CH_3-C=CH_2).
^{19}F NMR (470 MHz, $CDCl_3$) δ [ppm] = -152.82-152.86 (m, 2 F), -158.27 (t, *J* = 21.6 Hz, 1 F), -162.51-162.60 (m, 2 F).

5.3.19 General procedure for RAFT homopolymerization of pentafluorophenyl alcrylate (PFPA-1)

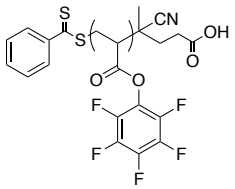

PFPA-1

A Schlenk tube was charged with **11** (5 g, 21.0 mmol, 85 equiv.) 4-cyano-4-(phenylcarbonothioylthio)pentanoic acid (**CTA-1**) (69 mg, 0.247 mmol, 1 equiv.), azobisisobutyronitrile (3.1 mg, 0.00282 mmol, 0.125 equiv.) and 1,4-dioxane (5 mL). Four freeze-pump-thaw cycles were performed to degas the solution. The Schlenk tube was refilled with argon and placed into a preheated oil bath at 80 °C. After three hours the reaction was stopped by placing the Schlenk tube into a liquid-nitrogen bath. The monomer conversion was determined by measuring ^{19}F NMR of the reaction mixture. The crude polymer was precipitated in cooled *n*-hexane three times from THF. The polymer was dried under vacuum and isolated in a yield of 63% as a slightly pink powder.
The theoretical M_n ($M_{n\ Theo}$) was calculated by using the linear RAFT equation: $M_n = ([M]_0/[RAFT]_0) \times$ monomer conversion $\times M_W$(Monomer)+ M_W(RAFT agent), $[M]_0$, $[RAFT]_0$, M_W (monomer) and M_W (RAFT agent) represent monomer and RAFT agent concentrations, molar mass of monomer and RAFT agent, respectively. The monomer conversion was directly determined after polymerization by ^{19}F NMR.

^{1}H NMR (400 MHz, $CDCl_3$) δ [ppm] = 3.09 (br s, 1H, C*H*-CH_2), 2.64 – 2.00 (br m, 2H, CH-CH_2) ppm.
^{19}F NMR (376 MHz, $CDCl_3$) δ [ppm] = -153.23 (br s, 2 F), -156.81 (br s, 1 F), -162.24 (br s, 2 F)
$M_{n\ Theo}$ =12400; M_n (GPC) =9100; PDI=1.3

5.3.20 General procedure for end-cap modification of poly(pentafluorophenyl acrylate) (PFPA-2)

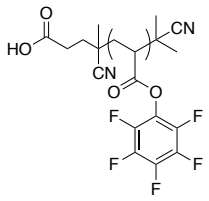

PFPA-2

The **PFPA-1** (1.3 g, 0.104 mmol, 1 equiv.) and azobisisobutyronitrile (170 mg, 1.04 mmol, 10 equiv.) were dissolved in dry dioxane (3 mL) under nitrogen atmosphere in a Schlenk tube. The resultant mixture was subjected to four freeze/thaw cycles and then heated to 80 °C. After three hours, the reaction was stopped by placing the Schlenk tube into a liquid-nitrogen bath. The polymer was precipitated in cold hexane from dioxane three times. The polymer was then dried in a vacuum oven to yield the desired poly(pentafluorophenyl acrylate) as a white solid compound and was directly used for side group modification without the need for further characterization.

5.3.21 General procedure for RAFT homopolymerization of pentafluorophenyl methalcrylate (PFPM-1)

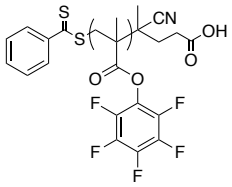

PFPM-1

A Schlenk tube was charged with **12** (5 g, 19.8 mmol, 85 equiv.) 4-cyano-4-(phenylcarbonothioylthio)pentanoic acid (**CTA-1**) (65 mg, 0.233 mmol, 1 equiv.), azobisisobutyronitrile (4.8 mg, 0.0202 mmol, 0.125 equiv.) and 1,4-dioxane (5 mL). Four freeze-pump-thaw cycles were performed to degas the solution. The Schlenk tube was refilled with argon and placed into a preheated oil bath at 80 °C. After three hours the reaction was stopped by placing the Schlenk tube into a liquid-nitrogen bath. The monomer conversion was determined by measuring ^{19}F NMR of the reaction mixture. The crude polymer was precipitated in cooled *n*-hexane three times from THF. The polymer was dried under vacuum and isolated in a yield of 57% as a slightly pink powder.
The theoretical M_n ($M_{n\ Theo}$) was calculated by using the linear RAFT equation: $M_n = ([M]_0/[RAFT]_0) \times$ monomer conversion $\times M_W$(Monomer)+ M_W(RAFT agent), $[M]_0$, $[RAFT]_0$, M_W (monomer) and M_W (RAFT agent) represent monomer and RAFT agent concentrations, molar mass of monomer and RAFT agent, respectively. The monomer conversion was directly determined after polymerization by ^{19}F NMR.

$M_{n\ Theo}$ =12400; M_n (GPC) = 12600; PDI=1.3
^{1}H NMR (400 MHz, $CDCl_3$) δ [ppm] = 2.43 (br s, 2H, C-CH_2), 1.25-1.60 (br m, 3H, C-CH_3).
^{19}F NMR (376 MHz, $CDCl_3$) δ [ppm] = -150.41-151.48 (m, 2F), -157.02 (br s, 1F) -162.15 (br s, 2 F)

5.3.22 General procedure for end-cap modification of poly(pentafluorophenyl methacrylate) (PFPM-2)

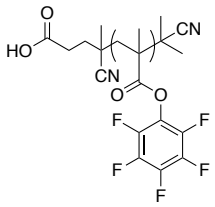

PFPM-2

The **PFPM-1** (2.2 g, 0.176 mmol, 1 equiv.) and azobisisobutyronitrile (577 mg, 3.5 mmol, 20 equiv.) were dissolved in dry dioxane (6 mL) under nitrogen atmosphere in a Schlenk tube. The resultant mixture was subjected to four freeze/thaw cycles and then heated to 80 °C. After three hours, the reaction was stopped by placing the Schlenk tube into a liquid-nitrogen bath. The polymer was precipitated in cold hexane from dioxane three times. The polymer was then dried in a vacuum oven to yield the desired poly(pentafluorophenyl methacrylate) as a white solid compound and was directly used for side group modification without the need for further characterization.

5.3.23 Poly(ethylene glycol) methyl ether amine (13)

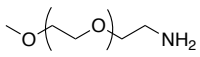

13

The synthesis of **13** was accomplished according to a modified literature procedure.[312] Methoxy poly(ethylene glycol) (10.0 g, 18.2 mmol, 1 equiv., MW 550) was charged in a 50 mL Schlenck flask and degassed at 80 °C in an oil bath while stirring for one hour to remove traces of water. The flask was purged with nitrogen, cooled with an ice bath and then thionyl chloride (2.0 g, 27.3 mmol, 1.5 equiv.) was added slowly. The reaction mixture was stirred for 2 hours while gradually reaching room temperature. The resulting crude product was dissolved in DMF (20 mL) and the solvent was subsequently removed *in vacuo* three times. The conversion of the reaction was tracked by IR-spectroscopy with the disappearance of the O-H stretching band and the appearance of a C-Cl stretch band. The obtained product was then added to a solution of sodium azide (1.8 g, 27.3 mmol, 1.5 equiv.) in DMF (100 mL) and stirred overnight at 85 °C. After cooling and solvent removal *in vacuo*, DCM (200 mL) was added. The resulting precipitate was filtered, and the solvent of the filtrate was removed *in vacuo*. The conversion of the reaction was tracked by IR-spectroscopy with the disappearance of a C-Cl stretch band and the appearance of an azide N=N=N stretch band. The product was redissolved in THF (150 mL) and triphenylphosphine (7.2 g, 27.3 mmol, 1.5 equiv.) was added. The reaction mixture was stirred at room temperature for 4 hours. Subsequently, deionized water (1 mL) was added and the reaction mixture was stirred overnight. THF was removed *in vacuo* and deionized water (100 mL) was added. The precipitate was filtered, and the filtrate was washed with toluene (3 x 50 mL) three times. The water was removed *in vacuo* yielding a clear yellow oil in a yield of 7.7 g.

^{1}H NMR (400 MHz, $CDCl_3$) δ [ppm] = 3.59 (m, 36H, CH_2-CH_2-O), 3.49 (m, 4H, CH_2-CH_2-N), 3.32 (s, 3H, O-CH_3), 2.64 (s, 2H, CH_2-NH_2).
IR (bulk): *ν*max (cm^{-1}) = 3500 (w), 2923 (m), 2120 (m), 1730 (m), 1562 (m), 1469 (m), 1418 (m), 1361 (m), 1305 (m), 1272 (m), 1260 (m), 1162 (s), 1110 (w), 986 (w), 969 (w), 654 (w), 617 (s).
ESI-TOF-MS for $[M+H]^+$: found 428.2845; calc. 428.2854

5.3.24 6-azido-hexylamine (14)

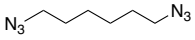

The synthesis of **14** was accomplished according to a modified literature procedure in two steps.[313] 1,6-Dibromohexane (8.0 g, 32.8 mmol, 1 equiv.) was dissolved in anhydrous DMF (50 mL) under nitrogen atmosphere. Sodium azide (6.4 g, 98.4 mmol, 3 equiv.) was added to the reaction vessel. The reaction mixture was heated to 60 °C and stirred for 4 hours. The DMF was then removed in *vacuo* and the residue was diluted with diethyl ether (100 mL). The organic phase was subsequently washed with saturated aqueous solution of $NaHCO_3$ (75 mL). The aqueous phase was extracted with diethyl ether (2 x50 mL) twice. The combined organic phases were dried over Na_2SO_4, filtered and the solvent was removed in *vacuo* resulting in a colourless oil in a yield of 63%.

^{1}H NMR (400 MHz, $CDCl_3$) δ [ppm] = 3.27 (t, *J* = 6.9 Hz, 4H, N_3-C*H*$_2$-CH_2), 1.66-1.58 (m, 4H, N_3-CH_2-C*H*$_2$), 1.44-1.38 (m, 4H, CH_2-C*H*$_2$-CH_2).

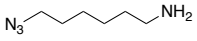

14

1,6-diazidohexane (3.5 g, 20.7 mmol, 1 equiv.) was dissolved in a mixture of diethyl ether/ethyl acetate (13 mL/13 mL). An aqueous solution of HCl 1M (20 mL) was added to the reaction vessel. The mixture was cooled with an ice bath while stirring. Triphenylphosphine (5.4 g, 20.6 mmol, 1 equiv.) was added to the reaction mixture over 20 minutes. After 3 hours of stirring at room temperature, the two layers were separated, and the aqueous layer was extracted with diethyl ether (2 x 50 mL). The aqueous layers were combined, basified with NaOH 1M (until pH 12) and extracted three times with diethyl ether (3 x 50 mL). The combined organic layers were then dried over Na_2SO_4 and filtered. The crude product was purified *via* column chromatography changing the eluent from pure DCM to DCM: MeOH (80:20). After removal of the solvent in *vacuo* the product was obtained as yellow oil in a yield of 59%.

^{1}H NMR (400 MHz, $CDCl_3$) δ [ppm] =3.26 (t, *J* = 6.9 Hz, 2H, N_3-C*H*$_2$-CH_2), 2.69 (t, *J* = 6.9 Hz, 2H, NH_2-C*H*$_2$-CH_2), 1.65 – 1.56 (m, 2H, NH_2-CH_2-C*H*$_2$), 1.49 – 1.42 (m, 2H), 1.40 – 1.33 (s, 6H, C*H*$_2$-C*H*$_2$-C*H*$_2$).
^{13}C NMR (101 MHz, $CDCl_3$) δ [ppm] = 51.51, 42.00, 28.92, 26.68, 26.53.
ESI-TOF-MS (m/z) for $[M+H]^+$: found 143.1295 calc. 143.1291

5.3.25 General procedure for post-modification with poly(ethylene glycol) methyl ether amine (13) and 6-azido-hexylamine (14) of PFPM (MPFPM-1)

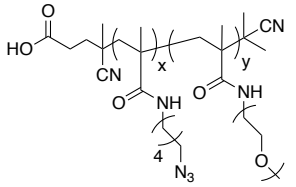

MPFPM-1

A Schlenk tube was charged with **PFPM-2** and dry DMF (3 mL) under nitrogen atmosphere. ω-Amino-PEG (0.8 equiv. relative to PFP subunits) and TEA (1 equiv.) were mixed in dry DMF (2 mL) before addition to the polymer solution. The Schlenk tube was placed into a preheated oil bath at 60 °C and stirred continuously. The conversion of the reaction was tracked with ^{19}F NMR spectroscopy. After reaching a conversion rate of 80%, 6-azidohexyl-1-amine **5** (0.3 equiv. relative to PFP subunits) was added. The reaction mixture was stirred till complete conversion according to ^{19}F NMR spectroscopy.

The final fully functionalized polymer was purified by dialysis in THF for three days. The pure product was obtained after removal of solvent *in vacuo*.

M_n (GPC) = 29700; PDI=1.6

5.3.26 General procedure for post-modification with poly(ethylene glycol) methyl ether amine (13) and 6-azido-hexylamine (14) of PFPA (MPFPA-1)

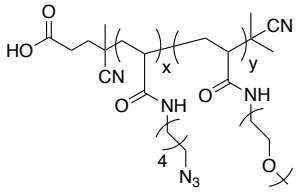

MPFPA-1

A Schlenk tube was charged with **PFPA-2** and dry DMF (3 mL) under nitrogen atmosphere. ω-Amino-PEG (0.8 equiv. relative to PFP subunits) and DMAP (0.2 equiv.) were mixed in dry DMF (2 mL) before addition to the polymer solution. The Schlenk tube was placed into a preheated oil bath at 50 °C and stirred continuously. The conversion of the reaction was tracked with ^{19}F NMR spectroscopy. After reaching a conversion rate of 80%, 6-azidohexyl-1-amine (0.3 equiv. relative to PFP subunits) was added. The reaction mixture was stirred till complete conversion according to ^{19}F NMR spectroscopy. The final fully functionalized polymer was purified by dialysis in THF for three days, and the pure product was obtained after solvent removal *in vacuo*.

M_n (GPC) = 22100; PDI=1.5

5.3.27 (4*S*,4'*S*)-2,2'-(hepta-1,6-diyne-4,4-diyl)bis(4-(*tert*-butyl)-oxazoline) (15)

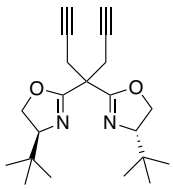

15

2,2-methylenebis[(4*S*)-4-*tert*-butyl-2-oxazoline] (400 mg, 1.5 mmol, 1 equiv.) was dissolved in dry THF (13 mL) and cooled to -55 °C. *n*-Butyllithium (1.32 mL of 2.5 M solution in hexane, 3.3 mmol, 2.2 equiv.) was added to the reaction vessel. The reaction was allowed to proceed for one hour at this temperature. Then propargyl bromide (393 mg of 80% solution in toluene, 3.3 mmol, 2.2 equiv.) was added and the reaction mixture was stirred at -10 °C. After three hours, the reaction was quenched by the addition of a saturated aqueous solution of NH_4Cl (10 mL). The resulting mixture was extracted with diethyl ether (2 x 50 mL), the organic phase was dried over Na_2SO_4 and filtered. Subsequently, the solvent was removed *in vacuo* and the crude product was purified by liquid chromatography using hexane: ethyl acetate dynamically (from 10:1 to 5:1) resulting in a yellow oil in a yield of 66%.

^{1}H NMR (400 MHz, $CDCl_3$) δ [ppm] = 4.21 – 4.15 (m, 2H, C-C*H*$_2$), 4.12 – 4.03 (m, 2H, C-C*H*$_2$), 3.89 (dd, *J* = 10.1, 7.6 Hz, 2H, N-C*H*-CH$_2$), 3.28 – 2.97 (m, 4H, CH-C*H*$_2$-O), 1.98 (t, *J* = 2.6 Hz, 2H, C*H*), 0.89 (s, 18H, C-C*H*$_3$).
^{13}C NMR (101 MHz, $CDCl_3$) δ [ppm] = 164.5, 79.7, 75.9, 71.1, 69.5, 45.2, 33.9, 25.9, 23.5.
ESI-TOF-MS (m/z) for $[M+H]^+$: found 343.2375 calc. 343.2380

5.3.28 (4*S*,4'*S*)-2,2'-(hepta-1,6-diyne-4,4-diyl)bis(4-phenyl-oxazoline) (16)

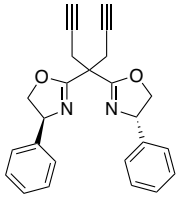

16

2,2-methylenebis[(4*S*)-4-phenyl-2-oxazoline] (400 mg, 1.31 mmoles, 1 equiv.) was dissolved in dry THF (13 mL) and cooled to -55 °C. *n*-Butyllithium (1.15 mL of 2.5 M solution in hexane, 2.88 mmol, 2.2 equiv.) was added to the reaction vessel. The reaction was allowed to proceed for one hour at this temperature. Then propargyl bromide (428 mg of 80% solution in toluene, 2.88 mmol, 2.2 equiv.) was added and the reaction mixture was stirred at -10 °C. After three hours, the reaction was quenched by the addition of a saturated aqueous solution of NH_4Cl (10 mL). The resulting mixture was extracted with diethyl ether (2 x 50 mL), the organic phase was dried over Na_2SO_4 and filtered. Subsequently, the solvent was removed *in vacuo* and the crude product was purified by column chromatography using hexane: ethyl acetate dynamically (from 10:1 to 3:1) resulting in a yellow oil in a yield of 52%.

^{1}H NMR (400 MHz, $CDCl_3$) δ [ppm] = 7.37 – 7.26 (m, 10H, phenyl-C*H*), 5.28 (dd, *J* = 10.2, 8.1 Hz, 2H, C-CH_2), 4.72 (dd, *J* = 10.2, 8.4 Hz, 2H, C-CH_2), 4.18 (t, *J* = 8.3 Hz, 2H, N-C*H*-CH$_2$), 3.33 – 3.21 (m, 4H, CH-CH_2-O), 2.10 (t, *J* = 2.6 Hz, 2H, C*H*).
^{13}C NMR (101 MHz, $CDCl_3$) δ [ppm] = 166.22, 141.93, 128.80, 127.87, 127.07, 79.38, 76.01, 71.71, 70.02, 45.30, 23.89.
ESI-TOF-MS (m/z) for $[M+H]^+$: found 383.1739 calc. 383.1754

5.3.29 General procedure for post-modification with poly(ethylene glycol) methyl ether amine (13) of PPFPA (MPFPA-2)

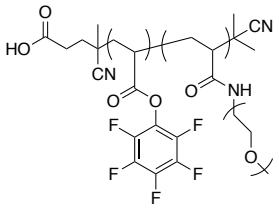

MPFPA-2

A Schlenk tube was charged with **PFPA-2** and dry THF (3 mL) under nitrogen atmosphere. ω-Amino-PEG (0.8 equiv. relative to PFP subunits) and DMAP (0.2 equiv.) were mixed in anhydrous THF (2 mL) before addition to the polymer solution. The Schlenk tube was placed into a preheated oil bath at 60 °C and stirred continuously. The conversion of the reaction was tracked with ^{19}F NMR spectroscopy. After reaching a conversion rate of 80%, the functionalized polymer was purified by dialysis in THF for three days. The product was obtained after solvent removal *in vacuo*.

M_n (GPC) = 18000; PDI=1.5

5.3.30 General procedure for post-modification with poly(ethylene glycol) methyl ether amine (13) of PPFPMA (MPFPM-2)

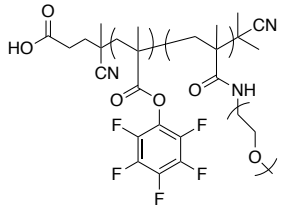

MPFPM-2

A Schlenk tube was charged with **PFPM-2** and anhydrous DMF (3 mL) under nitrogen atmosphere. ω-Amino-PEG (0.8 equiv. relative to PFP subunits) and TEA (1 equiv.) were mixed in anhydrous DMF (2 mL) before addition to the polymer solution. The Schlenk tube was placed into a preheated oil bath at 80 °C and stirred continuously. The conversion of the reaction was tracked with ^{19}F NMR spectroscopy. After reaching a conversion rate of 80%, the functionalized polymer was purified by dialysis in THF for three days. The product was obtained after solvent removal *in vacuo*.

M_n (GPC) = 25800; PDI=1.5

5.3.31 Bis(1-hexyl-3-(4-hydroxyundecyl)-2,3-dihydro-1*H*-imidazol-2-yl)copper(I) bromide (17)

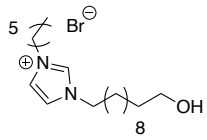

The synthesis of **17** was accomplished according to a modified literature procedure in two steps.[320] A suspension of 11-Bromo-1-undecanol (2.4 g, 9.6 mmol, 1 equiv.) was prepared in acetonitrile (20 mL). To this suspension, 1-hexylimidazole (1.52 mL, 10 mmol, 1.05 equiv.) was added, and the reaction mixture was stirred for 24 hours at 80 °C. The reaction mixture was allowed to return to room temperature and was subsequently diluted with diethyl ether (100 mL). The resulting precipitate was filtered off, washed three times with diethyl ether (3 x 50 mL) and dried *in vacuo* to result in the product as a colorless solid with a yield of 66%.

^{1}H NMR (400 MHz, DMSO-D$_6$) δ [ppm] = 9.20 (s, 1H, N-C*H*=N), 7.78 (m, 2H, N-C*H*=C*H*-N), 4.30 (t, *J* = 5.1 Hz, 1H, CH$_2$-O*H*), 4.14 (t, *J*=7.0 Hz, 4H, N-C*H*$_2$-CH$_2$), 3.36 (m, 2H, C*H*$_2$-OH), 1.77 (p, *J* = 7.2 Hz, H, N-CH$_2$-C*H*$_2$), 1.34-1.38 (m, 2H, C*H*$_2$-CH$_2$-OH), 1.28 – 1.15 (m, 20 H, -C*H*$_2$-), 0.88-0.77 (m, 3H, CH$_2$-C*H*$_3$).

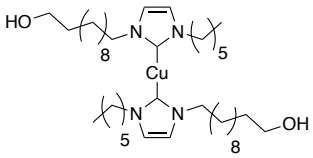

17

3-Hexyl-1-(11-hydroxyundecyl)-1H-imidazol-3-ium bromide (1.0 g, 2.50 mmol, 1 equiv.) and cooper oxide (Cu$_2$O) (1.8 g, 12.2 mmol, 5 equiv.) were suspended in dioxane (16.66 mL). The reaction mixture was stirred for 3 days at 100 °C. After cooling to room temperature, the excess of Cu$_2$O was filtered off and the solvent was removed *in vacuo*. The crude product was purified by column chromatography from pure chloroform (100: 0) to chloroform: methanol (20:1) resulting in the product as a white solid with a yield of 14%.

^{1}H NMR (400 MHz, $CDCl_3$) δ [ppm] = 6.16 (s, 4H, N-C*H*=C*H*-N), 3.62 (t, *J* = 6.7 Hz, 4H, CH_2-OH), 3.58 (t, *J* = 7.8 Hz, 8H, N-CH_2-CH_2), 1.70-1.60 (m, 8H, N-CH_2-CH_2), 1.59-1.48 (m, 4H, CH_2-CH_2-OH), 1.36-1.21 (m, 40H, -CH_2-), 0.93-0.82 (m, 6H, CH_2-CH_3).

4.2.2.36 General procedure for the single chain collapse in DMF *via* transesterification for MPFPM-2

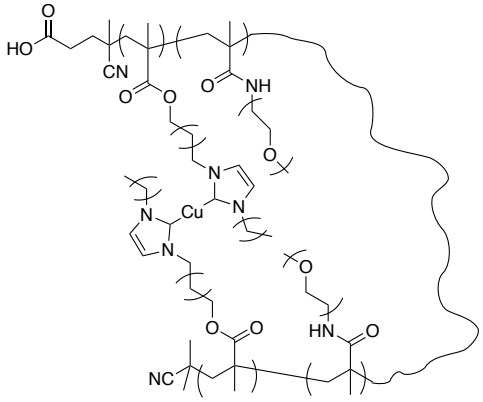

MPFPM-2 (50 mg) was dissolved in anhydrous DMF (95 mL). **17** (0.25 equiv related to PFP subunits) was dissolved in presence of catalyst (0.2 or 2 eq related to **17**) and 1,6-hexanediol (0.25 equiv. related to PFP subunits) in anhydrous DMF(5 mL). This solution was added to the polymer solution and stirred continuously for three days at 80 °C. Then the solvent DMF was reduced *in vacuo* and the residue was dialyzed against THF.

M_n (GPC) = 18400; PDI = 1.7

4.2.2.37 General procedure for the single chain collapse in DMF *via* transesterification for MPFPA-2

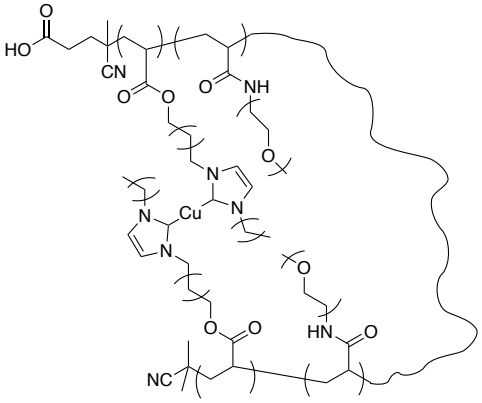

MPFPA-2 (50 mg) was dissolved in anhydrous DMF (95 mL). **17** (0.25 equiv. related to PFP subunits) was dissolved in presence of catalyst (0.2 eq related to **17**) and 1,6-hexanediol (0.25 equiv. related to PFP subunits) in anhydrous DMF (5 mL). This solution was added to the polymer solution and stirred continuously for three days at 80 °C. Then the solvent DMF was reduced *in vacuo* and the residue was dialyzed against THF.

M_n (GPC) = 14300; PDI = 1.5

6. References

(1) European Commision (2019) Communication from the commission to the European Parliament, the Council, the European Economic and Social Committee and the Committee of the Regions *The European Green Deal*, COM (2019) 640. **2019**. DOI: https://eur-lex.europa.eu/legal-content/EN/TXT/HTML/?uri=CELEX:52019DC0640.

(2) European Parliament and Council (2022) Corporate Sustainability Reporting Directive, (EU) 2022/2464 **2022**. DOI: http://data.europa.eu/eli/dir/2022/2464/oj.

(3) Kirchhoff, T. Problem oder Chance. *Nachr*. *Chem*. **2024**, *72* (1), 38-40. DOI: https://doi.org/10.1002/nadc.20244139751.

(4) Smith, R. F.; Boothroyd, S. C.; Thompson, R. L.; Khosravi, E. A facile route for rubber breakdown via cross metathesis reactions. *Green Chem*. **2016**, *18* (11), 3448-3455. DOI: https://doi.org/10.1039/C5GC03075G.

(5) Andler, R. Bacterial and enzymatic degradation of poly(cis-1,4-isoprene) rubber: Novel biotechnological applications. *Biotechnol*. *Adv*. **2020**, *44*, 107606. DOI: https://doi.org/10.1016/j.biotechadv.2020.107606.

(6) Anastas, P. T.; Warner, J. C. *Green Chemistry: Theory and Practice*; Oxford University Press, **1998**. ISBN: 0198502346.

(7) Winterton, N. Twelve more green chemistry principles. *Green Chem.* **2001**, *3* (6), G73-G81. DOI: https://doi.org/10.1039/B110187K.

(8) Altenhoff, A. L.; de Witt, J.; Andler, R.; Steinbuchel, A. Impact of additives of commercial rubber compounds on the microbial and enzymatic degradation of poly(cis-1,4-isoprene). *Biodegradation* **2019**, *30* (1), 13-26. DOI: https://doi.org/10.1007/s10532-018-9858-5.

(9) European Comission; Directorate-General for Internal Market, Industry, Entrepreneurship and SMEs. *Study on the review of the list of critical raw materials – Final report*; Publications Office of the European Union, **2017**. DOI: https://data.europa.eu/doi/10.2873/876644.

(10) European Commision; Directorate-General for Internal Market, Industry, Entrepreneurship and SMEs; Grohol, M.; Veeh, C. *Study on the critical raw materials for the EU 2023 – Final report*; Publications Office of the European Union, **2023**. DOI: https://data.europa.eu/doi/10.2873/725585.

(11) Jehanno, C.; Pérez-Madrigal, M. M.; Demarteau, J.; Sardon, H.; Dove, A. P. Organocatalysis for depolymerisation. *Polymer Chem*. **2019**, *10* (2), 172-186. DOI: https://doi.org/10.1039/C8PY01284A.

(12) Hosler, D.; Burkett, S. L.; Tarkanian, M. J. Prehistoric polymers: rubber processing in ancient mesoamerica. *Science* **1999**, *284* (5422), 1988-1991. DOI: https://doi.org/10.1126/science.284.5422.1988.

(13) Mooibroek, H.; Cornish, K. Alternative sources of natural rubber. *Appl*. *Microbiol*. *Biotechnol*. **2000**, *53* (4), 355-365. DOI: https://doi.org/10.1007/s002530051627.

(14) Tanaka, Y. Structure and biosynthesis mechanism of natural polyisoprene. *Progress in Polymer Science* **1989**, *14* (3), 339-371. DOI: https://doi.org/10.1016/0079-6700(89)90006-3.

(15) Berthelot, K.; Lecomte, S.; Estevez, Y.; Peruch, F. Hevea brasiliensis REF (Hev b 1) and SRPP (Hev b 3): An overview on rubber particle proteins. *Biochimie* **2014**, *106*, 1-9. DOI: https://doi.org/10.1016/j.biochi.2014.07.002.

(16) Vaysse, L.; Bonfils, F.; Sainte-Beuve, J.; Cartault, M. 10.17 - Natural Rubber. In *Polymer Science: A Comprehensive Reference*, Matyjaszewski, K., Möller, M. Eds.; Elsevier, **2012**; pp 281-293. ISBN: 044459387X

(17) Fang, Y.; Zhan, M.; Wang, Y. The status of recycling of waste rubber. *Mater*. *Des*. **2001**, *22* (2), 123-128. DOI: https://doi.org/10.1016/S0261-3069(00)00052-2.

(18) Morton, M. History of Synthetic Rubber. *J*. *Macromol*. *Sci*. *Part A* **1981**, *15*, 1289-1302. DOI: https://doi.org/10.1080/00222338108056786.

(19) Threadingham, D.; Obrecht, W.; Wieder, W.; Wachholz, G.; Engehausen, R. Rubber, 3. Synthetic Rubbers, Introduction and Overview. In *Ullmann's Encyclopedia of Industrial Chemistry*, Wiley-VCH, **2011**. ISBN: 9783527306732.

(20) Ciullo, P. A.; Hewitt, N. *The rubber formulary*; Noyes Publication/William Andrew Publishing, **1999**. ISBN: 081551929X.

(21) Williams, P. T. Pyrolysis of waste tyres: a review. *Waste Manag*. **2013**, *33* (8), 1714-1728. DOI: https://doi.org/10.1016/j.wasman.2013.05.003.

(22) Asua, J. M. Miniemulsion polymerization. *Prog*. *Polym*. *Sci*. **2002**, *27* (7), 1283-1346. DOI: https://doi.org/10.1016/S0079-6700(02)00010-2.
(23) Cheong, I. W.; Fellows, C. M.; Gilbert, R. G. Synthesis and cross-linking of polyisoprene latexes. *Polymer* **2004**, *45* (3), 769-781. DOI: https://doi.org/10.1016/j.polymer.2003.12.002.
(24) Lorenz, M. R.; Kohnle, M. V.; Dass, M.; Walther, P.; Hocherl, A.; Ziener, U.; Landfester, K.; Mailander, V. Synthesis of fluorescent polyisoprene nanoparticles and their uptake into various cells. *Macromol*. *Biosci*. **2008**, *8* (8), 711-727. DOI: https://doi.org/10.1002/mabi.200700336.
(25) Moad, G. Reversible addition–fragmentation chain transfer (co)polymerization of conjugated diene monomers: butadiene, isoprene and chloroprene. *Polym*. *Int*. **2017**, *66* (1), 26-41. DOI: https://doi.org/10.1002/pi.5173.
(26) Richards, D. H. The polymerization and copolymerization of butadiene. *Chem*. *Soc*. *Rev*. **1977**, *6* (2), 235-260. DOI: https://doi.org/10.1039/CS9770600235.
(27) Medalia, A. I.; Freedman, H. H. Configuration of Polybutadienes Prepared at High Temperatures1. *J*. *Am*. *Chem*. *Soc*. **1953**, *75* (19), 4790-4793. DOI: https://doi.org/10.1021/ja01115a051.
(28) Kerns, M.; Henning, S.; Rachita, M. Butadiene polymers. *Encyclopedia of Polymer Science and Technology*, John Wiley & Sons, Inc., **2002**. ISBN: 9780471440260
(29) Benoit, D.; Harth, E.; Fox, P.; Waymouth, R. M.; Hawker, C. J. Accurate Structural Control and Block Formation in the Living Polymerization of 1,3-Dienes by Nitroxide-Mediated Procedures. *Macromolecules* **2000**, *33* (2), 363-370. DOI: https://doi.org/10.1021/ma991187l.
(30) Harrisson, S.; Couvreur, P.; Nicolas, J. SG1 Nitroxide-Mediated Polymerization of Isoprene: Alkoxyamine Structure/Control Relationship and α,ω–Chain-End Functionalization. *Macromolecules* **2011**, *44* (23), 9230-9238. DOI: https://doi.org/10.1021/ma202078q.
(31) Harrisson, S.; Couvreur, P.; Nicolas, J. Use of Solvent Effects to Improve Control Over Nitroxide-Mediated Polymerization of Isoprene. *Macromol*. *Rapid Commun*. **2012**, *33* (9), 805-810. DOI: https://doi.org/10.1002/marc.201100866.
(32) Germack, D. S.; Wooley, K. L. Isoprene polymerization via reversible addition fragmentation chain transfer polymerization. *J*. *Polym*. *Sci., Part A: Polym*. *Chem*. **2007**, *45* (17), 4100-4108. DOI: https://doi.org/10.1002/pola.22226.
(33) Yu, H.-S.; Kim, J.-S.; Vasu, V.; Simpson, C. P.; Asandei, A. D. Cu-Mediated Butadiene ATRP. *ACS Catal*. **2020**, *10* (12), 6645-6663. DOI: https://doi.org/10.1021/acscatal.0c01207.
(34) Perrier, S.; Takolpuckdee, P.; Mars, C. A. Reversible Addition−Fragmentation Chain Transfer Polymerization: End Group Modification for Functionalized Polymers and Chain Transfer Agent Recovery. *Macromolecules* **2005**, *38* (6), 2033-2036. DOI: https://doi.org/10.1021/ma047611m.
(35) Jitchum, V.; Perrier, S. Living Radical Polymerization of Isoprene via the RAFT Process. *Macromolecules* **2007**, *40* (5), 1408-1412. DOI: https://doi.org/10.1021/ma061889s.
(36) Hillmyer, M. A.; Nguyen, S. T.; Grubbs, R. H. Utility of a Ruthenium Metathesis Catalyst for the Preparation of End-Functionalized Polybutadiene. *Macromolecules* **1997**, *30* (4), 718-721. DOI: https://doi.org/10.1021/ma961316n.
(37) Thomas, R. M.; Grubbs, R. H. Synthesis of Telechelic Polyisoprene via Ring-Opening Metathesis Polymerization in the Presence of Chain Transfer Agent. *Macromolecules* **2010**, *43* (8), 3705-3709. DOI: https://doi.org/10.1021/ma902749q.
(38) Puskas, J. E.; Gautriaud, E.; Deffieux, A.; Kennedy, J. P. Natural rubber biosynthesis—A living carbocationic polymerization? *Prog*. *Polym*. *Sci*. **2006**, *31* (6), 533-548. DOI: https://doi.org/10.1016/j.progpolymsci.2006.05.002.
(39) Richardson, W. S. The microstructure of diene polymers. III. Polyisoprenes and polybutadienes prepared with cationic catalysts. *J*. *Polym*. *Sci*. **1954**, *13* (70), 325-328. DOI: https://doi.org/10.1002/pol.1954.120137002.
(40) Gaylord, N.; Matyska, B.; Mach, K.; Vodehnal, J. Cyclo-and cyclized diene polymers. XII. Cationic polymerization of isoprene. *J*. *Polym*. *Sci*. *A-1 Polym*. *Chem*. **1966**, *4* (10), 2493-2511. DOI: https://doi.org/10.1002/pol.1966.150041014.
(41) Matyska, B.; Mach, K.; Vodehnal, J.; Kössler, I. Cyclo-and cyclized diene polymers. V. Cyclopolymerization of isoprene with a titanium tetrachloride-ethylaluminum dichloride catalyst. *Collect*. *Czech*. *Chem*. *Commun*. **1965**, *30* (8), 2569-2581. DOI: https://doi.org/10.1135/cccc19652569.

(42) Ouardad, S.; Deffieux, A.; Peruch, F. Polyisoprene synthesized via cationic polymerization: State of the art. *Pure Appl. Chem.* **2012**, *84* (10), 2065-2080. DOI: https://doi.org/10.1351/PAC-CON-12-02-05.

(43) Gaylord, N. G.; Kossler, I.; Stolka, M.; Vodehnal, J. Polymerization Of Conjugated Dienes To Ladder Cyclopolymers And The Cyclization Of Stereoregular Diene Polymers. *J. Am. Chem. Soc.* **1963**, *85* (5), 641-642. DOI: https://doi.org/10.1021/ja00888a037.

(44) Kostjuk, S. V.; Ouardad, S.; Peruch, F.; Deffieux, A.; Absalon, C.; Puskas, J. E.; Ganachaud, F. Carbocationic Polymerization of Isoprene Co-initiated by B(C6F5)3: An Alternative Route toward Natural Rubber Polymer Analogues? *Macromolecules* **2011**, *44* (6), 1372-1384. DOI: https://doi.org/10.1021/ma1027966.

(45) Rozentsvet, V. A.; Korovina, N. A.; Stotskaya, O. A.; Kuznetsova, M. G.; Peruch, F.; Kostjuk, S. V. Comprehensive structural characterization of polyisoprene synthesized via cationic mechanism. *J. Polym. Sci. Part A: Polym. Chem.* **2016**, *54* (15), 2430-2442. DOI: https://doi.org/10.1002/pola.28118.

(46) Rozentsvet, V. A.; Stotskaya, O. A.; Ivanova, V. P.; Kuznetsova, M. G.; Tolstoy, P. M.; Kostjuk, S. V. Structural characterization of polybutadiene synthesized via cationic mechanism. *J. Polym. Sci. Part A: Polym. Chem.* **2018**, *56* (4), 387-398. DOI: https://doi.org/10.1002/pola.28905.

(47) Forens, A.; Roos, K.; Dire, C.; Gadenne, B.; Carlotti, S. Accessible microstructures of polybutadiene by anionic polymerization. *Polymer* **2018**, *153*, 103-122. DOI: https://doi.org/10.1016/j.polymer.2018.07.071.

(48) Bywater, S.; Firat, Y.; Black, P. Microstructures of polybutadienes prepared by anionic polymerization in polar solvents. Ion-pair and solvent effects. *J. Polym. Sci. Polym. Chem. Ed.* **1984**, *22* (3), 669-672. DOI: https://doi.org/10.1002/pol.1984.170220316.

(49) Benvenuta-Tapia, J. J.; Tenorio-López, J. A.; Herrera-Nájera, R.; Ríos-Guerrero, L. Synthesis and distribution of structural units—Thermal property relationship of random and block butadiene-styrene copolymers with high trans 1,4 units content produced using an initiator composed of alkyl aluminum, n-butyl lithium, and barium alkoxide. *J. Appl. Polym. Sci.* **2010**, *116* (5), 3103-3110. DOI: https://doi.org/10.1002/app.31853.

(50) Oehme, A.; Gebauer, U.; Gehrke, K.; Beyer, P.; Hartmann, B.; Lechner, M. D. The influence of the catalyst preparation on the homo- and copolymerization of butadiene and isoprene. *Macromol. Chem. Phys.* **1994**, *195* (12), 3773-3781. DOI: https://doi.org/10.1002/macp.1994.021951203.

(51) Friebe, L.; Nuyken, O.; Obrecht, W. Neodymium-Based Ziegler/Natta Catalysts and their Application in Diene Polymerization. In *Neodymium Based Ziegler Catalysts – Fundamental Chemistry*, Nuyken, O. Ed.; Springer Berlin Heidelberg, **2006**; pp 1-154.

(52) Arndt, S.; Beckerle, K.; Zeimentz, P. M.; Spaniol, T. P.; Okuda, J. Cationic Yttrium Methyl Complexes as Functional Models for Polymerization Catalysts of 1,3-Dienes. *Angew. Chem. Int. Ed.* **2005**, *44* (45), 7473-7477. DOI: https://doi.org/10.1002/anie.200502915.

(53) Evans, W. J.; Giarikos, D. G. Chloride Effects in Lanthanide Carboxylate Based Isoprene Polymerization. *Macromolecules* **2004**, *37* (13), 5130-5132. DOI: https://doi.org/10.1021/ma034925l.

(54) Zhang, L.; Suzuki, T.; Luo, Y.; Nishiura, M.; Hou, Z. Cationic alkyl rare-earth metal complexes bearing an ancillary bis(phosphinophenyl)amido ligand: a catalytic system for living cis-1,4-polymerization and copolymerization of isoprene and butadiene. *Angew. Chem. Int. Ed.* **2007**, *46* (11), 1909-1913. DOI: https://doi.org/10.1002/anie.200604348.

(55) Ajellal, N.; Furlan, L.; Thomas, C. M.; Casagrande Jr, O. L.; Carpentier, J.-F. Mixed Aluminum-Magnesium-Rare Earth Allyl Catalysts for Controlled Isoprene Polymerization: Modulation of Stereocontrol. *Macromol. Rapid Commun.* **2006**, *27* (5), 338-343. DOI: https://doi.org/10.1002/marc.200500775.

(56) Kaita, S.; Yamanaka, M.; Horiuchi, A. C.; Wakatsuki, Y. Butadiene Polymerization Catalyzed by Lanthanide Metallocene−Alkylaluminum Complexes with Cocatalysts: Metal-Dependent Control of 1,4-Cis/Trans Stereoselectivity and Molecular Weight. *Macromolecules* **2006**, *39* (4), 1359-1363. DOI: https://doi.org/10.1021/ma051867q.

(57) Bonnet, F.; Visseaux, M.; Pereira, A.; Barbier-Baudry, D. Highly trans-Stereospecific Isoprene Polymerization by Neodymium Borohydrido Catalysts. *Macromolecules* **2005**, *38* (8), 3162-3169. DOI: https://doi.org/10.1021/ma047615r.

(58) Banar, M.; Akyıldız, V.; Özkan, A.; Çokaygil, Z.; Onay, Ö. Characterization of pyrolytic oil obtained from pyrolysis of TDF (Tire Derived Fuel). *Energ*. *Convers*. *Manag*. **2012**, *62*, 22-30. DOI: https://doi.org/10.1016/j.enconman.2012.03.019.
(59) Myhre, M.; MacKillop, D. A. Rubber recycling. *Rubber Chem*. *Technol*. **2002**, *75* (3), 429-474. DOI: https://doi.org/10.5254/1.3547678.
(60) Adhikari, J.; Das, A.; Sinha, T.; Saha, P.; Kim, J. K. Grinding of Waste Rubber. In *Rubber Recycling: Challenges and Developments*, Kim, J. K., Saha, P., Thomas, S., Haponiuk, J. T., Aswathi, M. K. Eds.; The Royal Society of Chemistry, **2018**. ISBN: 978-1-78801-084-9
(61) Lo Presti, D. Recycled Tyre Rubber Modified Bitumens for road asphalt mixtures: A literature review. *Constr*. *Build*. *Mater*. **2013**, *49*, 863-881. DOI: https://doi.org/10.1016/j.conbuildmat.2013.09.007.
(62) Adhikari, B.; De, D.; Maiti, S. Reclamation and recycling of waste rubber. *Prog*. *Polym*. *Sci*. **2000**, *25* (7), 909-948. DOI: https://doi.org/10.1016/S0079-6700(00)00020-4.
(63) Isayev, A. I. Recycling of natural and synthetic isoprene rubbers. In *Chemistry, Manufacture and Applications of Natural Rubber*, Woodhead Publishing Limited, **2014**; pp 395-435. ISBN: 9780857096838.
(64) Fazli, A.; Rodrigue, D. Waste Rubber Recycling: A Review on the Evolution and Properties of Thermoplastic Elastomers. *Materials* **2020**, *13* (3). DOI: https://doi.org/10.3390/ma13030782.
(65) Piton, M.; Rivaton, A. Photooxidation of polybutadiene at long wavelengths (λ > 300 nm). *Polym*. *Degrad*. *Stab.* **1996**, *53* (3), 343-359. DOI: https://doi.org/10.1016/0141-3910(96)00093-6.
(66) Adam, C.; Lacoste, J.; Lemaire, J. Photo-oxidation of polyisoprene. *Polym*. *Degrad*. *Stab*. **1991**, *32* (1), 51-69. DOI: https://doi.org/10.1016/0141-3910(91)90062-V.
(67) dos Santos, K. A. M.; Suarez, P. A. Z.; Rubim, J. C. Photo-degradation of synthetic and natural polyisoprenes at specific UV radiations. *Polym*. *Degrad*. *Stab*. **2005**, *90* (1), 34-43. DOI: https://doi.org/10.1016/j.polymdegradstab.2005.01.038.
(68) Singh, B.; Sharma, N. Mechanistic implications of plastic degradation. *Polym*. *Degrad*. *Stab*. **2008**, *93* (3), 561-584. DOI: https://doi.org/10.1016/j.polymdegradstab.2007.11.008.
(69) Nunes, A. T.; Santos, R. E. d.; Pereira, J. S.; Barbosa, R.; Ambrósio, J. D. Characterization of waste tire rubber devulcanized in twin-screw extruder with thermoplastics. *Prog*. *Rubber Plast*. *Recycl*. *Technol*. **2018**, *34* (3), 143-157. DOI: https://doi.org/10.1177/1477760618798413.
(70) de Sousa, F. D. B.; Scuracchio, C. H.; Hu, G.-H.; Hoppe, S. Devulcanization of waste tire rubber by microwaves. *Polym*. *Degrad*. *Stab*. **2017**, *138*, 169-181. DOI: https://doi.org/10.1016/j.polymdegradstab.2017.03.008.
(71) Antoniou, N.; Zabaniotou, A. Features of an efficient and environmentally attractive used tyres pyrolysis with energy and material recovery. *Renew*. *Sustain*. *Energy Rev*. **2013**, *20*, 539-558. DOI: https://doi.org/10.1016/j.rser.2012.12.005.
(72) Pan, D. L.; Jiang, W. T.; Guo, R. T.; Huang, Y.; Pan, W. G. Thermogravimetric and Kinetic Analysis of Co-Combustion of Waste Tires and Coal Blends. *ACS Omega* **2021**, *6* (8), 5479-5484. DOI: https://doi.org/10.1021/acsomega.0c05768.
(73) Al-Salem, S. M.; Lettieri, P.; Baeyens, J. Kinetics and product distribution of end of life tyres (ELTs) pyrolysis: a novel approach in polyisoprene and SBR thermal cracking. *J*. *Hazard*. *Mater*. **2009**, *172* (2-3), 1690-1694. DOI: https://doi.org/10.1016/j.jhazmat.2009.07.127.
(74) Brosse, J. C.; Campistron, I.; Derouet, D.; El Hamdaoui, A.; Houdayer, S.; Reyx, D.; Ritoit-Gillier, S. Chemical modifications of polydiene elastomers: A survey and some recent results. *J*. *Appl*. *Polym*. *Sci*. **2000**, *78* (8), 1461-1477. DOI: https://doi.org/10.1002/1097-4628(20001121)78:8<1461::AID-APP20>3.0.CO;2-V.
(75) Allison, A. R.; Stanley, I. J. Ozone Deterioration of Elastomeric Materials. *Anal*. *Chem*. **1952**, *24* (4), 630-635. DOI: https://doi.org/10.1021/ac60064a006.
(76) Salomon, G.; Van Der Schee, A. C. Infrared analysis of isomerized, vulcanized and oxidized natural rubber. *J*. *Polym*. *Sci*. **1954**, *14* (74), 181-192. DOI: https://doi.org/10.1002/pol.1954.120147405.
(77) Criegee, R. Mechanism of Ozonolysis. *Angew*. *Chem*. *Int*. *Ed*. **1975**, *14* (11), 745-752. DOI: https://doi.org/10.1002/anie.197507451.
(78) Nor, H. M.; Ebdon, J. R. Ozonolysis of natural rubber in chloroform solutionPart 1. A study by GPC and FTIR spectroscopy. *Polymer* **2000**, *41* (7), 2359-2365. DOI: https://doi.org/10.1016/S0032-3861(99)00417-6.

(79) Odinokov, V. N.; Ignatyuk, V. K.; Tolstikov, G. A.; Monakov, Y. B.; Berg, A. A.; Shakirova, A. M.; Rafikov, S. R.; Berlin, A. A. Synthesis of cis-1, 4-oligodien-α, ω-glycols by ozonolis of cis-1, 4-polydienes. *Bull*. *Acad*. *Sci*. *USSR, Div*. *Chem*. *Sci*. **1976**, *25* (7), 1475-1481. DOI: https://doi.org/10.1007/BF00920822.

(80) Phetphaisit, C. W.; Phinyocheep, P. Kinetics and parameters affecting degradation of purified natural rubber. *J*. *Appl*. *Polym*. *Sci*. **2003**, *90* (13), 3546-3555. DOI: https://doi.org/10.1002/app.12982.

(81) Ibrahim, S.; Daik, R.; Abdullah, I. Functionalization of Liquid Natural Rubber via Oxidative Degradation of Natural Rubber. *Polymers* **2014**, *6* (12), 2928-2941. DOI: https://doi.org/10.3390/polym6122928.

(82) Thuong, N. T.; Manh, N. D.; Tue, N. N. Characterization of liquid deproteinized natural rubber prepared via oxidative degradation. *Vietnam J*. *Chem*. **2020**, *58* (6), 826-831. DOI: https://doi.org/10.1002/vjch.202000093.

(83) El Hmadaoui, D. R. A.; Campistron, I.; Tétouani, S. F. Effet d'extrémité de chaîne dans l'oxydation du caoutchouc naturel accélérée par la phénylhydrazine. *Eur*. *Polym*. *J*. **1999**, *35*, 2165-2183. DOI: https://doi.org/10.1016/S0014-3057(99)00014-2.

(84) Kawabata, N.; Okuyama, B. I.; Yamashita, S. Reclamation of vulcanized rubber by chemical degradation. XV. Degradation of vulcanized synthetic isoprene by the phenylhydrazine–iron (II) chloride system. *J*. *Appl*. *Polym*. *Sci*. **1981**, *26* (4), 1417-1419. DOI: https://doi.org/10.1002/app.1981.070260431.

(85) Nor, H. M.; Ebdon, J. R. Telechelic liquid natural rubber: A review. *Prog*. *Polym*. *Sci*. **1998**, *23* (2), 143-177. DOI: https://doi.org/10.1016/S0079-6700(97)00028-2.

(86) Baptista, E. I. G.; Campese, M.; Zalloum, N. L.; Rubira, A. F.; Muniz, E. C. Degradation of polyisoprene induced by chloranil. *Polym*. *Degrad*. *Stab*. **1998**, *60*, 309-315. DOI: https://doi.org/10.1016/S0141-3910(97)00084-0.

(87) Mauler, R. S.; Martins, F. G.; Samios, D. Investigation on the styrene-butadiene rubber cleavage with periodic acid under the influence of ultrasonic radiation. *Polym*. *Bull*. **1995**, *35* (1), 151-156. DOI: https://doi.org/10.1007/BF00312907.

(88) Phinyocheep, P.; Phetphaisit, C. W.; Derouet, D.; Campistron, I.; Brosse, J. C. Chemical degradation of epoxidized natural rubber using periodic acid: Preparation of epoxidized liquid natural rubber. *J*. *Appl*. *Polym*. *Sci*. **2005**, *95* (1), 6-15. DOI: https://doi.org/10.1002/app.20812.

(89) Gillier-Ritoit, S.; Reyx, D. l.; Campistron, I. n.; Laguerre, A.; Pal Singh, R. Telecheliccis-1,4-oligoisoprenes through the selective oxidolysis of epoxidized monomer units and polyisoprenic monomer units incis-1,4-polyisoprenes. *J*. *Appl*. *Polym*. *Sci*. **2003**, *87* (1), 42-46. DOI: https://doi.org/10.1002/app.11661.

(90) Kébir, N.; Morandi, G.; Campistron, I.; Laguerre, A.; Pilard, J.-F. Synthesis of well defined amino telechelic cis-1,4-oligoisoprenes from carbonyl telechelic oligomers; first studies of their potentialities as polyurethane or polyurea materials precursors. *Polymer* **2005**, *46* (18), 6844-6854. DOI: https://doi.org/10.1016/j.polymer.2005.05.122.

(91) Sadaka, F.; Campistron, I.; Laguerre, A.; Pilard, J.-F. Controlled chemical degradation of natural rubber using periodic acid: Application for recycling waste tyre rubber. *Polym*. *Degrad*. *Stab*. **2012**, *97* (5), 816-828. DOI: https://doi.org/10.1016/j.polymdegradstab.2012.01.019.

(92) Zhou, Q.; Jie, S.; Li, B.-G. Preparation of Hydroxyl-Terminated Polybutadiene with High Cis-1,4 Content. *Ind*. *Eng*. *Chem*. *Res*. **2014**, *53* (46), 17884-17893. DOI: https://doi.org/10.1021/ie503652g.

(93) Zhou, Q.; Jie, S.; Li, B.-G. Facile synthesis of novel HTPBs and EHTPBs with high cis-1,4 content and extremely low glass transition temperature. *Polymer* **2015**, *67*, 208-215. DOI: https://doi.org/10.1016/j.polymer.2015.04.078.

(94) Xu, L.; Jie, S.; Bu, Z.; Li, B.-G. Preparation of primary amine-terminated polybutadiene from cis-polybutadiene. *Eur*. *Polym*. *J*. **2021**, *152*. DOI: https://doi.org/10.1016/j.eurpolymj.2021.110484.

(95) Berto, P.; Grelier, S.; Peruch, F. Controlled degradation of polyisoprene and polybutadiene: A comparative study of two methods. *Polym*. *Degrad*. *Stab*. **2018**, *154*, 295-303. DOI: https://doi.org/10.1016/j.polymdegradstab.2018.06.019.

(96) Alimuniar, A.; Yarmo, M. A.; Rahman, M. Z. A.; Kohjiya, S.; Ikeda, Y.; Yamashita, S. Metathesis degradation of natural rubber. *Polym*. *Bull*. **1990**, *23* (1), 119-126. DOI: https://doi.org/10.1007/BF00983973.

(97) Thorn-Csány, E.; Hammer, J.; Zilles, J. U. Metathetic ring-chain equilibrium; synthesis of 1,5,9-trimethyl-(1E,5E,9E)-cyclododecatriene from l,4-polyisoprene. *Macrmol*. *Rapid Commun*. **1994**, *15*, 797-800. DOI: https://doi.org/10.1002/marc.1994.030151008.
(98) Bidange, J.; Fischmeister, C.; Bruneau, C. Ethenolysis: A Green Catalytic Tool to Cleave Carbon-Carbon Double Bonds. *Chemistry* **2016**, *22* (35), 12226-12244. DOI: https://doi.org/10.1002/chem.201601052.
(99) Thorn-Csányi, E. Quantitative Metathetic Degradation of Rubbers and Sulfur Crosslinked Rubbers—Including Tires. *Rubber Chem*. *Technol*. **1994**, *67* (5), 786-796. DOI: https://doi.org/10.5254/1.3538710.
(100) Gutierras, S.; Vargas, S. M.; Tlenkopatchev, M. A. Computational study of metathesis degradation of rubber. distributions of products for the ethenolysis of 1,4-polyisoprene. *Polym*. *Degrad*. *Stab*. **2004**, *83* (1), 149-156. DOI: https://doi.org/10.1016/S0141-3910(03)00247-7.
(101) Spekreijse, J.; Sanders, J. P.; Bitter, J. H.; Scott, E. L. The Future of Ethenolysis in Biobased Chemistry. *ChemSusChem* **2017**, *10* (3), 470-482. DOI: https://doi.org/10.1002/cssc.201601256.
(102) Craig, S. W.; Manzer, J. A.; Coughlin, E. B. Highly Efficient Acyclic Diene Metathesis Depolymerization Using a Ruthenium Catalyst Containing a N-Heterocyclic Carbene Ligand. *Macromolecules* **2001**, *34* (23), 7929-7931. DOI: https://doi.org/10.1021/ma011188p.
(103) Sadaka, F.; Campistron, I.; Laguerre, A.; Pilard, J.-F. Telechelic oligomers obtained by metathetic degradation of both polyisoprene and styrene–butadiene rubbers. Applications for recycling waste tyre rubber. *Polym. Degrad*. *Stab.* **2013**, *98* (3), 736-742. DOI: https://doi.org/10.1016/j.polymdegradstab.2012.12.018.
(104) Gutiérrez, S.; Tlenkopatchev, M. A. Metathesis of renewable products: degradation of natural rubber via cross-metathesis with β-pinene using Ru-alkylidene catalysts. *Polym*. *Bull*. **2010**, *66* (8), 1029-1038. DOI: https://doi.org/10.1007/s00289-010-0330-x.
(105) Ogba, O. M.; Warner, N. C.; O'Leary, D. J.; Grubbs, R. H. Recent advances in ruthenium-based olefin metathesis. *Chem*. *Soc*. *Rev*. **2018**, *47* (12), 4510-4544. DOI: https://doi.org/10.1039/C8CS00027A.
(106) Wolf, S.; Plenio, H. On the ethenolysis of natural rubber and squalene. *Green Chem*. **2011**, *13* (8). DOI: https://doi.org/10.1039/C1GC15265C.
(107) Wolf, S.; Plenio, H. On the ethenolysis of end-of-life tire granulates. *Green Chem*. **2013**, *15* (2), 315-319. DOI: https://doi.org/10.1039/C2GC36417D.
(108) Mouawia, A.; Nourry, A.; Gaumont, A.-C.; Pilard, J.-F.; Dez, I. Controlled Metathetic Depolymerization of Natural Rubber in Ionic Liquids: From Waste Tires to Telechelic Polyisoprene Oligomers. *ACS Sustain*. *Chem*. *Eng*. **2016**, *5* (1), 696-700. DOI: https://doi.org/10.1021/acssuschemeng.6b01777.
(109) Ouardad, S.; Peruch, F. Metathetic degradation of trans-1,4-polyisoprene with ruthenium catalysts. *Polym*. *Degrad*. *Stab*. **2014**, *99*, 249-253. DOI: https://doi.org/10.1016/j.polymdegradstab.2013.10.022.
(110) Yikmis, M.; Steinbuchel, A. Historical and recent achievements in the field of microbial degradation of natural and synthetic rubber. *Appl*. *Environ*. *Microbiol*. **2012**, *78* (13), 4543-4551. DOI: https://doi.org/10.1128/AEM.00001-12.
(111) Rose, K.; Steinbuchel, A. Biodegradation of natural rubber and related compounds: recent insights into a hardly understood catabolic capability of microorganisms. *Appl*. *Environ*. *Microbiol*. **2005**, *71* (6), 2803-2812. DOI: https://doi.org/10.1128/AEM.71.6.2803-2812.2005.
(112) Jendrossek, D.; Birke, J. Rubber oxygenases. *Appl*. *Microbiol*. *Biotechnol*. **2019**, *103* (1), 125-142. DOI: https://doi.org/10.1007/s00253-018-9453-z.
(113) Linos, A.; Berekaa, M. M.; Steinbüchel, A.; Kim, K. K.; Sproer, C.; Kroppenstedt, R. M. Gordonia westfalica sp. nov., a novel rubber-degrading actinomycete. *Int. J. Syst. Evol*. *Microbiol*. **2002**, *52* (Pt 4), 1133-1139. DOI: https://doi.org/10.1099/00207713-52-4-1133.
(114) Ibrahim, E. M.; Arenskotter, M.; Luftmann, H.; Steinbuchel, A. Identification of poly(cis-1,4-Isoprene) degradation intermediates during growth of moderately thermophilic actinomycetes on rubber and cloning of a functional lcp homologue from Nocardia farcinica strain E1. *Appl*. *Environ*. *Microbiol*. **2006**, *72* (5), 3375-3382. DOI: https://doi.org/10.1128/AEM.72.5.3375-3382.2006.
(115) Linos, A.; Berekaa, M. M.; Reichelt, R.; Keller, U.; Schmitt, J.; Flemming, H. C.; Kroppenstedt, R. M.; Steinbüchel, A. Biodegradation of cis-1,4-polyisoprene rubbers by distinct actinomycetes:

microbial strategies and detailed surface analysis. *Appl*. *Environ*. *Microbiol*. **2000**, *66* (4), 1639-1645. DOI: https://doi.org/10.1128/AEM.66.4.1639-1645.2000.

(116) Bosco, F.; Antonioli, D.; Casale, A.; Gianotti, V.; Mollea, C.; Laus, M.; Malucelli, G. Biodegradation of unvulcanized natural rubber by microorganisms isolated from soil and rubber surface: A preliminary study. *Bioremediat*. *J*. **2018**, *22* (1-2), 43-52. DOI: https://doi.org/10.1080/10889868.2018.1476454.

(117) Tsuchii, A.; Takeda, K. Rubber-degrading enzyme from a bacterial culture. *Appl*. *Environ*. *Microbiol*. **1990**, *56* (1), 269-274. DOI: https://doi.org/10.1128/aem.56.1.269-274.1990.

(118) Bode, H. B.; Zeeck, A.; Plückhahn, K.; Jendrossek, D. Physiological and Chemical Investigations into Microbial Degradation of Synthetic Poly(cis-1,4-isoprene). *Appl*. *Environ*. *Microbiol*. **2000**, *66* (9), 3680-3685. DOI: https://doi.org/10.1128/AEM.66.9.3680-3685.2000.

(119) Rose, K.; Tenberge, K. B.; Steinbüchel, A. Identification and Characterization of Genes from Streptomyces sp. Strain K30 Responsible for Clear Zone Formation on Natural Rubber Latex and Poly(cis-1,4-isoprene) Rubber Degradation. *Biomacromolecules* **2005**, *6* (1), 180-188. DOI: https://doi.org/10.1021/bm0496110.

(120) Chengalroyen, M. D.; Dabbs, E. R. The Biodegradation of Latex Rubber: A Minireview. *J*. *Polym*. *Environ*. **2013**, *21* (3), 874-880. DOI: https://doi.org/10.1007/s10924-013-0593-z.

(121) Ali Shah, A.; Hasan, F.; Shah, Z.; Kanwal, N.; Zeb, S. Biodegradation of natural and synthetic rubbers: A review. *Int*. *Biodeterior*. *Biodegrad*. **2013**, *83*, 145-157. DOI: https://doi.org/10.1016/j.ibiod.2013.05.004.

(122) Tsuchii, A.; Suzuki, T.; Seiichi, F. Bacterial Degradation of 1,4-Type Poly butadiene. *Agric*. *Biol*. *Chem*. **2014**, *48* (3), 621-625. DOI: https://doi.org/10.1080/00021369.1984.10866194.

(123) Soares, F. A.; Steinbüchel, A. Natural rubber degradation products: Fine chemicals and reuse of rubber waste. *Eur*. *Polym*. *J*. **2022**, *165*. DOI: https://doi.org/10.1016/j.eurpolymj.2022.111001.

(124) Jendrossek, D.; Reinhardt, S. Sequence analysis of a gene product synthesized byXanthomonassp. during growth on natural rubber latex. *FEMS Microbiol*. *Lett*. **2003**, *224* (1), 61-65. DOI: https://doi.org/10.1016/S0378-1097(03)00424-5.

(125) Seidel, J.; Schmitt, G.; Hoffmann, M.; Jendrossek, D.; Einsle, O. Structure of the processive rubber oxygenase RoxA from Xanthomonas sp. *Proc*. *Natl*. *Acad*. *Sci*. *USA* **2013**, *110* (34), 13833-13838. DOI: https://doi.org/10.1073/pnas.1305560110.

(126) Braaz, R.; Armbruster, W.; Jendrossek, D. Heme-dependent rubber oxygenase RoxA of Xanthomonas sp. cleaves the carbon backbone of poly(cis-1,4-Isoprene) by a dioxygenase mechanism. *Appl*. *Environ*. *Microbiol*. **2005**, *71* (5), 2473-2478. DOI: https://doi.org/10.1128/AEM.71.5.2473-2478.2005.

(127) Schmitt, G.; Seiffert, G.; Kroneck, P. M. H.; Braaz, R.; Jendrossek, D. Spectroscopic properties of rubber oxygenase RoxA from Xanthomonas sp., a new type of dihaem dioxygenase. *Microbiology (Reading, Engl.)* **2010**, *156* (Pt 8), 2537-2548. DOI: https://doi.org/10.1099/mic.0.038992-0.

(128) Sharma, V.; Siedenburg, G.; Birke, J.; Mobeen, F.; Jendrossek, D.; Prakash, T. Metabolic and taxonomic insights into the Gram-negative natural rubber degrading bacterium Steroidobacter cummioxidans sp. nov., strain 35Y. *PLoS One* **2018**, *13* (5), e0197448. DOI: https://doi.org/10.1371/journal.pone.0197448.

(129) Birke, J.; Rother, W.; Jendrossek, D. RoxB Is a Novel Type of Rubber Oxygenase That Combines Properties of Rubber Oxygenase RoxA and Latex Clearing Protein (Lcp). *Appl*. *Environ*. *Microbiol*. **2017**, *83* (14). DOI: https://doi.org/10.1128/AEM.00721-17.

(130) Birke, J.; Rother, W.; Jendrossek, D. Rhizobacter gummiphilus NS21 has two rubber oxygenases (RoxA and RoxB) acting synergistically in rubber utilisation. *Appl*. *Microbiol*. *Biotechnol*. **2018**, *102* (23), 10245-10257. DOI: https://doi.org/10.1007/s00253-018-9341-6.

(131) Hiessl, S.; Schuldes, J.; Thurmer, A.; Halbsguth, T.; Broker, D.; Angelov, A.; Liebl, W.; Daniel, R.; Steinbuchel, A. Involvement of two latex-clearing proteins during rubber degradation and insights into the subsequent degradation pathway revealed by the genome sequence of Gordonia polyisoprenivorans strain VH2. *Appl*. *Environ*. *Microbiol*. **2012**, *78* (8), 2874-2887. DOI: https://doi.org/10.1128/AEM.07969-11.

(132) Watcharakul, S.; Rother, W.; Birke, J.; Umsakul, K.; Hodgson, B.; Jendrossek, D. Biochemical and spectroscopic characterization of purified Latex Clearing Protein (Lcp) from newly isolated rubber degrading Rhodococcus rhodochrous strain RPK1 reveals novel properties of Lcp. *BMC Microbiol*. **2016**, *16*, 92. DOI: https://doi.org/10.1186/s12866-016-0703-x.

(133) Vivod, R.; Andler, R.; Oetermann, S.; Altenhoff, A. L.; Seipel, N.; Holtkamp, M.; Hogeback, J.; Karst, U.; Steinbuchel, A. Characterization of the latex clearing protein of the poly(cis-1,4-isoprene) and poly(trans-1,4-isoprene) degrading bacterium Nocardia nova SH22a. *J*. *Gen*. *Appl*. *Microbiol*. **2020**, *65* (6), 293-300. DOI: https://doi.org/10.2323/jgam.2019.01.003.
(134) Birke, J.; Rother, W.; Jendrossek, D. Latex Clearing Protein (Lcp) of Streptomyces sp. Strain K30 Is a b-Type Cytochrome and Differs from Rubber Oxygenase A (RoxA) in Its Biophysical Properties. *Appl*. *Environ*. *Microbiol*. **2015**, *81* (11), 3793-3799. DOI: https://doi.org/10.1128/AEM.00275-15.
(135) Luo, Q.; Hiessl, S.; Poehlein, A.; Steinbuchel, A. Microbial gutta-percha degradation shares common steps with rubber degradation by Nocardia nova SH22a. *Appl*. *Environ*. *Microbiol*. **2013**, *79* (4), 1140-1149. DOI: https://doi.org/10.1128/AEM.03016-12.
(136) Luo, Q.; Hiessl, S.; Poehlein, A.; Daniel, R.; Steinbuchel, A. Insights into the microbial degradation of rubber and gutta-percha by analysis of the complete genome of Nocardia nova SH22a. *Appl*. *Environ*. *Microbiol*. **2014**, *80* (13), 3895-3907. DOI: https://doi.org/10.1128/AEM.00473-14.
(137) Hiessl, S.; Bose, D.; Oetermann, S.; Eggers, J.; Pietruszka, J.; Steinbuchel, A. Latex clearing protein-an oxygenase cleaving poly(cis-1,4-isoprene) rubber at the cis double bonds. *Appl*. *Environ*. *Microbiol.* **2014**, *80* (17), 5231-5240. DOI: https://doi.org/10.1128/AEM.01502-14.
(138) Ilcu, L.; Rother, W.; Birke, J.; Brausemann, A.; Einsle, O.; Jendrossek, D. Structural and Functional Analysis of Latex Clearing Protein (Lcp) Provides Insight into the Enzymatic Cleavage of Rubber. *Sci*. *Rep*. **2017**, *7* (1), 6179. DOI: https://doi.org/10.1038/s41598-017-05268-2.
(139) Rother, W.; Austen, S.; Birke, J.; Jendrossek, D. Cleavage of Rubber by the Latex Clearing Protein (Lcp) of Streptomyces sp. Strain K30: Molecular Insights. *Appl*. *Environ*. *Microbiol*. **2016**, *82* (22), 6593-6602. DOI: https://doi.org/10.1128/AEM.02176-16.
(140) Zhang, S.; Liu, Y. Mechanical Insights into the Enzymatic Cleavage of Double C-C Bond in Poly(cis-1,4-isoprene) by the Latex Clearing Protein. *Inorg*. *Chem*. **2020**, *59* (14), 9627-9637. DOI: https://doi.org/10.1021/acs.inorgchem.0c00726.
(141) Hassan, A. A.; Hanževački, M.; Pordea, A. Computational investigation of cis-1,4-polyisoprene binding to the latex-clearing protein LcpK30. *bioRxiv* **2023**, 2023.2006.2026.546638. DOI: https://doi.org/10.1101/2023.06.26.546638.
(142) Zhang, H.; Kong, D.; Wang, L.; Xia, W.; Yao, C.; Wu, J. Degradation of UV-pretreated polyolefins by latex clearing protein from Streptomyces sp. Strain K30. *Sci*. *Total*. *Environ*. **2022**, *806* (Pt 4), 150779. DOI: https://doi.org/10.1016/j.scitotenv.2021.150779.
(143) Enoki, M.; Doi, Y.; Iwata, T. Oxidative Degradation of cis- and trans-1,4-Polyisoprenes and Vulcanized Natural Rubber with Enzyme-Mediator Systems. *Biomacromolecules* **2003**, *4* (2), 314-320. DOI: https://doi.org/10.1021/bm025678g.
(144) Sato, S.; Honda, Y.; Kuwahara, M.; Watanabe, T. Degradation of Vulcanized and Nonvulcanized Polyisoprene Rubbers by Lipid Peroxidation Catalyzed by Oxidative Enzymes and Transition Metals. *Biomacromolecules* **2003**, *4* (2), 321-329. DOI: https://doi.org/10.1021/bm025683k.
(145) Andler, R.; D'Afonseca, V.; Pino, J.; Valdés, C.; Salazar-Viedma, M. Assessing the Biodegradation of Vulcanised Rubber Particles by Fungi Using Genetic, Molecular and Surface Analysis. *Front. Bioeng*. *Biotechnol*. **2021**, *9*. DOI: https://doi.org/10.3389/fbioe.2021.761510.
(146) Zhou, W.; Apkarian, R.; Wang, Z. L.; Joy, D. Fundamentals of Scanning Electron Microscopy (SEM). In *Scanning Microscopy for Nanotechnology: Techniques and Applications*, Zhou, W., Wang, Z. L. Eds.; Springer New York, 2007; pp 1-40. ISBN: 978-0-387-39620-0.
(147) Nawong, C.; Umsakul, K.; Sermwittayawong, N. Rubber gloves biodegradation by a consortium, mixed culture and pure culture isolated from soil samples. *Braz*. *J*. *Microbiol*. **2018**, *49* (3), 481-488. DOI: https://doi.org/10.1016/j.bjm.2017.07.006.
(148) Nanthini, J.; Sudesh, K. Biodegradation of Natural Rubber and Natural Rubber Products by Streptomyces sp. Strain CFMR 7. *J*. *Polym*. *Environ*. **2016**, *25* (3), 606-616. DOI: https://doi.org/10.1007/s10924-016-0840-1.
(149) Tripathy, A. R.; Morin, J. E.; Williams, D. E.; Eyles, S. J.; Farris, R. J. A Novel Approach to Improving the Mechanical Properties in Recycled Vulcanized Natural Rubber and Its Mechanism. *Macromolecules* **2002**, *35* (12), 4616-4627. DOI: https://doi.org/10.1021/ma012110b.
(150) Roy, R. V.; Das, M.; Banerjee, R.; Bhowmick, A. K. Comparative studies on crosslinked and uncrosslinked natural rubber biodegradation by Pseudomonas sp. *Bioresour*. *Technol*. **2006**, *97* (18), 2485-2488. DOI: https://doi.org/10.1016/j.biortech.2005.09.024.

(151) Tsuchii, A.; Tokiwa, Y. Microbial Degradation of the Natural Rubber in Tire Tread Compound by a Strain of Nocardia. *J. Polym. Environ.* **2006**, *14* (4), 403-409. DOI: https://doi.org/10.1007/s10924-006-0026-3.
(152) Birke, J.; Jendrossek, D. Rubber oxygenase and latex clearing protein cleave rubber to different products and use different cleavage mechanisms. *Appl. Environ. Microbiol.* **2014**, *80* (16), 5012-5020. DOI: https://doi.org/10.1128/AEM.01271-14.
(153) Dasgupta, P. K.; DeCesare, K.; Ullrey, J. C. Determination of atmospheric sulfur dioxide without tetrachloromercurate(II) and the mechanism of the Schiff reaction. *Anal. Chem.* **1980**, *52* (12), 1912-1922. DOI: https://doi.org/10.1021/ac50062a031.
(154) Dapson, R. W. Schiff and pseudo-Schiff reagents: the reactions and reagents of Hugo Schiff, including a classification of various kinds of histochemical reagents used to detect aldehydes. *Biotech. Histochem.* **2016**, *91* (8), 522-531. DOI: https://doi.org/10.1080/10520295.2016.1249518.
(155) Tsuchii, A.; Suzuki, T.; Takeda, K. Microbial degradation of natural rubber vulcanizates. *Appl. Environ. Microbiol.* **1985**, *50* (4), 965-970. DOI: https://doi.org/10.1128/aem.50.4.965-970.1985.
(156) Allen, C. F. H. The Identification of Cabonyl Compounds by Use of 2,4-Dinitrophenylhydrazine. *J. Am. Chem. Soc.* **1930**, *52* (7), 2955-2959. DOI: https://doi.org/10.1021/ja01370a058.
(157) Brady, O. L. CIII.—The use of 2 : 4-dinitrophenylhydrazine as a reagent for carbonyl compounds. *J. Chem. Soc.* **1931**, (0), 756-759. DOI: http://dx.doi.org/10.1039/JR9310000756.
(158) Yusa, S.-i. Chapter 6 - Polymer characterization. In *Polymer Science and Nanotechnology*, Narain, R. Ed.; Elsevier, **2020**; pp 105-124. ISBN: 978-0-12-816806-6.
(159) Dragostin, O.; Profire, L. 5 - Molecular weight of polymers used in biomedical applications. In *Characterization of Polymeric Biomaterials*, Tanzi, M. C., Farè, S. Eds.; Woodhead Publishing, **2017**; pp 101-121. ISBN: 9780081007433.
(160) Andler, R.; Valdes, C.; Diaz-Barrera, A.; Steinbuchel, A. Biotransformation of poly(cis-1,4-isoprene) in a multiphase enzymatic reactor for continuous extraction of oligo-isoprenoid molecules. *N. Biotechnol.* **2020**, *58*, 10-16. DOI: https://doi.org/10.1016/j.nbt.2020.05.001.
(161) Rother, W.; Birke, J.; Grond, S.; Beltran, J. M.; Jendrossek, D. Production of functionalized oligo-isoprenoids by enzymatic cleavage of rubber. *Microb. Biotechnol.* **2017**, *10* (6), 1426-1433. DOI: https://doi.org/10.1111/1751-7915.12748.
(162) Andler, R.; Altenhoff, A. L.; Masing, F.; Steinbuchel, A. In vitro studies on the degradation of poly(cis-1,4-isoprene). *Biotechnol. Prog.* **2018**, *34* (4), 890-899. DOI: https://doi.org/10.1002/btpr.2631.
(163) Andler, R.; Hiessl, S.; Yucel, O.; Tesch, M.; Steinbuchel, A. Cleavage of poly(cis-1,4-isoprene) rubber as solid substrate by cultures of Gordonia polyisoprenivorans. *N. Biotechnol.* **2018**, *44*, 6-12. DOI: https://doi.org/10.1016/j.nbt.2018.03.002.
(164) Leal-Calderon, F.; Bibette, J.; Schmitt, V. Introduction. In *Emulsion Science: Basic Principles*, Leal-Calderon, F., Bibette, J., Schmitt, V. Eds.; Springer New York, **2007**; pp 1-4. ISBN: 978-0-387-39683-5.
(165) Kabalnov, A. Thermodynamic and theoretical aspects of emulsions and their stability. *Curr. Opin. Colloid Interface Sci.* **1998**, *3* (3), 270-275. DOI: https://doi.org/10.1016/S1359-0294(98)80071-X.
(166) Perrin, L.; Desobry-Banon, S.; Gillet, G.; Desobry, S. Review of High-Frequency Ultrasounds Emulsification Methods and Oil/Water Interfacial Organization in Absence of any Kind of Stabilizer. *Foods* **2022**, *11* (15), 2194. DOI: https://doi.org/10.3390/foods11152194.
(167) Aben, S.; Holtze, C.; Tadros, T.; Schurtenberger, P. Rheological Investigations on the Creaming of Depletion-Flocculated Emulsions. *Langmuir* **2012**, *28* (21), 7967-7975. DOI: https://doi.org/10.1021/la300221m.
(168) Borwankar, R. P.; Lobo, L. A.; Wasan, D. T. Emulsion stability — kinetics of flocculation and coalescence. *Colloids Surf.* **1992**, *69* (2), 135-146. DOI: https://doi.org/10.1016/0166-6622(92)80224-P.
(169) Weiss, J.; Herrmann, N.; McClements, D. J. Ostwald Ripening of Hydrocarbon Emulsion Droplets in Surfactant Solutions. *Langmuir* **1999**, *15* (20), 6652-6657. DOI: https://doi.org/10.1021/la981739d.
(170) Sakai, T. Surfactant-free emulsions. *Curr. Opin. Colloid Interface Sci.* **2008**, *13* (4), 228-235. DOI: https://doi.org/10.1016/j.cocis.2007.11.013.

(171) Bhargava, N.; Mor, R. S.; Kumar, K.; Sharanagat, V. S. Advances in application of ultrasound in food processing: A review. *Ultrason*. *Sonochem*. **2021**, *70*, 105293. DOI: https://doi.org/10.1016/j.ultsonch.2020.105293.
(172) Yao, C.; Zhao, S.; Liu, L.; Liu, Z.; Chen, G. Ultrasonic emulsification: basic characteristics, cavitation, mechanism, devices and application. *Front*. *Chem*. *Sci*. *Eng*. **2022**, *16* (11), 1560-1583. DOI: https://doi.org/10.1007/s11705-022-2160-4.
(173) Reddy, S. R.; Fogler, H. S. Emulsion stability of acoustically formed emulsions. *J*. *Phys*. *Chem*. **1980**, *84* (12), 1570-1575. DOI: https://doi.org/10.1021/j100449a027.
(174) Marinova, K. G.; Alargova, R. G.; Denkov, N. D.; Velev, O. D.; Petsev, D. N.; Ivanov, I. B.; Borwankar, R. P. Charging of Oil−Water Interfaces Due to Spontaneous Adsorption of Hydroxyl Ions. *Langmuir* **1996**, *12* (8), 2045-2051. DOI: https://doi.org/10.1021/la950928i.
(175) Beattie, J. K.; Djerdjev, A. M. The Pristine Oil/Water Interface: Surfactant-Free Hydroxide-Charged Emulsions. *Angew*. *Chem*. *Int*. *Ed*. **2004**, *43* (27), 3568-3571. DOI: https://doi.org/10.1002/anie.200453916.
(176) Sakai, T.; Kamogawa, K.; Nishiyama, K.; Sakai, H.; Abe, M. Molecular Diffusion of Oil/Water Emulsions in Surfactant-Free Conditions. *Langmuir* **2002**, *18* (6), 1985-1990. DOI: https://doi.org/10.1021/la0111248.
(177) Davis, S. S.; Round, H. P.; Purewal, T. S. Ostwald ripening and the stability of emulsion systems: an explanation for the effect of an added third component. *J*. *Colloid Interface Sci*. **1981**, *80* (2), 508-511. DOI: https://doi.org/10.1016/0021-9797(81)90210-1.
(178) Kamogawa, K.; Matsumoto, M.; Kobayashi, T.; Sakai, T.; Sakai, H.; Abe, M. Dispersion and Stabilizing Effects of n-Hexadecane on Tetralin and Benzene Metastable Droplets in Surfactant-Free Conditions. *Langmuir* **1999**, *15* (6), 1913-1917. DOI: https://doi.org/10.1021/la9806799.
(179) Kamogawa, K.; Kuwayama, N.; Katagiri, T.; Akatsuka, H.; Sakai, T.; Sakai, H.; Abe, M. Dispersion and Stabilization in Water of Droplets of Hydrophobic Organic Liquids with the Addition of Hydrophobic Polymers. *Langmuir* **2003**, *19*, 4063-4069. DOI: https://doi.org/10.1021/la020749i.
(180) Bhattacharjee, S. DLS and zeta potential – What they are and what they are not? *J*. *Control*. *Release* **2016**, *235*, 337-351. DOI: https://doi.org/10.1016/j.jconrel.2016.06.017.
(181) Stachurski, J.; Michałek, M. The Effect of the ζ Potential on the Stability of a Non-Polar Oil-in-Water Emulsion. *J*. *Colloid Interface Sci*. **1996**, *184* (2), 433-436. DOI: https://doi.org/10.1006/jcis.1996.0637.
(182) Babick, F. Chapter 3.2.1 - Dynamic light scattering (DLS). In *Characterization of Nanoparticles*, Hodoroaba, V.-D., Unger, W. E. S., Shard, A. G. Eds.; Elsevier, 2020; pp 137-172. ISBN: 978-0-12-814182-3.
(183) Kamogawa, K.; Okudaira, G.; Matsumoto, M.; Sakai, T.; Sakai, H.; Abe, M. Preparation of Oleic Acid/Water Emulsions in Surfactant-Free Condition by Sequential Processing Using Midsonic-Megasonic Waves. *Langmuir* **2004**, *20*, 2043-2047. DOI: https://doi.org/10.1021/la030160z.
(184) Nakabayashi, K.; Amemiya, F.; Fuchigami, T.; Machida, K.; Takeda, S.; Tamamitsu, K.; Atobe, M. Highly clear and transparent nanoemulsion preparation under surfactant-free conditions using tandem acoustic emulsification. *Chem*. *Commun*. **2011**, *47* (20), 5765-5767. DOI: https://doi.org/10.1039/C1CC10558B.
(185) Takei, K.; Watanabe, M.; Kawasaki, K.; Sakai, T. Colloidal Stability of Emulsifier-free Triolein-in-Water Emulsions: Effects of Temperature. *J*. *Oleo Sci*. **2022**, *71* (1), 75-81. DOI: https://doi.org/10.5650/jos.ess21234.
(186) Andler, R.; Valdés, C.; Díaz-Barrera, A.; Steinbüchel, A. Biotransformation of poly(cis-1,4-isoprene) in a multiphase enzymatic reactor for continuous extraction of oligo-isoprenoid molecules. *N*. *Biotechnol*. **2020**, *58*, 10-16. DOI: https://doi.org/10.1016/j.nbt.2020.05.001.
(187) Bell, E. L.; Hutton, A. E.; Burke, A. J.; O'Connell, A.; Barry, A.; O'Reilly, E.; Green, A. P. Strategies for designing biocatalysts with new functions. *Chem*. *Soc*. *Rev*. **2024**. DOI: http://dx.doi.org/10.1039/D3CS00972F.
(188) Bornscheuer, U. T.; Hauer, B.; Jaeger, K. E.; Schwaneberg, U. Directed Evolution Empowered Redesign of Natural Proteins for the Sustainable Production of Chemicals and Pharmaceuticals. *Angew*. *Chem*. *Int*. *Ed*. **2019**, *58* (1), 36-40. DOI: https://doi.org/10.1002/anie.201812717.
(189) Brakmann, S. Discovery of Superior Enzymes by Directed Molecular Evolution. *ChemBioChem* **2001**, *2* (12), 865-871. DOI: https://doi.org/10.1002/1439-7633(20011203)2:12<865::AID-CBIC865>3.0.CO;2-6.

(190) Stemmer, W. P. C. Rapid evolution of a protein in vitro by DNA shuffling. *Nature* **1994**, *370* (6488), 389-391. DOI: https://doi.org/10.1038/370389a0.
(191) Quin, M. B.; Schmidt-Dannert, C. Engineering of Biocatalysts: from Evolution to Creation. *ACS Catal*. **2011**, *1* (9), 1017-1021. DOI: https://doi.org/10.1021/cs200217t.
(192) Reetz, M. T.; Carballeira, J. D.; Vogel, A. Iterative saturation mutagenesis on the basis of B factors as a strategy for increasing protein thermostability. *Angew*. *Chem. Int. Ed*. **2006**, *45* (46), 7745-7751. DOI: https://doi.org/10.1002/anie.200602795.
(193) Sulaiman, S.; Yamato, S.; Kanaya, E.; Kim, J.-J.; Koga, Y.; Takano, K.; Kanaya, S. Isolation of a Novel Cutinase Homolog with Polyethylene Terephthalate-Degrading Activity from Leaf-Branch Compost by Using a Metagenomic Approach. *Appl*. *Environ*. *Microbiol*. **2012**, *78* (5), 1556-1562. DOI: https://doi.org/10.1128/AEM.06725-11.
(194) Tournier, V.; Topham, C. M.; Gilles, A.; David, B.; Folgoas, C.; Moya-Leclair, E.; Kamionka, E.; Desrousseaux, M. L.; Texier, H.; Gavalda, S.; Cot, M.; Guemard, E.; Dalibey, M.; Nomme, J.; Cioci, G.; Barbe, S.; Chateau, M.; Andre, I.; Duquesne, S.; Marty, A. An engineered PET depolymerase to break down and recycle plastic bottles. *Nature* **2020**, *580* (7802), 216-219. DOI: https://doi.org/10.1038/s41586-020-2149-4.
(195) Chandler, P. G.; Broendum, S. S.; Riley, B. T.; Spence, M. A.; Jackson, C. J.; McGowan, S.; Buckle, A. M. Strategies for Increasing Protein Stability. In *Protein Nanotechnology: Protocols, Instrumentation, and Applications*, Gerrard, J. A., Domigan, L. J. Eds.; Springer US, **2020**; pp 163-181. ISBN: 978-1-4939-9869-2.
(196) Goldenzweig, A.; Goldsmith, M.; Hill, Shannon E.; Gertman, O.; Laurino, P.; Ashani, Y.; Dym, O.; Unger, T.; Albeck, S.; Prilusky, J.; Lieberman, Raquel L.; Aharoni, A.; Silman, I.; Sussman, Joel L.; Tawfik, Dan S.; Fleishman, Sarel J. Automated Structure- and Sequence-Based Design of Proteins for High Bacterial Expression and Stability. *Mol*. *Cell* **2016**, *63* (2), 337-346. DOI: https://doi.org/10.1016/j.molcel.2016.06.012.
(197) Steipe, B.; Schiller, B.; Plückthun, A.; Steinbacher, S. Sequence Statistics Reliably Predict Stabilizing Mutations in a Protein Domain. *J*. *Mol*. *Biol*. **1994**, *240* (3), 188-192. DOI: https://doi.org/10.1006/jmbi.1994.1434.
(198) Fleishman, S. J.; Leaver-Fay, A.; Corn, J. E.; Strauch, E.-M.; Khare, S. D.; Koga, N.; Ashworth, J.; Murphy, P.; Richter, F.; Lemmon, G.; Meiler, J.; Baker, D. RosettaScripts: A Scripting Language Interface to the Rosetta Macromolecular Modeling Suite. *PLoS ONE* **2011**, *6* (6), e20161. DOI: https://doi.org/10.1371/journal.pone.0020161.
(199) Khersonsky, O.; Lipsh, R.; Avizemer, Z.; Ashani, Y.; Goldsmith, M.; Leader, H.; Dym, O.; Rogotner, S.; Trudeau, D. L.; Prilusky, J.; Amengual-Rigo, P.; Guallar, V.; Tawfik, D. S.; Fleishman, S. J. Automated Design of Efficient and Functionally Diverse Enzyme Repertoires. *Mol*. *Cell* **2018**, *72* (1), 178-186.e175. DOI: https://doi.org/10.1016/j.molcel.2018.08.033.
(200) Wittmund, M.; Cadet, F.; Davari, M. D. Learning Epistasis and Residue Coevolution Patterns: Current Trends and Future Perspectives for Advancing Enzyme Engineering. *ACS Catal*. **2022**, *12* (22), 14243-14263. DOI: https://doi.org/10.1021/acscatal.2c01426.
(201) Verde-Sesto, E.; Arbe, A.; Moreno, A. J.; Cangialosi, D.; Alegría, A.; Colmenero, J.; Pomposo, J. A. Single-chain nanoparticles: opportunities provided by internal and external confinement. *Mater*. *Horiz*. **2020**, *7* (9), 2292-2313. DOI: https://doi.org/10.1039/D0MH00846J.
(202) Gonzalez-Burgos, M.; Latorre-Sanchez, A.; Pomposo, J. A. Advances in single chain technology. *Chem*. *Soc*. *Rev*. **2015**, *44* (17), 6122-6142. DOI: https://doi.org/10.1039/C5CS00209E.
(203) Wijker, S.; Palmans, A. R. A. Protein-Inspired Control over Synthetic Polymer Folding for Structured Functional Nanoparticles in Water. *ChemPlusChem* **2023**, *88* (7), e202300260. DOI: https://doi.org/10.1002/cplu.202300260.
(204) Terashima, T.; Sugita, T.; Fukae, K.; Sawamoto, M. Synthesis and Single-Chain Folding of Amphiphilic Random Copolymers in Water. *Macromolecules* **2014**, *47* (2), 589-600. DOI: https://doi.org/10.1021/ma402355v.
(205) Chen, J.; Li, K.; Bonson, S. E.; Zimmerman, S. C. A Bioorthogonal Small Molecule Selective Polymeric "Clickase". *J*. *Am*. *Chem*. *Soc*. **2020**, *142* (32), 13966-13973. DOI: https://doi.org/10.1021/jacs.0c06553.
(206) Garmendia, S.; Lawrenson, S. B.; Arno, M. C.; O'Reilly, R. K.; Taton, D.; Dove, A. P. Catalytically Active N-Heterocyclic Carbene Release from Single-Chain Nanoparticles Following a Thermolysis-Driven Unfolding Strategy. *Macromol*. *Rapid Commun.* **2019**, *40* (15), e1900071. DOI: https://doi.org/10.1002/marc.201900071.

(207) ter Huurne, G. M.; Gillissen, M. A. J.; Palmans, A. R. A.; Voets, I. K.; Meijer, E. W. The Coil-to-Globule Transition of Single-Chain Polymeric Nanoparticles with a Chiral Internal Secondary Structure. *Macromolecules* **2015**, *48* (12), 3949-3956. DOI: https://doi.org/10.1021/acs.macromol.5b00604.
(208) Lyon, C. K.; Prasher, A.; Hanlon, A. M.; Tuten, B. T.; Tooley, C. A.; Frank, P. G.; Berda, E. B. A brief user's guide to single-chain nanoparticles. *Polym*. *Chem*. **2015**, *6* (2), 181-197. DOI: https://doi.org/10.1039/C4PY01217H.
(209) Tuten, B. T.; Chao, D.; Lyon, C. K.; Berda, E. B. Single-chain polymer nanoparticles via reversible disulfide bridges. *Polym*. *Chem*. **2012**, *3* (11), 3068-3071. DOI: http://dx.doi.org/10.1039/C2PY20308A.
(210) Altintas, O.; Willenbacher, J.; Wuest, K. N. R.; Oehlenschlaeger, K. K.; Krolla-Sidenstein, P.; Gliemann, H.; Barner-Kowollik, C. A Mild and Efficient Approach to Functional Single-Chain Polymeric Nanoparticles via Photoinduced Diels–Alder Ligation. *Macromolecules* **2013**, *46* (20), 8092-8101. DOI: https://doi.org/10.1021/ma4015033.
(211) Liang, J.; Struckhoff, J. J.; Hamilton, P. D.; Ravi, N. Preparation and Characterization of Biomimetic beta-Lens Crystallins Using Single-Chain Polymeric Nanoparticles. *Langmuir* **2017**, *33* (31), 7660-7668. DOI: https://doi.org/10.1021/acs.langmuir.7b01290.
(212) Berda, E. B.; Foster, E. J.; Meijer, E. W. Toward Controlling Folding in Synthetic Polymers: Fabricating and Characterizing Supramolecular Single-Chain Nanoparticles. *Macromolecules* **2010**, *43* (3), 1430-1437. DOI: https://doi.org/10.1021/ma902393h.
(213) Mes, T.; van der Weegen, R.; Palmans, A. R.; Meijer, E. W. Single-chain polymeric nanoparticles by stepwise folding. *Angew*. *Chem*. *Int*. *Ed.* **2011**, *50* (22), 5085-5089. DOI: https://doi.org/10.1002/anie.201100104.
(214) Garcia, E. S.; Xiong, T. M.; Lifschitz, A.; Zimmerman, S. C. Tandem catalysis using an enzyme and a polymeric ruthenium-based artificial metalloenzyme. *Polym*. *Chem*. **2021**, *12* (46), 6755-6760. DOI: https://doi.org/10.1039/D1PY01255J.
(215) Artar, M.; Souren, E. R. J.; Terashima, T.; Meijer, E. W.; Palmans, A. R. A. Single Chain Polymeric Nanoparticles as Selective Hydrophobic Reaction Spaces in Water. *ACS Macro Lett*. **2015**, *4* (10), 1099-1103. DOI: https://doi.org/10.1021/acsmacrolett.5b00652.
(216) Sanchez-Sanchez, A.; Arbe, A.; Colmenero, J.; Pomposo, J. A. Metallo-Folded Single-Chain Nanoparticles with Catalytic Selectivity. *ACS Macro Lett*. **2014**, *3* (5), 439-443. DOI: https://doi.org/10.1021/mz5001477.
(217) Knofel, N. D.; Rothfuss, H.; Willenbacher, J.; Barner-Kowollik, C.; Roesky, P. W. Platinum(II)-Crosslinked Single-Chain Nanoparticles: An Approach towards Recyclable Homogeneous Catalysts. *Angew*. *Chem*. *Int*. *Ed*. **2017**, *56* (18), 4950-4954. DOI: https://doi.org/10.1002/anie.201700718.
(218) Willenbacher, J.; Altintas, O.; Trouillet, V.; Knöfel, N.; Monteiro, M. J.; Roesky, P. W.; Barner-Kowollik, C. Pd-complex driven formation of single-chain nanoparticles. *Polym*. *Chem*. **2015**, *6* (24), 4358-4365. DOI: https://doi.org/10.1039/C5PY00389J.
(219) Lambert, R.; Wirotius, A.-L.; Garmendia, S.; Berto, P.; Vignolle, J.; Taton, D. Pd(ii)–NHC coordination-driven formation of water-soluble catalytically active single chain nanoparticles. *Polym*. *Chem*. **2018**, *9* (23), 3199-3204. DOI: https://doi.org/10.1039/C8PY00326B.
(220) Wang, W.; Wang, J.; Li, S.; Li, C.; Tan, R.; Yin, D. Iron(ii)-folded single-chain nanoparticles: a metalloenzyme mimicking sustainable catalyst for highly enantioselective sulfa-Michael addition in water. *Green Chem*. **2020**, *22* (14), 4645-4655. DOI: https://doi.org/10.1039/D0GC00949K.
(221) Thanneeru, S.; Duay, S. S.; Jin, L.; Fu, Y.; Angeles-Boza, A. M.; He, J. Single Chain Polymeric Nanoparticles to Promote Selective Hydroxylation Reactions of Phenol Catalyzed by Copper. *ACS Macro Lett.* **2017**, *6* (7), 652-656. DOI: https://doi.org/10.1021/acsmacrolett.7b00300.
(222) Huerta, E.; Stals, P. J. M.; Meijer, E. W.; Palmans, A. R. A. Consequences of Folding a Water-Soluble Polymer Around an Organocatalyst. *Angew*. *Chem*. *Int*. *Ed*. **2013**, *52* (10), 2906-2910. DOI: https://doi.org/10.1002/anie.201207123.
(223) Lambert, R.; Wirotius, A. L.; Taton, D. Intramolecular Quaternization as Folding Strategy for the Synthesis of Catalytically Active Imidazolium-Based Single Chain Nanoparticles. *ACS Macro Lett*. **2017**, *6* (5), 489-494. DOI: https://doi.org/10.1021/acsmacrolett.7b00161.
(224) Mundsinger, K.; Izuagbe, A.; Tuten, B. T.; Roesky, P. W.; Barner-Kowollik, C. Single Chain Nanoparticles in Catalysis. *Angew*. *Chem*. *Int*. *Ed*. **2024**, *63* (7), e202311734. DOI: https://doi.org/10.1002/anie.202311734.

(225) Stals, P. J. M.; Cheng, C. Y.; van Beek, L.; Wauters, A. C.; Palmans, A. R. A.; Han, S.; Meijer, E. W. Surface water retardation around single-chain polymeric nanoparticles: critical for catalytic function? *Chem*. *Sci*. **2016**, *7* (3), 2011-2015. DOI: https://doi.org/10.1039/C5SC02319J.
(226) Schwuger, M.-J.; Stickdorn, K.; Schomaecker, R. Microemulsions in Technical Processes. *Chem*. *Rev*. **1995**, *95* (4), 849-864. DOI: https://doi.org/10.1021/cr00036a003.
(227) Hamzah, Y. B.; Hashim, S.; Rahman, W. A. W. A. Synthesis of polymeric nano/microgels: a review. *J. Polym*. *Res*. **2017**, *24* (9), 134. DOI: https://doi.org/10.1007/s10965-017-1281-9.
(228) Canselier, J. P.; Delmas, H.; Wilhelm, A. M.; Abismaïl, B. Ultrasound Emulsification—An Overview. *J*. *Disper*. *Sci*. *Technol*. **2002**, *23* (1-3), 333-349. DOI: https://doi.org/10.1080/01932690208984209.
(229) Gunsteren, N. F. A. v. d. V. a. W. F. v. Entropic Contributions in Cosolvent Binding to Hydrophobic Solutes in Water. *J*. *Phys*. *Chem*. *B* **2004** *108* (3), 1056-1064. DOI: https://doi.org/10.1021/jp030532c.
(230) Zhou, L.; Zhang, J.; Xing, L.; Zhang, W. Applications and effects of ultrasound assisted emulsification in the production of food emulsions: A review. *Trends Food Sci*. *Technol*. **2021**, *110*, 493-512. DOI: https://doi.org/10.1016/j.tifs.2021.02.008.
(231) Leong, T. S. H.; Wooster, T. J.; Kentish, S. E.; Ashokkumar, M. Minimising oil droplet size using ultrasonic emulsification. *Ultrason*. *Sonochem*. **2009**, *16* (6), 721-727. DOI: https://doi.org/10.1016/j.ultsonch.2009.02.008.
(232) Consoli, L.; de Figueiredo Furtado, G.; da Cunha, R. L.; Hubinger, M. D. High solids emulsions produced by ultrasound as a function of energy density. *Ultrason*. *Sonochem*. **2017**, *38*, 772-782. DOI: https://doi.org/10.1016/j.ultsonch.2016.11.038.
(233) Modarres-Gheisari, S. M. M.; Gavagsaz-Ghoachani, R.; Malaki, M.; Safarpour, P.; Zandi, M. Ultrasonic nano-emulsification – A review. *Ultrason*. *Sonochem*. **2019**, *52*, 88-105. DOI: https://doi.org/10.1016/j.ultsonch.2018.11.005.
(234) Schneider, C. A.; Rasband, W. S.; Eliceiri, K. W. NIH Image to ImageJ: 25 years of image analysis. *Nat*. *Methods* **2012**, *9* (7), 671-675. DOI: https://doi.org/10.1038/nmeth.2089.
(235) Schindelin, J.; Rueden, C. T.; Hiner, M. C.; Eliceiri, K. W. The ImageJ ecosystem: An open platform for biomedical image analysis. *Mol*. *Reprod*. *Dev*. **2015**, *82* (7-8), 518-529. DOI: https://doi.org/10.1002/mrd.22489.
(236) Weiss, J.; Coupland, J. N.; McClements, D. J. Solubilization of Hydrocarbon Emulsion Droplets Suspended in Nonionic Surfactant Micelle Solutions. *J*. *Phys*. *Chem.* **1996**, *100* (3), 1066-1071. DOI: https://doi.org/10.1021/jp9524892.
(237) Senske, M.; Constantinescu-Aruxandei, D.; Havenith, M.; Herrmann, C.; Weingärtner, H.; Ebbinghaus, S. The temperature dependence of the Hofmeister series: thermodynamic fingerprints of cosolute–protein interactions. *Phys*. *Chem*. *Chem*. *Phys*. **2016**, *18* (43), 29698-29708. DOI: https://doi.org/10.1039/C6CP05080H.
(238) Rother, W.; Birke, J.; Jendrossek, D. Assays for the Detection of Rubber Oxygenase Activities. *Bio-protocol* **2017**, *7* (6), e2188. DOI: https://doi.org/10.21769/BioProtoc.2188.
(239) Braaz, R.; Fischer, P.; Jendrossek, D. Novel type of heme-dependent oxygenase catalyzes oxidative cleavage of rubber (poly-cis-1,4-isoprene). *Appl*. *Environ*. *Microbiol*. **2004**, *70* (12), 7388-7395. DOI: https://doi.org/10.1128/AEM.70.12.7388-7395.2004.
(240) Andler, R.; Guajardo, C.; Sepúlveda, C.; Pino, V.; Sanhueza, V.; D'Afonseca, V. Biodegradation of rubber in cultures of Rhodococcus rhodochrous and by its enzyme latex clearing protein. *Biodegradation* **2022**, *33*, 1-12. DOI: https://doi.org/10.1007/s10532-022-09998-7.
(241) Andler, R.; Steinbuchel, A. A simple, rapid and cost-effective process for production of latex clearing protein to produce oligopolyisoprene molecules. *J*. *Biotechnol*. **2017**, *241*, 184-192. DOI: https://doi.org/10.1016/j.jbiotec.2016.12.008.
(242) Giver, L.; Gershenson, A.; Freskgard, P.-O.; Arnold, F. H. Directed evolution of a thermostable esterase. *Proc*. *Natl*. *Acad*. *Sci*. *USA* **1998**, *95* (22), 12809-12813. DOI: https://doi.org/10.1073/pnas.95.22.12809.
(243) Vazquez-Figueroa, E.; Yeh, V.; Broering, J. M.; Chaparro-Riggers, J. F.; Bommarius, A. S. Thermostable variants constructed via the structure-guided consensus method also show increased stability in salts solutions and homogeneous aqueous-organic media. *Protein Eng*. *Des*. *Sel*. **2008**, *21* (11), 673-680. DOI: https://doi.org/10.1093/protein/gzn048.
(244) Gazi, R.; Maity, S.; Jana, M. Conformational Features and Hydration Dynamics of Proteins in Cosolvents: A Perspective from Computational Approaches. *ACS Omega* **2023**, *8* (3), 2832-2843. DOI: https://doi.org/10.1021/acsomega.2c08009.

(245) Bren, K. L. Engineered Biomolecular Catalysts. *J. Am. Chem. Soc.* **2017**, *139* (41), 14331-14334. DOI: https://doi.org/10.1021/jacs.7b09896.
(246) Speer, S. L.; Stewart, C. J.; Sapir, L.; Harries, D.; Pielak, G. J. Macromolecular Crowding Is More than Hard-Core Repulsions. *Annu. Rev. Biophys.* **2022**, *51* (1), 267-300. DOI: https://doi.org/10.1146/annurev-biophys-091321-071829.
(247) Kokkonen, P.; Bednar, D.; Pinto, G.; Prokop, Z.; Damborsky, J. Engineering enzyme access tunnels. *Biotechnol. Adv.* **2019**, *37* (6), 107386. DOI: https://doi.org/10.1016/j.biotechadv.2019.04.008.
(248) Samak, N. A.; Jia, Y.; Sharshar, M. M.; Mu, T.; Yang, M.; Peh, S.; Xing, J. Recent advances in biocatalysts engineering for polyethylene terephthalate plastic waste green recycling. *Environ. Int.* **2020**, *145*, 106144. DOI: https://doi.org/10.1016/j.envint.2020.106144.
(249) DePristo, M. A.; Weinreich, D. M.; Hartl, D. L. Missense meanderings in sequence space: a biophysical view of protein evolution. *Nat. Rev. Genet.* **2005**, *6* (9), 678-687. DOI: https://doi.org/10.1038/nrg1672.
(250) Wolf, Y. L. Latex-degrading Enzym LcpK30 - Expression- and Stabilityimprovement by PROSS Algorithm as well as first Steps of Directed Evolution, Bachelor Thesis. Martin-Luther University Halle-Wittenberg, **2020.**
(251) Lu, H.; Diaz, D. J.; Czarnecki, N. J.; Zhu, C.; Kim, W.; Shroff, R.; Acosta, D. J.; Alexander, B. R.; Cole, H. O.; Zhang, Y.; Lynd, N. A.; Ellington, A. D.; Alper, H. S. Machine learning-aided engineering of hydrolases for PET depolymerization. *Nature* **2022**, *604* (7907), 662-667. DOI: https://doi.org/10.1038/s41586-022-04599-z.
(252) Bharadwaj, S.; Nayar, D.; Dalgicdir, C.; van der Vegt, N. F. A. A cosolvent surfactant mechanism affects polymer collapse in miscible good solvents. *Commun. Chem.* **2020**, *3* (1). DOI: https://doi.org/10.1038/s42004-020-00405-x.
(253) Oetermann, S.; Vivod, R.; Hiessl, S.; Hogeback, J.; Holtkamp, M.; Karst, U.; Steinbüchel, A. Histidine at Position 195 is Essential for Association of Heme-b in Lcp1VH2. *Earth Syst. Environ.* **2018**, *2* (1), 5-14. DOI: https://doi.org/10.1007/s41748-018-0041-2.
(254) Simeonov, A. Recent developments in the use of differential scanning fluorometry in protein and small molecule discovery and characterization. *Expert Opin. Drug. Discov.* **2013**, *8* (9), 1071-1082. DOI: https://doi.org/10.1517/17460441.2013.806479.
(255) Tsuchii, A.; Suzuki, T.; Takeda, K. Microbial degradation of natural rubber vulcanizates. *Appl. Environ. Microbiol.* **1985**, *50* (4), 965-970. DOI: https://doi.org/10.1128/aem.50.4.965-970.1985.
(256) Kolmel, D. K.; Kool, E. T. Oximes and Hydrazones in Bioconjugation: Mechanism and Catalysis. *Chem. Rev.* **2017**, *117* (15), 10358-10376. DOI: https://doi.org/10.1021/acs.chemrev.7b00090.
(257) Wang, S. L.; Wang, Y.; Wu, L.; Cai, Y. Y.; Wang, Z. C.; Alolga, R. N.; Qi, L. W.; Li, B.; Huang, F. Q. Paired Derivatization Approach with H/D-Labeled Hydroxylamine Reagents for Sensitive and Accurate Analysis of Monosaccharides by Liquid Chromatography Tandem Mass Spectrometry. *Anal. Chem.* **2022**, *94* (8), 3590-3599. DOI: https://doi.org/10.1021/acs.analchem.1c04924.
(258) Kotoku, N.; Tsujita, H.; Hiramatsu, A.; Mori, C.; Koizumi, N.; Kobayashi, M. Synthesis and Biological Evaluation of Purealin and Analogues as Cytoplasmic Dynein Heavy Chain Inhibitors. *Tetrahedron* **2005**, *61*, 7211-7218. DOI: https://doi.org/10.1021/jm051030l.
(259) Tschierske, C. Microsegregation: From Basic Concepts to Complexity in Liquid Crystal Self-Assembly. *Isr. J. Chem.* **2012**, *52* (10), 935-959. DOI: https://doi.org/10.1002/ijch.201200053.
(260) Jegannathan, K. R.; Nielsen, P. H. Environmental assessment of enzyme use in industrial production – a literature review. *J. Clean. Prod.* **2013**, *42*, 228-240. DOI: https://doi.org/10.1016/j.jclepro.2012.11.005.
(261) Foresti, M. L.; Ferreira, M. L. Frequent analytical/experimental problems in lipase-mediated synthesis in solvent-free systems and how to avoid them. *Anal. Bioanal. Chem.* **2005**, *381* (7), 1408-1425. DOI: https://doi.org/10.1007/s00216-005-3087-6.
(262) Liesener, A.; Karst, U. Monitoring enzymatic conversions by mass spectrometry: a critical review. *Anal. Bioanal. Chem.* **2005**, *382* (7), 1451-1464. DOI: https://doi.org/10.1007/s00216-005-3305-2.
(263) Hiller, W.; Sinha, P.; Hehn, M.; Pasch, H.; Hofe, T. Separation Analysis of Polyisoprenes Regarding Microstructure by Online LCCC-NMR and SEC-NMR. *Macromolecules* **2011**, *44* (6), 1311-1318. DOI: https://doi.org/10.1021/ma102750s.

(264) Wolf, Y. L. Creation of a broader variety of rubber-degrading enzymes through protein engineering to enable the degradation of synthetic rubber polymers, Master Thesis. Martin-Luther University Halle-Wittenberg, **2023**.
(265) Shinde, K. S.; Michael, P.; Rössle, M.; Thiele, S.; Binder, W. H. Cyclopropanation of poly(isoprene) using NHC-Cu(I) catalysts: Introducing carboxylates. *J. Polym. Sci.* **2020**, *58* (20), 2864-2874. DOI: https://doi.org/10.1002/pol.20200404.
(266) Dalpozzo, R.; Bartoli, G.; Bencivenni, G. Asymmetric Cyclopropanation Reactions. *Synthesis* **2014**, *46* (08), 979-1029. DOI: https://doi.org/10.1055/s-0033-1340838.
(267) Østergaard, N.; Jensen, J. F.; Tanner, D. Scope and limitations of chiral bis(oxazoline) ligands in the copper-catalysed asymmetric cyclopropanation of trisubstituted alkenes. *Tetrahedron* **2001**, *57* (28), 6083-6088. DOI: https://doi.org/10.1016/S0040-4020(01)00583-X.
(268) Mavila, S.; Rozenberg, I.; Lemcoff, N. G. A general approach to mono- and bimetallic organometallic nanoparticles. *Chem. Sci.* **2014**, *5* (11), 4196-4203. DOI: https://doi.org/10.1039/C4SC01231C.
(269) Crispino, G. A.; Ho, P. T.; Sharpless, K. B. Selective Perhydroxylation of Squalene: Taming the Arithmetic Demon. *Science* **1993**, *259* (5091), 64-66. DOI: https://doi.org/10.1126/science.8418495.
(270) Ford, A.; Miel, H.; Ring, A.; Slattery, C. N.; Maguire, A. R.; McKervey, M. A. Modern Organic Synthesis with alpha-Diazocarbonyl Compounds. *Chem. Rev.* **2015**, *115* (18), 9981-10080. DOI: https://doi.org/10.1021/acs.chemrev.5b00121.
(271) Díaz-Requejo, M. M.; Pérez, P. J. Copper, silver and gold-based catalysts for carbene addition or insertion reactions. *J. Organomet. Chem.* **2005**, *690* (24-25), 5441-5450. DOI: https://doi.org/10.1016/j.jorganchem.2005.07.092.
(272) Fructos, M. R.; Belderrain, T. R.; Nicasio, M. C.; Nolan, S. P.; Kaur, H.; Díaz-Requejo, M. M.; Pérez, P. J. Complete Control of the Chemoselectivity in Catalytic Carbene Transfer Reactions from Ethyl Diazoacetate: An N-Heterocyclic Carbene−Cu System That Suppresses Diazo Coupling. *J. Am. Chem. Soc.* **2004**, *126* (35), 10846-10847. DOI: https://doi.org/10.1021/ja047284y.
(273) Carreras, J.; Caballero, A.; Perez, P. J. Enantio- and Diastereoselective Cyclopropanation of 1-Alkenylboronates: Synthesis of 1-Boryl-2,3-Disubstituted Cyclopropanes. *Angew. Chem. Int. Ed.* **2018**, *57* (9), 2334-2338. DOI: https://doi.org/10.1002/anie.201710415.
(274) Li, J.; Zheng, L.; Chen, H.; Wang, L.; Sun, X.-L.; Zhu, J.; Tang, Y. Highly enantioselective cyclopropanation of trisubstituted olefins. *Sci. China Chem.* **2018**, *61* (5), 526-530. DOI: https://doi.org/10.1007/s11426-017-9200-9.
(275) Evans, D. A.; Woerpel, K. A.; Hinman, M. M.; Faul, M. M. Bis(oxazolines) as chiral ligands in metal-catalyzed asymmetric reactions. Catalytic, asymmetric cyclopropanation of olefins. *J. Am. Chem. Soc.* **2002**, *113* (2), 726-728. DOI: https://doi.org/10.1021/ja00002a080.
(276) Azzouzi-Zriba, K.; Bonnet-Delpon, D.; Crousse, B. Transition metal-catalyzed cyclopropanation of alkenes in fluorinated alcohols. *J. Fluorine Chem.* **2011**, *132* (10), 811-814. DOI: https://doi.org/10.1016/j.jfluchem.2011.05.018.
(277) Kaur, P.; Tyagi, V. Recent Advances in Iron-Catalyzed Chemical and Enzymatic Carbene-Transfer Reactions. *Adv. Synth. Catal.* **2021**, *363* (4), 877-905. DOI: https://doi.org/10.1002/adsc.202001158.
(278) Yang, Y.; Arnold, F. H. Navigating the Unnatural Reaction Space: Directed Evolution of Heme Proteins for Selective Carbene and Nitrene Transfer. *Acc. Chem. Res.* **2021**, *54* (5), 1209-1225. DOI: https://doi.org/10.1021/acs.accounts.0c00591.
(279) Biewend, M.; Neumann, S.; Michael, P.; Binder, W. H. Synthesis of polymer-linked copper(i) bis(N-heterocyclic carbene) complexes of linear and chain extended architecture. *Polym. Chem.* **2019**, *10* (9), 1078-1088. DOI: https://doi.org/10.1039/C8PY01751D.
(280) Rupp, H.; Binder, W. H. Multicomponent Stress-Sensing Composites Fabricated by 3D-Printing Methodologies. *Macromol. Rapid Commun.* **2021**, *42* (1), 2000450. DOI: https://doi.org/10.1002/marc.202000450.
(281) Terashima, T.; Mes, T.; De Greef, T. F.; Gillissen, M. A.; Besenius, P.; Palmans, A. R.; Meijer, E. W. Single-chain folding of polymers for catalytic systems in water. *J. Am. Chem. Soc.* **2011**, *133* (13), 4742-4745. DOI: https://doi.org/10.1021/ja2004494.
(282) Hua, Z.; Pitto-Barry, A.; Kang, Y.; Kirby, N.; Wilks, T. R.; O'Reilly, R. K. Micellar nanoparticles with tuneable morphologies through interactions between nucleobase-containing synthetic polymers in aqueous solution. *Polym. Chem.* **2016**, *7* (25), 4254-4262. DOI: https://doi.org/10.1039/C6PY00716C.

(283) Kohman, R. E.; Cha, C.; Zimmerman, S. C.; Kong, H. Tuning hydrogel properties and function using substituent effects. *Soft Matter* **2010**, *6* (10), 2150-2152. DOI: https://doi.org/10.1039/C001548B.
(284) Kikuchi, S.; Chen, Y.; Ichinohe, E.; Kitano, K.; Sato, S.-i.; Duan, Q.; Shen, X.; Kakuchi, T. Synthesis and Thermoresponsive Property of Linear, Cyclic, and Star-Shaped Poly(N,N-diethylacrylamide)s Using B(C6F5)3-Catalyzed Group Transfer Polymerization as Facile End-Functionalization Method. *Macromolecules* **2016**, *49* (13), 4828-4838. DOI: https://doi.org/10.1021/acs.macromol.6b01075.
(285) Zhang, Z.-J.; Zhang, H.-Y.; Wang, H.; Liu, Y. A Twin-Axial Hetero[7]rotaxane. *Angew*. *Chem*. *Int*. *Ed*. **2011**, *50* (46), 10834-10838. DOI: https://doi.org/10.1002/anie.201105375.
(286) Gondi, S. R.; Vogt, A. P.; Sumerlin, B. S. Versatile Pathway to Functional Telechelics via RAFT Polymerization and Click Chemistry. *Macromolecules* **2007**, *40* (3), 474-481. DOI: https://doi.org/10.1021/ma061959v.
(287) Rieger, J.; Zhang, W.; Stoffelbach, F.; Charleux, B. Surfactant-Free RAFT Emulsion Polymerization Using Poly(N,N-dimethylacrylamide) Trithiocarbonate Macromolecular Chain Transfer Agents. *Macromolecules* **2010**, *43* (15), 6302-6310. DOI: https://doi.org/10.1021/ma1009269.
(288) Perrier, S. 50th Anniversary Perspective: RAFT Polymerization—A User Guide. *Macromolecules* **2017**, *50* (19), 7433-7447. DOI: https://doi.org/10.1021/acs.macromol.7b00767.
(289) Rulkens, R.; Schulze, M.; Wegner, G. Rigid-rod polyelectrolytes: synthesis of sulfonated poly(p-phenylene)s. *Macromol. Rapid Commun*. **1994**, *15* (9), 669-676. DOI: https://doi.org/10.1002/marc.1994.030150902.
(290) Huang, F.; Hou, L.; Wu, H.; Wang, X.; Shen, H.; Cao, W.; Yang, W.; Cao, Y. High-Efficiency, Environment-Friendly Electroluminescent Polymers with Stable High Work Function Metal as a Cathode: Green- and Yellow-Emitting Conjugated Polyfluorene Polyelectrolytes and Their Neutral Precursors. *J*. *Am*. *Chem*. *Soc*. **2004**, *126* (31), 9845-9853. DOI: https://doi.org/10.1021/ja0476765.
(291) He, H.; Zhong, M.; Adzima, B.; Luebke, D.; Nulwala, H.; Matyjaszewski, K. A Simple and Universal Gel Permeation Chromatography Technique for Precise Molecular Weight Characterization of Well-Defined Poly(ionic liquid)s. *J*. *Am*. *Chem*. *Soc*. **2013**, *135* (11), 4227-4230. DOI: https://doi.org/10.1021/ja4012645.
(292) Grignon, E.; An, S. Y.; Battaglia, A. M.; Seferos, D. S. Catechol Homopolymers and Networks through Postpolymerization Modification. *Macromolecules* **2022**, *55* (22), 10167-10175. DOI: https://doi.org/10.1021/acs.macromol.2c01513.
(293) Chen, J.; Wang, J.; Li, K.; Wang, Y.; Gruebele, M.; Ferguson, A. L.; Zimmerman, S. C. Polymeric "Clickase" Accelerates the Copper Click Reaction of Small Molecules, Proteins, and Cells. *J*. *Am*. *Chem*. *Soc*. **2019**, *141* (24), 9693-9700. DOI: https://doi.org/10.1021/jacs.9b04181.
(294) Liu, Y.; Pujals, S.; Stals, P. J. M.; Paulohrl, T.; Presolski, S. I.; Meijer, E. W.; Albertazzi, L.; Palmans, A. R. A. Catalytically Active Single-Chain Polymeric Nanoparticles: Exploring Their Functions in Complex Biological Media. *J*. *Am*. *Chem*. *Soc*. **2018**, *140* (9), 3423-3433. DOI: https://doi.org/10.1021/jacs.8b00122.
(295) Theato, P. Synthesis of well-defined polymeric activated esters. *J*. *Polym*. *Sci*. *A Polym*. *Chem*. **2008**, *46* (20), 6677-6687. DOI: https://doi.org/10.1002/pola.22994.
(296) Eberhardt, M.; Mruk, R.; Zentel, R.; Théato, P. Synthesis of pentafluorophenyl(meth)acrylate polymers: New precursor polymers for the synthesis of multifunctional materials. *Eur*. *Polym*. *J*. **2005**, *41* (7), 1569-1575. DOI: https://doi.org/10.1016/j.eurpolymj.2005.01.025.
(297) Alex, J.; Ulbrich, J.; Rosales-Guzmán, M.; Weber, C.; Schubert, U. S.; Guerrero-Sanchez, C. Kinetic investigations on homo- and co-polymerizations of pentafluorophenyl (meth)acrylates. *Eur*. *Polym*. *J*. **2021**, *143*. DOI: https://doi.org/10.1016/j.eurpolymj.2020.110175.
(298) Eberhardt, M.; Théato, P. RAFT Polymerization of Pentafluorophenyl Methacrylate: Preparation of Reactive Linear Diblock Copolymers. *Macromol*. *Rapid Commun*. **2005**, *26* (18), 1488-1493. DOI: https://doi.org/10.1002/marc.200500390.
(299) Das, A.; Theato, P. Multifaceted Synthetic Route to Functional Polyacrylates by Transesterification of Poly(pentafluorophenyl acrylates). *Macromolecules* **2015**, *48* (24), 8695-8707. DOI: https://doi.org/10.1021/acs.macromol.5b02293.
(300) Jochum, F. D.; Theato, P. Temperature and light sensitive copolymers containing azobenzene moieties prepared via a polymer analogous reaction. *Polymer* **2009**, *50* (14), 3079-3085. DOI: https://doi.org/10.1016/j.polymer.2009.05.041

(301) Bou Zerdan, R.; Geng, Z.; Narupai, B.; Diaz, Y. J.; Bates, M. W.; Laitar, D. S.; Souvagya, B.; Van Dyk, A. K.; Hawker, C. J. Efficient synthesis of branched poly(acrylic acid) derivatives via postpolymerization modification. *J. Polym. Sci.* **2020**, *58* (14), 1989-1997. DOI: https://doi.org/10.1002/pol.20200287.
(302) Santa Chalarca, C. F.; Dalal, R. J.; Chapa, A.; Hanson, M. G.; Reineke, T. M. Cation Bulk and pKa Modulate Diblock Polymer Micelle Binding to pDNA. *ACS Macro Lett.* **2022**, *11* (4), 588-594. DOI: https://doi.org/10.1021/acsmacrolett.2c00015.
(303) Battistella, C.; Yang, Y.; Chen, J.; Klok, H. A. Synthesis and Postpolymerization Modification of Fluorine-End-Labeled Poly(Pentafluorophenyl Methacrylate) Obtained via RAFT Polymerization. *ACS Omega* **2018**, *3* (8), 9710-9721. DOI: https://doi.org/10.1021/acsomega.8b01654.
(304) Barz, M.; Tarantola, M.; Fischer, K.; Schmidt, M.; Luxenhofer, R.; Janshoff, A.; Theato, P.; Zentel, R. From Defined Reactive Diblock Copolymers to Functional HPMA-Based Self-Assembled Nanoaggregates. *Biomacromolecules* **2008**, *9* (11), 3114-3118. DOI: https://doi.org/10.1021/bm800684b.
(305) Moad, G.; Rizzardo, E.; Thang, S. H. End-functional polymers, thiocarbonylthio group removal/transformation and reversible addition–fragmentation–chain transfer (RAFT) polymerization. *Polym. Int.* **2011**, *60* (1), 9-25. DOI: https://doi.org/10.1002/pi.2988.
(306) Carmean, R. N.; Figg, C. A.; Scheutz, G. M.; Kubo, T.; Sumerlin, B. S. Catalyst-Free Photoinduced End-Group Removal of Thiocarbonylthio Functionality. *ACS Macro Lett.* **2017**, *6* (2), 185-189. DOI: https://doi.org/10.1021/acsmacrolett.7b00038.
(307) Eisenreich, F.; Palmans, A. R. A. Direct C−H Trifluoromethylation of (Hetero)Arenes in Water Enabled by Organic Photoredox-Active Amphiphilic Nanoparticles. *Chem. Eur. J.* **2022**, *28* (52), e202201322. DOI: https://doi.org/10.1002/chem.202201322.
(308) Thümmler, J. F.; Roos, A. H.; Krüger, J.; Hinderberger, D.; Schmitt, F.-J.; Tang, G.; Golmohamadi, F. G.; Laufer, J.; Binder, W. H. Tuning the Internal Compartmentation of Single-Chain Nanoparticles as Fluorescent Contrast Agents. *Macromol. Rapid Commun.* **2023**, *44* (2), 2200618. DOI: https://doi.org/10.1002/marc.202200618.
(309) Liu, M.; Miao, D.; Wang, X.; Wang, C.; Deng, W. Precise synthesis of heterogeneous glycopolymers with well-defined saccharide motifs in the side chain via post-polymerization modification and recognition with lectin. *J. Polym. Sci.* **2020**, *58* (15), 2074-2087. DOI: https://doi.org/10.1002/pol.20200008.
(310) Chua, G. B. H.; Roth, P. J.; Duong, H. T. T.; Davis, T. P.; Lowe, A. B. Synthesis and Thermoresponsive Solution Properties of Poly[oligo(ethylene glycol) (meth)acrylamide]s: Biocompatible PEG Analogues. *Macromolecules* **2012**, *45* (3), 1362-1374. DOI: https://doi.org/10.1021/ma202700y.
(311) Gibson, M. I.; Fröhlich, E.; Klok, H.-A. Postpolymerization modification of poly(pentafluorophenyl methacrylate): Synthesis of a diverse water-soluble polymer library. *J. Polym. Sci. A Polym. Chem.* **2009**, *47* (17), 4332-4345. DOI: https://doi.org/10.1002/pola.23486.
(312) Liu, W.; Greytak, A. B.; Lee, J.; Wong, C. R.; Park, J.; Marshall, L. F.; Jiang, W.; Curtin, P. N.; Ting, A. Y.; Nocera, D. G.; Fukumura, D.; Jain, R. K.; Bawendi, M. G. Compact Biocompatible Quantum Dots via RAFT-Mediated Synthesis of Imidazole-Based Random Copolymer Ligand. *J. Am. Chem. Soc.* **2010**, *132* (2), 472-483. DOI: https://doi.org/10.1021/ja908137d.
(313) Romuald, C.; Busseron, E.; Coutrot, F. Very Contracted to Extended co-Conformations with or without Oscillations in Two- and Three-Station [c2]Daisy Chains. *J. Org. Chem.* **2010**, *75* (19), 6516-6531. DOI: https://doi.org/10.1021/jo101234u.
(314) Liu, Y.; Pauloehrl, T.; Presolski, S. I.; Albertazzi, L.; Palmans, A. R.; Meijer, E. W. Modular Synthetic Platform for the Construction of Functional Single-Chain Polymeric Nanoparticles: From Aqueous Catalysis to Photosensitization. *J. Am. Chem. Soc.* **2015**, *137* (40), 13096-13105. DOI: https://doi.org/10.1021/jacs.5b08299.
(315) Gaballa, H.; Shang, J.; Meier, S.; Theato, P. The glucose-responsive behavior of a block copolymer featuring boronic acid and glycine. *J. Polym. Sci., Part A: Polym. Chem.* **2018**, *57* (3), 422-431. DOI: https://doi.org/10.1002/pola.29226.
(316) Liu, M.; Wang, X.; Miao, D.; Wang, C.; Deng, W. Synthesis of well-defined heteroglycopolymers via combining sequential click reactions and PPM: the effects of linker and heterogeneity on Con A binding. *Polym. Chem.* **2020**, *11* (17), 3054-3065. DOI: https://doi.org/10.1039/D0PY00302F.

(317) Beija, M.; Li, Y.; Lowe, A. B.; Davis, T. P.; Boyer, C. Factors influencing the synthesis and the post-modification of PEGylated pentafluorophenyl acrylate containing copolymers. *Eur*. *Polym*. *J*. **2013**, *49* (10), 3060-3071. DOI: https://doi.org/10.1016/j.eurpolymj.2013.05.003.
(318) Hoffmann, J. F.; Roos, A. H.; Schmitt, F. J.; Hinderberger, D.; Binder, W. H. Fluorescent and Water Dispersible Single-Chain Nanoparticles: Core-Shell Structured Compartmentation. *Angew*. *Chem*. *Int*. *Ed*. **2021**, *60* (14), 7820-7827. DOI: https://doi.org/10.1002/anie.202015179.
(319) Danopoulos, A. A.; Simler, T.; Braunstein, P. N-Heterocyclic Carbene Complexes of Copper, Nickel, and Cobalt. *Chem*. *Rev*. **2019**, *119* (6), 3730-3961. DOI: https://doi.org/10.1021/acs.chemrev.8b00505.
(320) Sammon, M. S.; Biewend, M.; Michael, P.; Schirra, S.; Oncak, M.; Binder, W. H.; Beyer, M. K. Activation of a Copper Biscarbene Mechano-Catalyst Using Single-Molecule Force Spectroscopy Supported by Quantum Chemical Calculations. *Chem*. *Eur*. *J*. **2021**, *27* (34), 8723-8729. DOI: https://doi.org/10.1002/chem.202100555.
(321) van Oers, M. C.; Abdelmohsen, L. K.; Rutjes, F. P.; van Hest, J. C. Aqueous asymmetric cyclopropanation reactions in polymersome membranes. *Chem*. *Commun*. **2014**, *50* (31), 4040-4043. DOI: https://doi.org/10.1039/C3CC48865A.
(322) Engelke, J.; Brandt, J.; Barner-Kowollik, C.; Lederer, A. Strengths and limitations of size exclusion chromatography for investigating single chain folding – current status and future perspectives. *Polym*. *Chem*. **2019**, *10* (25), 3410-3425. DOI: https://doi.org/10.1039/C9PY00336C.
(323) Gou, X.; Wang, G.; Yang, J.; Park, J.; Wexler, D. Chemical synthesis, characterisation and gas sensing performance of copper oxide nanoribbons. *J*. *Mater*. *Chem*. **2008**, *18* (9), 965-969. DOI: https://doi.org/10.1039/B716745H.
(324) Liu, D.; Kottke, I. Subcellular localization of copper in the root cells of Allium sativum by electron energy loss spectroscopy (EELS). *Bioresour*. *Technol*. **2004**, *94* (2), 153-158. DOI: https://doi.org/10.1016/j.biortech.2003.12.003.
(325) Leapman, R. D.; Andrews, S. B. Characterization of biological macromolecules by combined mass mapping and electron energy-loss spectroscopy. *J*. *Microsc*. **1992**, *165* (2), 225-238. DOI: https://doi.org/10.1111/j.1365-2818.1992.tb01482.x.
(326) Evans, D. A.; Barnes, D. M.; Johnson, J. S.; Lectka, T.; von Matt, P.; Miller, S. J.; Murry, J. A.; Norcross, R. D.; Shaughnessy, E. A.; Campos, K. R. Bis(oxazoline) and Bis(oxazolinyl)pyridine Copper Complexes as Enantioselective Diels−Alder Catalysts: Reaction Scope and Synthetic Applications. *J*. *Am*. *Chem*. *Soc*. **1999**, *121* (33), 7582-7594. DOI: https://doi.org/10.1021/ja991191c.
(327) Evans, D. A.; Kozlowski, M. C.; Murry, J. A.; Burgey, C. S.; Campos, K. R.; Connell, B. T.; Staples, R. J. C2-Symmetric Copper(II) Complexes as Chiral Lewis Acids. Scope and Mechanism of Catalytic Enantioselective Aldol Additions of Enolsilanes to (Benzyloxy)acetaldehyde. *J*. *Am*. *Chem*. *Soc*. **1999**, *121* (4), 669-685. DOI: https://doi.org/10.1021/ja9829822.
(328) Johnson, J. S.; Evans, D. A. Chiral Bis(oxazoline) Copper(II) Complexes: Versatile Catalysts for Enantioselective Cycloaddition, Aldol, Michael, and Carbonyl Ene Reactions. *Acc*. *Chem*. *Res*. **2000**, *33* (6), 325-335. DOI: https://doi.org/10.1021/ar960062n.
(329) Williamson, K. S.; Yoon, T. P. Iron Catalyzed Asymmetric Oxyamination of Olefins. *J*. *Am*. *Chem*. *Soc*. **2012**, *134* (30), 12370-12373. DOI: https://doi.org/10.1021/ja3046684.
(330) Fu, N.; Song, L.; Liu, J.; Shen, Y.; Siu, J. C.; Lin, S. New Bisoxazoline Ligands Enable Enantioselective Electrocatalytic Cyanofunctionalization of Vinylarenes. *J*. *Am*. *Chem*. *Soc*. **2019**, *141* (37), 14480-14485. DOI: https://doi.org/10.1021/jacs.9b03296.
(331) Püllmann, P.; Ulpinnis, C.; Marillonnet, S.; Gruetzner, R.; Neumann, S.; Weissenborn, M. J. Golden Mutagenesis: An efficient multi-site-saturation mutagenesis approach by Golden Gate cloning with automated primer design. *Sci*. *Rep*. **2019**, *9* (1), 10932. DOI: https://doi.org/10.1038/s41598-019-47376-1.
(332) Cabantous, S.; Waldo, G. S. In vivo and in vitro protein solubility assays using split GFP. *Nat*. *Methods* **2006**, *3* (10), 845-854. DOI: https://doi.org/10.1038/nmeth932.
(333) Kröger, A. P. P.; Paats, J.-W. D.; Boonen, R. J. E. A.; Hamelmann, N. M.; Paulusse, J. M. J. Pentafluorophenyl-based single-chain polymer nanoparticles as a versatile platform towards protein mimicry. *Polym*. *Chem*. **2020**, *11* (37), 6056-6065. DOI: https://doi.org/10.1039/D0PY00922A.

Curriculum Vitae

Vor- und Zuname: Vico Keve Bernhard Adjedje, M.Sc. Chemie

Arbeitserfahrung

03/2019-11/2023	Wissenschaftlicher Mitarbeiter– Martin-Luther Universität Halle-Wittenberg
06/2014-06/2015	Werkstudent im QM für Forgings – Siemens AG (Gasturbinenwerk Berlin)
08/2009-09/2011	Gründer und stellvertretender Geschäftsführer – Eventgarde UG

Studium

03/2019 - heute	Promotion zum Thema „Enzymatic and Chemical Modifications of Oligoenes and Polyenes “ Martin-Luther-Universität Halle Wittenberg, Naturwissenschaftliche Fakultät II, Institut für Chemie, Makromolekulare Chemie
04/2015 - 05/2018	Master of Science (Chemistry), Freie Universität Berlin Masterthesis: „Synthesis & Characterization of Biodegradable Polymers” AK Prof. Dr. Marie Weinhart (Polymere und Biomaterialien) Forschungspraktika: AK Prof. Dr. Daniel Klinger, Ingénierie et Archtitectures Macromoléculaires bei Dr. Christine Joly-Duhamel, AK Prof. Dr. Christian Müller
09/2016 - 03/2017	ERASMUS: Ecole Nationale Supérieur de Chimie Montpellier
10/2013 - 09/2016	Bachelor of Science (Chemistry), Freie Universität Berlin Bachelorthesis: „Coordination Chemistry of 2-(2-Pyridyl)-4,6-diphenyl-λ^3-Phosphinine with Gold(I) & Silver(I)“ AK Prof. Dr. Christian Müller (Phosphorchemie)

Schulausbildung

09/2002 - 12/2011	Melanchthon Gymnasium Nürnberg
09/1998 - 07/2002	Bartholomäus-Grundschule Nürnberg

Wissenschaftliche Veröffentlichungen

Als Erstautor:

“Enzymatic degradation of synthetic polyisoprenes *via* surfactant-free polymer emulsification” V. K. B. Adjedje, E. Schell, Y. L. Wolf, A. Laub, M. J. Weissenborn, W. H. Binder, *Green Chem. 2021*, *23*, 9433-9438. DOI: 10.1039/D1GC03515K

“Rubber Oxygenase Degradation Assay by UV-Labeling and Gel Permeation Chromatography” V. K. B. Adjedje, Y. L. Wolf, M. J. Weissenborn, W. H. Binder, *Macromol. Rapid Commun.* **2024**, 2400032. DOI: 10.1002/marc.202400032

Als Coautor:

*“*Design, Synthesis and Characterization of Vitrimers with Low Topology Freezing Transition Temperature*”,* B. P. Krishnan, K. Saalwächter, V. K. B. Adjedje, W. H. Binder, *Polymers* **2022**, *14*, 2456. DOI: 10.3390/polym14122456

Konferenzbeiträge:

“Enzymatic degradation of synthetic polyisoprenes via surfactant-free polymer emulsification”, Vico K. B. Adjedje, Eugen Schell, Yannick L. Wolf, Annegret Laub, Martin J. Weissenborn, Wolfgang H. Binder, *Bordeaux Polymer Conference* **2022**, Poster

Eigenständigkeitserklärung

Hiermit erkläre ich an Eides statt, dass ich die vorliegende Arbeit selbstständig und ohne fremde Hilfe verfasst habe. Andere als die angegebenen Quellen und Hilfsmittel wurden nicht benutzt und die den benutzten Werken wörtlich oder inhaltlich entnommenen Stellen wurden als solche kenntlich gemacht.
Außerdem erkläre ich, die vorliegende Dissertation an keiner anderen wissenschaftlichen Einrichtung zur Erlangung eines akademischen Grades eingereicht zu haben.

Halle (Saale), den

_____

Vico Keve Bernhard Adjedje

7. Appendix

7. 1 Procedures by collaborators

Expression in shake flask

For expression of Lcp_{K30}-WT and all PROSS or FuncLib variants an overnight grown pre-culture (TB medium and 50 µg/ml kanamycin) was used to inoculate the main culture 1:100, consisting of auto-induction TB medium with the addition of heme precursors (100 µM $FeCl_3$ and 100 µM 5-aminolevulinic acid) and antibiotics (50 µg/ml kanamycin). For best cell growth the culture was incubated at 120 rpm and 37 °C for 3h before the cultures were cooled on ice for half an hour and afterwards incubated at 120 rpm and 25 °C for 24 hours. Harvest of the cells was performed by centrifugation at 4 °C and 3000 g for 30 minutes in large centrifuge bakers and following transfer to weighed falcon tubes.

Protein purification

Cell pellets were resuspended in lysis buffer (100 mM KPi pH 7.7; 150 mM NaCl, 1 mg/mL lysozyme, 100 µg/mL DNAse I), homogenized by sonication (Bandelin Sonoplus HD3100: 3x30 s, 70 % amplitude, pulse mode) and lysed using a cell disruptor (2 cycles, 1,3 kbar, model TS2, Constant Systems Ltd, Daventry, United Kingdom). After centrifugation (15500 g, 4 °C, 20 min) the cleared cell extract was applied onto a 5 mL Strep-Tactin®XT gravity flow column (IBA GmbH, Göttingen, Germany). Unbound protein was washed out with 5x5 mL binding buffer (100 mM KPi pH 7,7; 150 mM NaCl) and the protein of interest was eluted with 6x2 mL of binding buffer containing 50 mM biotin.
For buffer exchange PD-10 columns were used according to the manufacturer's protocol (GE Healthcare Europe GmbH, Freiburg, Germany). 20 mM KPi pH 7 was used as storage buffer. Samples were then flash frozen in liquid nitrogen and stored at -20 °C. The concentration of purified Lcp_{K30} was determined by absorbance at 412 nm (ε=80000 M-1 cm-1)[3 SI].

Potassium phosphate activity maximum optimum determination

Latex milk stock solution (60 % PI) was diluted with freshly prepared potassium phosphate buffer pH 7 to result in a 0.2 w/v% and in either 1 mM or 2 mM or 5 mM or 10 mM or 20 mM or 50 mM or 100 mM KPi concentration at a volume of 1 mL. The Lcp_{K30} was added, and the reaction was conducted at room temperature. The degradation products were extracted via liquid to liquid extraction with ethyl acetate and the solvent of the extracts was evaporated in vacuo. UHPLC analysis was performed to track the oligoisoprenoidic fragments produced during the enzymatic degradation and compare their peak intensity at different potassium phosphate buffer concentrations.

7. 2 Supplementary Data

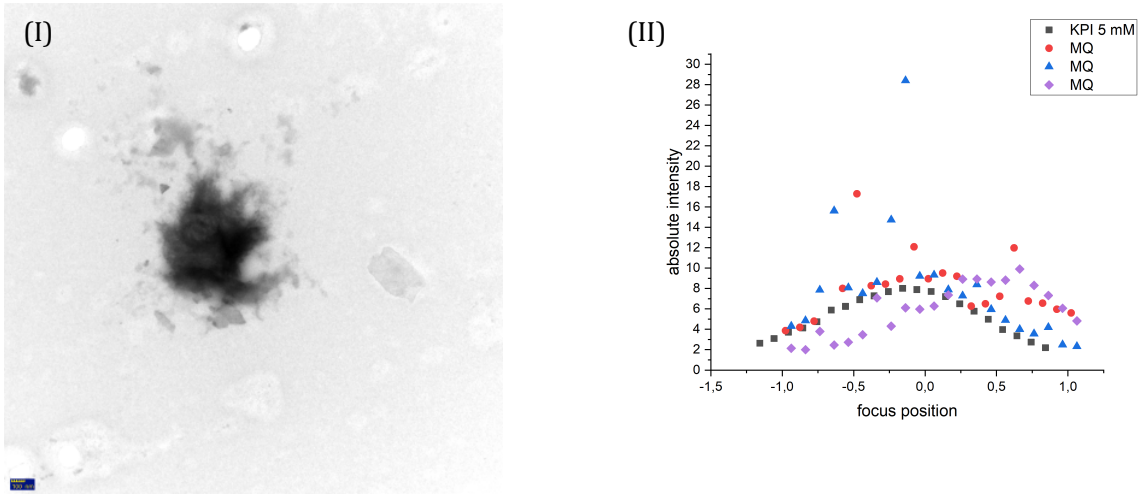

Figure A1. TEM image of acoustically emulsified **PI 3000** (**A 1**) as micrometer-sized polyisoprene droplet. **PI 3000** as **A 1** was dispersed but no supramolecular structure can be determined. (I) Refractive index determination of KPi 5 mM. (II)

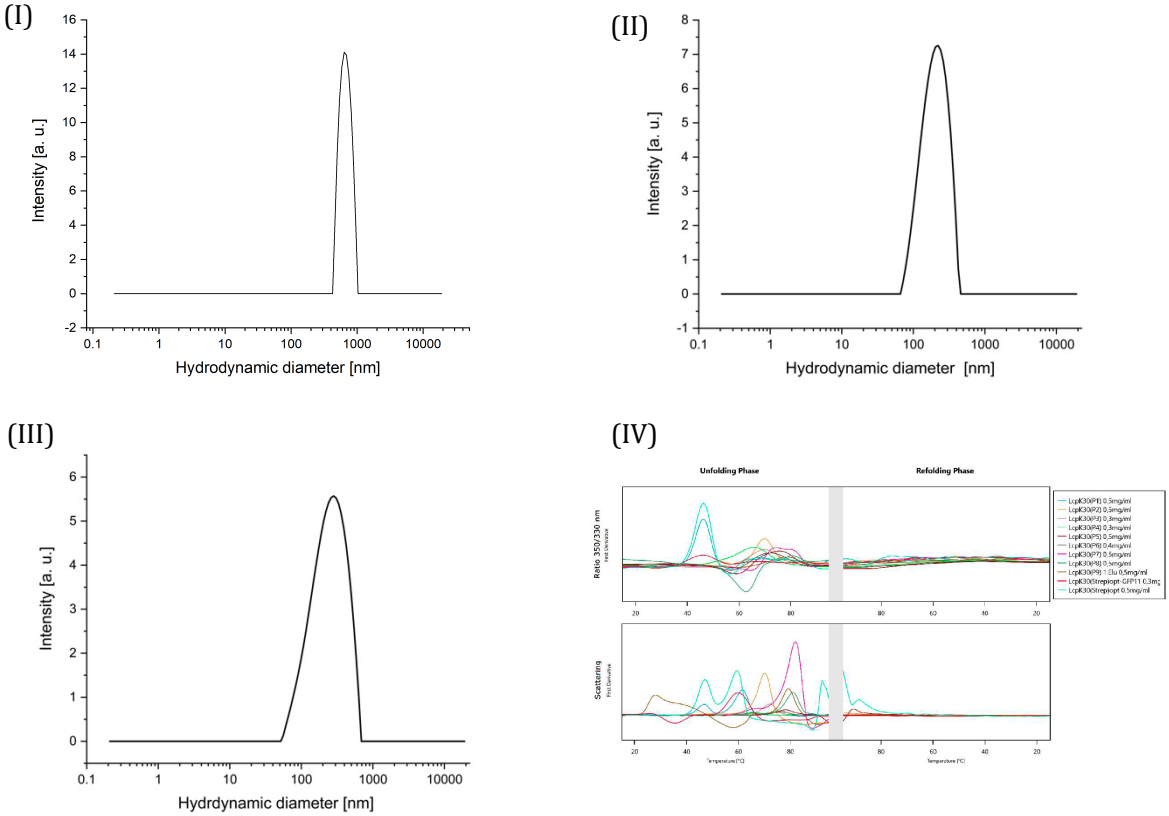

Figure A2. Dynamic light scattering (DLS) of latex milk sample L 1 with a hydrodynamic diameter of 750 nm. (I) DLS of **PI 4500** with a hydrodynamic diameter of 200 nm. (II) DLS of **PB 12000** with a hydrodynamic diameter of 240 nm. (III) Determination of T_M and T_A-values of Lcp_{K30}-PROSS-Variants by Nano-DSF. First derivative of the fluorescence at 350 nm to 330 nm (ratio) and light scattering are plotted against temperature. Provided by E. Schell and Y. L. Wolf (IV).

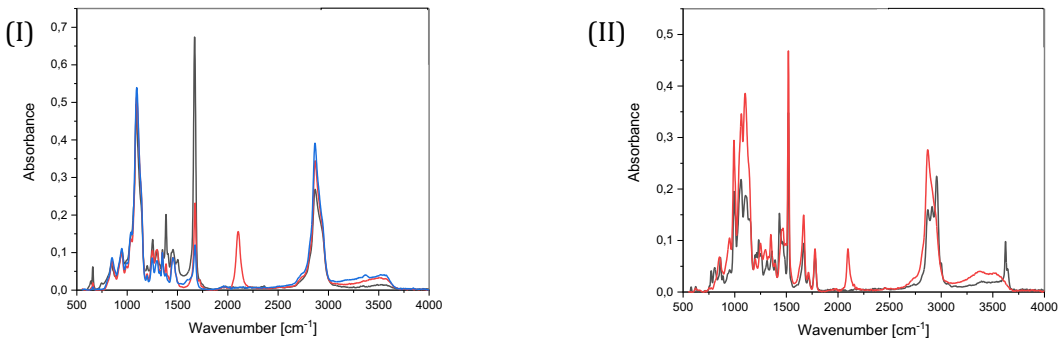

Figure A3. End group modification according to IR spectroscopy of **13**, PEG-Cl (black), PEG-N_3 (red), PEG-NH_2 (blue) (I). Conversion of **MPFPM-1** (red) according to copper catalzyed alkyne azide catalyzed collapse strategy (red) according to IR spectroscopy (II). In collaboration with Mohamed Hassan.

7. 3 UHPLC-Data

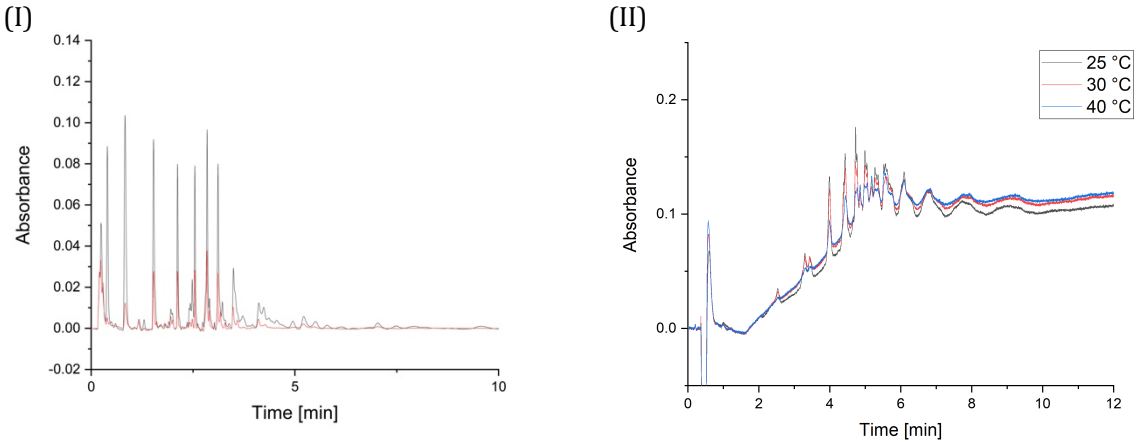

Figure A4. Stacked UHPLC chromatogram for the degradation inhibition by *n*-hexadecane at different ratios. Stacked UHPLC curves of two degradations runs with weight ratios of **PI *cis* 7000**: *n*-hexadecane of 1:1 (black) and 1:10 (red). (I) Stacked UV-UHPLC chromatograms, with gradient, of the enzymatic degradation of **PI 3000** at 25 °C (black), 30 °C (red) and 40 °C (blue). (II)

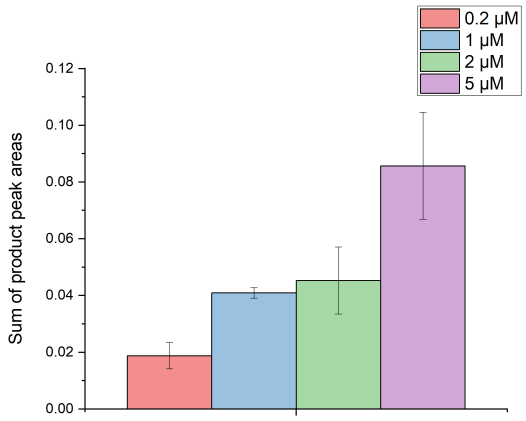

Figure A5. Integrated sum area of product peaks of enzymatic degradations of **PI 3000** at different enzyme loadings measured using UV-UHPLC measurements. Enzyme concentrations of 0.2 µM (red), 1 µM (blue), 2 µM (green) and 5 µM (purple). Triplicates to determine the standard deviation. In collaboration with E. Schell.

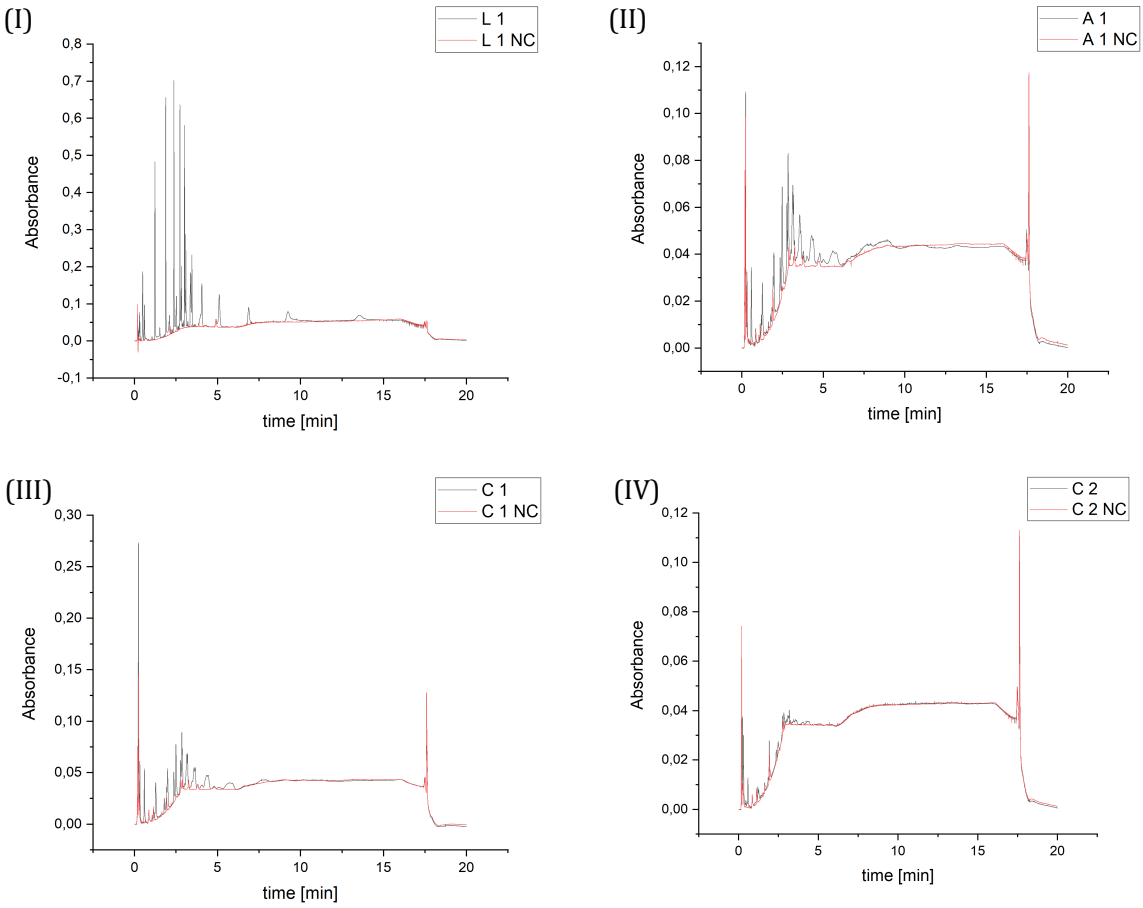

Figure A6. Separation of latex milk derived polyisoprene cleavage products (**L 1**; black) and negative control (L 1 NC; red) with UHPLC. (I), Separation of acoustically emulsified **PI 3000** derived polyisoprene cleavage products (**A 1**; black) and negative control (A 1 NC; red) with UHPLC. (II), Separation of co-solvent stabilized **PI 3000** derived polyisoprene cleavage products (**C 1**; black) and negative control (C 1 NC; red) with UHPLC. (III), Separation of co-solvent stabilized **PI 15 000** derived polyisoprene cleavage products (**C 2**; black) and negative control (C 2 NC; red) with UHPLC. (IV)

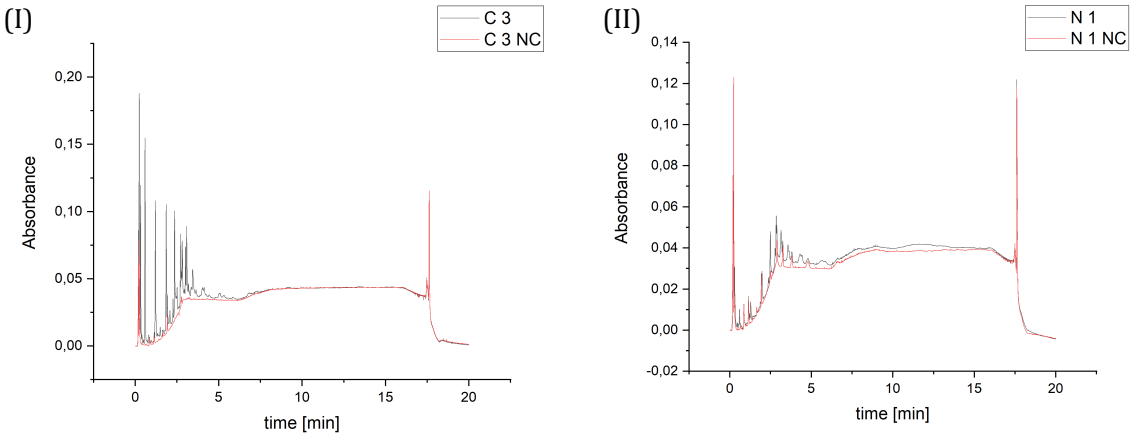

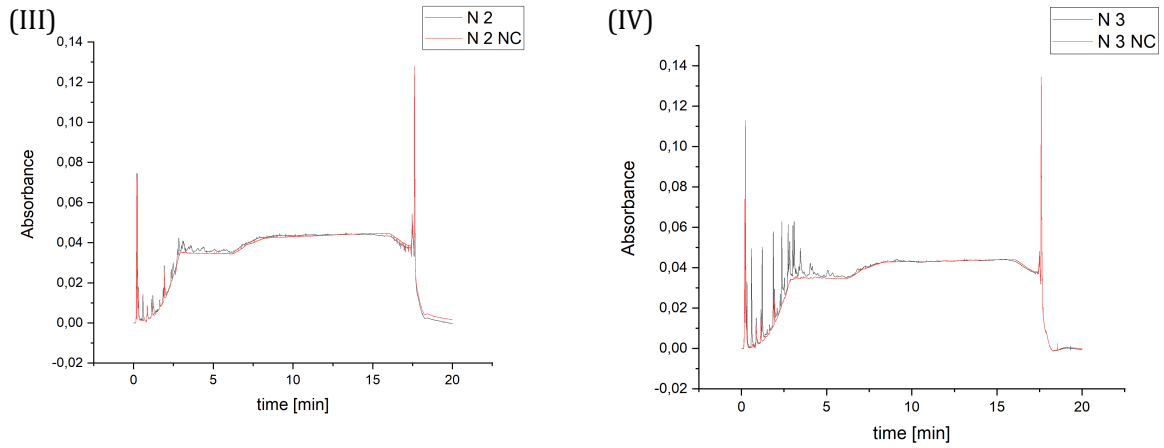

Figure A7. Separation of co-solvent stabilized **PI *cis* 7000** derived polyisoprene cleavage products (**C 3**; black) and negative control (C 3 NC; red) with UHPLC. (I) Separation of non-emulsified **PI 3000** derived polyisoprene cleavage products (**N 1**; black) and negative control (N 1 NC; red) with UHPLC. (II) Separation of non-emulsified **PI 15 000** derived polyisoprene cleavage products (**N 2**; black) and negative control (N 2 NC; red) with UHPLC. (III) Separation of non-emulsified **PI *cis* 7000** derived polyisoprene cleavage products (**N 3**; black) and negative control (N 3 NC; red) with UHPLC. (IV)

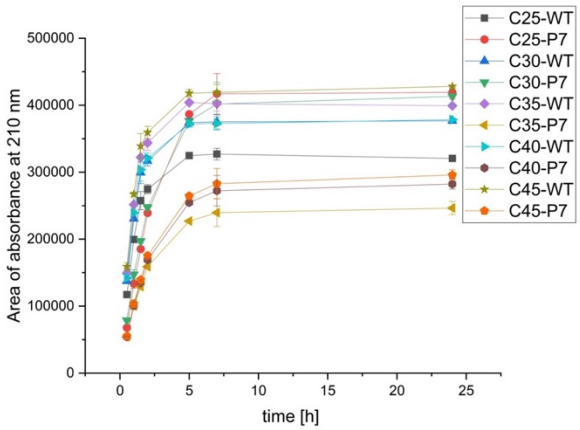

Figure A8. Area of absorbance of **L 1** degradation fragments of Lcp_{K30} and Lcp_{K30}-P7 according to UHPLC over reaction duration of 24 hours. In collaboration with Y. L. Wolf.

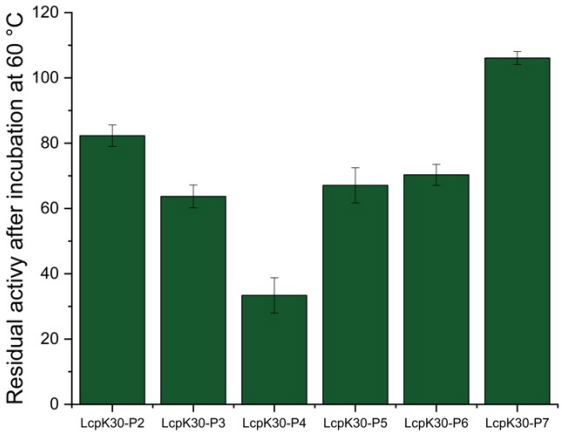

Figure A9. Initial screening of residual activity of Lcp_{K30}-PROSS Variants according to degradation fragment determination by area integration with UHPLC. In collaboration with E. Schell.

7.4 NMR-Data

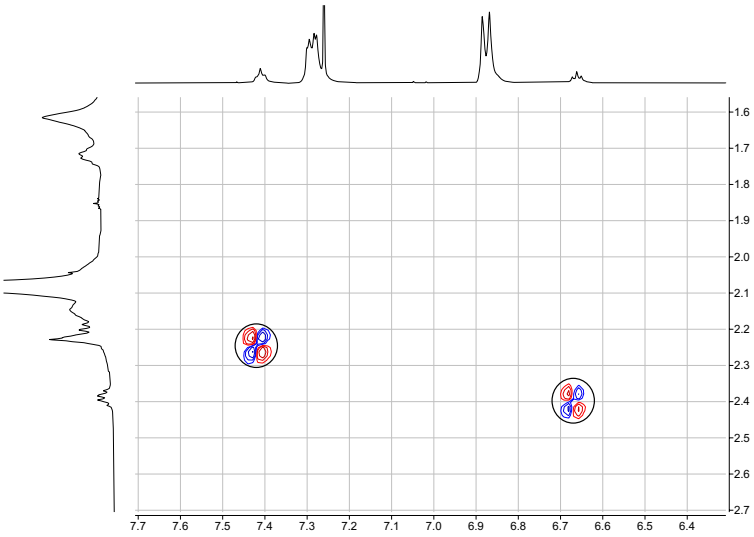

Figure A10. ^{1}H-^{1}H COSY 2D NMR of the respective derivatized end groups of **PB-200k-D**.

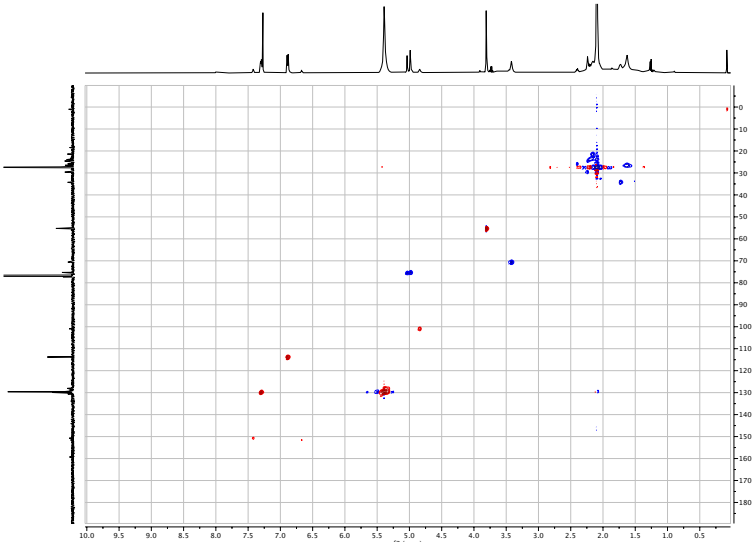

Figure A11**.** $^{1}H/^{3}C$ HSQC NMR of **PB 200k-D**.

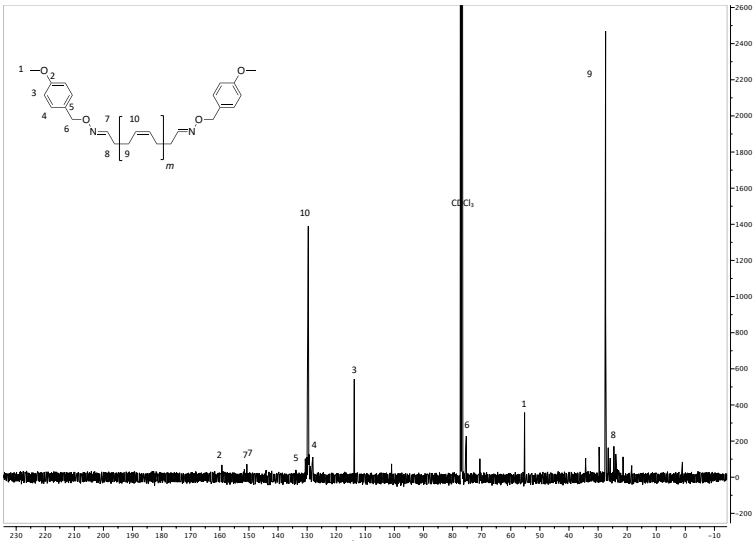

Figure A12. ^{13}C NMR of **PB 200k-D.**

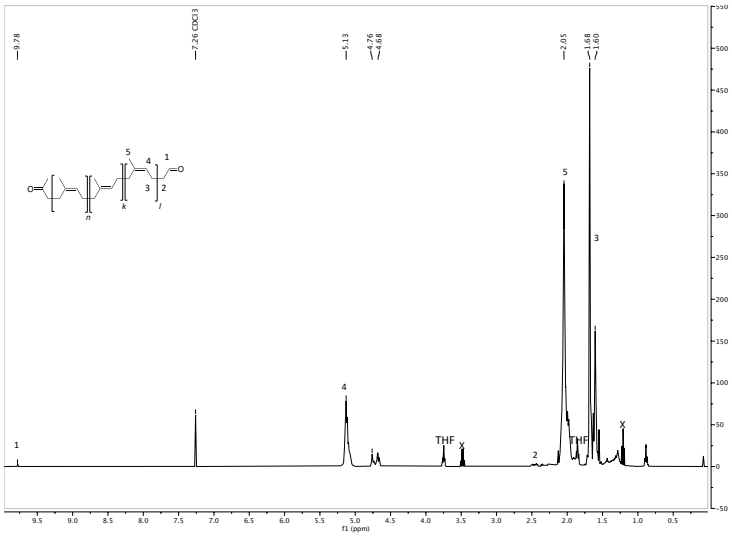

Figure A13. ^{1}H NMR of **PI 3000-Ox**. THF = residual tetrahydrofuran; X = residual diethyl ether.

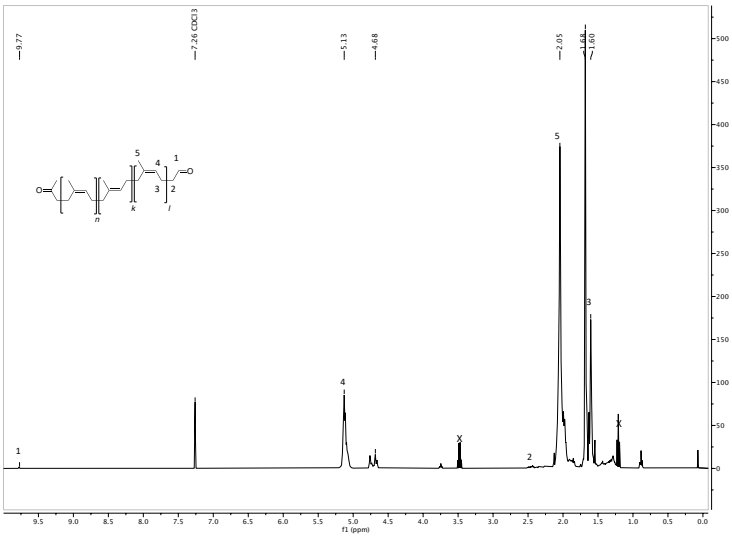

Figure A14. ^{1}H NMR of **PI 4500-Ox**. X = residual diethyl ether.

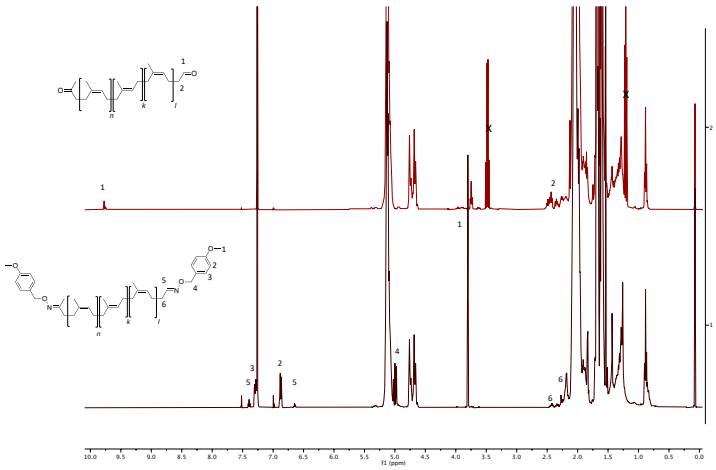

Figure A15**.** Stacked ^{1}H NMRs of **PI 3000-Ox** and **PI 3000-D**. X= diethylether.

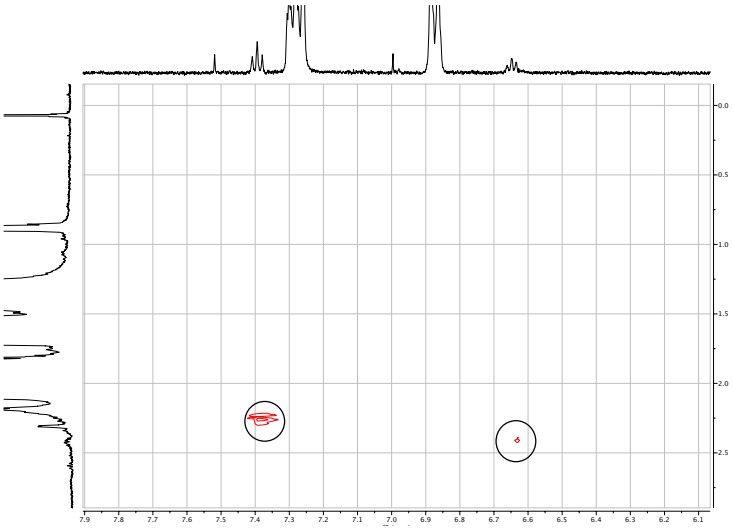

Figure A16. COSY NMR of the respective derivatized end groups of **PI 3000-D**.

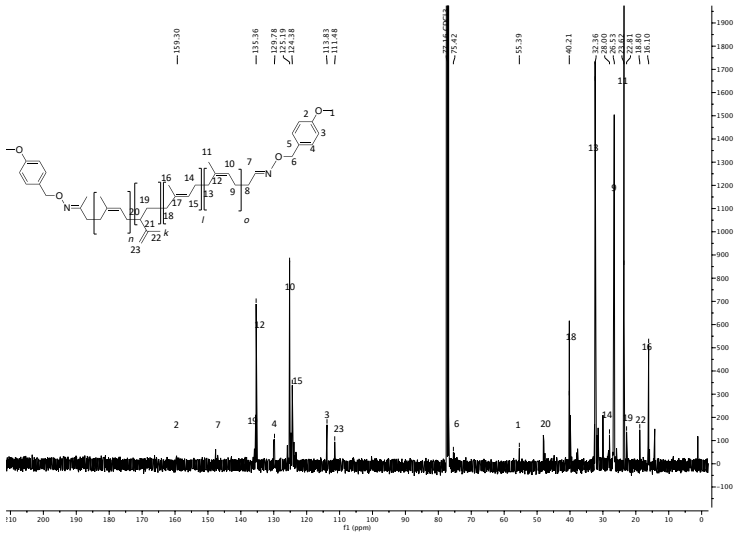

Figure A17. ^{13}C NMR of **PI 3000-D**.

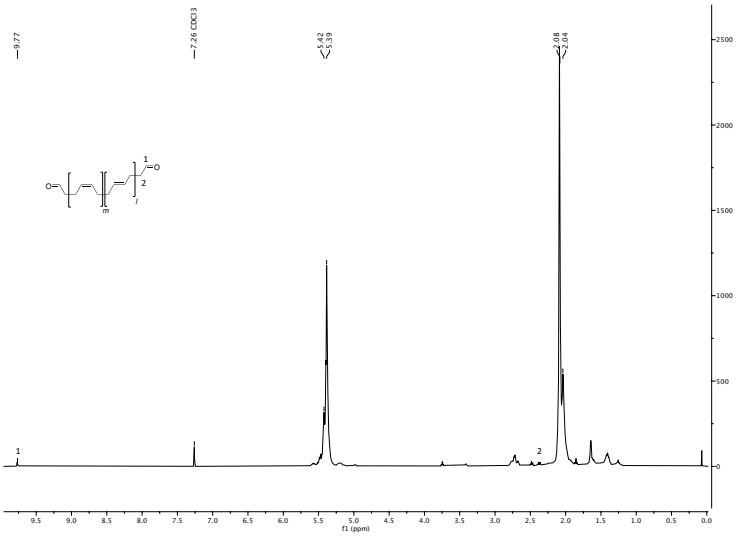

Figure A18. ^{1}H NMR of **PB 3500-Ox**.

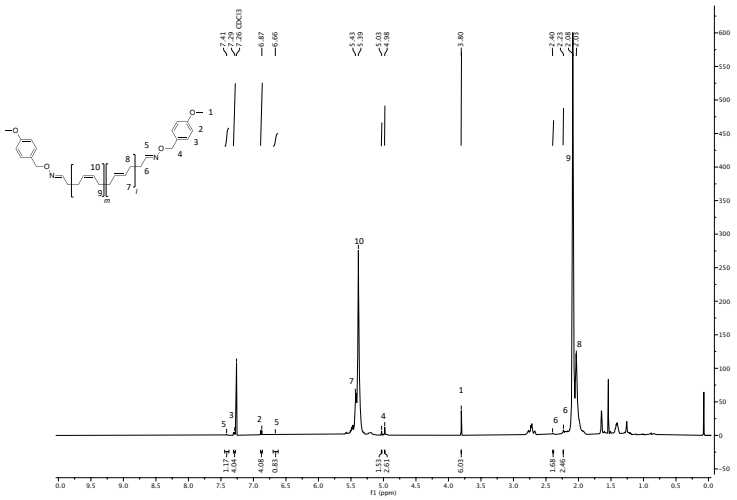

Figure A19. ^{1}H NMR of **PB 3500-D**.

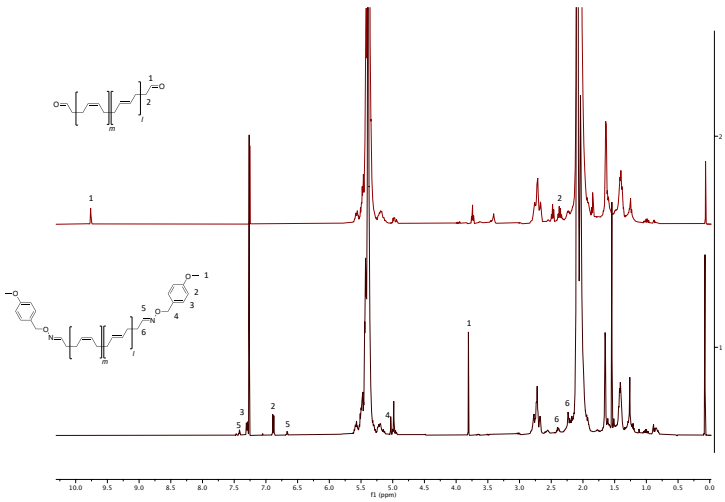

Figure A20. Stacked ^{1}H NMRs of **PB 3500-Ox** and **PB 3500-D**.

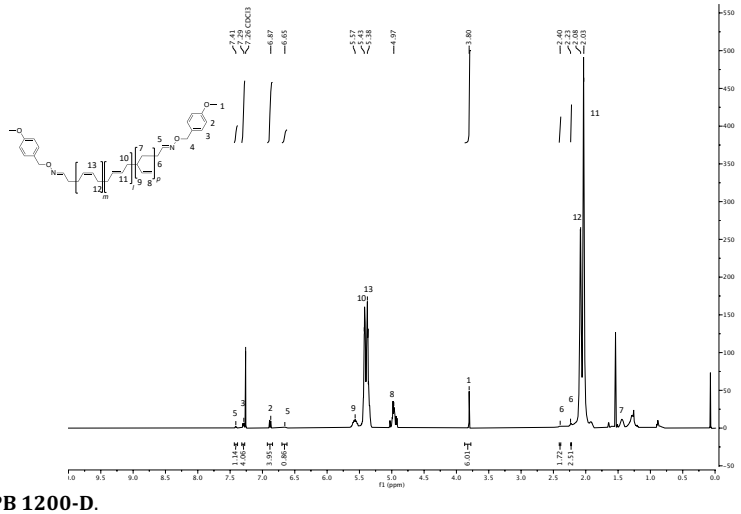

Figure A21. ^{1}H NMR of **PB 1200-D**.

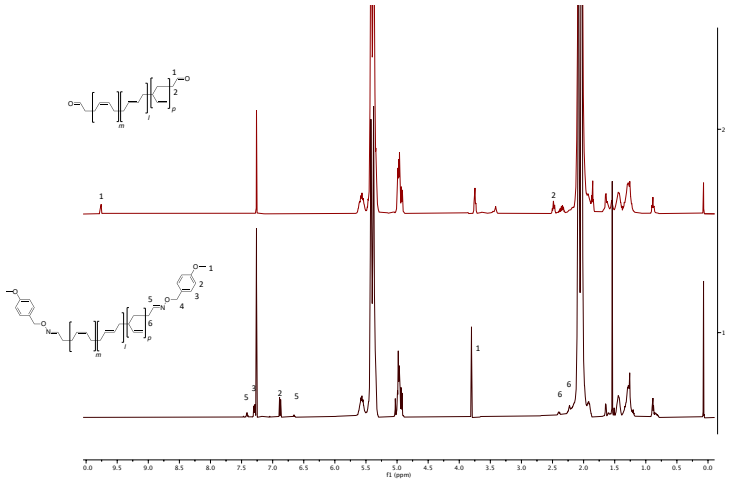

Figure A22. Stacked ^{1}H NMRs of **PB 12000-Ox** and **PB 12000-D**.

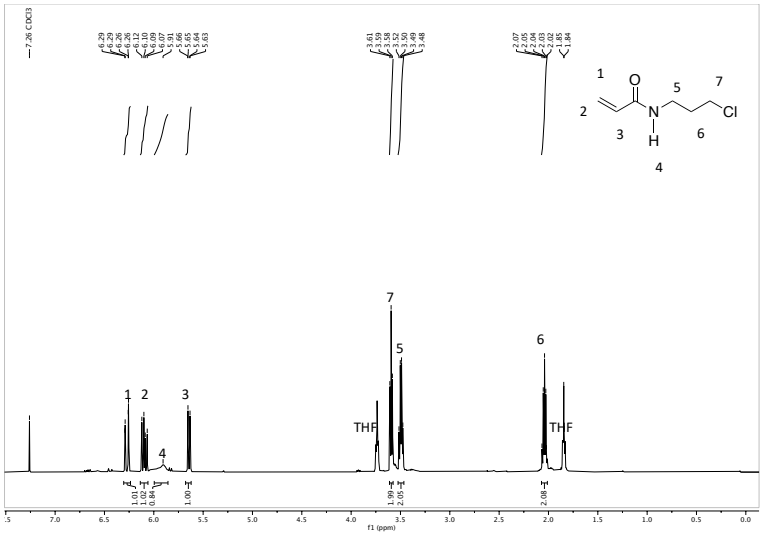

Figure A23. ^{1}H NMR of **1**.

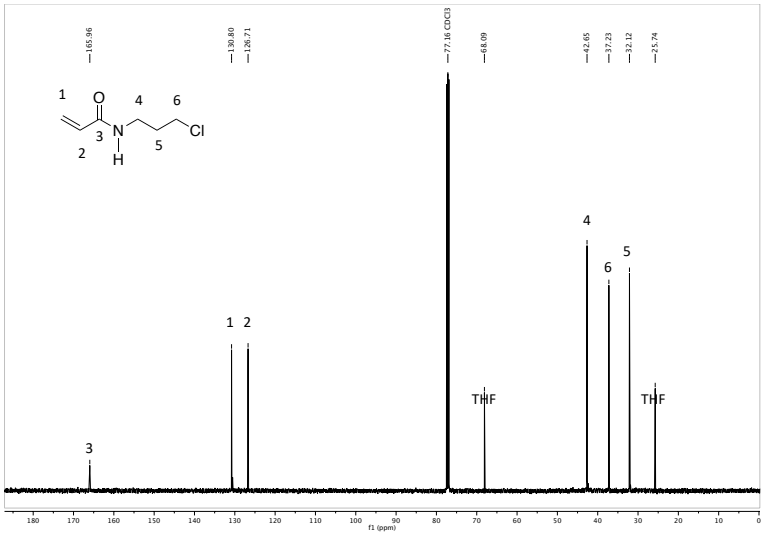

Figure A24. ^{13}C NMR of **1**.

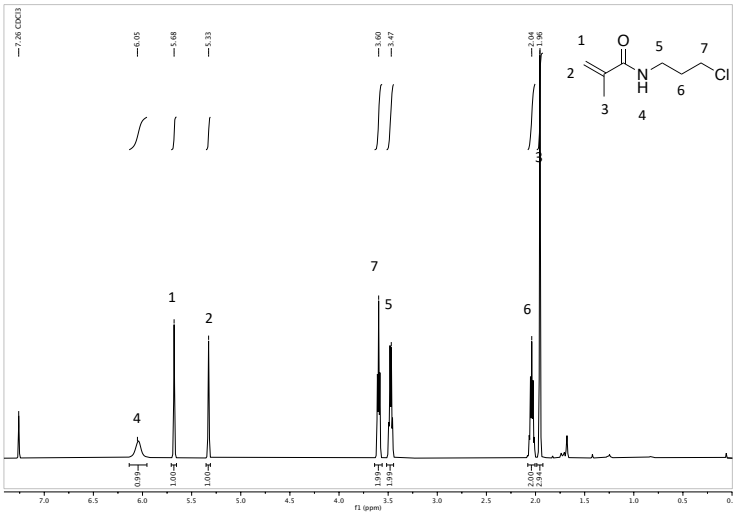

Figure A25. ^{1}H NMR of **2**.

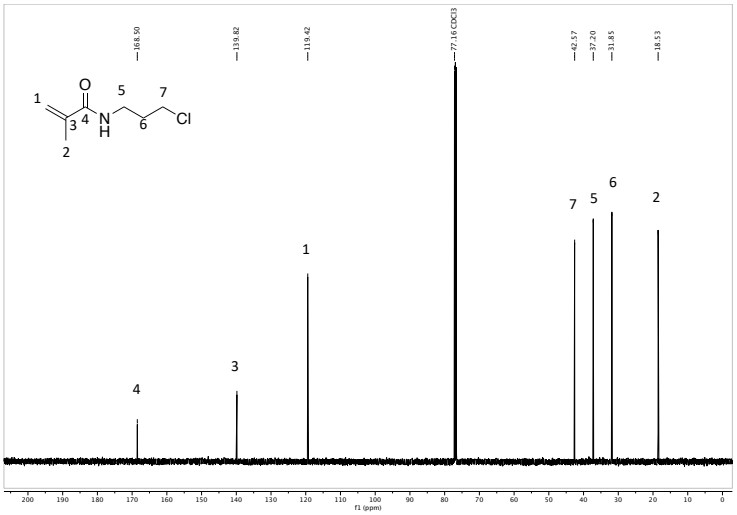

Figure A26. ^{13}C NMR of **2**.

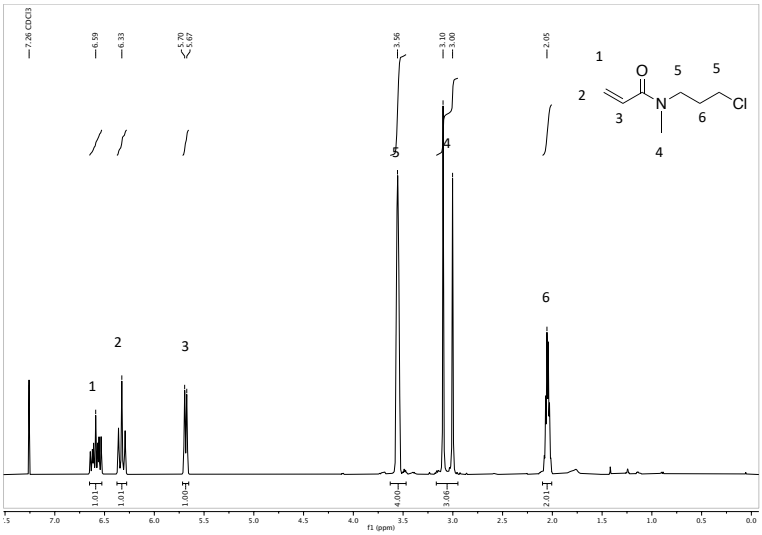

Figure A27. ^{1}H NMR of **3**.

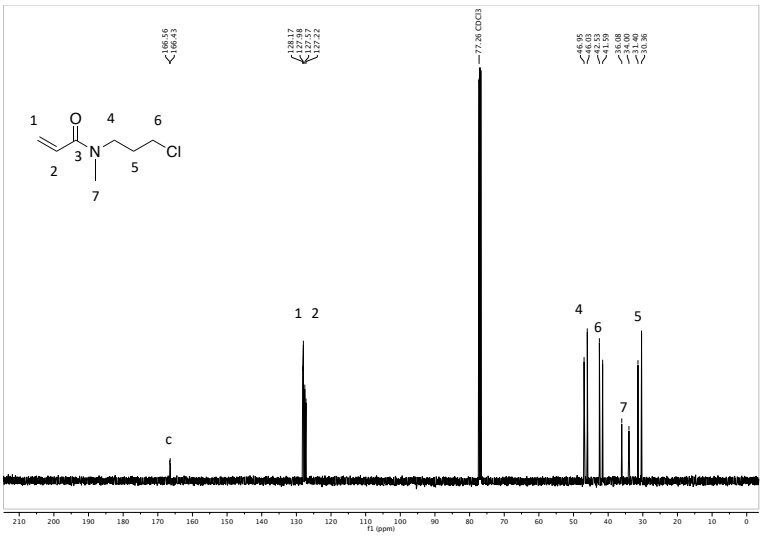

Figure A28. ^{13}C NMR of **3**.

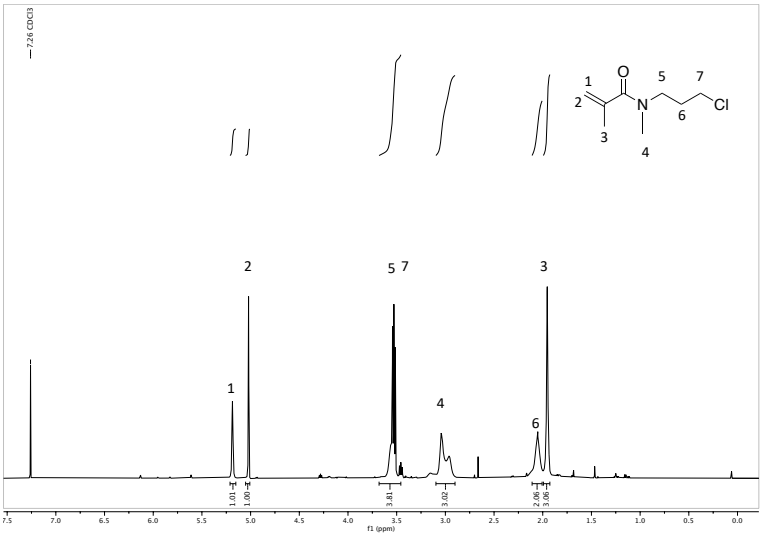

Figure A29. ^{1}H NMR of **4**.

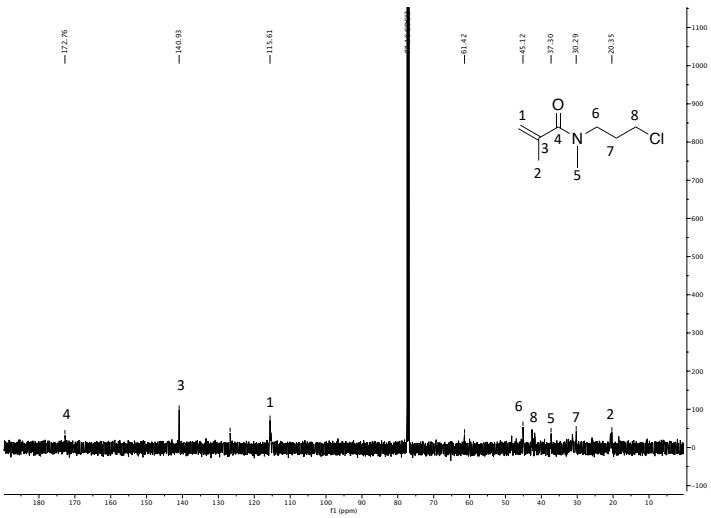

Figure A30. ^{13}C NMR of **4**.

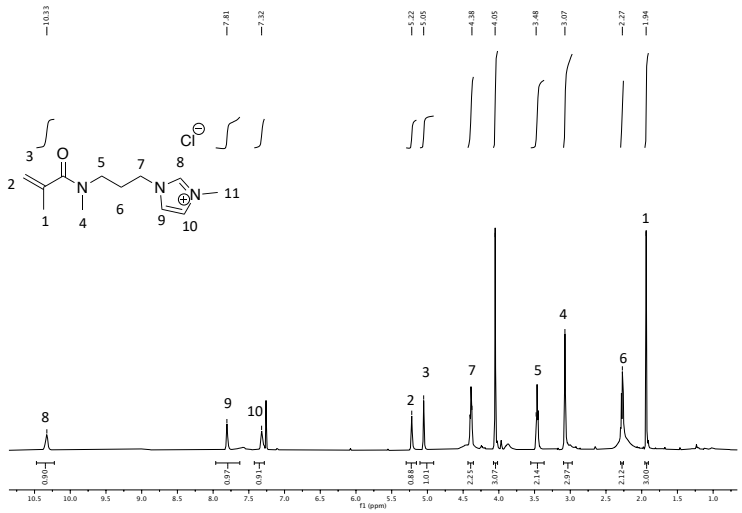

Figure A31. ^{1}H NMR of **5**.

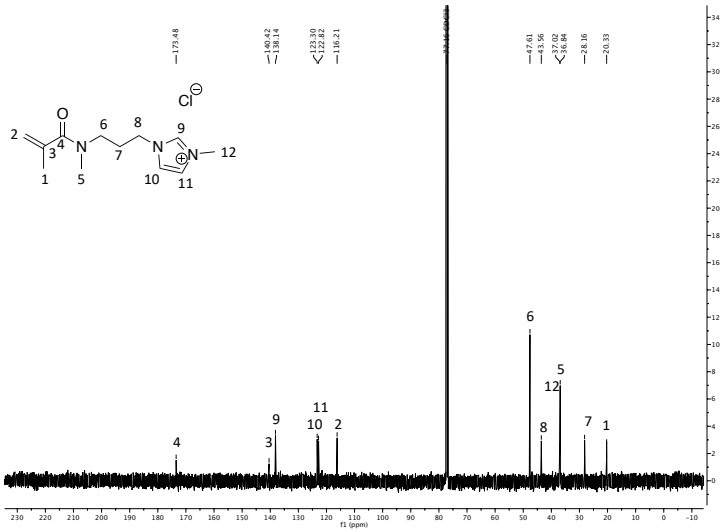

Figure A32. ^{13}C NMR of **5**.

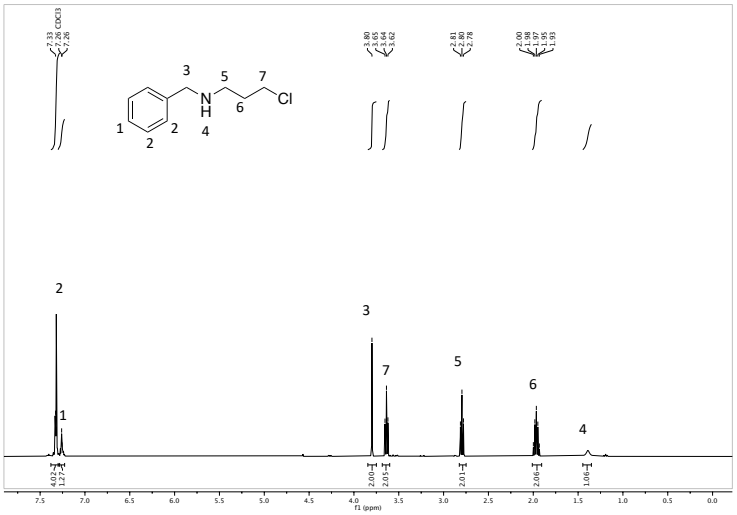

Figure A33. ^{1}H NMR of **6**.

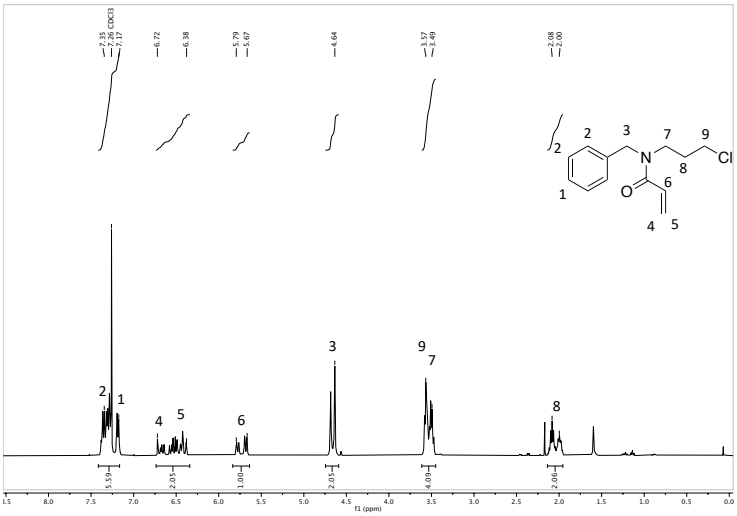

Figure A34. ^{1}H NMR of **7.**

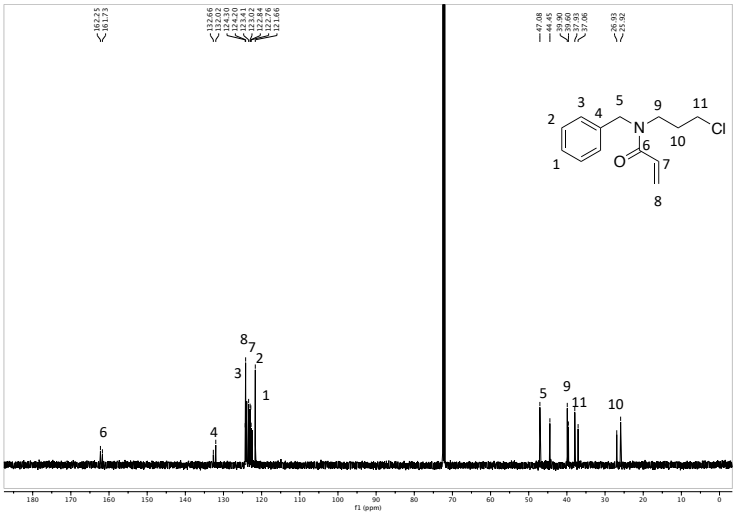

Figure A35. ^{13}C NMR of **7.**

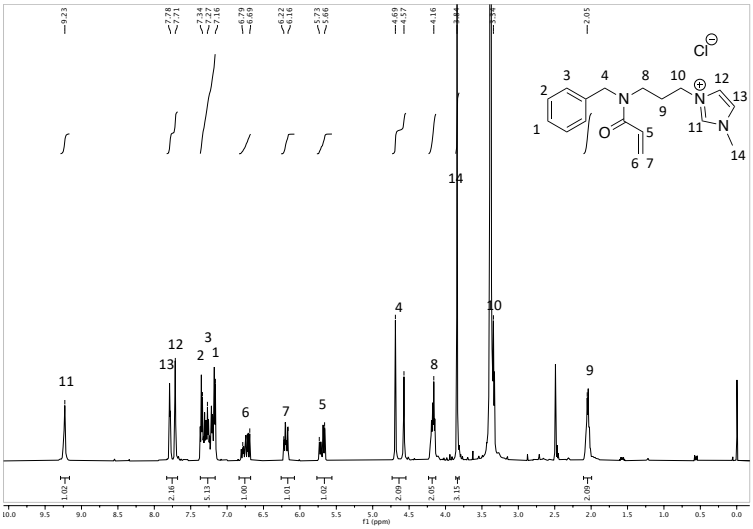

Figure A35. ^{1}H NMR of **8.**

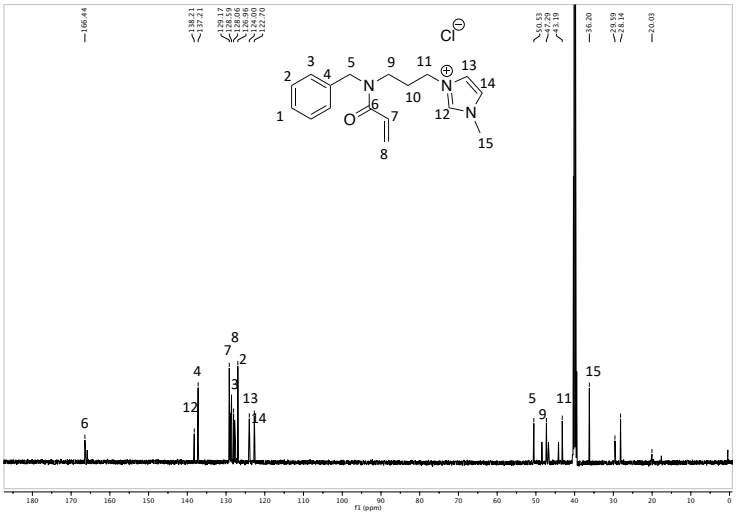

Figure A36. ^{13}C NMR of **8.**

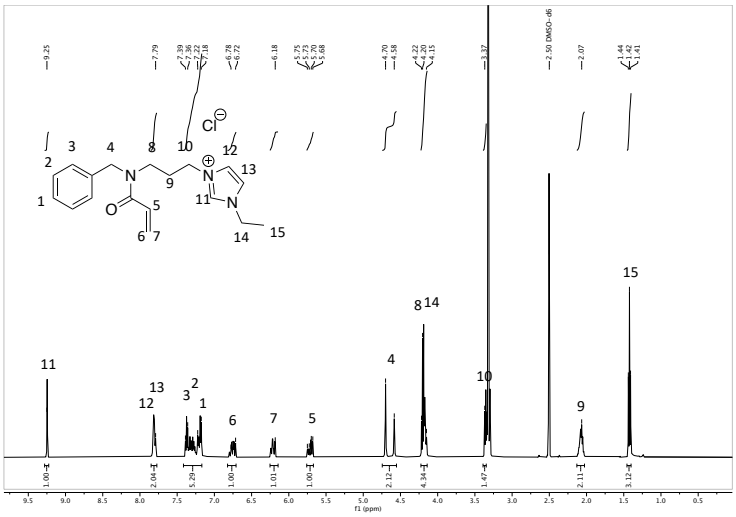

Figure A37. ^{1}H NMR of **9.**

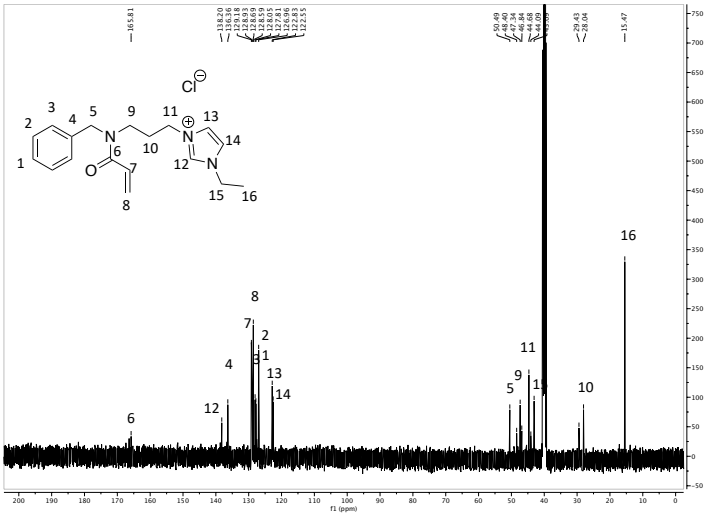

Figure A38. ^{13}C NMR of **9.**

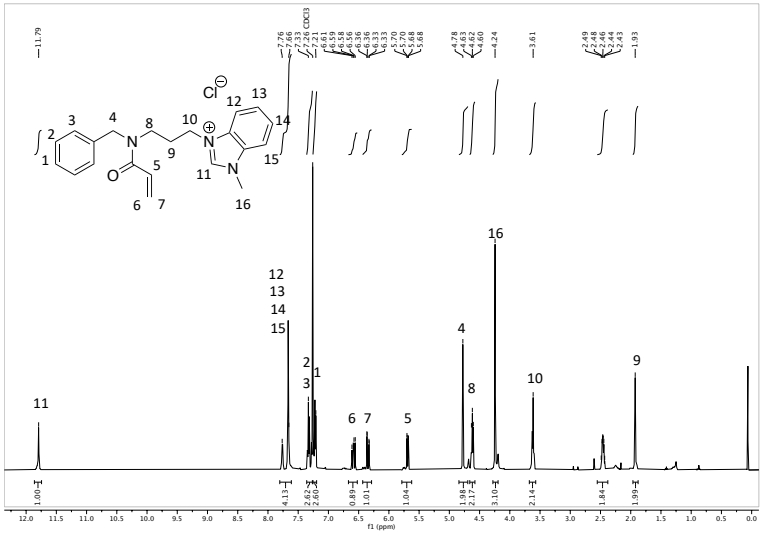

Figure A39. ^{1}H NMR of **10**.

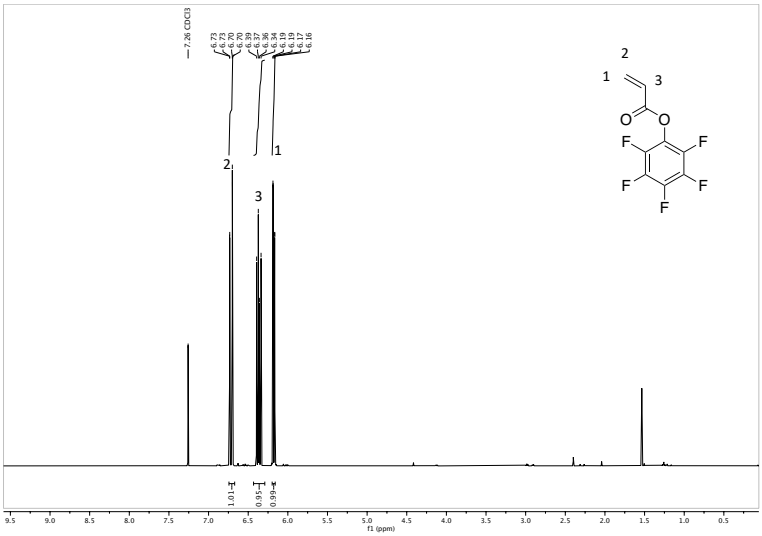

Figure A40. ^{1}H NMR of **11**.

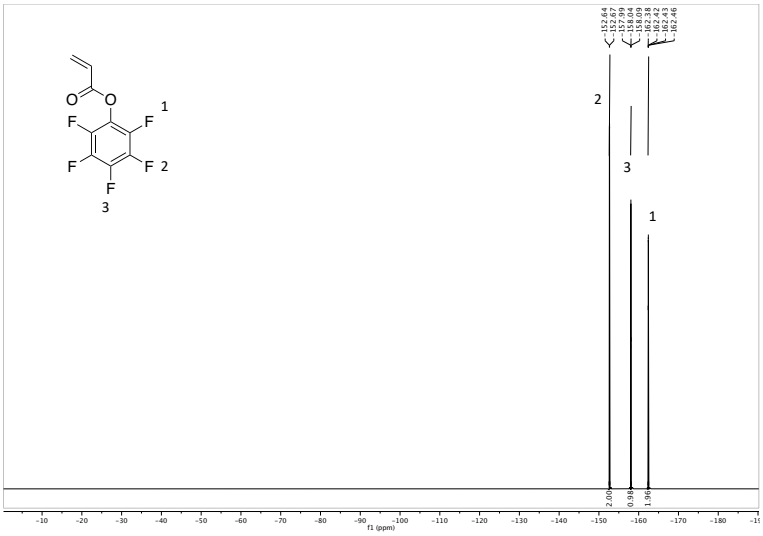

Figure A41. ^{19}F NMR of **11**.

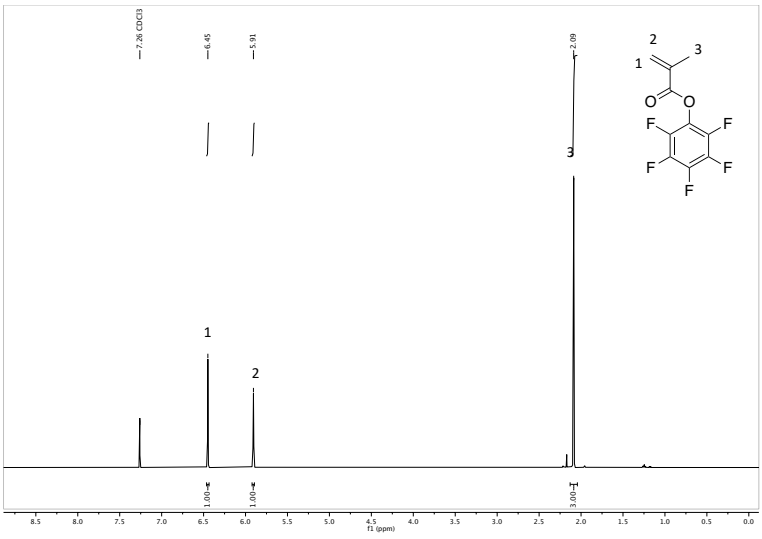

Figure A42. ^{1}H NMR of **12**.

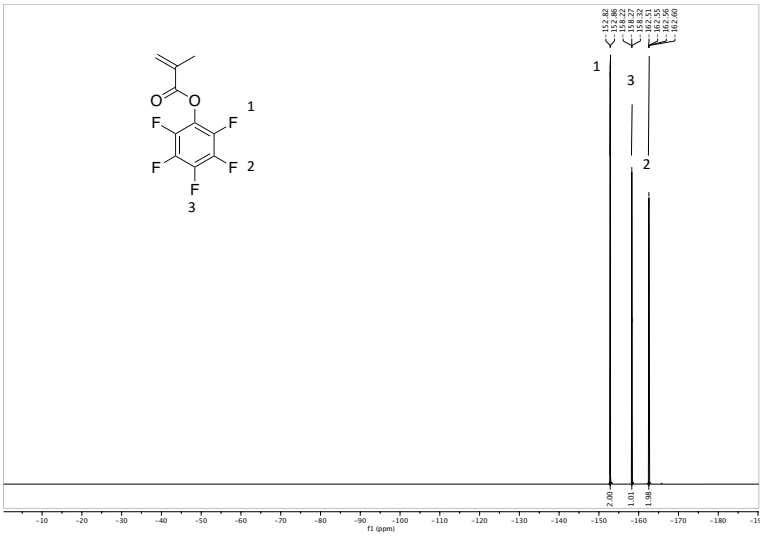

Figure A43. ^{19}F NMR of **12**.

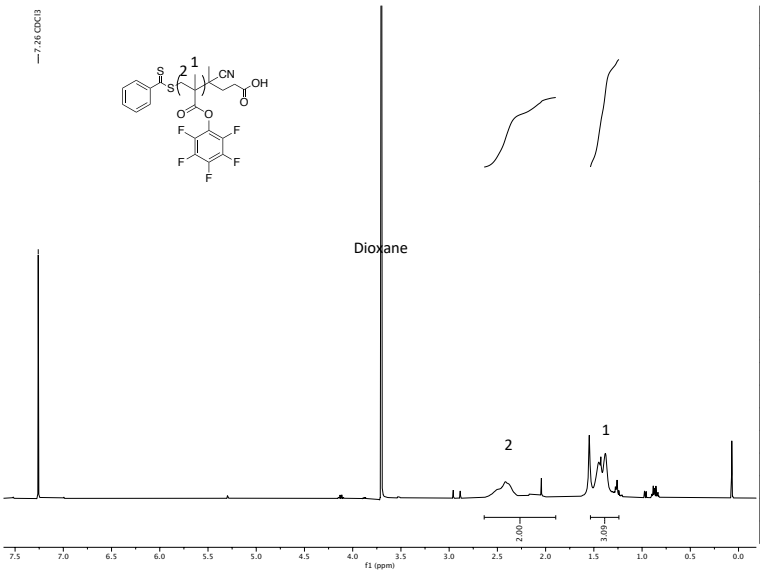

Figure A44. ^{1}H NMR of **PFPA-1**.

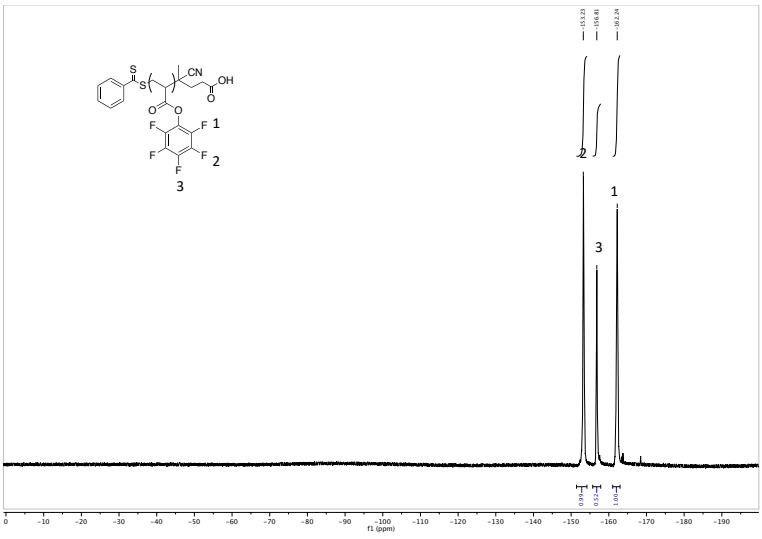

Figure A45. ^{19}F NMR of **PFPA-1**.

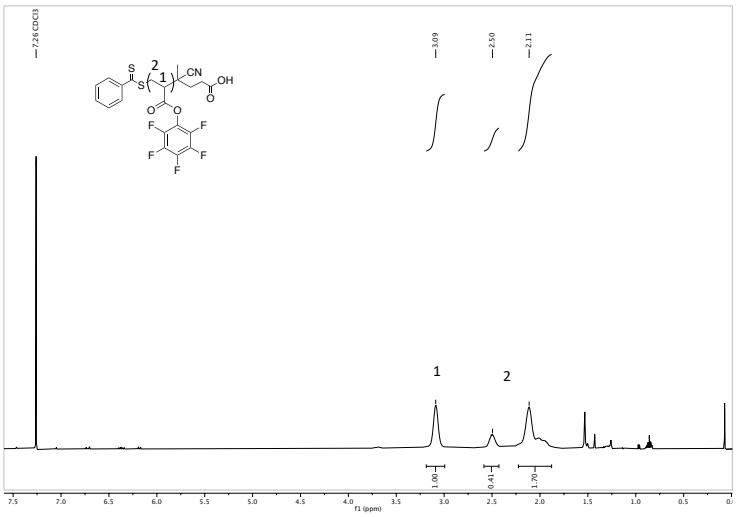

Figure A46. ^{1}H NMR of **PFPM-1**.

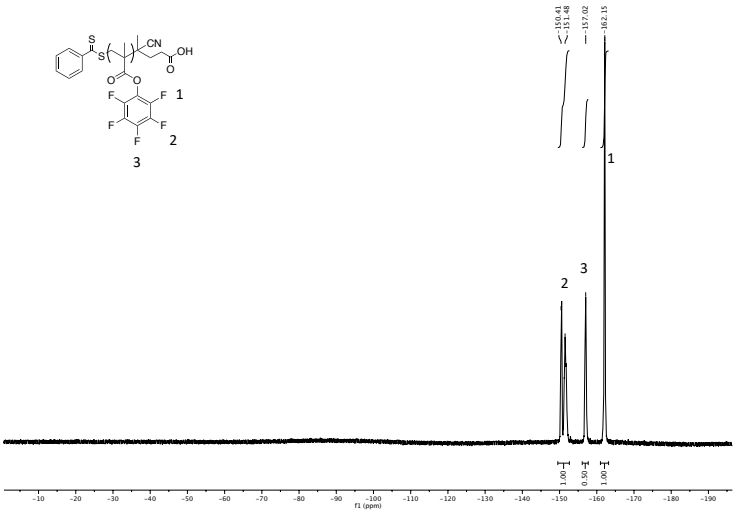

Figure A47. ^{19}F NMR of **PFPM-1**.

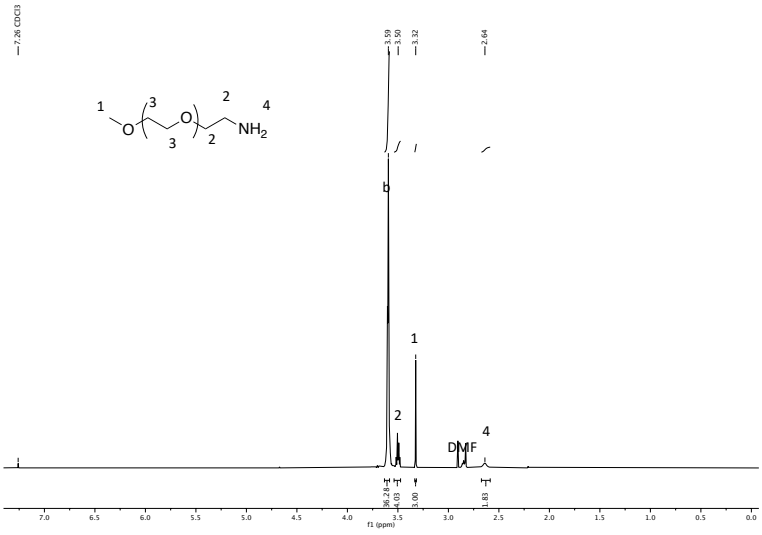

Figure A48. ^{1}H NMR of **13**.

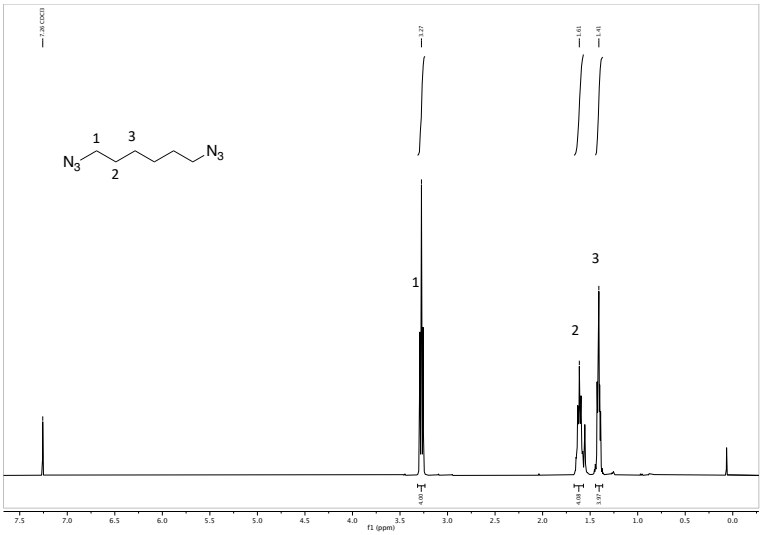

Figure A49. ^{1}H NMR of reactant for **14**.

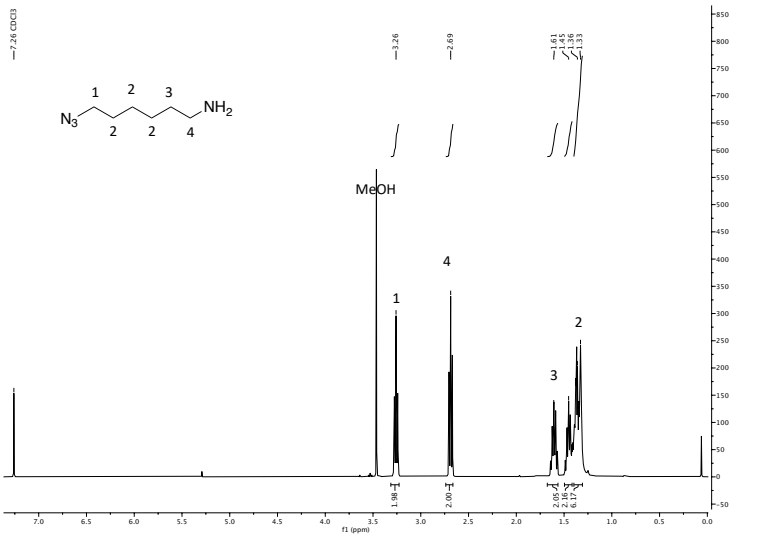

Figure A50. ^{1}H NMR of **14**.

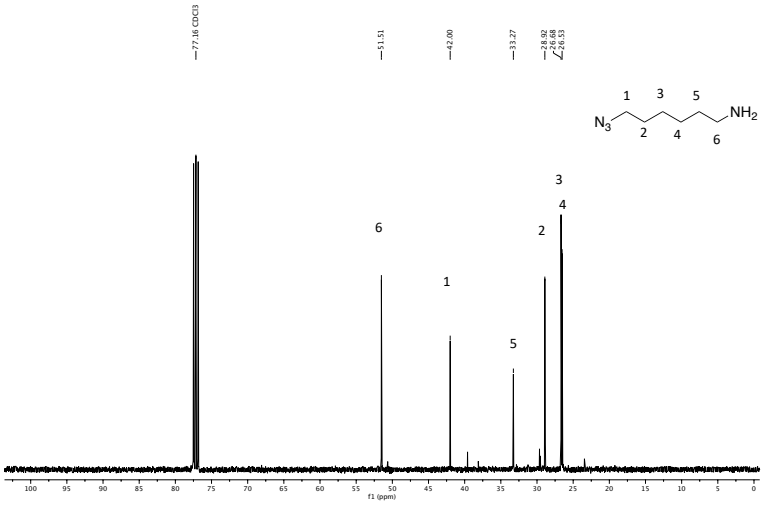

Figure A51. ^{13}C NMR of **14**.

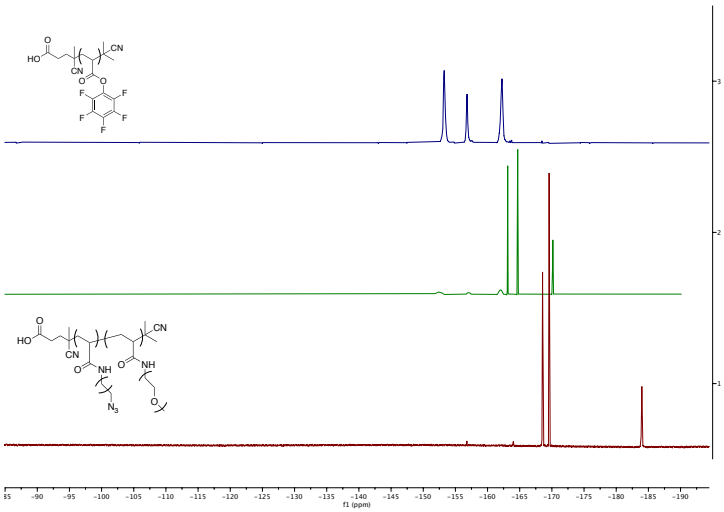

Figure A52. Conversion of **PFPA-2** to **MPFPA-1** according to ^{19}F NMR.

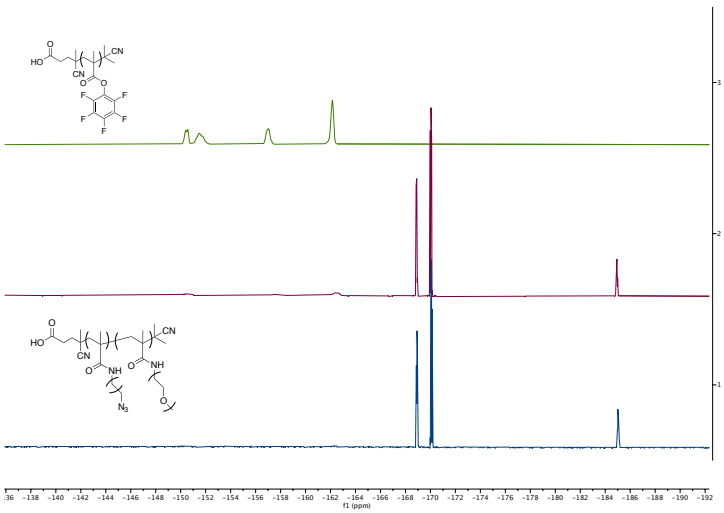

Figure A53. Conversion of **PFPM-2** to **MPFPM-1** according to ^{19}F NMR.

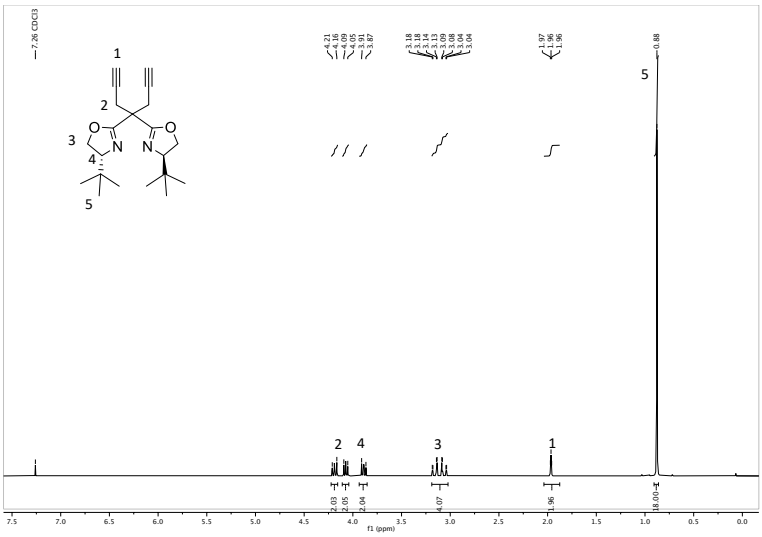

Figure A54. ^{1}H NMR of **15**.

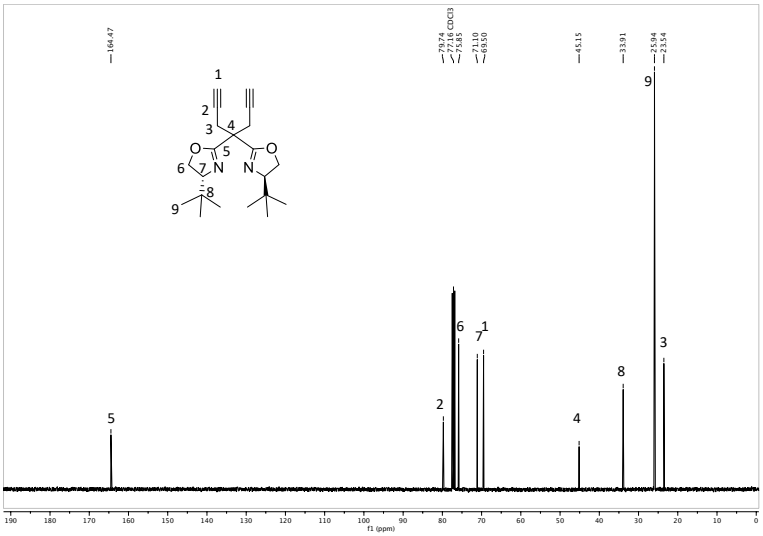

Figure A55. ^{13}C NMR of **15**.

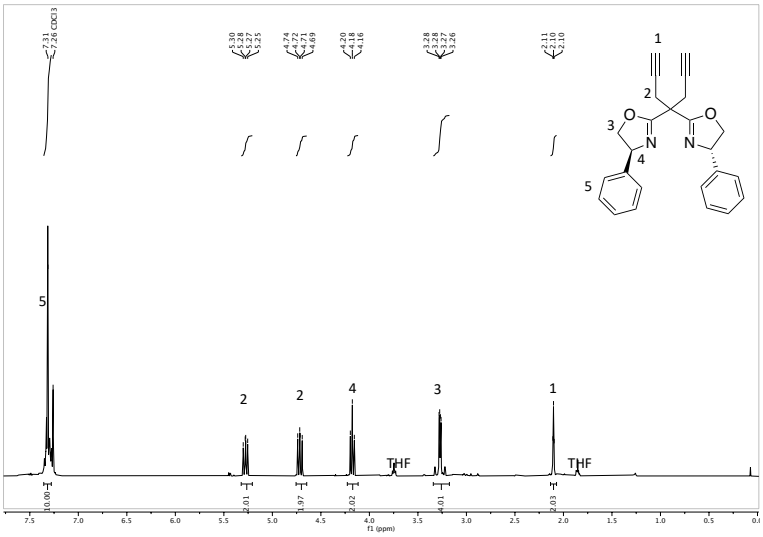

Figure A56. ^{1}H NMR of **16**.

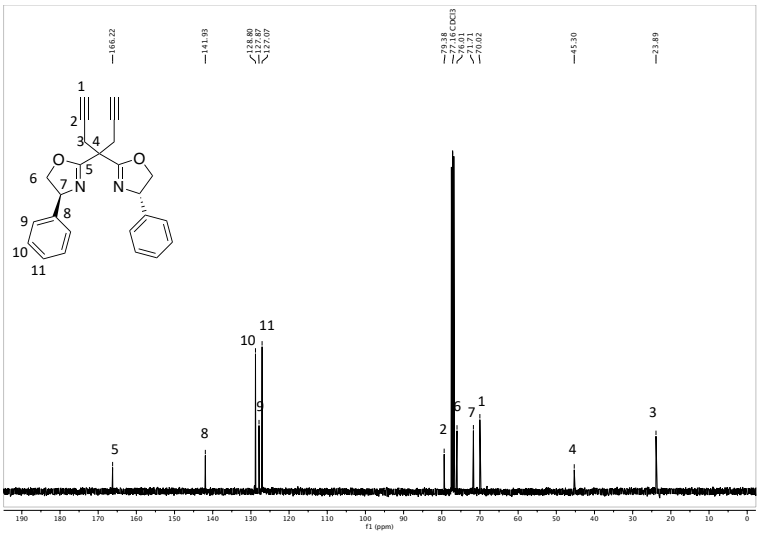

Figure A57. ^{13}C NMR of **16**.

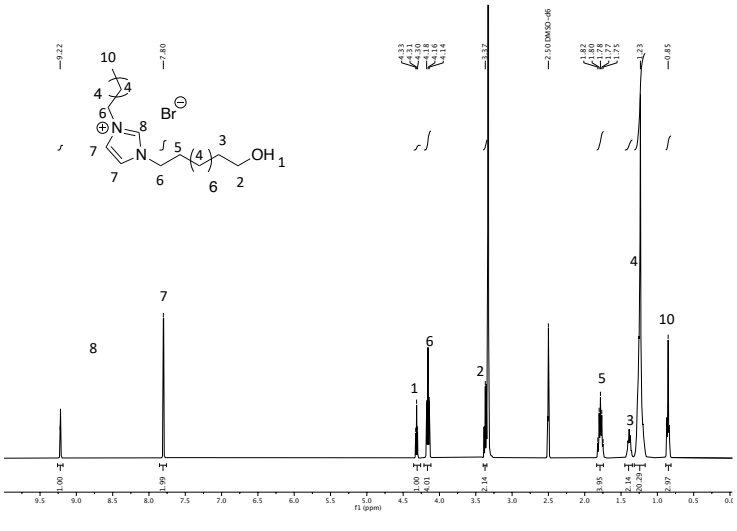

Figure A58. ^{1}H NMR of reactant for **17**.

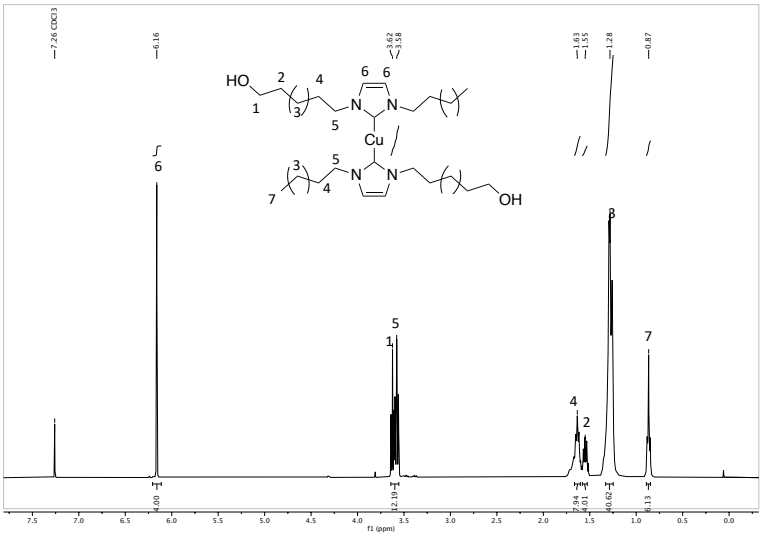

Figure A59. ^{1}H NMR of **17**.

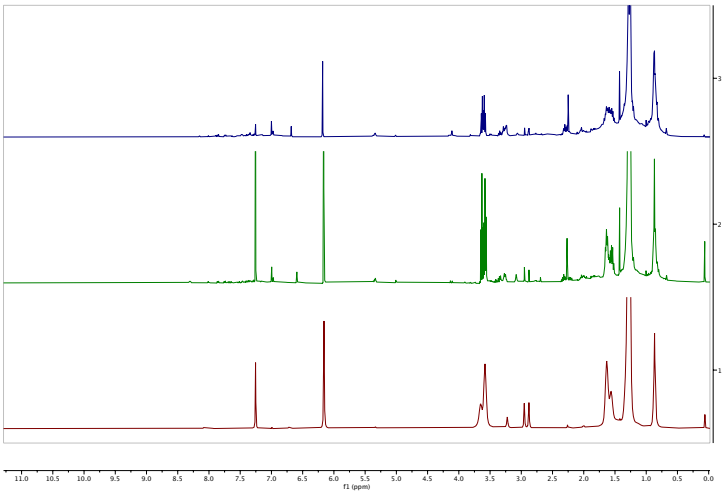

Figure A60. ^{1}H-NMR spectra of **17** during the reaction with DMAP for 2 (red), 24 (green) and 73 hours (blue). In collaboration with Mohamed Hassan.

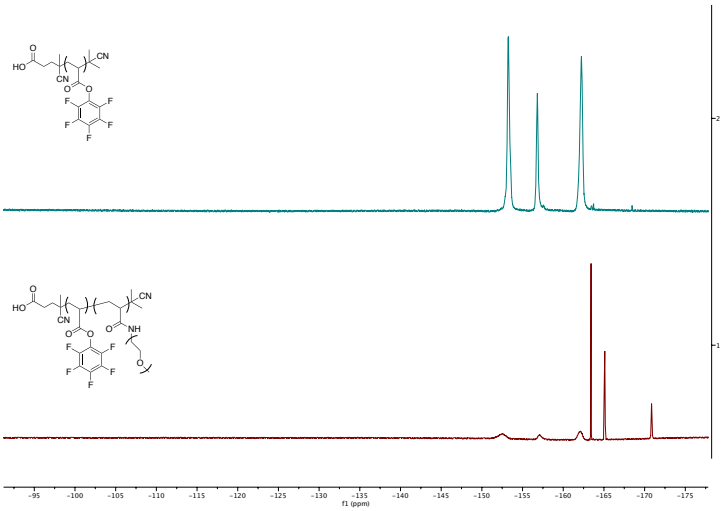

Figure A61. Conversion of **PFPA-2** to **MPFPA-2** according to ^{19}F NMR.

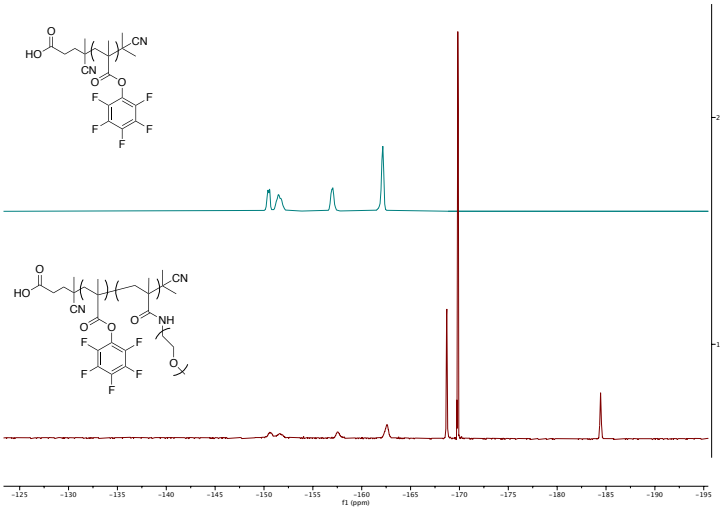

Figure A62. Conversion of **PFPM-2** to **MPFPM-2** according to ^{19}F NMR.

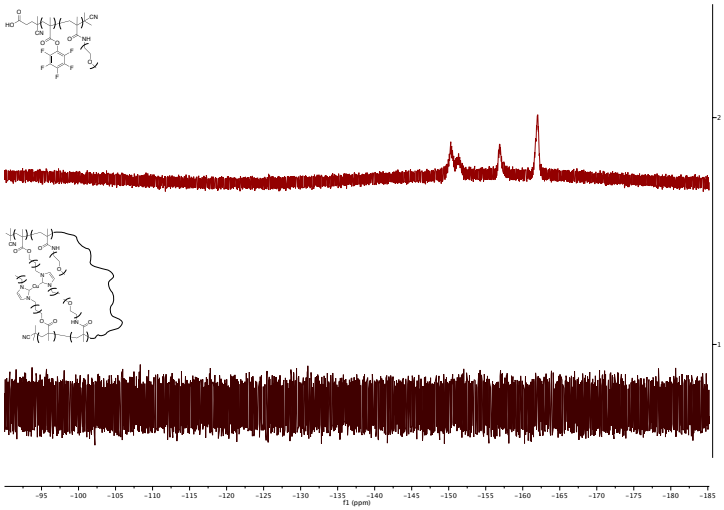

Figure A63. Conversion of **MPFPM-2** to **NP 1** according to ^{19}F NMR.

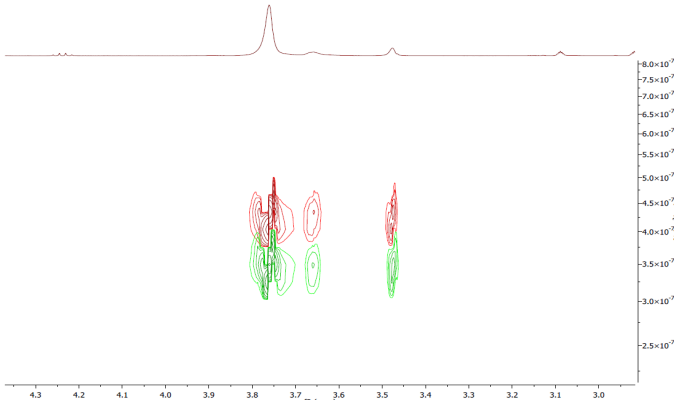

Figure A64. DOSY spectra comparison of **MPFPM-2** (green) and **NP 1** (red). In collaboration with Mohamed Hassan.

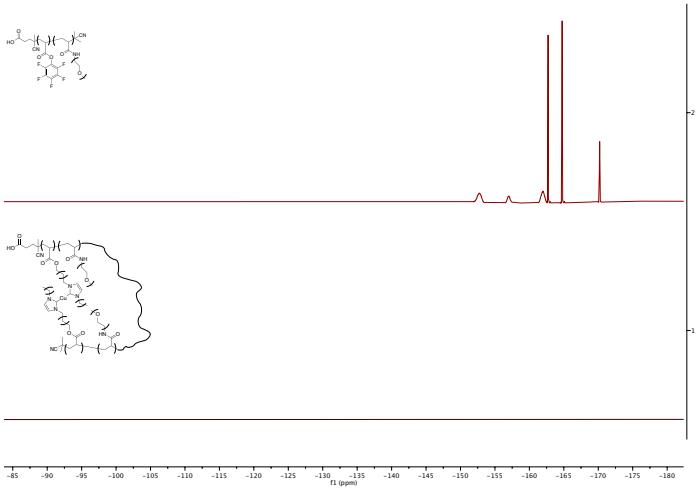

Figure A65. Conversion of **MPFPA-2** to **NP 2** according to ^{19}F NMR.

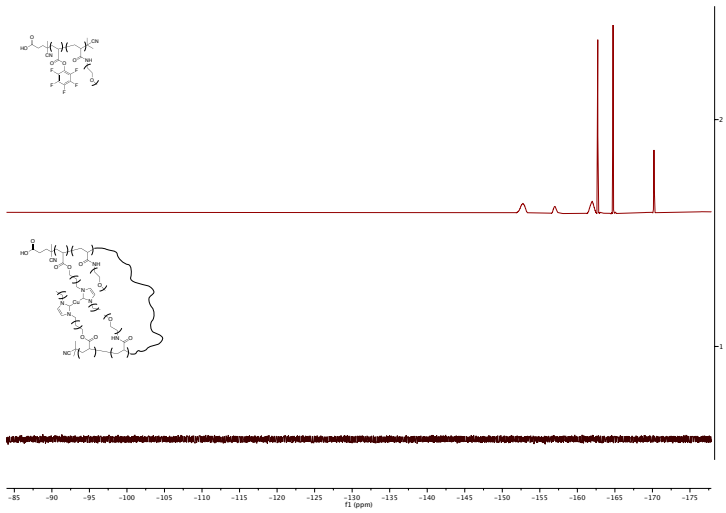

Figure A66. Conversion of **MPFPA-2** to **NP 3** according to ^{19}F NMR.

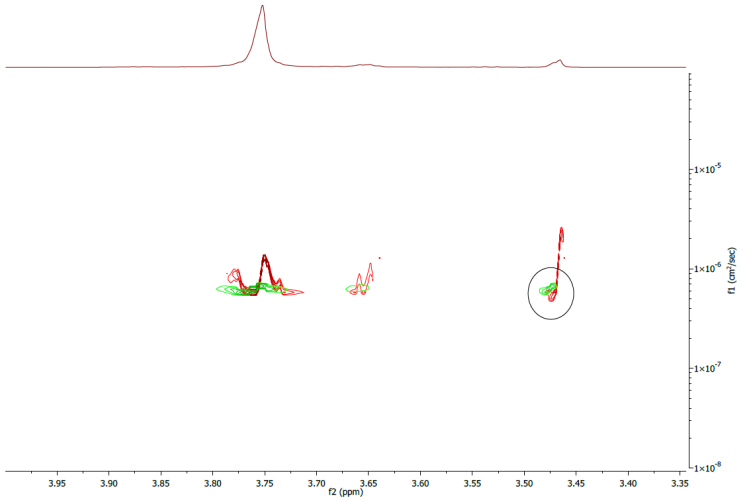

Figure A67. COSY NMR spectra of **MPFPA-2** (red) and **NP 3**. In collaboration with Mohamed Hassan.

7.5 Mass spectrometric data

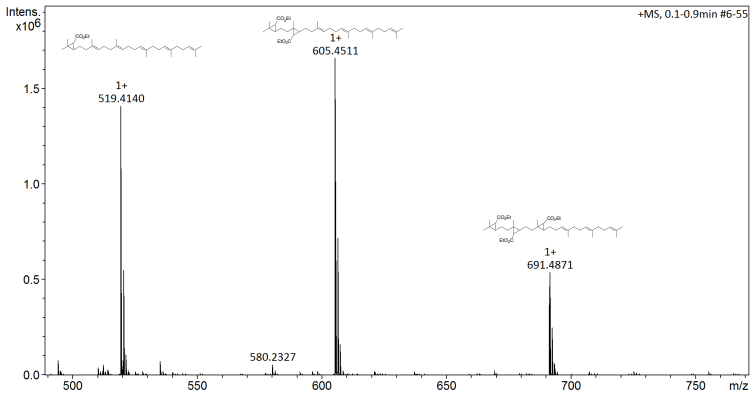

Figure A68. Exemplary equimolar reaction product formation according to ESI-TOF-MS of cyclopropanation of Squalene.

Table A1. ESI-TOF-MS degradation fragments of enzymatich degradation with Lcp_{K30}

m/z $[M+Na+CH_3OH]^+$ (calculated)	N 1 (measured) $[m/z]$	N 2 (measured) $[m/z]$	N 3 (measured) $[m/z]$	A 1 (measured) $[m/z]$	C 1 (measured) $[m/z]$	C 2 (measured) $[m/z]$	C 3 (measured) $[m/z]$
427.32	427.32	427.31	427.31	427.32	427.32	427.31	427.32
495.38	495.40	495.37	495.37	495.40	495.40	495.38	495.38
563.44	563.47	563.44	562.42	563.46	563.46	563.44	563.44
631.50	631.53	631.51	631.50	631.52	631.52	631.51	631.50
699.57	699.62	699.57	699.55	699.57	699.58	699.57	699.56
767.63	767.65	767.63	767.61	767.65	767.65	767.62	767.62
835.69	835.72	835.69	835.68	835.72	835.71	835.69	835.68

Table A2. ESI-TOF-MS of degradation fragment with m/z 427 of enzymatically degraded samples.

ID	m/z $[M+Na+CH_3OH]^+$	ID	m/z $[M+Na+CH_3OH]^+$
N 1	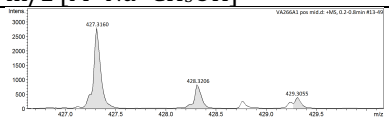	A 1	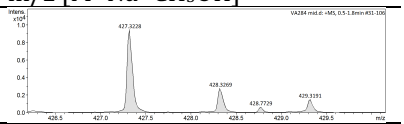
N 2	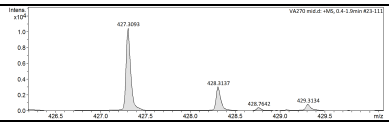	C 1	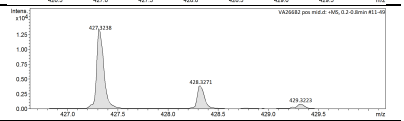
N 3	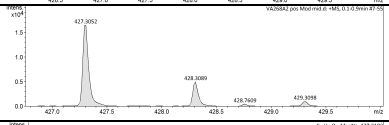	C 2	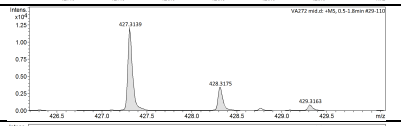
Simulated pattern	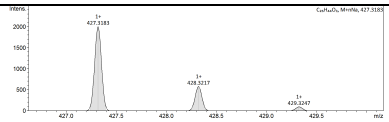	C 3	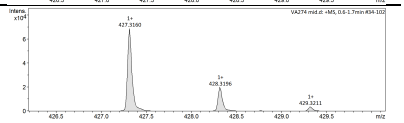

Table A3. ESI-TOF-MS of degradation fragment with m/z 495 of enzymatically degraded samples.

ID	m/z $[M+Na+CH_3OH]^+$	ID	m/z $[M+Na+CH_3OH]^+$
N 1	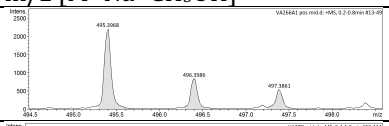	A 1	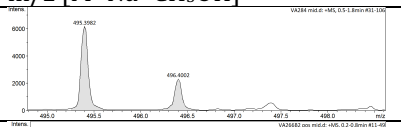
N 2	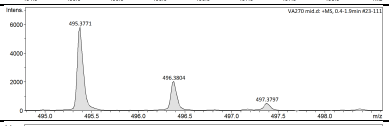	C 1	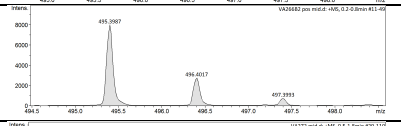
N 3	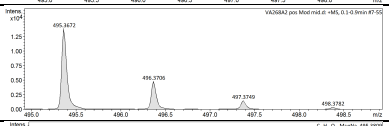	C 2	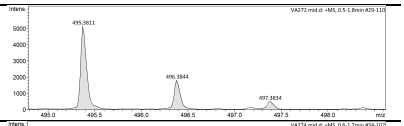
Simulated pattern	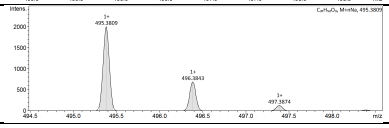	C 3	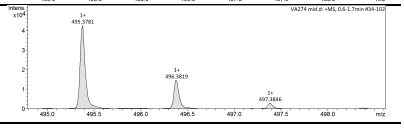

Table A4. ESI-TOF-MS of degradation fragment with m/z 563 of enzymatically degraded samples.

ID	m/z $[M+Na+CH_3OH]^+$	ID	m/z $[M+Na+CH_3OH]^+$
N 1	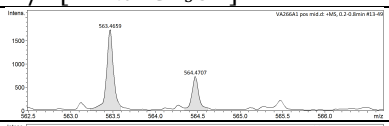	A 1	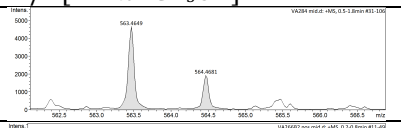
N 2	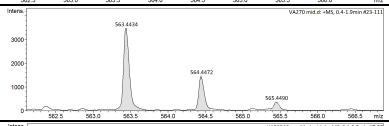	C 1	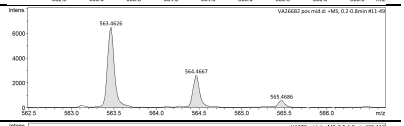
N 3	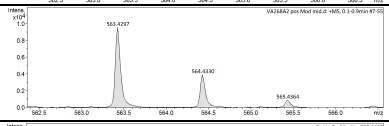	C 2	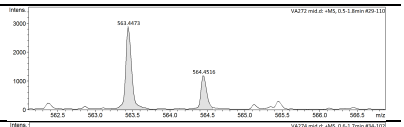
Simulated pattern	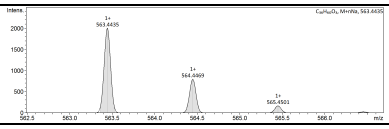	C 3	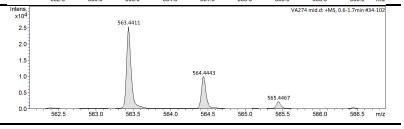

Table A5. ESI-TOF-MS of degradation fragment with m/z 631 of enzymatically degraded samples.

ID	m/z $[M+Na+CH_3OH]^+$	ID	m/z $[M+Na+CH_3OH]^+$
N 1	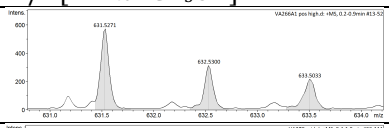	A 1	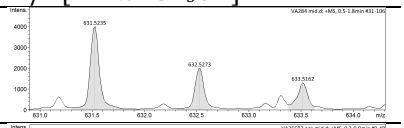
N 2	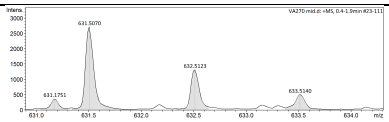	C 1	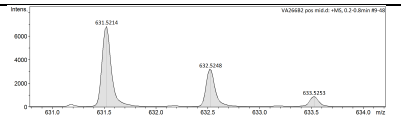
N 3	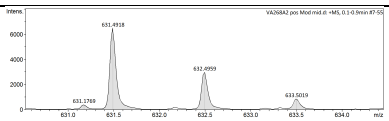	C 2	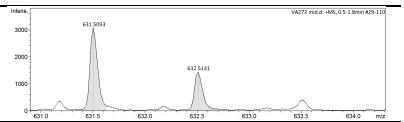
Simulated pattern	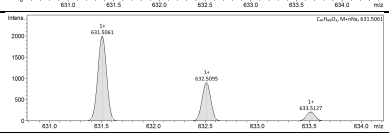	C 3	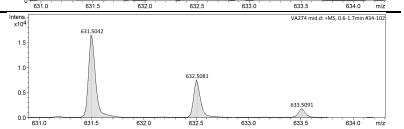

Table A6. ESI-TOF-MS of degradation fragment with m/z 699 of enzymatically degraded samples.

ID	m/z $[M+Na+CH_3OH]^+$	ID	m/z $[M+Na+CH_3OH]^+$
N 1	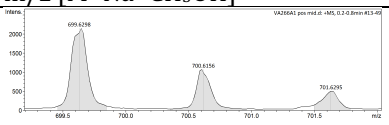	A 1	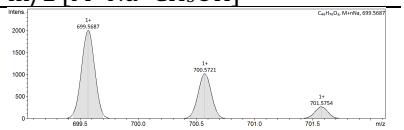
N 2	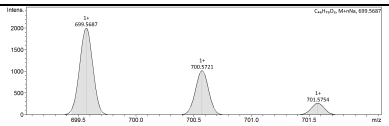	C1	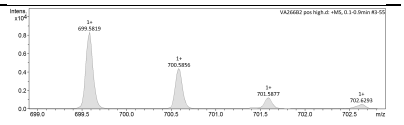
N 3	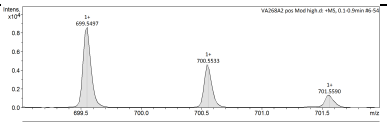	C 2	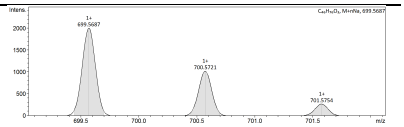
Simulated pattern	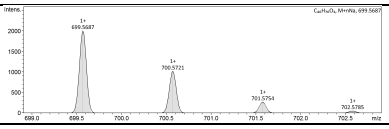	C 3	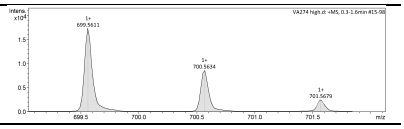

Table A7. ESI-TOF-MS of degradation fragment with m/z 767 of enzymatically degraded samples.

ID	m/z $[M+Na+CH_3OH]^+$	ID	m/z $[M+Na+CH_3OH]^+$
N 1	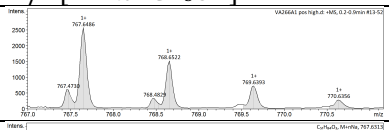	A 1	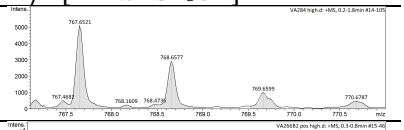
N 2	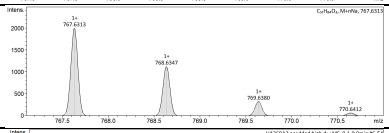	C 1	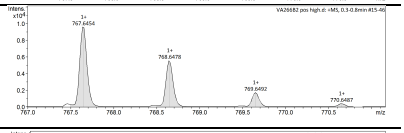
N 3	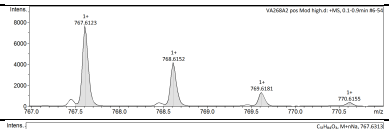	C 2	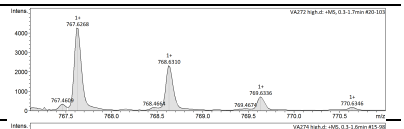
Simulated pattern	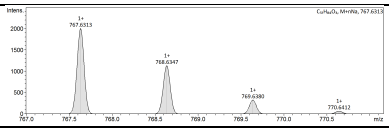	C 3	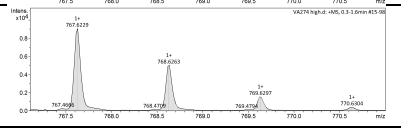

Table A8. ESI-TOF-MS of degradation fragment with m/z 835 of enzymatically degraded samples.

ID	m/z $[M+Na+CH_3OH]^+$	ID	m/z $[M+Na+CH_3OH]^+$
N 1	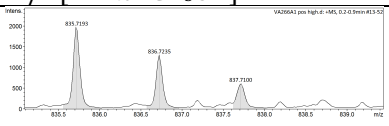	A 1	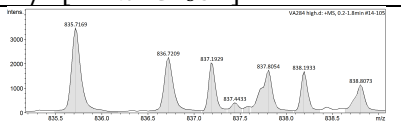
N 2	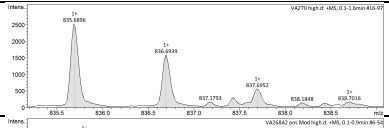	C 1	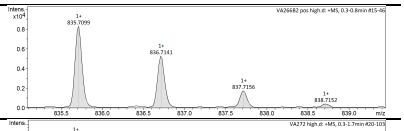
N 3	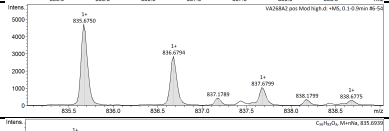	C 2	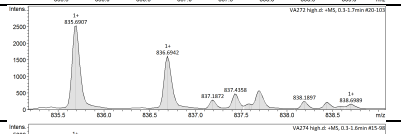
Simulated pattern	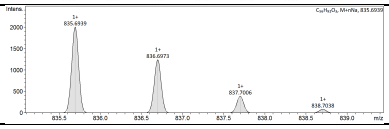	C 3	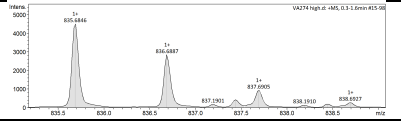

Table A9. Degradation fragments generated by enzymatic cleavage of co-solvent emulsified SPI (C 1) by Lcp_{K30} according to UHPLC-ESI-HRMS in positive ion mode

Number of intact isoprene units	$[M+H]^+$ measured	$[M+H]^+$ calculated	Elemental Composition	RDBE[e]
1	169.1224	169.1223	$C_{10}H_{17}O_2^+$	2.5
2	237.1850	237.1849	$C_{15}H_{25}O_2^+$	3.5
3	305.2475	305.2475	$C_{20}H_{33}O_2^+$	4.5
4	373.3096	373.3101	$C_{25}H_{41}O_2^+$	5.5
5	441.3725	441.3727	$C_{30}H_{49}O_2^+$	6.5
6	509.4346	509.4353	$C_{35}H_{57}O_2^+$	7.5
7	577.4969	577.4979	$C_{40}H_{65}O_2^+$	8.5
8	645.5595	645.5605	$C_{45}H_{73}O_2^+$	9.5
9	713.6230	713.6231	$C_{50}H_{81}O_2^+$	10.5
10	781.6857	781.6857	$C_{55}H_{89}O_2^+$	11.5
11	849.7474	849.7483	$C_{60}H_{97}O_2^+$	12.5
12	917.8104	917.8109	$C_{65}H_{105}O_2^+$	13.5
13	985.8733	985.8735	$C_{70}H_{113}O_2^+$	14.5

[e]RDBE = ring double bond equivalent;

Table A10. Degradation fragments generated by enzymatic cleavage of co-solvent emulsified synthetic polyisoprene (C 1) and of reference latex milk (L 1) by Lcp_{K30} according to UHPLC-UV-ESI-HRMS (QTOF) in positive ion mode

RT (min) L 1	**RT (min) C 1**	**RT_{UV} (min) L 1**	**RT_{UV} (min) C 1**	**[M-H]+ measured L1**	**[M-H]+ measured C 1**	**[M-H]+ calculated**	**Error (ppm) Latex**	**Elemental Composition**	**RDBE**
n.d	0.64	n.d.	0.58	-	169.1217	169.1223	-3.6, S	$C_{10}H_{17}O_2$	2.5
1.12	1.17	1.051	.1.02	237.1843	237.1852	237.1849	-2.6	$C_{15}H_{24}O_2$	3.5
2.57	2.59	2.54	2.55	305.2476	305.2475	305.2475	0.3	$C_{20}H_{32}O_2$	4.5
3.48	3.50	3.43	3.47	373.3103	373.3089	373.3101	0.5	$C_{25}H_{40}O_2$	5.5
4.02	4.03	3.98	3.97	441.3722	441.3714	441.3727	-1.2	$C_{30}H_{48}O_2$	6.5
4.40	4.40	4.36	4.39	509.4336	509.4350	509.4353	-3.4	$C_{35}H_{56}O_2$	7.5
4.67	4.65	4.65	4.72	577.4979	577.4968	577.4979	0.1	$C_{40}H_{64}O_2$	8.5
4.93	4.94	4.90	5.02	645.5621	645.5593	645.5605	2.5	$C_{45}H_{73}O_2$	9.5
5.17	5.15	5.13	5.29	713.6221	713.6212	713.6231	0.8	$C_{50}H_{80}O_2$	10.5
5.46	5.44	5.42	5.64	781.6848	781.6828	781.6857	-1.2	$C_{55}H_{88}O_2$	11.5
5.83	5.80	5.78	5.81	849.7466	849.7463	849.7483	-2.0	$C_{60}H_{96}O_2$	12.5
6.32	n.d.	6.28	n.d.	917.8092	n.d.	917.8109	-1.9	$C_{65}H_{104}O_2$	13.5
7.04	n.d.	6.96	n.d.	985.8713	n.d.	985.8735	-2.2	$C_{70}H_{112}O_2$	14.5
8.05	n.d.	7.98	n.d.	1053.9330	n.d.	1053.9361	-3.0	$C_{75}H_{120}O_2$	15.5
9.18	n.d.	9.21	n.d.	1121.9984	n.d.	1121.9987	-0.3	$C_{80}H_{129}O_2$	16.5
n.d.	n.d.	10.95	n.d.	n.d.	n.d.	1191	n.d.	$C_{85}H_{137}O_2$	n.d.

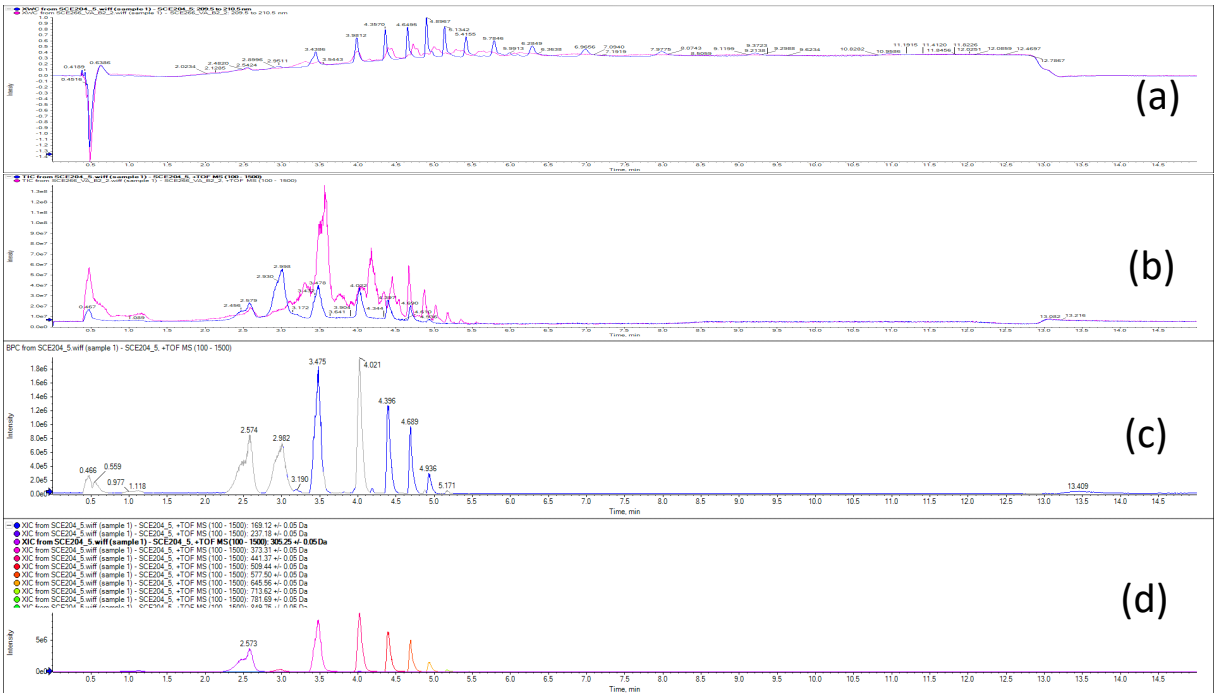

Figure A69. Stacked UV-curves (a) of enzymatically degraded **L 1** (blue) and enzymatically degraded **C 1** (pink), stacked total ion chromatograms (TIC) (b) of enzymatically degraded **L 1** (blue) and enzymatically degraded **C 1** (pink) and extracted ion chromatograms (EICs) of enzymatically degraded **L 1** (c) and enzymatically degraded **C 1** (d) acquired during UHPLC-UV-ESI-HRMS measurement.

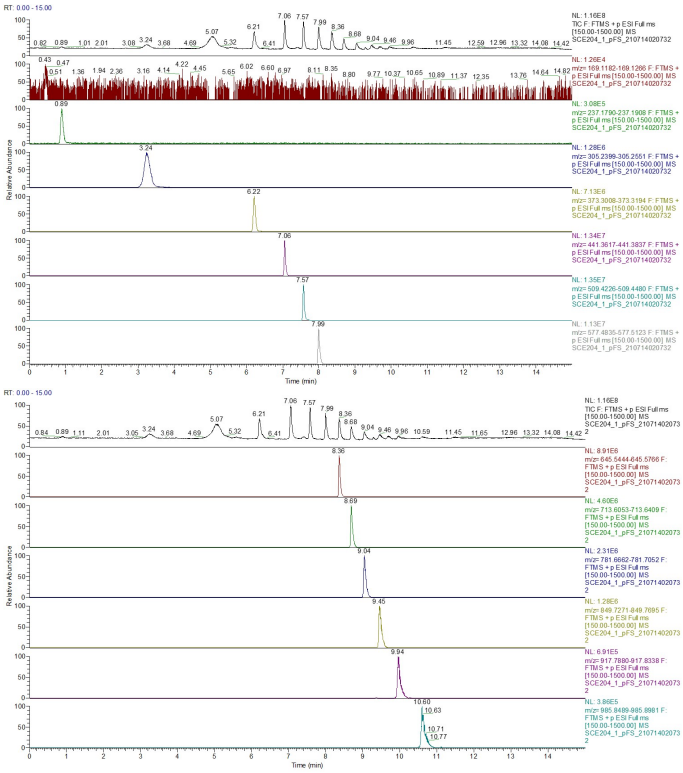

Figure A70. Total ion chromatogram (TIC) and extracted ion chromatograms (EICs) of enzymatically degraded **L 1** acquired during UHPLC-ESI-HRMS measurement. For the data evaluation, the target *m/z* values were extracted from the TIC using a 25 ppm mass window with a mass accuracy of four decimals to obtain the corresponding EIC for each analyte according to the degradation patterns.

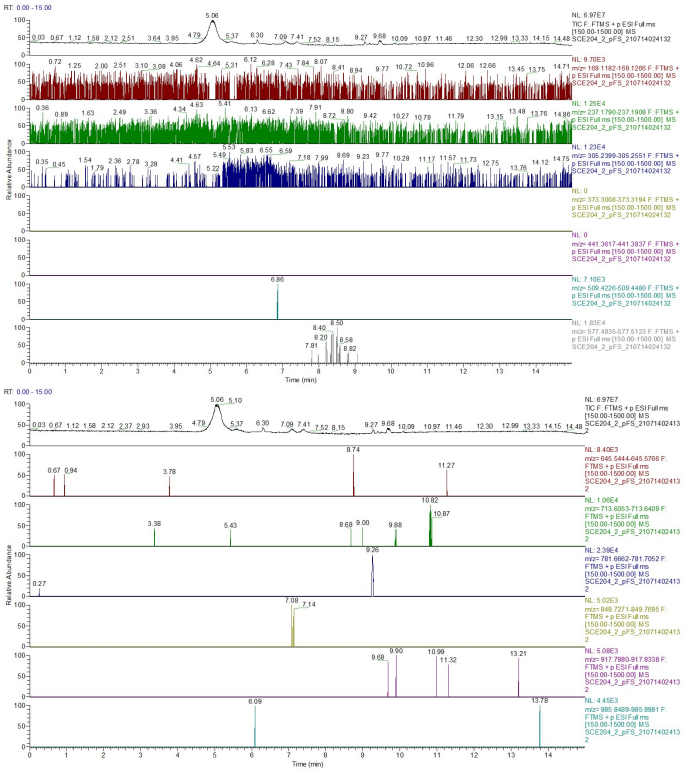

Figure A71. Total ion chromatogram (TIC) and extracted ion chromatograms (EICs) of the negative control of **L 1** acquired during UHPLC-ESI-HRMS measurement. For the data evaluation, the target *m/z* values were extracted from the TIC using a 25 ppm mass window with a mass accuracy of four decimals to obtain the corresponding EIC for each analyte according to the degradation patterns.

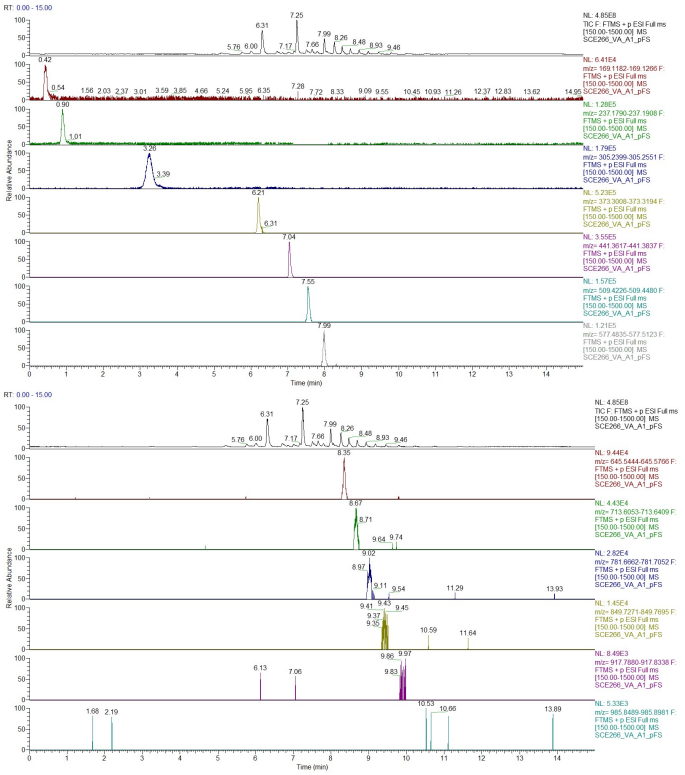

Figure A72. Total ion chromatogram (TIC) and extracted ion chromatograms (EICs) of enzymatically degraded **N 1** acquired during UHPLC-ESI-HRMS measurement. For the data evaluation, the target *m/z* values were extracted from the TIC using a 25 ppm mass window with a mass accuracy of four decimals to obtain the corresponding EIC for each analyte according to the degradation patterns.

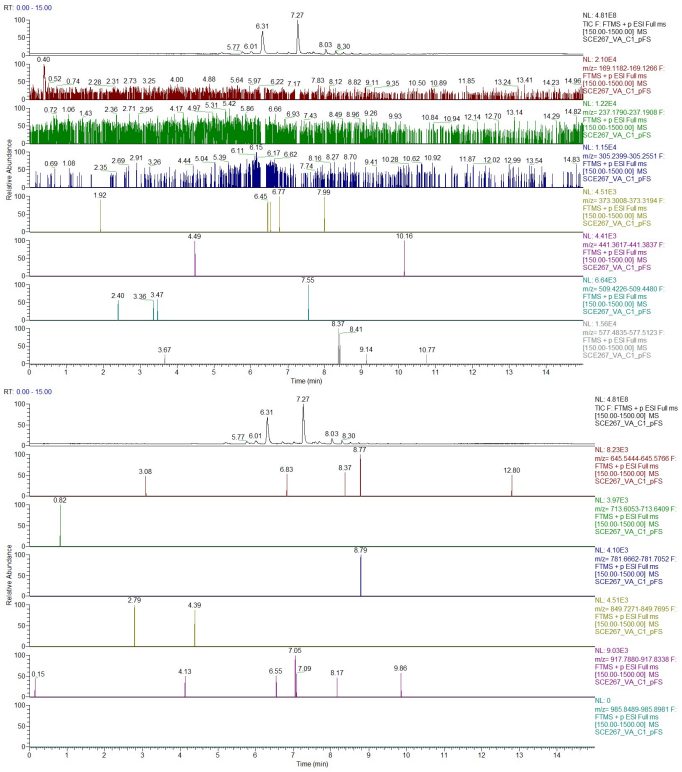

Figure A73. Total ion chromatogram (TIC) and extracted ion chromatograms (EICs) of the negative control of **N 1** acquired during UHPLC-ESI-HRMS measurement. For the data evaluation, the target *m/z* values were extracted from the TIC using a 25 ppm mass window with a mass accuracy of four decimals to obtain the corresponding EIC for each analyte according to the degradation patterns.

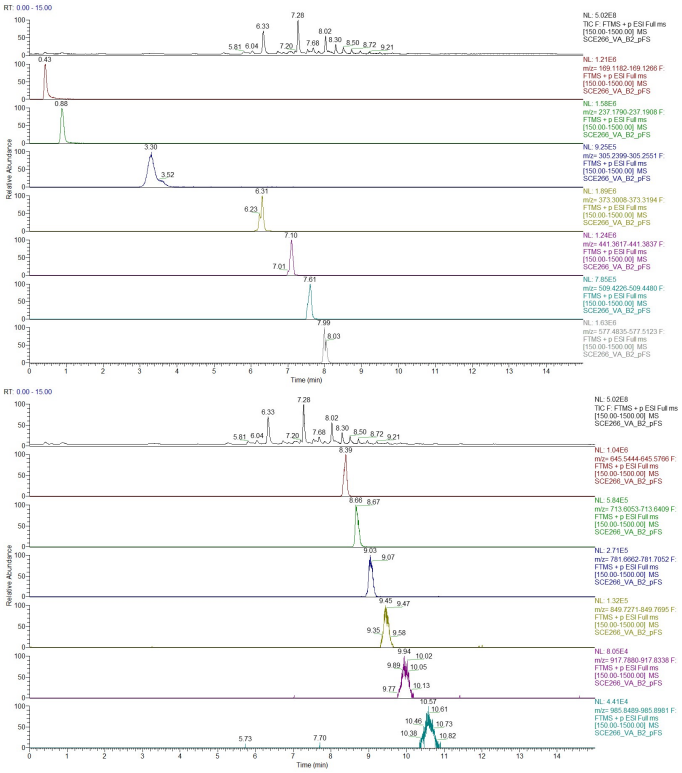

Figure A74. Total ion chromatogram (TIC) and extracted ion chromatograms (EICs) of enzymatically degraded **C 1** acquired during UHPLC-ESI-HRMS measurement. For the data evaluation, the target *m/z* values were extracted from the TIC using a 25 ppm mass window with a mass accuracy of four decimals to obtain the corresponding EIC for each analyte according to the degradation patterns.

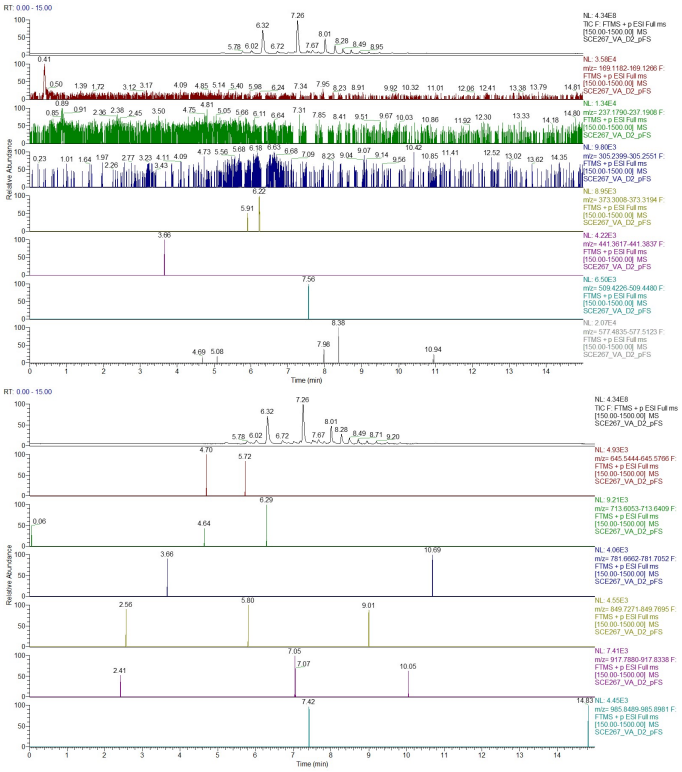

Figure A75. Total ion chromatogram (TIC) and extracted ion chromatograms (EICs) of the negative control of C 1 acquired during UHPLC-ESI-HRMS measurement. For the data evaluation, the target *m/z* values were extracted from the TIC using a 25 ppm mass window with a mass accuracy of four decimals to obtain the corresponding EIC for each analyte according to the degradation patterns.

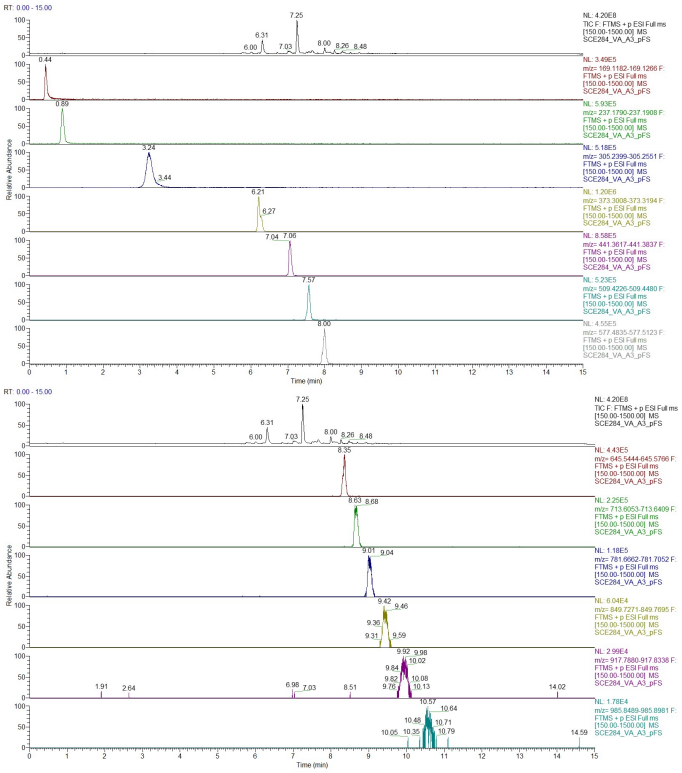

Figure A76. Total ion chromatogram (TIC) and extracted ion chromatograms (EICs) of enzymatically degraded **A 1** acquired during UHPLC-ESI-HRMS measurement. For the data evaluation, the target *m/z* values were extracted from the TIC using a 25 ppm mass window with a mass accuracy of four decimals to obtain the corresponding EIC for each analyte according to the degradation patterns.

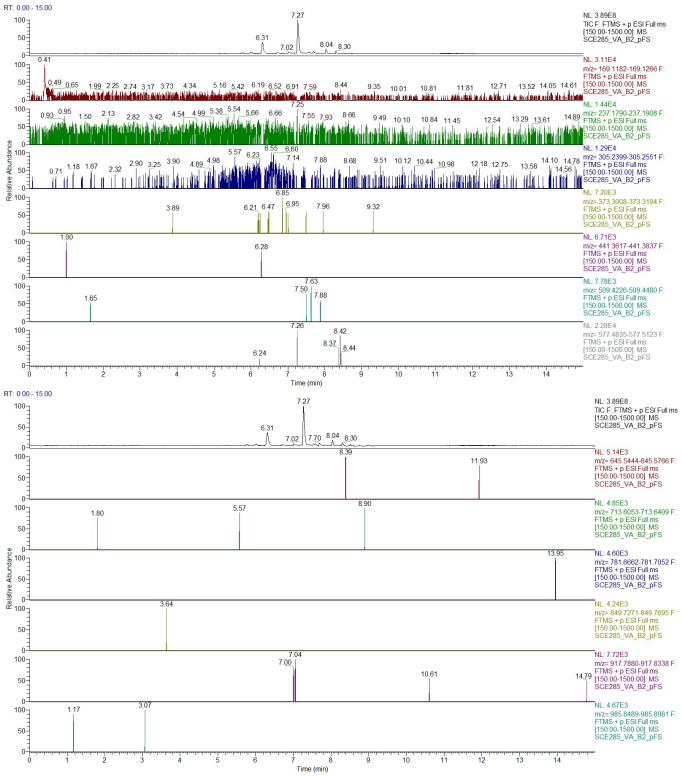

Figure A77. Total ion chromatogram (TIC) and extracted ion chromatograms (EICs) of the negative control of A 1 acquired during UHPLC-ESI-HRMS measurement. For the data evaluation, the target *m/z* values were extracted from the TIC using a 25 ppm mass window with a mass accuracy of four decimals to obtain the corresponding EIC for each analyte according to the degradation patterns.

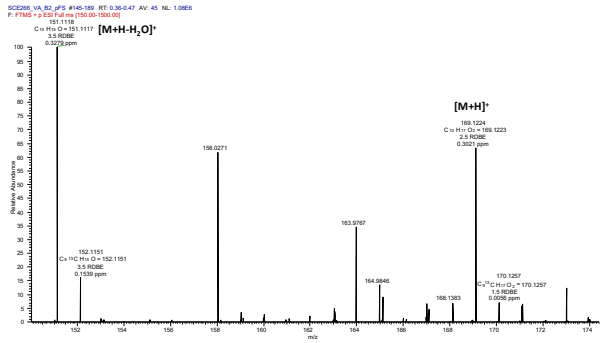

Figure A78. (+)-ESI-HRMS spectrum of the degradation fragments with elemental composition of $C_{10}H_{16}O_2$. obtained from **C 1**.

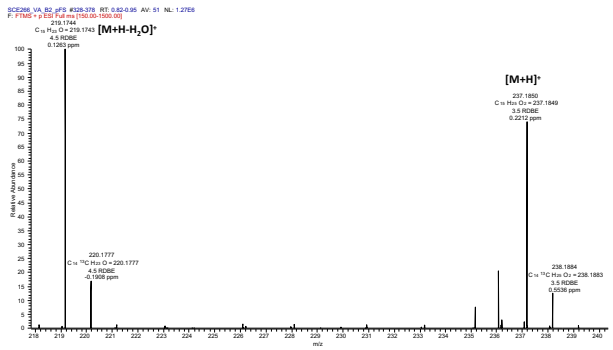

Figure A79. (+)-ESI-HRMS spectrum of the degradation fragments with elemental composition of $C_{15}H_{24}O_2$ obtained from **C 1**.

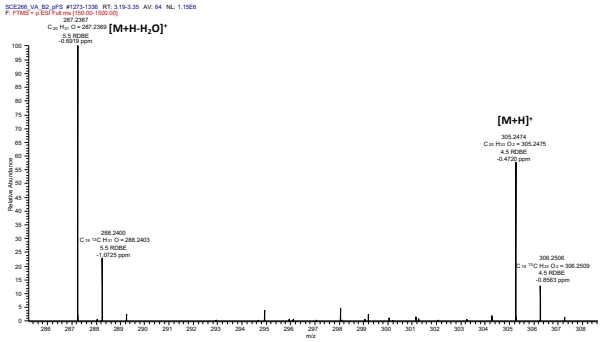

Figure A80. (+)-ESI-HRMS spectrum of the degradation fragments with elemental composition of $C_{20}H_{32}O_2$ obtained from **C 1**.

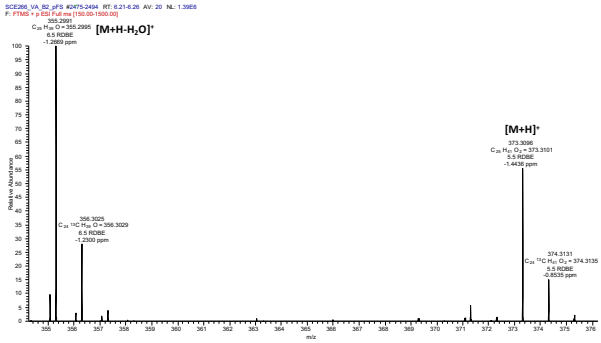

Figure A81. (+)-ESI-HRMS spectrum of the degradation fragments with elemental composition of $C_{25}H_{40}O_2$ obtained from **C 1**.

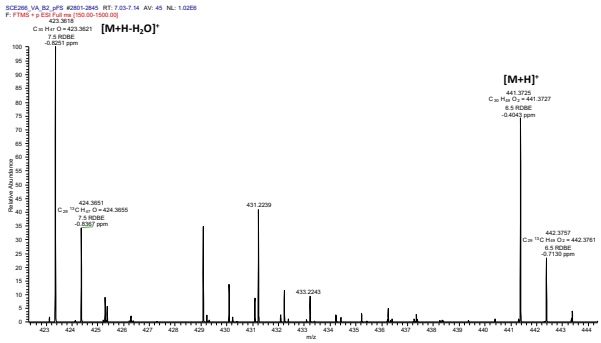

Figure A82. (+)-ESI-HRMS spectrum of the degradation fragments with elemental composition of $C_{30}H_{48}O_2$ obtained from **C 1**.

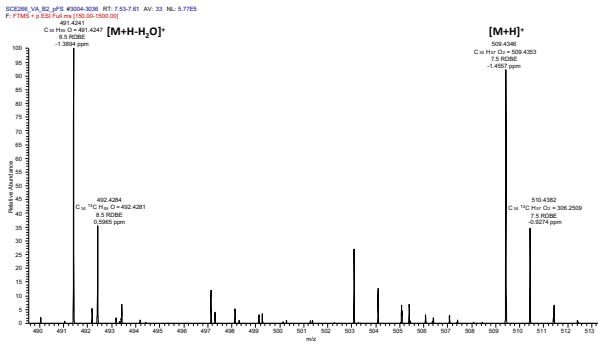

Figure A83. (+)-ESI-HRMS spectrum of the degradation fragments with elemental composition of $C_{35}H_{56}O_2$ obtained from **C 1**.

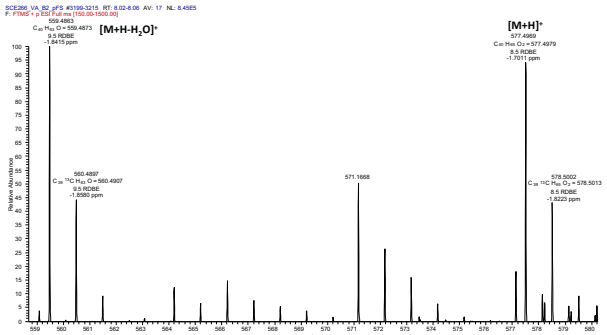

Figure A84. (+)-ESI-HRMS spectrum of the degradation fragments with elemental composition of $C_{40}H_{64}O_2$ obtained from **C 1**.

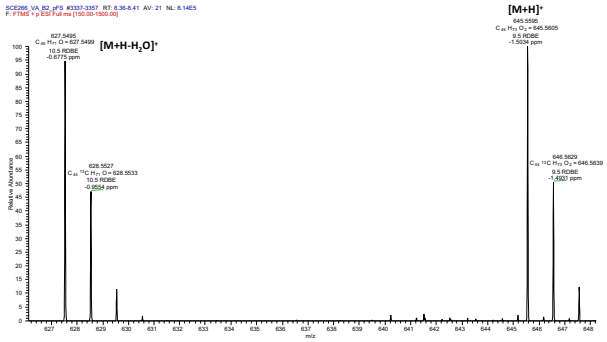

Figure A85. (+)-ESI-HRMS spectrum of the degradation fragments with elemental composition of $C_{45}H_{72}O_2$ obtained from **C 1**.

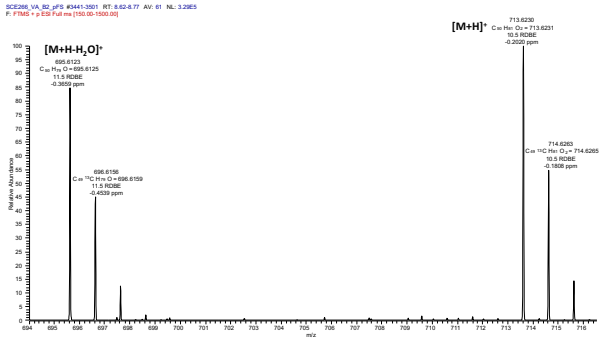

Figure A86. (+)-ESI-HRMS spectrum of the degradation fragments with elemental composition of $C_{50}H_{80}O_2$ obtained from **C 1**.

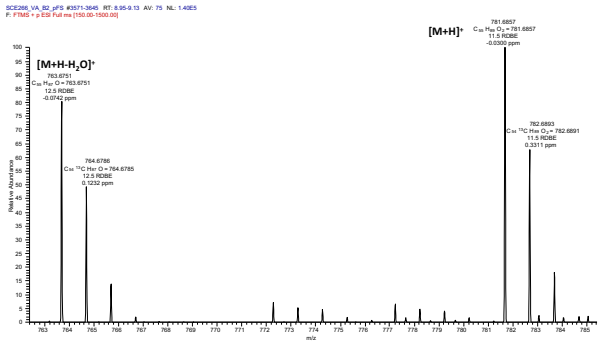

Figure A87. (+)-ESI-HRMS spectrum of the degradation fragments with elemental composition of $C_{55}H_{88}O_2$ obtained from **C 1**.

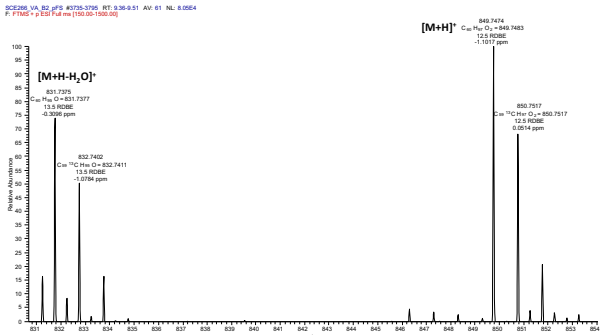

Figure A88. (+)-ESI-HRMS spectrum of the degradation fragments with elemental composition of $C_{60}H_{96}O_2$ obtained from **C 1**.

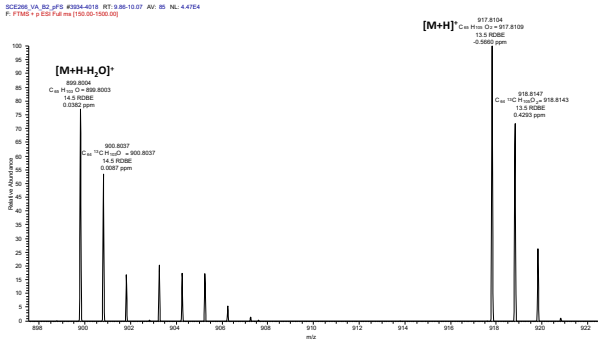

Figure A89. (+)-ESI-HRMS spectrum of the degradation fragments with elemental composition of $C_{65}H_{104}O_2$ obtained from **C 1**.

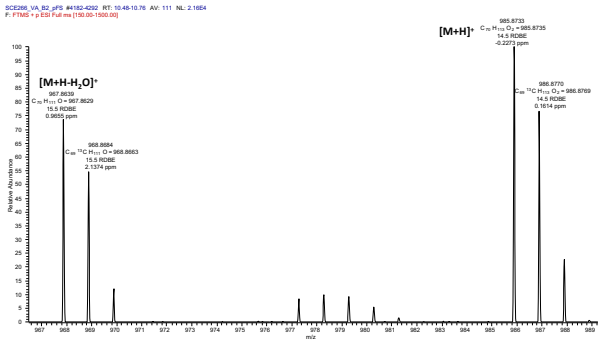

Figure A90. (+)-ESI-HRMS spectrum of the degradation fragments with elemental composition of $C_{70}H_{112}O_2$ obtained from **C 1**.

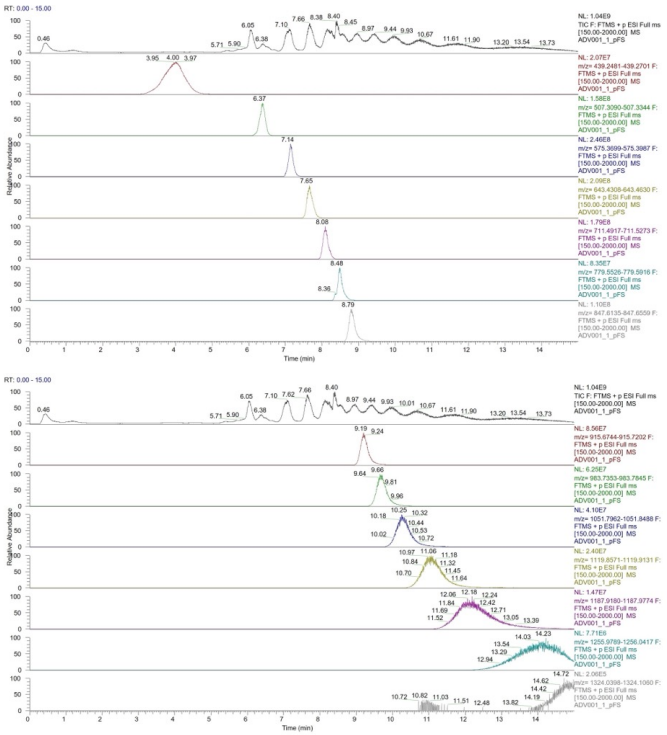

Figure A91. Total ion chromatogram (TIC) and extracted ion chromatograms (EICs) of **PI 3000-D** acquired during UHPLC-ESI-HRMS measurement. For the data evaluation, the target *m/z* values were extracted from the total ion chromatogram (TIC) using a 25 ppm mass window with a mass accuracy of four decimals to obtain the corresponding extracted ion chromatogram (EIC) for each analyte according to the expected degradation fragments of **PI 3000-D**.

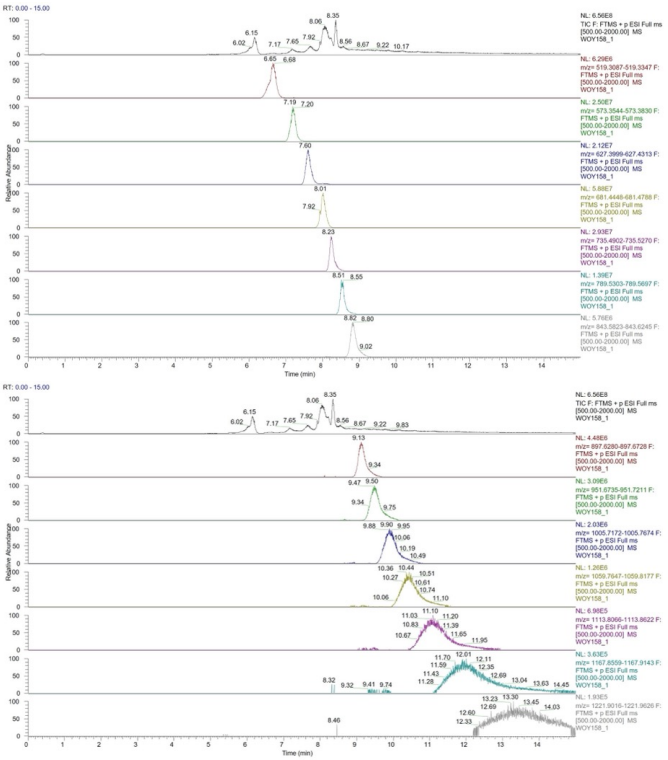

Figure A92. Total ion chromatogram (TIC) and extracted ion chromatograms (EICs) of **PB 3500-D** acquired during UHPLC-ESI-HRMS measurement. For the data evaluation, the target *m/z* values were extracted from the TIC using a 25 ppm mass window with a mass accuracy of four decimals to obtain the corresponding EIC for each analyte according to the expected degradation fragments.

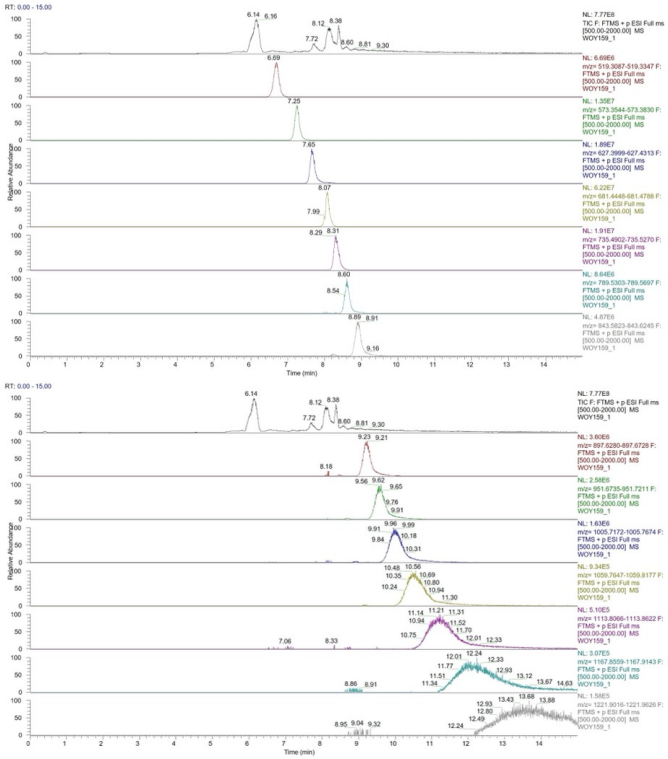

Figure A93. Total ion chromatogram (TIC) and extracted ion chromatograms (EICs) of **PB 12000-D** acquired during UHPLC-ESI-HRMS measurement. For the data evaluation, the target *m/z* values were extracted from the TIC using a 25 ppm mass window with a mass accuracy of four decimals to obtain the corresponding EIC for each analyte according to the expected degradation fragments.

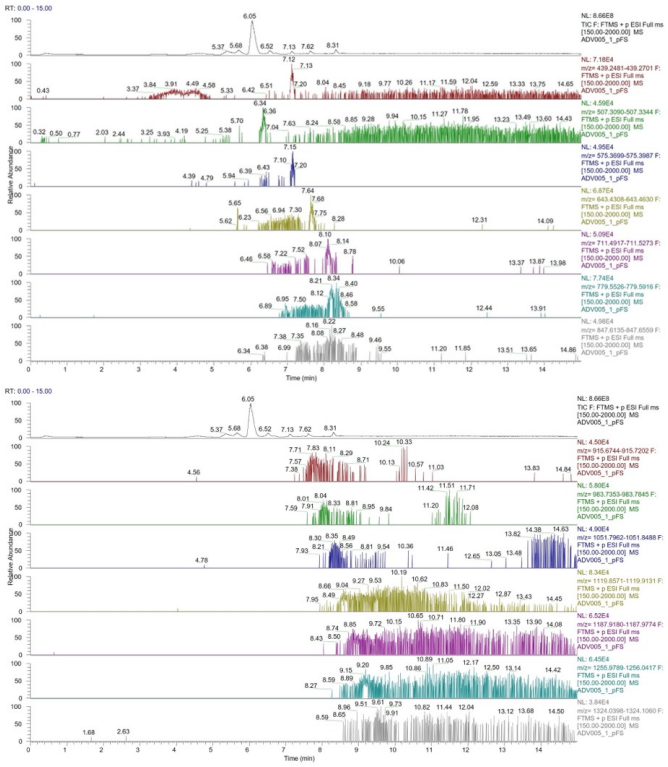

Figure A94. Total ion chromatogram (TIC) and extracted ion chromatograms (EICs) of **PI 3000 NC** acquired during UHPLC-ESI-HRMS measurement. For the data evaluation, the target *m/z* values were extracted from the TIC using a 25 ppm mass window with a mass accuracy of four decimals to obtain the corresponding EIC for each analyte according to the expected degradation fragments.

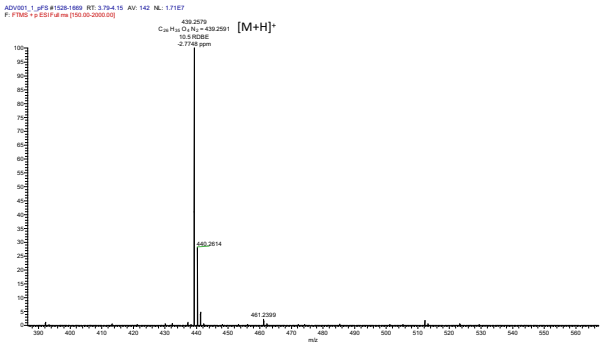

Figure A95. (+)-ESI-HRMS spectrum of the degradation fragments with elemental composition of $C_{26}H_{34}N_2O_4$ obtained from **PI 3000-D.**

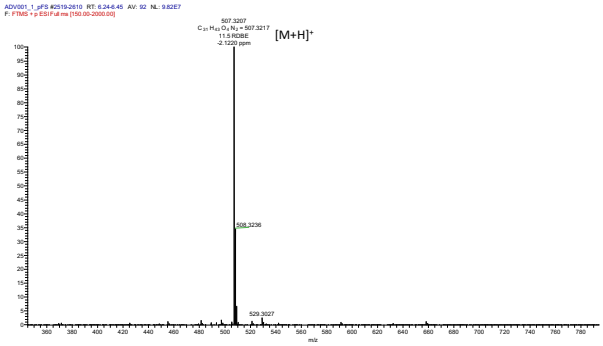

Figure A96. (+)-ESI-HRMS spectrum of the degradation fragments with elemental composition of $C_{31}H_{42}N_2O_4$ obtained from **PI 3000-D**.

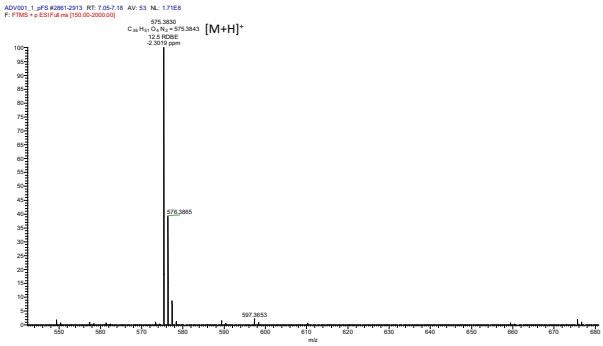

Figure A97. (+)-ESI-HRMS spectrum of the degradation fragments with elemental composition of $C_{36}H_{50}N_2O_4$ obtained from **PI 3000-D**.

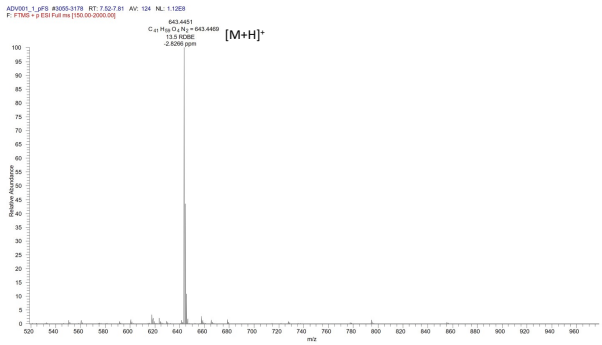

Figure A98. (+)-ESI-HRMS spectrum of the degradation fragments with elemental composition of $C_{41}H_{58}N_2O_4$ obtained from **PI 3000-D**.

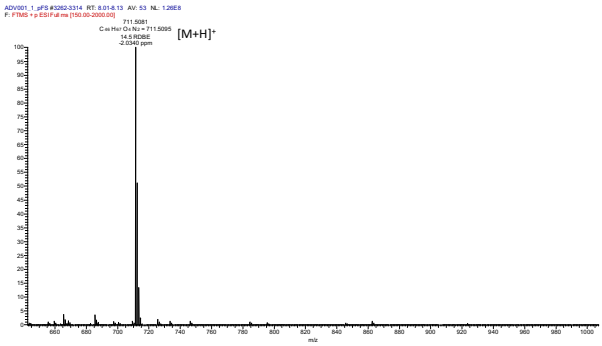

Figure A99. (+)-ESI-HRMS spectrum of the degradation fragments with elemental composition of $C_{46}H_{66}N_2O_4$ obtained from **PI 3000-D**.

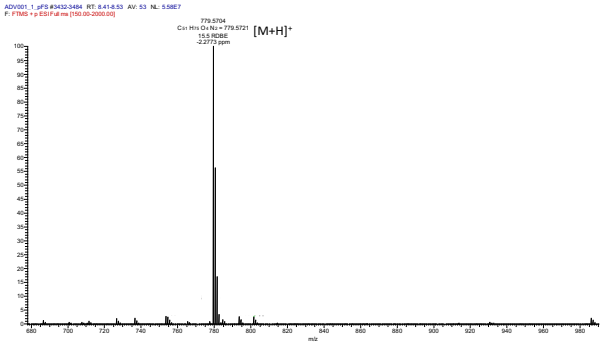

Figure A100. (+)-ESI-HRMS spectrum of the degradation fragments with elemental composition of $C_{51}H_{74}N_2O_4$ obtained from **PI 3000-D**.

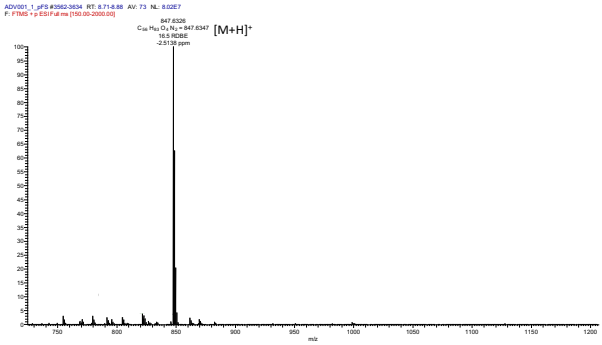

Figure A101. (+)-ESI-HRMS spectrum of the degradation fragments with elemental composition of $C_{56}H_{82}N_2O_4$ obtained from **PI 3000-D**.

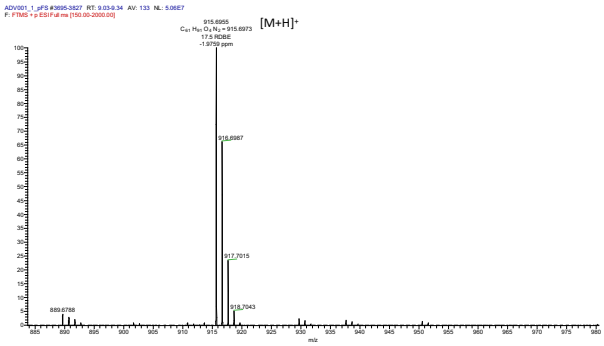

Figure A102. (+)-ESI-HRMS spectrum of the degradation fragments with elemental composition of $C_{61}H_{90}N_2O_4$ obtained from **PI 3000-D**.

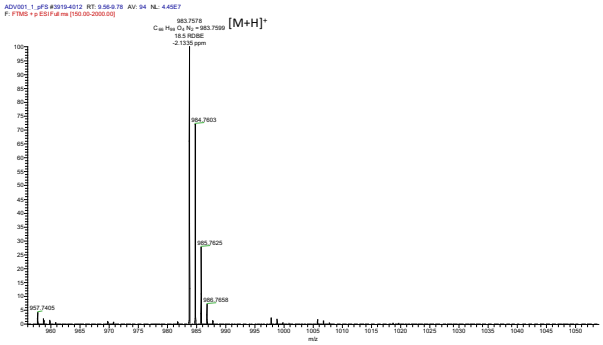

Figure A103. (+)-ESI-HRMS spectrum of the degradation fragments with elemental composition of $C_{66}H_{98}N_2O_4$ obtained from **PI 3000-D**.

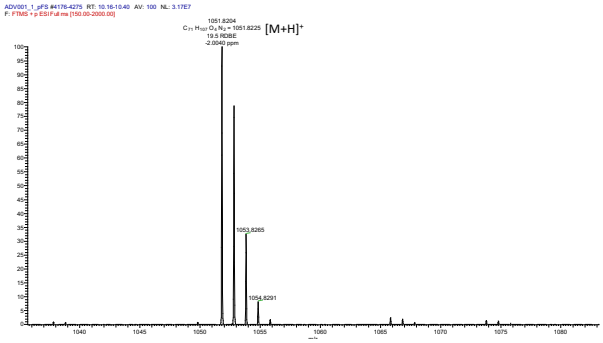

Figure A104. (+)-ESI-HRMS spectrum of the degradation fragments with elemental composition of $C_{71}H_{106}N_2O_4$ obtained from **PI 3000-D**.

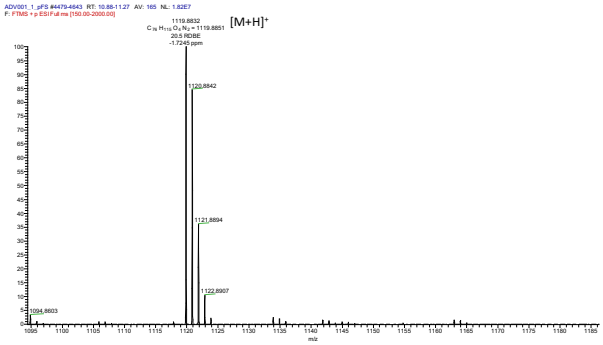

Figure 105. (+)-ESI-HRMS spectrum of the degradation fragments with elemental composition of $C_{76}H_{114}N_2O_4$ obtained from **PI 3000-D**.

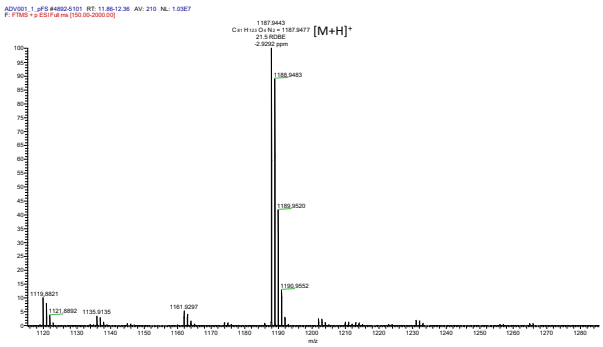

Figure A106. (+)-ESI-HRMS spectrum of the degradation fragments with elemental composition of $C_{81}H_{122}N_2O_4$ obtained from **PI 3000-D**.

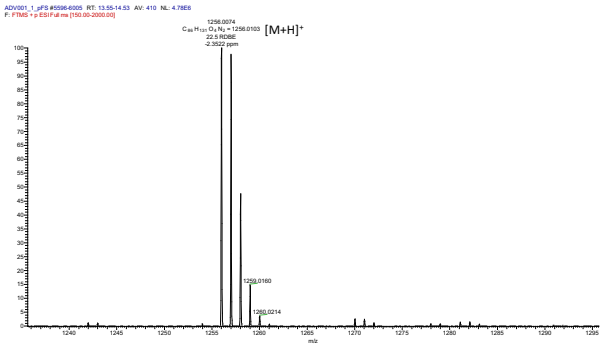

Figure A107. (+)-ESI-HRMS spectrum of the degradation fragments with elemental composition of $C_{86}H_{130}N_2O_4$ obtained from **PI 3000-D**.

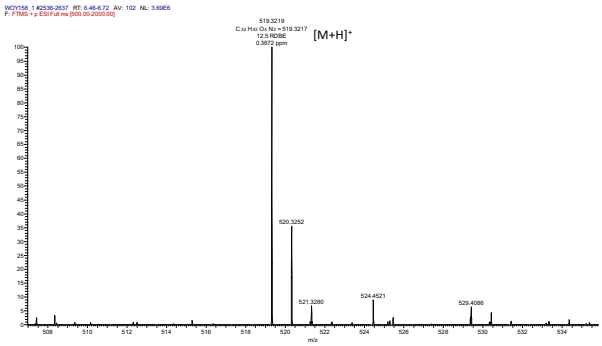

Figure A108. (+)-ESI-HRMS spectrum of the degradation fragments with elemental composition of $C_{32}H_{42}N_2O_4$ obtained from **PB 3500-D**.

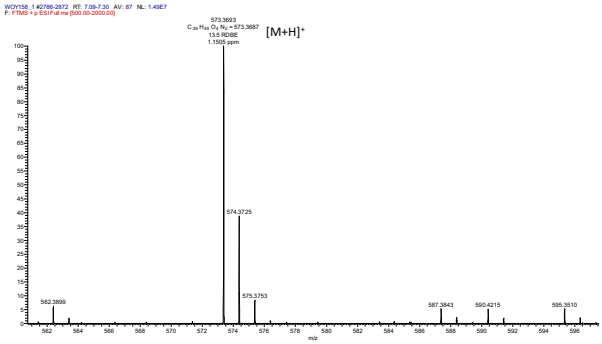

Figure A109. (+)-ESI-HRMS spectrum of the degradation fragments with elemental composition of $C_{36}H_{48}N_2O_4$ obtained from **PB 3500-D**.

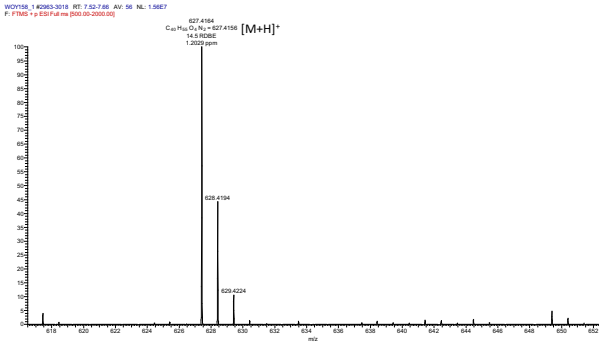

Figure A110. (+)-ESI-HRMS spectrum of the degradation fragments with elemental composition of $C_{40}H_{54}N_2O_4$ obtained from **PB 3500-D**.

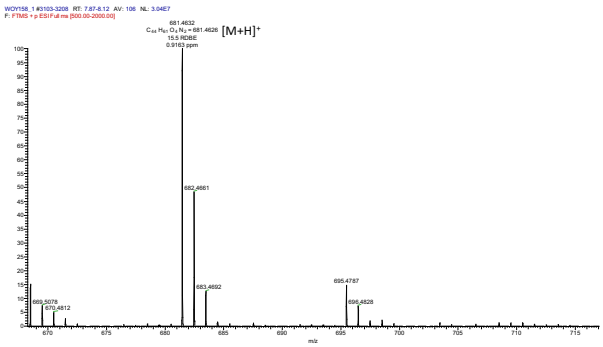

Figure A111. (+)-ESI-HRMS spectrum of the degradation fragments with elemental composition of $C_{44}H_{60}N_2O_4$ obtained from **PB 3500-D**.

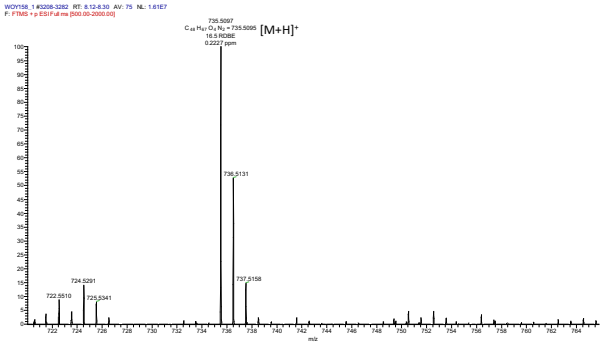

Figure A112. (+)-ESI-HRMS spectrum of the degradation fragments with elemental composition of $C_{48}H_{66}N_2O_4$ obtained from **PB 3500-D**.

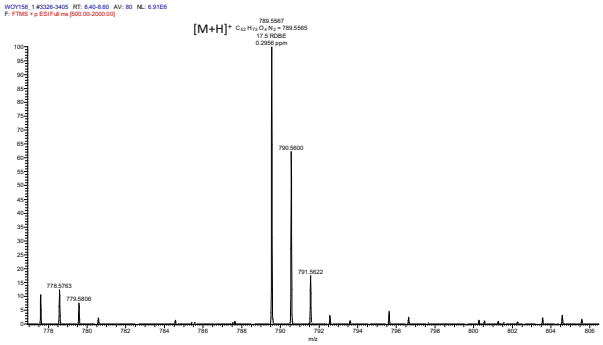

Figure A113. (+)-ESI-HRMS spectrum of the degradation fragments with elemental composition of $C_{52}H_{72}N_2O_4$ obtained from **PB 3500-D**.

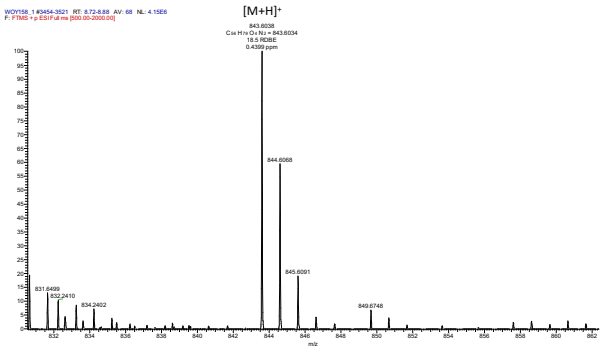

Figure A114. (+)-ESI-HRMS spectrum of the degradation fragments with elemental composition of $C_{56}H_{78}N_2O_4$ obtained from **PB 3500-D**.

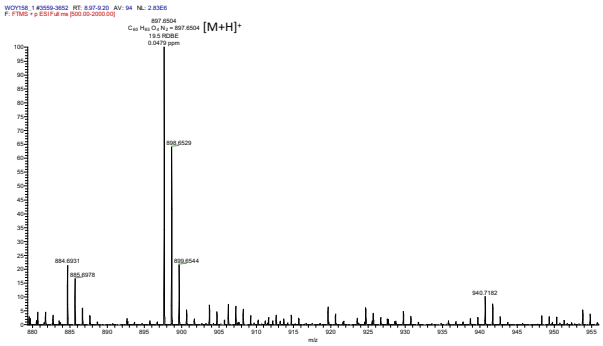

Figure A115. (+)-ESI-HRMS spectrum of the degradation fragments with elemental composition of $C_{60}H_{84}N_2O_4$ obtained from **PB 3500-D**.

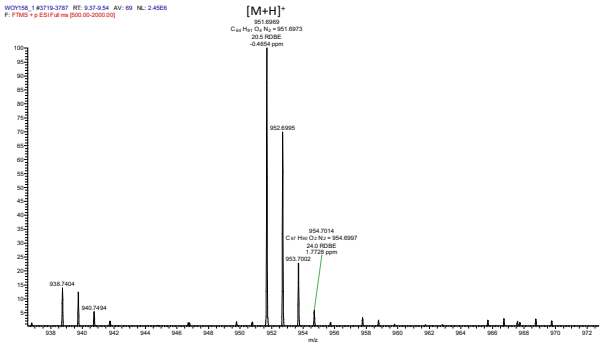

Figure A116. (+)-ESI-HRMS spectrum of the degradation fragments with elemental composition of $C_{64}H_{90}N_2O_4$ obtained from **PB 3500-D**.

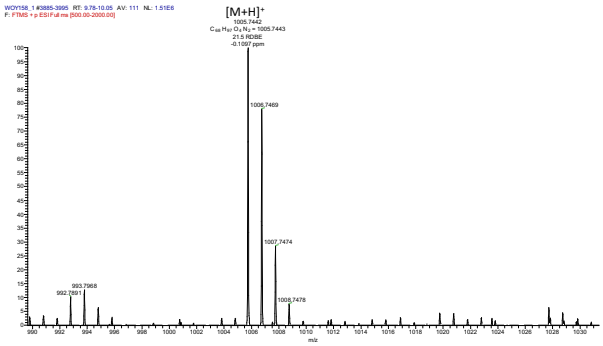

Figure A117. (+)-ESI-HRMS spectrum of the degradation fragments with elemental composition of $C_{68}H_{96}N_2O_4$ obtained from **PB 3500-D**.

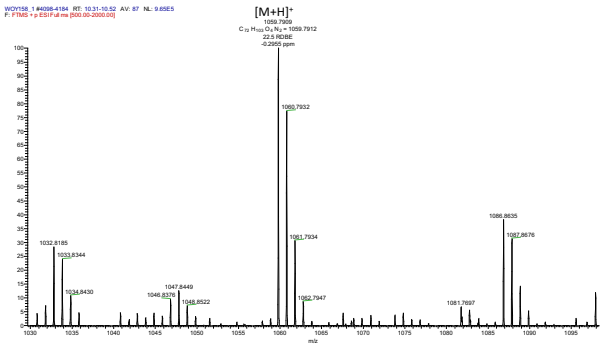

Figure A118. (+)-ESI-HRMS spectrum of the degradation fragments with elemental composition of $C_{72}H_{102}N_2O_4$ obtained from **PB 3500-D**.

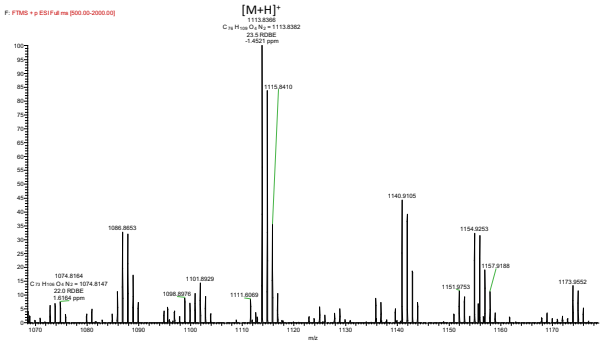

Figure A119. (+)-ESI-HRMS spectrum of the degradation fragments with elemental composition of $C_{76}H_{108}N_2O_4$ obtained from **PB 3500-D**.

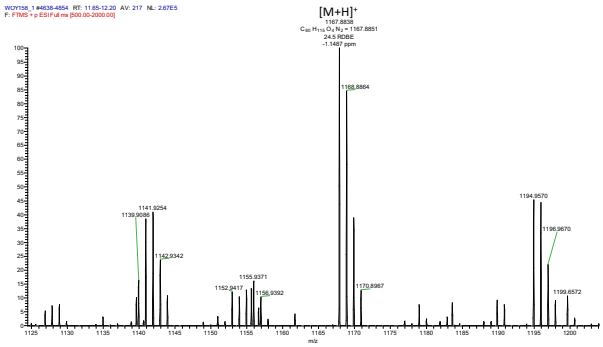

Figure A120. (+)-ESI-HRMS spectrum of the degradation fragments with elemental composition of $C_{80}H_{114}N_2O_4$ obtained from **PB 3500-D**.

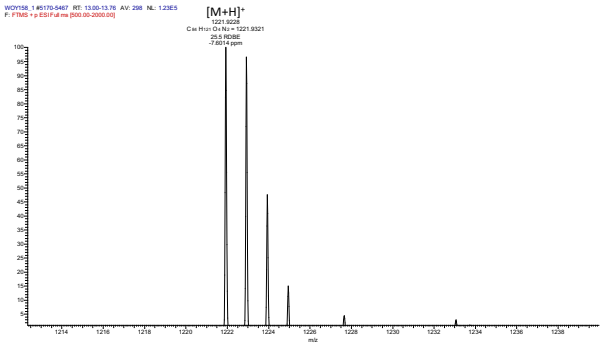

Figure A121. (+)-ESI-HRMS spectrum of the degradation fragments with elemental composition of $C_{84}H_{120}N_2O_4$ obtained from **PB 3500-D**.

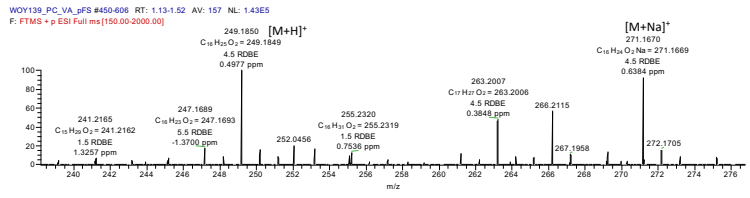

Figure A122. (+)-ESI-HRMS spectrum of the degradation fragments with elemental composition of $C_{16}H_{24}O_2$ obtained from **PB 200k-Ox**.

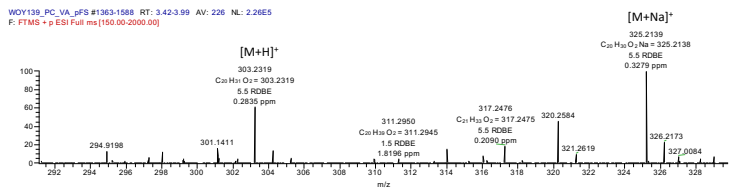

Figure A123. (+)-ESI-HRMS spectrum of the degradation fragments with elemental composition of $C_{20}H_{30}O_2$ obtained from **PB 200k-Ox**.

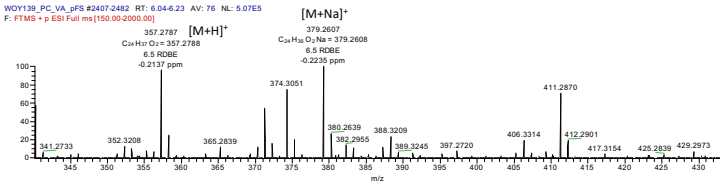

Figure A124. (+)-ESI-HRMS spectrum of the degradation fragments with elemental composition of $C_{24}H_{36}O_2$ obtained from **PB 200k-Ox**.

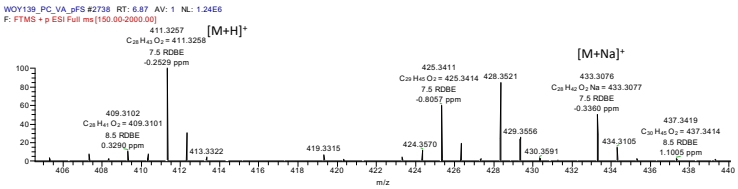

Figure A125. (+)-ESI-HRMS spectrum of the degradation fragments with elemental composition of $C_{28}H_{42}O_2$ obtained from **PB 200k-Ox**.

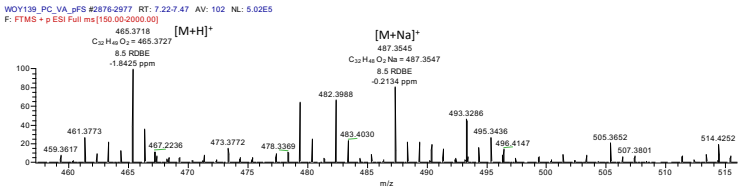

Figure A126. (+)-ESI-HRMS spectrum of the degradation fragments with elemental composition of $C_{32}H_{48}O_2$ obtained from **PB 200k-Ox**.

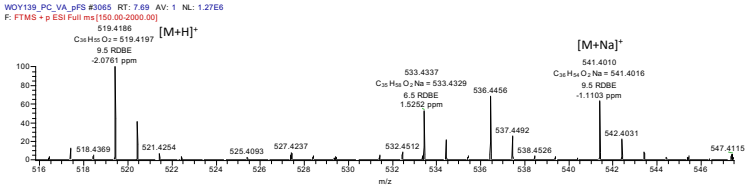

Figure A127. (+)-ESI-HRMS spectrum of the degradation fragments with elemental composition of $C_{36}H_{54}O_2$ obtained from **PB 200k-Ox**.

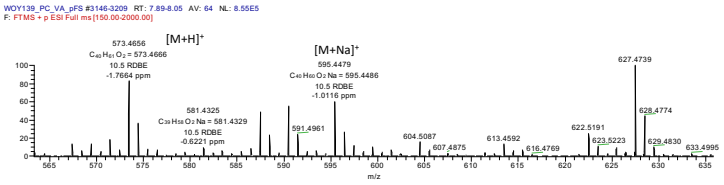

Figure A128. (+)-ESI-HRMS spectrum of the degradation fragments with elemental composition of $C_{40}H_{60}O_2$ obtained from **PB 200k-Ox**.

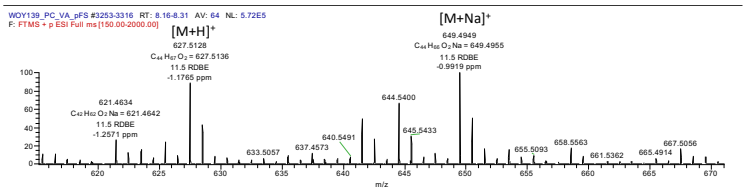

Figure A129. (+)-ESI-HRMS spectrum of the degradation fragments with elemental composition of $C_{44}H_{66}O_2$ obtained from **PB 200k-Ox**.

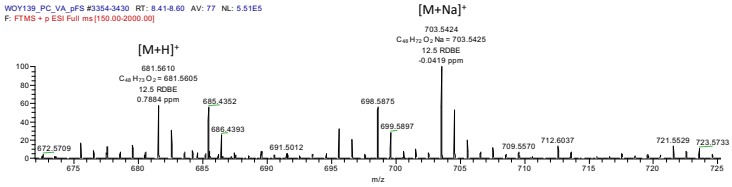

Figure A130. (+)-ESI-HRMS spectrum of the degradation fragments with elemental composition of $C_{48}H_{72}O_2$ obtained from **PB 200k-Ox**.

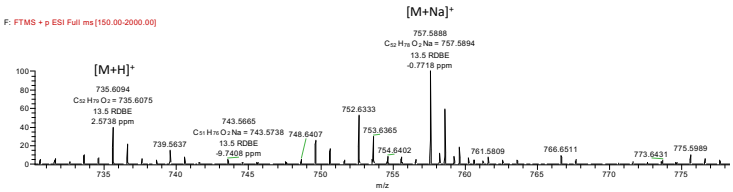

Figure A131. (+)-ESI-HRMS spectrum of the degradation fragments with elemental composition of $C_{52}H_{78}O_2$ obtained from **PB 200k-Ox**.

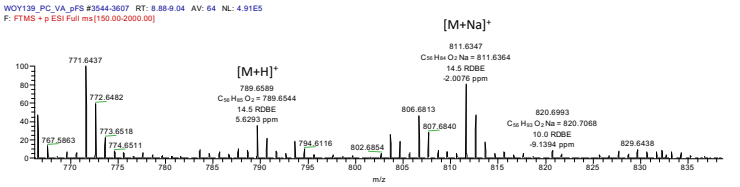

Figure A132. (+)-ESI-HRMS spectrum of the degradation fragments with elemental composition of $C_{56}H_{84}O_2$ obtained from **PB 200k-Ox**.

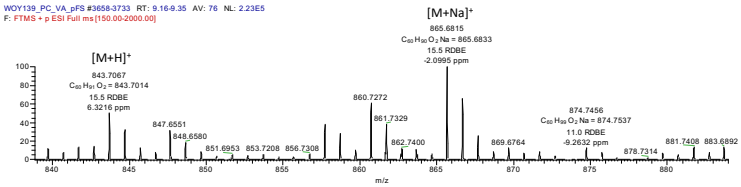

Figure A133. (+)-ESI-HRMS spectrum of the degradation fragments with elemental composition of $C_{60}H_{90}O_2$ obtained from **PB 200k-Ox**.

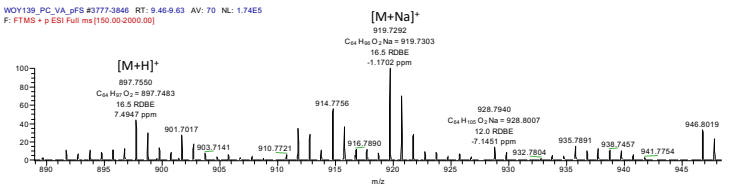

Figure A134. (+)-ESI-HRMS spectrum of the degradation fragments with elemental composition of $C_{64}H_{96}O_2$ obtained from **PB 200k-Ox**.

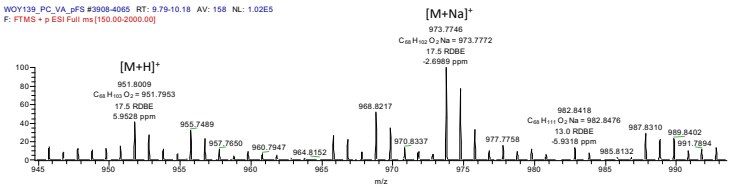

Figure A135. (+)-ESI-HRMS spectrum of the degradation fragments with elemental composition of $C_{68}H_{102}O_2$ obtained from **PB 200k-Ox**.

7.6 GPC-Data

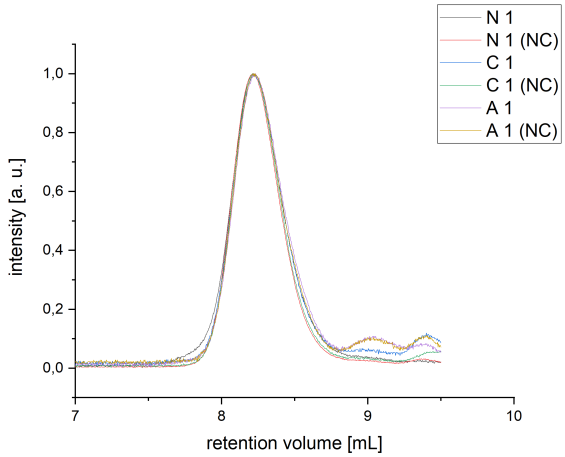

Figure A136. Stacked normalized GPC traces of Lcp_{K30} enzymatically degraded **PI 3000** with corresponding negative controls without the addition of enzyme. (**N 1**=black, N 1 (NC)=red, **C 1**= blue, C 1 (NC)= green, **A 1**=purple and A 1 (NC) light brown)

Table A11. Comparison number average molar mass NMR and GPC

Samples	$M_{n(GPC)}$	$M_{n(NMR)}$
PI 3000-Ox	1700	6100
PI 4500-Ox	2300	9700
PB 3500-Ox	2400	5600
PB 12000-Ox	5400	7100

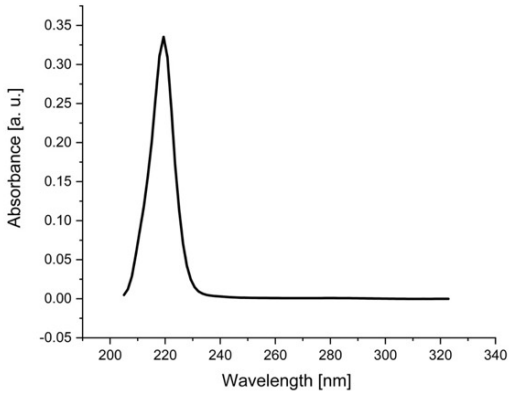

Figure A137. UV spectrum of **PI 3000** acquired with gel permeation chromatography.

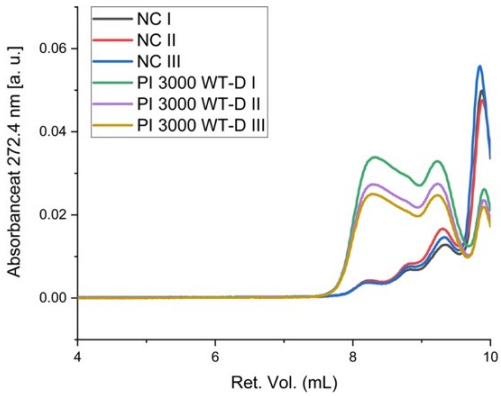

Figure A138. Stacked UV-GPC trace of triplicate of PI 3000 NC (negative control) at 272.4 nm (black, red, blue) and triplicate of PI 3000 WT-D at 272.4 nm (green, purple, yellow).

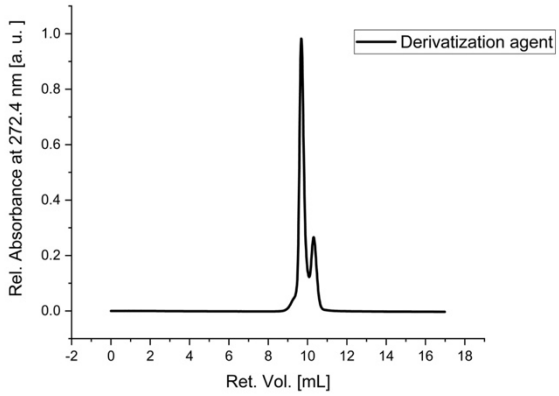

Figure A139. UV-GPC trace of the derivatization agent O-(4-methoxybenzyl)-hydroxylamine hydrochloride.

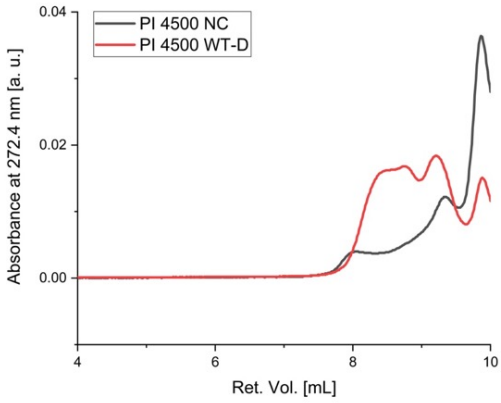

Figure A140. Stacked UV-GPC traces of PI 4500 NC (negative control) at 272.4 nm (black) and PI 4500 WT-D at 272.4 nm (red).

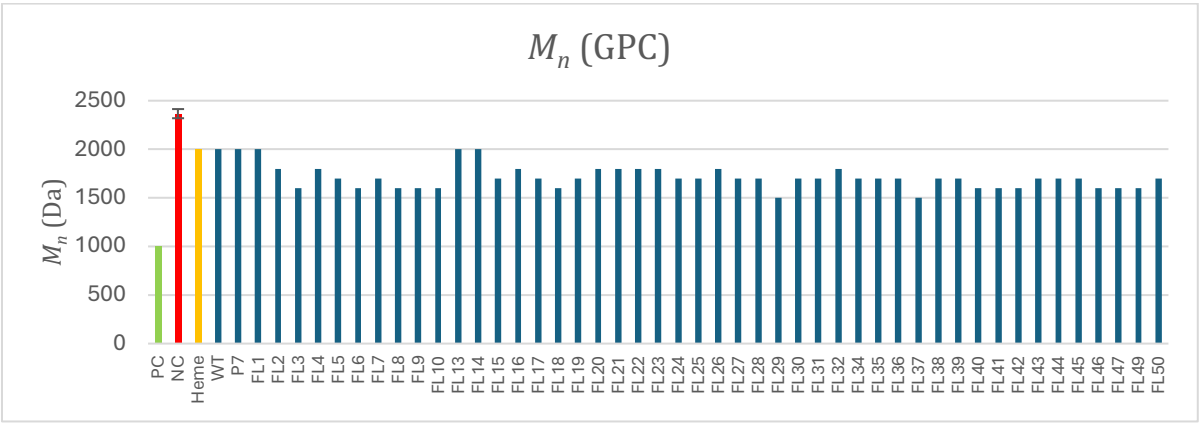

Figure A141. M_n of GPC of PB after reaction with the different Lcp_{K30}-FuncLib variants. As a positive control, a sample with chemically degraded polybutadiene was used. In collaboration with Yannick L. Wolf.

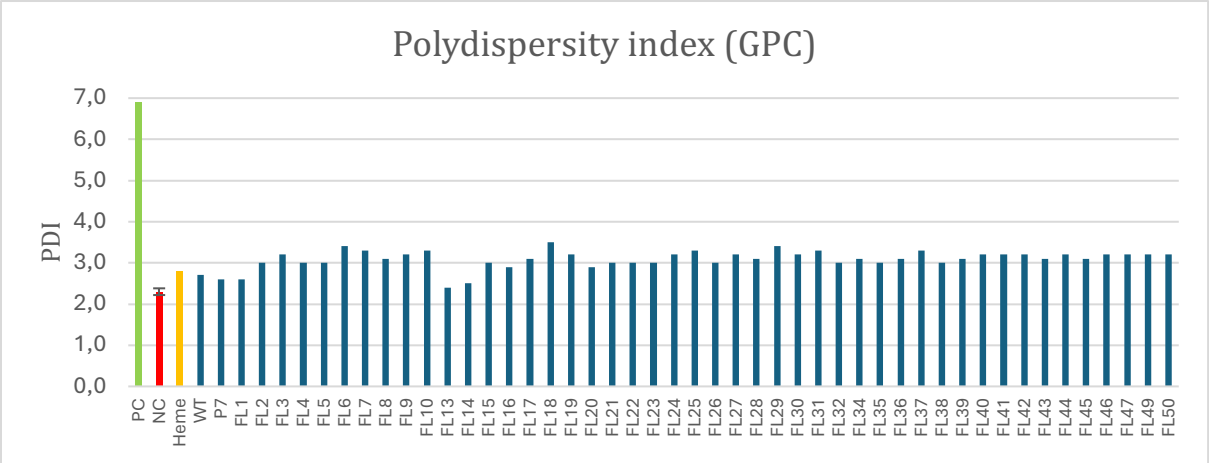

Figure A142. PDI of GPC graph of PB after reaction with the different Lcp_{K30}-FuncLib variants. As a positive control, a sample with chemically degraded polybutadiene was used. In collaboration with Yannick L. Wolf.

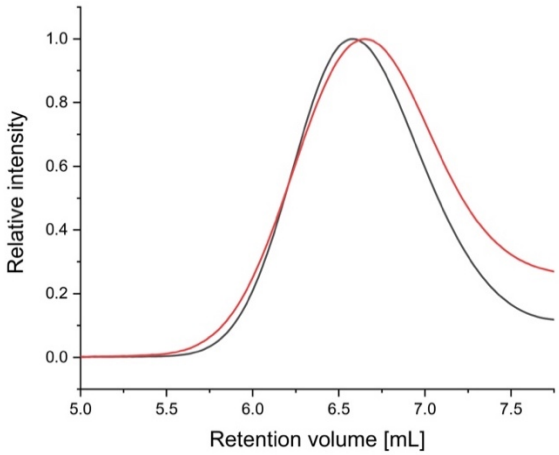

Figure A143. Comparison of the retention time of **MPFPM-2** (red) and **NP 1** (black). In collaboration with Mohamed Hassan.

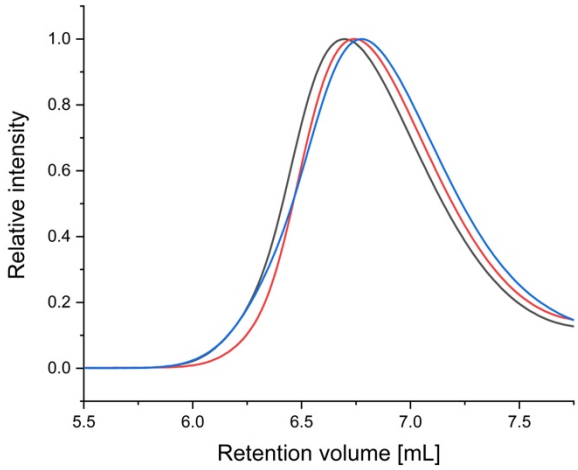

Figure A144. Comparison of the retention time of **MPFPA-2** (black) to **NP 2** (blue) and **NP 3** (red). In collaboration with Mohamed Hassan.

7.7 Protein sequences

Lcp_{K30}
PLWTWSPSASVAGTGVGVDPEYVWDEEADPVLAAVIDRGEVPAVNALLKQWTRNDQALPGGLPGDLREFMEHA
RRMPSWADKAALDRGAQFSKTKGIYVGALYGLGSGLMSTAIPRESRAVYYSKGGADMKDRIAKTARLGYDIGDLDA
YLPHGSMIVTAVKTRMVHAAVRHLLPQSPAWSQTSGGQKIPISQADIMVTWHSLATFVMRKMKQWGVRVNTAD
AEAYLHVWQVSAHMLGVSDEYIPATWDAANAQSKQVLDPILAHTPEGEALTEVLLGIVAELDAGLTRPLIGAFSRY
TLGGEVGDMIGLAKQPVLERLIATAWPLLVAFREGLIPLPAVPAVLWTLEEALRKFVLLFLSEGRRIAIDIPD

Lcp_{K30}-P7
PLWTWSPSGSVAGTGTGVDPEWVWDDEADPVVAAVIDRGEVPAVNALLRTWTRNGQPLPDGLPADLRDFMEQ
ARRLPSWADKAKLDRAAQFNKTKGFYIGVLYGLGSGMMSTAIPREARAVYYSKGGADMKDRIAKTAKLGYDIGDL
NAYRPDGSMIVTAVKTRLVHAAVRHLLPQSPAWSQTSGGQKIPISQADMMVTWHSLATFVMRKMKEWGVRVPA
ADAEAYLHMWQVAAHMLGVRDEYIPATWDAANAQAKQVLDPILAPTPEGKALADVLLNIVAELDAGLTRPLINA
FARYMLGDEIGDWIGLPRQPVWEALIATAWPLLVAFREGLIPLPLVPEVLWTLEEALRKFVLLFLSEGRRIHIEIPD

Lcp_{K30}-P7-FL01
PLWTWSPSGSVAGTGTGVDPEWVWDDEADPVVAAVIDRGEVPAVNALLRTWTRNGQPLPDGLPADLRDFMEQ
ARRLPSWADKAKLDRAAQFNKTKGFYIGVLYGLGSGMMSTAIPREARSIYYSKGGADMKDRIAKSAKLGYDIGDLN
AYRPDGSMIVTAVKVRLVHAAVRHLLPQSPAWSQTSGGQKIPLSQADMMVTWHSLATFVMRKMKEWGVRVPAA
DAEAYLHMWQVAAHMLGVRDEYIPATWDAANAQAKQVLDPILAPTPEGKALADVLLNIVAELDAGLTRPLINAF
ARYMLGDEIGDWIGLPRQPVWEALIATAWPLLVAFREGLIPLPLVPEVLWTLEEALRKFVLLFLSEGRRIHIEIPD

Lcp_{K30}-P7-FL02
PLWTWSPSGSVAGTGTGVDPEWVWDDEADPVVAAVIDRGEVPAVNALLRTWTRNGQPLPDGLPADLRDFMEQ
ARRLPSWADKAKLDRAAQFNKTKGFYIGVLYGLGSGMMSTAIPREARAVYYSKGGADMKDRIAKTAKLGYDIGDL
NAYRPDGSMIVTAVKVRLVHAAVRHLLPQSPAWSQTSGGQKIPLSQADMMVTWHSLATFVMRKMKEWGVRVPA
ADAEAYLHMWQVAAHMLGVRDEYIPATWDAANAQAKQVLDPILAPTPEGKALADVLLNIVAELDAGLTRPLINA
FARYMLGDEIGDWIGLPRQPVWEALIATAWPLLVAFREGLIPLPLVPEVLWTLEEALRKFVLLFLSEGRRIHFEIPD

Lcp_{K30}-P7-FL03
PLWTWSPSGSVAGTGTGVDPEWVWDDEADPVVAAVIDRGEVPAVNALLRTWTRNGQPLPDGLPADLRDFMEQ
ARRLPSWADKAKLDRAAQFNKTKGFYIGVLYGLGSGMMSTAIPREARAVYYSKGGADMKDRIAKTAKIGYDIGDL
NAYRPDGSMIVTAVKVRLVHAAVRHLLPQSPAWSQTSGGQKIPLSQADMMVTWHSLATFVMRKMKEWGVRVPA
ADAEAYLHMWQVAAHMLGVRDEYIPATWDAANAQAKQVLDPILAPTPEGKALADVLLNIVAELDAGLTRPLINA
FARYMLGDEIGDWIGLPRQPVWEALIATAWPLLVAFREGLIPLPLVPEVLWTLEEALRKFVLLFLSEGRRIHVEIPD

Lcp_{K30}-P7-FL04
PLWTWSPSGSVAGTGTGVDPEWVWDDEADPVVAAVIDRGEVPAVNALLRTWTRNGQPLPDGLPADLRDFMEQ
ARRLPSWADKAKLDRAAQFNKTKGFYIGVLYGLGSGMMSTAIPREARAVYYSKGGADMKDRIAKTAKVGYDIGDL
NAYRPDGSMIVTAVKVRLVHAAVRHLLPQSPAWSQTSGGQKIPLSQADMMVTWHSLATFVMRKMKEWGVRVPA
ADAEAYLHMWQVAAHMLGVRDEYIPATWDAANAQAKQVLDPILAPTPEGKALADVLLNIVAELDAGLTRPLINA
FARYMLGDEIGDWIGLPRQPVWEALIATAWPLLVAFREGLIPLPLVPEVLWTLEEALRKFVLLFLSEGRRIHIEIPD

Lcp_{K30}-P7-FL05
PLWTWSPSGSVAGTGTGVDPEWVWDDEADPVVAAVIDRGEVPAVNALLRTWTRNGQPLPDGLPADLRDFMEQ
ARRLPSWADKAKLDRAAQFNKTKGFYIGVLYGLGSGMMSTAIPREARAVYYSKGGADMKDRIAKSAKLGYDIGDL
NAYRPDGSMIVTAVKVRLVHAAVRHLLPQSPAWSQTSGGQKIPLSQADMMVTWHSLATFVMRKMKEWGVRVPA
ADAEAYLHMWQVAAHMLGVRDEYIPATWDAANAQAKQVLDPILAPTPEGKALADVLLNIVAELDAGLTRPLINA
FARYMLGDEIGDWIGLPRQPVWEALIATAWPLLVAFREGLIPLPLVPEVLWTLEEALRKFVLLFLSEGRRIHVEIPD

Lcp_{K30}-P7-FL06
PLWTWSPSGSVAGTGTGVDPEWVWDDEADPVVAAVIDRGEVPAVNALLRTWTRNGQPLPDGLPADLRDFMEQ
ARRLPSWADKAKLDRAAQFNKTKGFYIGVLYGLGSGMMSTAIPREARAVYYAKGGADMKDRIAKTAKLGYDIGDL
NAYRPDGSMIVTAVKVRLVHAAVRHLLPQSPAWSQTSGGQKIPLSQADMMVTWHSLATFVMRKMKEWGVRVPA
ADAEAYLHMWQVAAHMLGVRDEYIPATWDAANAQAKQVLDPILAPTPEGKALADVLLNIVAELDAGLTRPLINA
FARYMLGDEIGDWIGLPRQPVWEALIATAWPLLVAFREGLIPLPLVPEVLWTLEEALRKFVLLFLSEGRRIHVEIPD

Lcp_{K30}-P7-FL07
PLWTWSPSGSVAGTGTGVDPEWVWDDEADPVVAAVIDRGEVPAVNALLRTWTRNGQPLPDGLPADLRDFMEQ
ARRLPSWADKAKLDRAAQFNKTKGFYIGVLYGLGSGMMSTAIPREARAVYYAKGGADMKDRIAKTAKIGYDIGDL
NAYRPDGSMIVTAVKTRLVHAAVRHLLPQSPAWSQTSGGQKIPLSQADMMVTWHSLATFVMRKMKEWGVRVPA
ADAEAYLHMWQVAAHMLGVRDEYIPATWDAANAQAKQVLDPILAPTPEGKALADVLLNIVAELDAGLTRPLINA
FARYMLGDEIGDWIGLPRQPVWEALIATAWPLLVAFREGLIPLPLVPEVLWTLEEALRKFVLLFLSEGRRIHIEIPD

Lcp_{K30}-P7-FL08
PLWTWSPSGSVAGTGTGVDPEWVWDDEADPVVAAVIDRGEVPAVNALLRTWTRNGQPLPDGLPADLRDFMEQ
ARRLPSWADKAKLDRAAQFNKTKGFYIGVLYGLGSGMMSTAIPREARAVYYAKGGADMKDRIAKTAKMGYDIGDL
NAYRPDGSMIVTAVKVRLVHAAVRHLLPQSPAWSQTSGGQKIPLSQADMMVTWHSLATFVMRKMKEWGVRVPA
ADAEAYLHMWQVAAHMLGVRDEYIPATWDAANAQAKQVLDPILAPTPEGKALADVLLNIVAELDAGLTRPLINA
FARYMLGDEIGDWIGLPRQPVWEALIATAWPLLVAFREGLIPLPLVPEVLWTLEEALRKFVLLFLSEGRRIHIEIPD

Lcp_{K30}-P7-FL09
PLWTWSPSGSVAGTGTGVDPEWVWDDEADPVVAAVIDRGEVPAVNALLRTWTRNGQPLPDGLPADLRDFMEQ
ARRLPSWADKAKLDRAAQFNKTKGFYIGVLYGLGSGMMSTAIPREARAIYYSKGGADMKDRIAKTAKLGYDIGDLN
AYRPDGSMIVTAVKVRLVHAAVRHLLPQSPAWSQTSGGQKIPLSQADMMVTWHSLATFVMRKMKEWGVRVPAA
DAEAYLHMWQVAAHMLGVRDEYIPATWDAANAQAKQVLDPILAPTPEGKALADVLLNIVAELDAGLTRPLINAF
ARYMLGDEIGDWIGLPRQPVWEALIATAWPLLVAFREGLIPLPLVPEVLWTLEEALRKFVLLFLSEGRRIHIEIPD

Lcp_{K30}-P7-FL10
PLWTWSPSGSVAGTGTGVDPEWVWDDEADPVVAAVIDRGEVPAVNALLRTWTRNGQPLPDGLPADLRDFMEQ
ARRLPSWADKAKLDRAAQFNKTKGFYIGVLYGLGSGMMSTAIPREARAIYYSKGGADMKDRIAKTAKMGYDIGDL
NAYRPDGSMIVTAVKVRLVHAAVRHLLPQSPAWSQTSGGQKIPLSQADMMVTWHSLATFVMRKMKEWGVRVPA
ADAEAYLHMWQVAAHMLGVRDEYIPATWDAANAQAKQVLDPILAPTPEGKALADVLLNIVAELDAGLTRPLINA
FARYMLGDEIGDWIGLPRQPVWEALIATAWPLLVAFREGLIPLPLVPEVLWTLEEALRKFVLLFLSEGRRIHFEIPD

Lcp_{K30}-P7-FL11
PLWTWSPSGSVAGTGTGVDPEWVWDDEADPVVAAVIDRGEVPAVNALLRTWTRNGQPLPDGLPADLRDFMEQ
ARRLPSWADKAKLDRAAQFNKTKGFYIGVLYGLGSGMMSTAIPREARAIYYSKGGADMKDRIAKTAKMGYDIGDL
NAYRPDGSMIVTAVKVRLVHAAVRHLLPQSPAWSQTSGGQKIPLSQADMMVSWHSLATFVMRKMKEWGVRVPA
ADAEAYLHMWQVAAHMLGVRDEYIPATWDAANAQAKQVLDPILAPTPEGKALADVLLNIVAELDAGLTRPLINA
FARYMLGDEIGDWIGLPRQPVWEALIATAWPLLVAFREGLIPLPLVPEVLWTLEEALRKFVLLFLSEGRRIHIEIPD

Lcp_{K30}-P7-FL12
PLWTWSPSGSVAGTGTGVDPEWVWDDEADPVVAAVIDRGEVPAVNALLRTWTRNGQPLPDGLPADLRDFMEQ
ARRLPSWADKAKLDRAAQFNKTKGFYIGVLYGLGSGMMSTAIPREARAIYYSKGGADMKDRIAKTAKVGYDIGDL
NAYRPDGSMIVTAVKTRLVHAAVRHLLPQSPAWSQTSGGQKIPLSQADMMVTWHSLATFVMRKMKEWGVRVPA
ADAEAYLHMWQVAAHMLGVRDEYIPATWDAANAQAKQVLDPILAPTPEGKALADVLLNIVAELDAGLTRPLINA
FARYMLGDEIGDWIGLPRQPVWEALIATAWPLLVAFREGLIPLPLVPEVLWTLEEALRKFVLLFLSEGRRIHIEIPD

Lcp_{K30}-P7-FL13
PLWTWSPSGSVAGTGTGVDPEWVWDDEADPVVAAVIDRGEVPAVNALLRTWTRNGQPLPDGLPADLRDFMEQ
ARRLPSWADKAKLDRAAQFNKTKGFYIGVLYGLGSGMMSTAIPREARAIYYSKGGADMKDRIAKTAKVGYDIGDL
NAYRPDGSMIVTAVKVRLVHAAVRHLLPQSPAWSQTSGGQKIPLSQADMMVTWHSLATFVMRKMKEWGVRVPA
ADAEAYLHMWQVAAHMLGVRDEYIPATWDAANAQAKQVLDPILAPTPEGKALADVLLNIVAELDAGLTRPLINA
FARYMLGDEIGDWIGLPRQPVWEALIATAWPLLVAFREGLIPLPLVPEVLWTLEEALRKFVLLFLSEGRRIHVEIPD

Lcp_{K30}-P7-FL14
PLWTWSPSGSVAGTGTGVDPEWVWDDEADPVVAAVIDRGEVPAVNALLRTWTRNGQPLPDGLPADLRDFMEQ
ARRLPSWADKAKLDRAAQFNKTKGFYIGVLYGLGSGMMSTAIPREARAIYYSKGGADMKDRIAKSAKLGYDIGDLN
AYRPDGSMIVTAVKVRLVHAAVRHLLPQSPAWSQTSGGQKIPLSQADMMVSWHSLATFVMRKMKEWGVRVPAA
DAEAYLHMWQVAAHMLGVRDEYIPATWDAANAQAKQVLDPILAPTPEGKALADVLLNIVAELDAGLTRPLINAF
ARYMLGDEIGDWIGLPRQPVWEALIATAWPLLVAFREGLIPLPLVPEVLWTLEEALRKFVLLFLSEGRRIHIEIPD

Lcp_{K30}-P7-FL15
PLWTWSPSGSVAGTGTGVDPEWVWDDEADPVVAAVIDRGEVPAVNALLRTWTRNGQPLPDGLPADLRDFMEQ
ARRLPSWADKAKLDRAAQFNKTKGFYIGVLYGLGSGMMSTAIPREARAIYYSKGGADMKDRIAKSAKIGYDIGDLN
AYRPDGSMIVTAVKVRLVHAAVRHLLPQSPAWSQTSGGQKIPLSQADMMVTWHSLATFVMRKMKEWGVRVPAA

DAEAYLHMWQVAAHMLGVRDEYIPATWDAANAQAKQVLDPILAPTPEGKALADVLLNIVAELDAGLTRPLINAF
ARYMLGDEIGDWIGLPRQPVWEALIATAWPLLVAFREGLIPLPLVPEVLWTLEEALRKFVLLFLSEGRRIHIEIPD

Lcp$_{K30}$-P7-FL16
PLWTWSPSGSVAGTGTGVDPEWVWDDEADPVVAAVIDRGEVPAVNALLRTWTRNGQPLPDGLPADLRDFMEQ
ARRLPSWADKAKLDRAAQFNKTKGFYIGVLYGLGSGMMSTAIPREARAIYYSKGGADMKDKIAKTAKIGYDIGDLN
AYRPDGSMIVTAVKVRLVHAAVRHLLPQSPAWSQTSGGQKIPLSQADMMVTWHSLATFVMRKMKEWGVRVPAA
DAEAYLHMWQVAAHMLGVRDEYIPATWDAANAQAKQVLDPILAPTPEGKALADVLLNIVAELDAGLTRPLINAF
ARYMLGDEIGDWIGLPRQPVWEALIATAWPLLVAFREGLIPLPLVPEVLWTLEEALRKFVLLFLSEGRRIHIEIPD

Lcp$_{K30}$-P7-FL17
PLWTWSPSGSVAGTGTGVDPEWVWDDEADPVVAAVIDRGEVPAVNALLRTWTRNGQPLPDGLPADLRDFMEQ
ARRLPSWADKAKLDRAAQFNKTKGFYIGVLYGLGSGMMSTAIPREARAIYYAKGGADMKDRIAKTAKLGYDIGDL
NAYRPDGSMIVTAVKVRLVHAAVRHLLPQSPAWSQTSGGQKIPLSQADMMVTWHSLATFVMRKMKEWGVRVPA
ADAEAYLHMWQVAAHMLGVRDEYIPATWDAANAQAKQVLDPILAPTPEGKALADVLLNIVAELDAGLTRPLINA
FARYMLGDEIGDWIGLPRQPVWEALIATAWPLLVAFREGLIPLPLVPEVLWTLEEALRKFVLLFLSEGRRIHLEIPD

Lcp$_{K30}$-P7-FL18
PLWTWSPSGSVAGTGTGVDPEWVWDDEADPVVAAVIDRGEVPAVNALLRTWTRNGQPLPDGLPADLRDFMEQ
ARRLPSWADKAKLDRAAQFNKTKGFYIGVLYGLGSGMMSTAIPREARAIYYAKGGADMKDRIAKTAKLGYDIGDL
NAYRPDGSMIVTAVKVRLVHAAVRHLLPQSPAWSQTSGGQKIPLSQADMMVSWHSLATFVMRKMKEWGVRVPA
ADAEAYLHMWQVAAHMLGVRDEYIPATWDAANAQAKQVLDPILAPTPEGKALADVLLNIVAELDAGLTRPLINA
FARYMLGDEIGDWIGLPRQPVWEALIATAWPLLVAFREGLIPLPLVPEVLWTLEEALRKFVLLFLSEGRRIHIEIPD

Lcp$_{K30}$-P7-FL19
PLWTWSPSGSVAGTGTGVDPEWVWDDEADPVVAAVIDRGEVPAVNALLRTWTRNGQPLPDGLPADLRDFMEQ
ARRLPSWADKAKLDRAAQFNKTKGFYIGVLYGLGSGMMSTAIPREARAIYYAKGGADMKDRIAKTAKIGYDIGDLN
AYRPDGSMIVTAVKTRLVHAAVRHLLPQSPAWSQTSGGQKIPLSQADMMVTWHSLATFVMRKMKEWGVRVPAA
DAEAYLHMWQVAAHMLGVRDEYIPATWDAANAQAKQVLDPILAPTPEGKALADVLLNIVAELDAGLTRPLINAF
ARYMLGDEIGDWIGLPRQPVWEALIATAWPLLVAFREGLIPLPLVPEVLWTLEEALRKFVLLFLSEGRRIHVEIPD

Lcp$_{K30}$-P7-FL20
PLWTWSPSGSVAGTGTGVDPEWVWDDEADPVVAAVIDRGEVPAVNALLRTWTRNGQPLPDGLPADLRDFMEQ
ARRLPSWADKAKLDRAAQFNKTKGFYIGVLYGLGSGMMSTAIPREARAIYYAKGGADMKDRIAKTAKIGYDIGDLN
AYRPDGSMIVTAVKVRLVHAAVRHLLPQSPAWSQTSGGQKIPLSQADMMVTWHSLATFVMRKMKEWGVRVPAA
DAEAYLHMWQVAAHMLGVRDEYIPATWDAANAQAKQVLDPILAPTPEGKALADVLLNIVAELDAGLTRPLINAF
ARYMLGDEIGDWIGLPRQPVWEALIATAWPLLVAFREGLIPLPLVPEVLWTLEEALRKFVLLFLSEGRRIHIEIPD

Lcp$_{K30}$-P7-FL21
PLWTWSPSGSVAGTGTGVDPEWVWDDEADPVVAAVIDRGEVPAVNALLRTWTRNGQPLPDGLPADLRDFMEQ
ARRLPSWADKAKLDRAAQFNKTKGFYIGVLYGLGSGMMSTAIPREARAIYYAKGGADMKDRIAKSAKLGYDIGDL
NAYRPDGSMIVTAVKVRLVHAAVRHLLPQSPAWSQTSGGQKIPLSQADMMVTWHSLATFVMRKMKEWGVRVPA
ADAEAYLHMWQVAAHMLGVRDEYIPATWDAANAQAKQVLDPILAPTPEGKALADVLLNIVAELDAGLTRPLINA
FARYMLGDEIGDWIGLPRQPVWEALIATAWPLLVAFREGLIPLPLVPEVLWTLEEALRKFVLLFLSEGRRIHIEIPD

Lcp$_{K30}$-P7-FL22
PLWTWSPSGSVAGTGTGVDPEWVWDDEADPVVAAVIDRGEVPAVNALLRTWTRNGQPLPDGLPADLRDFMEQ
ARRLPSWADKAKLDRAAQFNKTKGFYIGVLYGLGSGMMSTAIPREARALYYSKGGADMKDRIAKTAKIGYDIGDLN
AYRPDGSMIVTAVKVRLVHAAVRHLLPQSPAWSQTSGGQKIPLSQADMMVTWHSLATFVMRKMKEWGVRVPAA
DAEAYLHMWQVAAHMLGVRDEYIPATWDAANAQAKQVLDPILAPTPEGKALADVLLNIVAELDAGLTRPLINAF
ARYMLGDEIGDWIGLPRQPVWEALIATAWPLLVAFREGLIPLPLVPEVLWTLEEALRKFVLLFLSEGRRIHIEIPD

Lcp$_{K30}$-P7-FL23
PLWTWSPSGSVAGTGTGVDPEWVWDDEADPVVAAVIDRGEVPAVNALLRTWTRNGQPLPDGLPADLRDFMEQ
ARRLPSWADKAKLDRAAQFNKTKGFYIGVLYGLGSGMMSTAIPREARALYYSKGGADMKDKIAKTAKLGYDIGDL
NAYRPDGSMIVTAVKVRLVHAAVRHLLPQSPAWSQTSGGQKIPLSQADMMVTWHSLATFVMRKMKEWGVRVPA
ADAEAYLHMWQVAAHMLGVRDEYIPATWDAANAQAKQVLDPILAPTPEGKALADVLLNIVAELDAGLTRPLINA
FARYMLGDEIGDWIGLPRQPVWEALIATAWPLLVAFREGLIPLPLVPEVLWTLEEALRKFVLLFLSEGRRIHVEIPD

Lcp_{K30}-P7-FL24
PLWTWSPSGSVAGTGTGVDPEWVWDDEADPVVAAVIDRGEVPAVNALLRTWTRNGQPLPDGLPADLRDFMEQ
ARRLPSWADKAKLDRAAQFNKTKGFYIGVLYGLGSGMMSTAIPREARALYYSKGGADMKDKIAKTAKVGYDIGDL
NAYRPDGSMIVTAVKVRLVHAAVRHLLPQSPAWSQTSGGQKIPLSQADMMVTWHSLATFVMRKMKEWGVRVPA
ADAEAYLHMWQVAAHMLGVRDEYIPATWDAANAQAKQVLDPILAPTPEGKALADVLLNIVAELDAGLTRPLINA
FARYMLGDEIGDWIGLPRQPVWEALIATAWPLLVAFREGLIPLPLVPEVLWTLEEALRKFVLLFLSEGRRIHIEIPD

Lcp_{K30}-P7-FL25
PLWTWSPSGSVAGTGTGVDPEWVWDDEADPVVAAVIDRGEVPAVNALLRTWTRNGQPLPDGLPADLRDFMEQ
ARRLPSWADKAKLDRAAQFNKTKGFYIGVLYGLGSGMMSTAIPREARAMYYSKGGADMKDRIAKTAKMGYDIGD
LNAYRPDGSMIVTAVKVRLVHAAVRHLLPQSPAWSQTSGGQKIPLSQADMMVTWHSLATFVMRKMKEWGVRVP
AADAEAYLHMWQVAAHMLGVRDEYIPATWDAANAQAKQVLDPILAPTPEGKALADVLLNIVAELDAGLTRPLIN
AFARYMLGDEIGDWIGLPRQPVWEALIATAWPLLVAFREGLIPLPLVPEVLWTLEEALRKFVLLFLSEGRRIHVEIP
D

Lcp_{K30}-P7-FL26
PLWTWSPSGSVAGTGTGVDPEWVWDDEADPVVAAVIDRGEVPAVNALLRTWTRNGQPLPDGLPADLRDFMEQ
ARRLPSWADKAKLDRAAQFNKTKGFYIGVLYGLGSGMMSTAIPREARAMYYSKGGADMKDKIAKTAKMGYDIGD
LNAYRPDGSMIVTAVKVRLVHAAVRHLLPQSPAWSQTSGGQKIPLSQADMMVTWHSLATFVMRKMKEWGVRVP
AADAEAYLHMWQVAAHMLGVRDEYIPATWDAANAQAKQVLDPILAPTPEGKALADVLLNIVAELDAGLTRPLIN
AFARYMLGDEIGDWIGLPRQPVWEALIATAWPLLVAFREGLIPLPLVPEVLWTLEEALRKFVLLFLSEGRRIHIEIP
D

Lcp_{K30}-P7-FL27
PLWTWSPSGSVAGTGTGVDPEWVWDDEADPVVAAVIDRGEVPAVNALLRTWTRNGQPLPDGLPADLRDFMEQ
ARRLPSWADKAKLDRAAQFNKTKGFYIGVLYGLGSGMMSTAIPREARAMYYAKGGADMKDRIAKTAKLGYDIGDL
NAYRPDGSMIVTAVKVRLVHAAVRHLLPQSPAWSQTSGGQKIPLSQADMMVTWHSLATFVMRKMKEWGVRVPA
ADAEAYLHMWQVAAHMLGVRDEYIPATWDAANAQAKQVLDPILAPTPEGKALADVLLNIVAELDAGLTRPLINA
FARYMLGDEIGDWIGLPRQPVWEALIATAWPLLVAFREGLIPLPLVPEVLWTLEEALRKFVLLFLSEGRRIHFEIPD

Lcp_{K30}-P7-FL28
PLWTWSPSGSVAGTGTGVDPEWVWDDEADPVVAAVIDRGEVPAVNALLRTWTRNGQPLPDGLPADLRDFMEQ
ARRLPSWADKAKLDRAAQFNKTKGFYIGVLYGLGSGMMSTAIPREARAMYYAKGGADMKDKIAKTAKLGYDIGDL
NAYRPDGSMIVTAVKVRLVHAAVRHLLPQSPAWSQTSGGQKIPLSQADMMVTWHSLATFVMRKMKEWGVRVPA
ADAEAYLHMWQVAAHMLGVRDEYIPATWDAANAQAKQVLDPILAPTPEGKALADVLLNIVAELDAGLTRPLINA
FARYMLGDEIGDWIGLPRQPVWEALIATAWPLLVAFREGLIPLPLVPEVLWTLEEALRKFVLLFLSEGRRIHIEIPD

Lcp_{K30}-P7-FL29
PLWTWSPSGSVAGTGTGVDPEWVWDDEADPVVAAVIDRGEVPAVNALLRTWTRNGQPLPDGLPADLRDFMEQ
ARRLPSWADKAKLDRAAQFNKTKGFYIGVLYGLGSGMMSTAIPREARNVYYAKGGADMKDRIAKTAKIGYDIGDL
NAYRPDGSMIVTAVKVRLVHAAVRHLLPQSPAWSQTSGGQKIPLSQADMMVTWHSLATFVMRKMKEWGVRVPA
ADAEAYLHMWQVAAHMLGVRDEYIPATWDAANAQAKQVLDPILAPTPEGKALADVLLNIVAELDAGLTRPLINA
FARYMLGDEIGDWIGLPRQPVWEALIATAWPLLVAFREGLIPLPLVPEVLWTLEEALRKFVLLFLSEGRRIHIEIPD

Lcp_{K30}-P7-FL30
PLWTWSPSGSVAGTGTGVDPEWVWDDEADPVVAAVIDRGEVPAVNALLRTWTRNGQPLPDGLPADLRDFMEQ
ARRLPSWADKAKLDRAAQFNKTKGFYIGVLYGLGSGMMSTAIPREARSIYYSKGGADMKDRIAKTAKLGYDIGDLN
AYRPDGSMIVTAVKVRLVHAAVRHLLPQSPAWSQTSGGQKIPLSQADMMVTWHSLATFVMRKMKEWGVRVPAA
DAEAYLHMWQVAAHMLGVRDEYIPATWDAANAQAKQVLDPILAPTPEGKALADVLLNIVAELDAGLTRPLINAF
ARYMLGDEIGDWIGLPRQPVWEALIATAWPLLVAFREGLIPLPLVPEVLWTLEEALRKFVLLFLSEGRRIHFEIPD

Lcp_{K30}-P7-FL31
PLWTWSPSGSVAGTGTGVDPEWVWDDEADPVVAAVIDRGEVPAVNALLRTWTRNGQPLPDGLPADLRDFMEQ
ARRLPSWADKAKLDRAAQFNKTKGFYIGVLYGLGSGMMSTAIPREARSIYYSKGGADMKDRIAKTAKIGYDIGDLN
AYRPDGSMIVTAVKVRLVHAAVRHLLPQSPAWSQTSGGQKIPLSQADMMVTWHSLATFVMRKMKEWGVRVPAA
DAEAYLHMWQVAAHMLGVRDEYIPATWDAANAQAKQVLDPILAPTPEGKALADVLLNIVAELDAGLTRPLINAF
ARYMLGDEIGDWIGLPRQPVWEALIATAWPLLVAFREGLIPLPLVPEVLWTLEEALRKFVLLFLSEGRRIHIEIPD

Lcp_{K30}-P7-FL32
PLWTWSPSGSVAGTGTGVDPEWVWDDEADPVVAAVIDRGEVPAVNALLRTWTRNGQPLPDGLPADLRDFMEQ
ARRLPSWADKAKLDRAAQFNKTKGFYIGVLYGLGSGMMSTAIPREARSMYYSKGGADMKDRIAKTAKLGYDIGDL
NAYRPDGSMIVTAVKVRLVHAAVRHLLPQSPAWSQTSGGQKIPLSQADMMVTWHSLATFVMRKMKEWGVRVPA
ADAEAYLHMWQVAAHMLGVRDEYIPATWDAANAQAKQVLDPILAPTPEGKALADVLLNIVAELDAGLTRPLINA
FARYMLGDEIGDWIGLPRQPVWEALIATAWPLLVAFREGLIPLPLVPEVLWTLEEALRKFVLLFLSEGRRIHIEIPD

Lcp_{K30}-P7-FL33
PLWTWSPSGSVAGTGTGVDPEWVWDDEADPVVAAVIDRGEVPAVNALLRTWTRNGQPLPDGLPADLRDFMEQ
ARRLPSWADKAKLDRAAQFNKTKGFYIGVLYGLGSGMMSTAIPRESRAVYYAKGGADMKDRIAKTAKLGYDIGDL
NAYRPDGSMIVTAVKVRLVHAAVRHLLPQSPAWSQTSGGQKIPLSQADMMVTWHSLATFVMRKMKEWGVRVPA
ADAEAYLHMWQVAAHMLGVRDEYIPATWDAANAQAKQVLDPILAPTPEGKALADVLLNIVAELDAGLTRPLINA
FARYMLGDEIGDWIGLPRQPVWEALIATAWPLLVAFREGLIPLPLVPEVLWTLEEALRKFVLLFLSEGRRIHFEIPD

Lcp_{K30}-P7-FL34
PLWTWSPSGSVAGTGTGVDPEWVWDDEADPVVAAVIDRGEVPAVNALLRTWTRNGQPLPDGLPADLRDFMEQ
ARRLPSWADKAKLDRAAQFNKTKGFYIGVLYGLGSGMMSTAIPRESRAIYYSKGGADMKDRIAKTAKLGYDIGDLN
AYRPDGSMIVTAVKVRLVHAAVRHLLPQSPAWSQTSGGQKIPLSQADMMVTWHSLATFVMRKMKEWGVRVPAA
DAEAYLHMWQVAAHMLGVRDEYIPATWDAANAQAKQVLDPILAPTPEGKALADVLLNIVAELDAGLTRPLINAF
ARYMLGDEIGDWIGLPRQPVWEALIATAWPLLVAFREGLIPLPLVPEVLWTLEEALRKFVLLFLSEGRRIHFEIPD

Lcp_{K30}-P7-FL35
PLWTWSPSGSVAGTGTGVDPEWVWDDEADPVVAAVIDRGEVPAVNALLRTWTRNGQPLPDGLPADLRDFMEQ
ARRLPSWADKAKLDRAAQFNKTKGFYIGVLYGLGSGMMSTAIPRESRAIYYSKGGADMKDRIAKTAKIGYDIGDLN
AYRPDGSMIVTAVKVRLVHAAVRHLLPQSPAWSQTSGGQKIPLSQADMMVTWHSLATFVMRKMKEWGVRVPAA
DAEAYLHMWQVAAHMLGVRDEYIPATWDAANAQAKQVLDPILAPTPEGKALADVLLNIVAELDAGLTRPLINAF
ARYMLGDEIGDWIGLPRQPVWEALIATAWPLLVAFREGLIPLPLVPEVLWTLEEALRKFVLLFLSEGRRIHIEIPD

Lcp_{K30}-P7-FL36
PLWTWSPSGSVAGTGTGVDPEWVWDDEADPVVAAVIDRGEVPAVNALLRTWTRNGQPLPDGLPADLRDFMEQ
ARRLPSWADKAKLDRAAQFNKTKGFYIGVLYGLGSGMMSTAIPRESRAIYYSKGGADMKDRIAKTAKMGYDIGDL
NAYRPDGSMIVTAVKTRLVHAAVRHLLPQSPAWSQTSGGQKIPLSQADMMVTWHSLATFVMRKMKEWGVRVPA
ADAEAYLHMWQVAAHMLGVRDEYIPATWDAANAQAKQVLDPILAPTPEGKALADVLLNIVAELDAGLTRPLINA
FARYMLGDEIGDWIGLPRQPVWEALIATAWPLLVAFREGLIPLPLVPEVLWTLEEALRKFVLLFLSEGRRIHIEIPD

Lcp_{K30}-P7-FL37
PLWTWSPSGSVAGTGTGVDPEWVWDDEADPVVAAVIDRGEVPAVNALLRTWTRNGQPLPDGLPADLRDFMEQ
ARRLPSWADKAKLDRAAQFNKTKGFYIGVLYGLGSGMMSTAIPRQARAVYYSKGGADMKDRIAKTAKIGYDIGDL
NAYRPDGSMIVTAVKVRLVHAAVRHLLPQSPAWSQTSGGQKIPLSQADMMVTWHSLATFVMRKMKEWGVRVPA
ADAEAYLHMWQVAAHMLGVRDEYIPATWDAANAQAKQVLDPILAPTPEGKALADVLLNIVAELDAGLTRPLINA
FARYMLGDEIGDWIGLPRQPVWEALIATAWPLLVAFREGLIPLPLVPEVLWTLEEALRKFVLLFLSEGRRIHFEIPD

Lcp_{K30}-P7-FL38
PLWTWSPSGSVAGTGTGVDPEWVWDDEADPVVAAVIDRGEVPAVNALLRTWTRNGQPLPDGLPADLRDFMEQ
ARRLPSWADKAKLDRAAQFNKTKGFYIGVLYGLGSGMMSTAIPRQARAVYYSKGGADMKDRIAKSAKIGYDIGDL
NAYRPDGSMIVTAVKVRLVHAAVRHLLPQSPAWSQTSGGQKIPLSQADMMVTWHSLATFVMRKMKEWGVRVPA
ADAEAYLHMWQVAAHMLGVRDEYIPATWDAANAQAKQVLDPILAPTPEGKALADVLLNIVAELDAGLTRPLINA
FARYMLGDEIGDWIGLPRQPVWEALIATAWPLLVAFREGLIPLPLVPEVLWTLEEALRKFVLLFLSEGRRIHIEIPD

Lcp_{K30}-P7-FL39
PLWTWSPSGSVAGTGTGVDPEWVWDDEADPVVAAVIDRGEVPAVNALLRTWTRNGQPLPDGLPADLRDFMEQ
ARRLPSWADKAKLDRAAQFNKTKGFYIGVLYGLGSGMMSTAIPRQARAVYYAKGGADMKDRIAKTAKLGYDIGDL
NAYRPDGSMIVTAVKVRLVHAAVRHLLPQSPAWSQTSGGQKIPLSQADMMVTWHSLATFVMRKMKEWGVRVPA
ADAEAYLHMWQVAAHMLGVRDEYIPATWDAANAQAKQVLDPILAPTPEGKALADVLLNIVAELDAGLTRPLINA
FARYMLGDEIGDWIGLPRQPVWEALIATAWPLLVAFREGLIPLPLVPEVLWTLEEALRKFVLLFLSEGRRIHLEIPD

Lcp_{K30}-P7-FL40
PLWTWSPSGSVAGTGTGVDPEWVWDDEADPVVAAVIDRGEVPAVNALLRTWTRNGQPLPDGLPADLRDFMEQ
ARRLPSWADKAKLDRAAQFNKTKGFYIGVLYGLGSGMMSTAIPRQARAVYYAKGGADMKDRIAKTAKLGYDIGDL
NAYRPDGSMIVTAVKVRLVHAAVRHLLPQSPAWSQTSGGQKIPLSQADMMVSWHSLATFVMRKMKEWGVRVPA

ADAEAYLHMWQVAAHMLGVRDEYIPATWDAANAQAKQVLDPILAPTPEGKALADVLLNIVAELDAGLTRPLINA
FARYMLGDEIGDWIGLPRQPVWEALIATAWPLLVAFREGLIPLPLVPEVLWTLEEALRKFVLLFLSEGRRIHIEIPD

Lcp_{K30}-P7-FL41
PLWTWSPSGSVAGTGTGVDPEWVWDDEADPVVAAVIDRGEVPAVNALLRTWTRNGQPLPDGLPADLRDFMEQ
ARRLPSWADKAKLDRAAQFNKTKGFYIGVLYGLGSGMMSTAIPRQARAVYYAKGGADMKDRIAKTAKVGYDIGDL
NAYRPDGSMIVTAVKVRLVHAAVRHLLPQSPAWSQTSGGQKIPLSQADMMVTWHSLATFVMRKMKEWGVRVPA
ADAEAYLHMWQVAAHMLGVRDEYIPATWDAANAQAKQVLDPILAPTPEGKALADVLLNIVAELDAGLTRPLINA
FARYMLGDEIGDWIGLPRQPVWEALIATAWPLLVAFREGLIPLPLVPEVLWTLEEALRKFVLLFLSEGRRIHIEIPD

Lcp_{K30}-P7-FL42
PLWTWSPSGSVAGTGTGVDPEWVWDDEADPVVAAVIDRGEVPAVNALLRTWTRNGQPLPDGLPADLRDFMEQ
ARRLPSWADKAKLDRAAQFNKTKGFYIGVLYGLGSGMMSTAIPRQARAIYYSKGGADMKDRIAKTAKLGYDIGDL
NAYRPDGSMIVTAVKVRLVHAAVRHLLPQSPAWSQTSGGQKIPLSQADMMVTWHSLATFVMRKMKEWGVRVPA
ADAEAYLHMWQVAAHMLGVRDEYIPATWDAANAQAKQVLDPILAPTPEGKALADVLLNIVAELDAGLTRPLINA
FARYMLGDEIGDWIGLPRQPVWEALIATAWPLLVAFREGLIPLPLVPEVLWTLEEALRKFVLLFLSEGRRIHLEIPD

Lcp_{K30}-P7-FL43
PLWTWSPSGSVAGTGTGVDPEWVWDDEADPVVAAVIDRGEVPAVNALLRTWTRNGQPLPDGLPADLRDFMEQ
ARRLPSWADKAKLDRAAQFNKTKGFYIGVLYGLGSGMMSTAIPRQARAIYYSKGGADMKDRIAKTAKMGYDIGDL
NAYRPDGSMIVTAVKVRLVHAAVRHLLPQSPAWSQTSGGQKIPLSQADMMVTWHSLATFVMRKMKEWGVRVPA
ADAEAYLHMWQVAAHMLGVRDEYIPATWDAANAQAKQVLDPILAPTPEGKALADVLLNIVAELDAGLTRPLINA
FARYMLGDEIGDWIGLPRQPVWEALIATAWPLLVAFREGLIPLPLVPEVLWTLEEALRKFVLLFLSEGRRIHIEIPD

Lcp_{K30}-P7-FL44
PLWTWSPSGSVAGTGTGVDPEWVWDDEADPVVAAVIDRGEVPAVNALLRTWTRNGQPLPDGLPADLRDFMEQ
ARRLPSWADKAKLDRAAQFNKTKGFYIGVLYGLGSGMMSTAIPRQARALYYSKGGADMKDKIAKTAKLGYDIGDL
NAYRPDGSMIVTAVKVRLVHAAVRHLLPQSPAWSQTSGGQKIPLSQADMMVTWHSLATFVMRKMKEWGVRVPA
ADAEAYLHMWQVAAHMLGVRDEYIPATWDAANAQAKQVLDPILAPTPEGKALADVLLNIVAELDAGLTRPLINA
FARYMLGDEIGDWIGLPRQPVWEALIATAWPLLVAFREGLIPLPLVPEVLWTLEEALRKFVLLFLSEGRRIHIEIPD

Lcp_{K30}-P7-FL45
PLWTWSPSGSVAGTGTGVDPEWVWDDEADPVVAAVIDRGEVPAVNALLRTWTRNGQPLPDGLPADLRDFMEQ
ARRLPSWADKAKLDRAAQFNKTKGFYIGVLYGLGSGMMSTAIPRQARAMYYSKGGADMKDRIAKTAKLGYDIGDL
NAYRPDGSMIVTAVKVRLVHAAVRHLLPQSPAWSQTSGGQKIPLSQADMMVTWHSLATFVMRKMKEWGVRVPA
ADAEAYLHMWQVAAHMLGVRDEYIPATWDAANAQAKQVLDPILAPTPEGKALADVLLNIVAELDAGLTRPLINA
FARYMLGDEIGDWIGLPRQPVWEALIATAWPLLVAFREGLIPLPLVPEVLWTLEEALRKFVLLFLSEGRRIHVEIPD

Lcp_{K30}-P7-FL46
PLWTWSPSGSVAGTGTGVDPEWVWDDEADPVVAAVIDRGEVPAVNALLRTWTRNGQPLPDGLPADLRDFMEQ
ARRLPSWADKAKLDRAAQFNKTKGFYIGVLYGLGSGMMSTAIPRQARAMYYSKGGADMKDRIAKTAKVGYDIGDL
NAYRPDGSMIVTAVKVRLVHAAVRHLLPQSPAWSQTSGGQKIPLSQADMMVTWHSLATFVMRKMKEWGVRVPA
ADAEAYLHMWQVAAHMLGVRDEYIPATWDAANAQAKQVLDPILAPTPEGKALADVLLNIVAELDAGLTRPLINA
FARYMLGDEIGDWIGLPRQPVWEALIATAWPLLVAFREGLIPLPLVPEVLWTLEEALRKFVLLFLSEGRRIHIEIPD

Lcp_{K30}-P7-FL47
PLWTWSPSGSVAGTGTGVDPEWVWDDEADPVVAAVIDRGEVPAVNALLRTWTRNGQPLPDGLPADLRDFMEQ
ARRLPSWADKAKLDRAAQFNKTKGFYIGVLYGLGSGMMSTAIPRQARSVYYSKGGADMKDRIAKTAKIGYDIGDLN
AYRPDGSMIVTAVKVRLVHAAVRHLLPQSPAWSQTSGGQKIPLSQADMMVTWHSLATFVMRKMKEWGVRVPAA
DAEAYLHMWQVAAHMLGVRDEYIPATWDAANAQAKQVLDPILAPTPEGKALADVLLNIVAELDAGLTRPLINAF
ARYMLGDEIGDWIGLPRQPVWEALIATAWPLLVAFREGLIPLPLVPEVLWTLEEALRKFVLLFLSEGRRIHIEIPD

Lcp_{K30}-P7-FL48
PLWTWSPSGSVAGTGTGVDPEWVWDDEADPVVAAVIDRGEVPAVNALLRTWTRNGQPLPDGLPADLRDFMEQ
ARRLPSWADKAKLDRAAQFNKTKGFYIGVLYGLGSGMMSTAIPRQSRAVYYSKGGADMKDRIAKTAKIGYDIGDLN
AYRPDGSMIVTAVKVRLVHAAVRHLLPQSPAWSQTSGGQKIPLSQADMMVTWHSLATFVMRKMKEWGVRVPAA
DAEAYLHMWQVAAHMLGVRDEYIPATWDAANAQAKQVLDPILAPTPEGKALADVLLNIVAELDAGLTRPLINAF
ARYMLGDEIGDWIGLPRQPVWEALIATAWPLLVAFREGLIPLPLVPEVLWTLEEALRKFVLLFLSEGRRIHIEIPD

Lcp_{K30}-P7-FL49
PLWTWSPSGSVAGTGTGVDPEWVWDDEADPVVAAVIDRGEVPAVNALLRTWTRNGQPLPDGLPADLRDFMEQ
ARRLPSWADKAKLDRAAQFNKTKGFYIGVLYGLGSGMMSTAIPHEARAIYYSKGGADMKDRIAKTAKIGYDIGDLN
AYRPDGSMIVTAVKVRLVHAAVRHLLPQSPAWSQTSGGQKIPLSQADMMVTWHSLATFVMRKMKEWGVRVPAA
DAEAYLHMWQVAAHMLGVRDEYIPATWDAANAQAKQVLDPILAPTPEGKALADVLLNIVAELDAGLTRPLINAF
ARYMLGDEIGDWIGLPRQPVWEALIATAWPLLVAFREGLIPLPLVPEVLWTLEEALRKFVLLFLSEGRRIHIEIPD

Lcp_{K30}-P7-FL50
PLWTWSPSGSVAGTGTGVDPEWVWDDEADPVVAAVIDRGEVPAVNALLRTWTRNGQPLPDGLPADLRDFMEQ
ARRLPSWADKAKLDRAAQFNKTKGFYIGVLYGLGSGMMSTAIPKEARAIYYSKGGADMKDRIAKTAKMGYDIGDL
NAYRPDGSMIVTAVKVRLVHAAVRHLLPQSPAWSQTSGGQKIPLSQADMMVTWHSLATFVMRKMKEWGVRVPA
ADAEAYLHMWQVAAHMLGVRDEYIPATWDAANAQAKQVLDPILAPTPEGKALADVLLNIVAELDAGLTRPLINA
FARYMLGDEIGDWIGLPRQPVWEALIATAWPLLVAFREGLIPLPLVPEVLWTLEEALRKFVLLFLSEGRRIHIEIPD